Torrefaction and Combustion Properties of some Nigerian Biomass

by

Femi Seun Akinrinola

Submitted in accordance with the requirements for the degree of Doctor of Philosophy

The University of Leeds

School of Chemical and Process Engineering

December 2014

The candidate confirms that the work submitted is his/her own, except where work which has formed part of jointly-authored publications has been included. The contribution of the candidate and the other authors to this work has been explicitly indicated below. The candidate confirms that appropriate credit has been given within the thesis where reference has been made to the work of others. Further details of the jointly-authored publications and the contributions of the candidate and the other authors to the work are listed below.

Chapter 4 is based on the publication listed below:

Femi S. Akinrinola, Leilani I. Darvell, Jenny M. Jones, Alan Williams and Joseph A. Fuwape., "**Characterisation of selected Nigerian Biomass for Combustion and Pyrolysis Applications**" Energy & Fuels 2014, (28), 3821−3832, American Chemical Society.

I carried out all experiment, except for metal and lignocellulose analyses which were conducted in TES Bretby and IBERS Analytical Chemistry Laboratory respectively. I analysed the result and wrote the paper, Fuwape advised on the fuels & helped with the delivery of the fuels, while other authors provided guidance, advice and supervision.

Chapter 5 contains part of the publication in a conference paper as listed below:

Femi S. Akinrinola, Leilani I. Darvell, Jenny M. Jones, and Alan Williams. "**Increasing Wood Fuel Utilisation in Nigeria via Torrefaction**" Presented at the 6th Annual NAEE/IAEE International Conference: Energy Resource Management in a Federal System: Challenges, Constraints And Strategies, Sheraton Hotel, Lagos, Nigeria (22-23 April, 2013).

I was the lead author and also carried out all experimental data respectively. Other authors provided guidance, advice and supervision.

Chapter 5, 6 and 7 of this work contains part of the publication that is listed below:

Femi S. Akinrinola, Nwigwudu Ikechukwu, Leilani I. Darvell, Jenny M. Jones and Alan Williams., "**Upgrading of Nigerian biomass by torrefaction for combustion applications**" (in pipeline).

I was the lead author. Nwigwudu Ikechukwu, an MSc student under my supervision (April-Jun 2012) prepared samples for single particle combustion experiment (Chapter 7), and we both did the gindability test for torrefied fuels in Chapter 5, while I worked on the calibration of the Retsch ball mill and gindability test for raw samples. I solely carried out all the experimental work in Chapter 6. All other authors mentioned in this publication provided guidance, advice and supervision.

This copy has been supplied on the understanding that it is copyright material and that no quotation from the thesis may be published without proper acknowledgement.

© <2014> <University of Leeds> <Femi Seun Akinrinola>

ACKNOWLEDGEMENTS

"Now to Him who is able to do exceedingly abundantly above all that we ask or think, according to the power that works in us, to Him be glory".

During the last few days of this writeup, I have felt like I was about to complete a marathon and to get here, I have journeyed for years on a hilly road with many twists and turns where my mental strength have been tested. I have grown and further developed as a person.

First and foremost, my sincere gratitude goes to my supervisors, Professor Jenny M. Jones, Professor Alan Williams and Dr. Leilani Darvel for providing invaluable support and guidance during the course of this work. They guided me into the complex and exciting world of wood chemistry, and without them, I don't see myself coming this far. My thanks also goes to Robert Fowell for proofreading this thesis and for showing sincere interest in the contents of the documents and also to Prof. Joseph Fuwape for helping out towards the delivery of the Nigerian biomass to the UK.

This research work would not have been possible without the help of several individuals from this institution. Therefore I would like to thank Adrian Cunliff, Simon Lloyd, Sara Dona, Jude Onwudili, Peter Dawson, Amanda Lea-Langton, Xiaomian Baxter, Abby Saddawi, Bijal Gudka, Raimie Ibrahim, Thomas Robin, Richard Riley, Chibi Takaya, Paula Mcnamee, Ben Dooley, Farooq Atiku, Peinong Xing, Patrick Mason, Yee Chin, Kelechi Anyikude, Ugochinyere Ekpo, Stephen Chilton, Bala Fakandu, Adewale Oladipo, Adeolu Adebulugbe, Nwigwudu Ikechukwu, Efosa Osaghie, Mayowa Amusat, Felix Olakuleyin, Charles Ikonwa, Joshua Alabi, Heather Strachan, and Dave Haynes. Some of them have left the university and I send my best wishes for the future.

To David Lancaster (communication studies, University of Leeds) I will always be in your debt. You helped me to find inspiration, encourage me to tackle new tasks and helped me into a good mood when I was down. You supported my family when we needed it. A big thank you to Mrs Akindolire, Joan Ojukwu and Preye Ombu, Sayo Dairo, Ehoniyotans, Iyokos, Odedeyis, Alabis, Odins, Jacobs and Ayobami Alao who all baby sit my children and support my family during the course of this work.

I would also like to acknowledge the Energy Programme, who are the Research Councils UK cross council initiative led by Engineering and Physical Sciences Research Council (EPSRC) and contributed to by Economic and Social Research Council (ESRC), National Environment Research Council (NERC), Biotechnology and Biological Sciences Research Council (BBSRC) and Science and Technology Facilities Council (STFC), as well as the scholarship received from Niger Delta Development Commission for the financial support. I will also like to appreciate Quintas Renewable Energy Solutions Limited for the role they played towards the success of this project.

I say a very resounding thank you to my family. Words cannot express how grateful I am to my siblings, mother-in law, father-in-law, my two grandmothers (camp and Sango) my mummy, and daddy for all of the sacrifices that you've made on my behalf. Dad, I really appreciate your willpower for hanging on till now despite all odds. Mum, your prayers for me were what sustained and kept me going me thus far.

Finally, my deepest gratitude to my beloved wife Olusola and lovely children Mercy and Majesty to whom this thesis is dedicated. You guys are fantastic. You always inspire, support and encourage me in the moments when there was no one to answer my queries. You felt my mental absence, gave me space and waited patiently for this work to be completed. I am forever grateful to you all. Thank you Olusola for looking through the videos on single particle combustion to ensure that my analysis is error free. Mercy, I will never forget to thank you for always checking on me in the middle of the nights during the course of writing this thesis.

ABSTRACT

Many countries are seeking to expand their use of solid biomass for electricity and heat generation. Nigeria, too, is exploring its own potential energy crops and indigenous residues. It is expected that 75% of electricity generation in Nigeria will come from renewable energy by the end of 2025 [1], and this includes hydro, solar, wind and biomass. The use of this biomass for energy production is, however, limited by some critical factors such as high moisture content, low bulk density and low energy density, all of which negatively affect the viability of biomass energy. Torrefaction is a mild pyrolysis method which shows promise for improving the energy density and some of the other undesirable properties of raw biomass.

This study examines the torrefaction and combustion properties of four Nigerian woody biomass, *Gmelina arborea, Terminalia superba, Nauclea diderrichii*, *Lophira alata* and a residue; palm kernel expeller (PKE). Two of these woods (*Gmelina* and *Terminalia*) are energy crops under cultivation trials in Nigeria, and two (*Nauclea* and *Lophira*) are woods used in the timber industry which results in large quantities of sawmill residues. Fuels were torrefied at 270 and 290^{o}C for either 30 or 60 min, and assessed for pyrolysis and combustion characteristics in comparison to their untreated (raw) counterparts. Torrefied fuels were analysed for proximate, ultimate and higher heating value, and mass and energy yields were calculated. Results show that the Nigerian fuels have low N, S, Cl and high carbon contents. The high carbon content in the Nigerian fuels resulted in a relatively higher calorific value compared to typical European biomass such as willow. These two together makes the biomass very attractive for energy production. For the Nigerian fuels mass yields were in the range 70-93% and energy yields in the range 79-93%. Energy densities of the woods improved from 19.2-21.2 MJ/kg for the raw fuels to 21.5-24.6 MJ/kg for the torrefied fuels. The torrefaction process also results in loss of nitrogen from the fuel, mainly in the tar (condensables). Generally, while the wt% N increases in the torrefied fuel compared to the original material, the N content on an energy basis, generally decrease. This is very significant since amount of NOx that is formed in combustion is related, in part, to fuel nitrogen (fuel dependent N/GJ).

A modified Hardgove Index test was used to study the milling behaviour of the fuels, which demonstrated improved grindability of the woods upon torrefaction, especially

for *Nauclea.* This is important for pulverized fuel combustion applications where energy in milling and mill throughput are expected to decrease for the torrefied fuels. However, torrefaction had very little effect on the grindability of PKE. The apparent first order kinetics for pyrolysis were determined by thermogravimetric analysis (TGA). After torrefaction, the fuels become less reactive as evidenced by both the slightly higher temperature of maximum pyrolysis rate and by the lower reactivity rate (as calculated at 300^{o}C). The A and Ea values for the fuels ranged from 10 – 24.9 s^{-1} and 78.8 -156 kJ/mol respectively. Overall, *Nauclea* and *Gmelina* were the most reactive fuels, whilst PKE was the least reactive.

The combustion behaviour of the selected raw and some of the torrefied fuels was examined by suspending particles in a methane air flame and interrogating using a high-speed camera. The observations showed that torrefaction changes the combustion properties of biomass resulting in shorter ignition delay, shorter duration of volatile combustion and longer duration of char burn out. TGA combustion analysis of chars and apparent first order kinetic parameters for char combustion revealed that torrefaction of biomass results in an increase in activation energy, Ea, resulting in a slower apparent reactivity in combustion i.e. torrefied chars are less reactive than their raw counterparts and the more severe the torrefaction conditions, the less reactive the fuels become. The fuels are becoming more coal-like in their combustion behaviour.

In summary, the Nigerian biomass and torrefied biomass show high potential for large scale electricity production. Their high calorific value, low nitrogen, low sulphur and high melting ash, together with their combustion properties make them an attractive resource. Future studies should examine the sustainability of supply chains for these fuels to ensure good carbon reduction. Torrefaction shows promise for improving many characteristics of the fuels for use in both large scale power stations and more widely for domestic purposes.

TABLE OF CONTENTS

LIST OF FIGURES

LIST OF TABLES

LIST OF PUBLICATIONS

Femi S. Akinrinola, Leilani I. Darvell, Jenny M. Jones, and Alan Williams. "INCREASING WOOD FUEL UTILISATION IN NIGERIA VIA TORREFACTION" Presented at the 6th Annual NAEE/IAEE International Conference: ENERGY RESOURCE MANAGEMENT IN A FEDERAL SYSTEM: CHALLENGES, CONSTRAINTS AND STRATEGIES, Sheraton Hotel, Lagos, Nigeria (22-23 April, 2013).

Femi S. Akinrinola, Leilani I. Darvell, Jenny M. Jones, Alan Williams and Joseph A. Fuwape., "CHARACTERISATION OF SELECTED NIGERIAN BIOMASS FOR COMBUSTION AND PYROLYSIS APPLICATIONS" Energy & Fuels 2014, (28), 3821−3832, American Chemical Society.

Femi S. Akinrinola, Nwigwudu Ikechukwu, Leilani I. Darvell, Jenny M. Jones and Alan Williams., "UPGRADING OF NIGERIAN BIOMASS BY TORREFACTION FOR COMBUSTION APPLICATIONS" (the manuscript is submitted).

LIST OF ABBREVIATIONS

AC	Ash Content
AD	After air drying
ADF	Acid Detergent Fiber
ADL	Acid Detergent Lignin
AR	As received
$CaCO_3$	Calcium Carbonate
CaC_2O_4	Calcium Oxalate
CBD	Convention on Biological Diversity
CDM	Clean Development Mechanism
CHNS	Carbon-Hydrogen-Nitrogen-Sulphur
CH_4	Methane
CO	Carbon Monoxide
CO_2	Carbon Dioxide
CV	Calorific Value
daf	dry ash free basis
db	dry basis
DCM	Dichloromethane
DSC	Differential Scanning Calorimetry
DTA	Differential Thermal Analysis
DTG	Differential Thermogravimetric Analysis
EA	Elemental Analyser

EU	European Union
FC	Fixed Carbon
FCC	Fixed Carbon Content
FGN	Federal Government of Nigeria
fps	frame(s) per second
FTIR	Fourier Transform Infra-Red
GC	Gas Chromatography
GDP	Gross Domestic Product
GHG	Green House Gases
GJ	Gigajoule
GWh	Gigawatt hour
HGI	Hardgrove Grindability Index
HHV	Higher Heating Value
HFC	hydrofluorocarbons
ICP	Inductively Coupled Plasma
IR	Infra-red
K	Potassium
KW	Kilowatt
KWhm	Kilowatt Hour Meter
LHV	Lower Heating Value (KJ/kg)
M_{ad}	Moisture Content after oven drying

MC	Moisture Content
MS	Mass Spectrometry
MW	Megawatt
N	Nitrogen
NA	Not Applicable
ND	Not Detected
NDF	Neutral Detergent Fiber
NO	Nitric Oxide
N_2O	Nitrous Oxide
NO_2	Nitrogen dioxide
OLS	Ordinary Least Squares Regression
PFC	Perfluorocarbons
PLS	Particle Least Squares Regression
Py-GCMS	Pyrolysis Gas chromatography
R	Reaction
RO	Renew
RPR	Residue to Product Ratio
RT	Retention Time
SPC	Single Particle Combustion
SRC	Short Rotation Coppice
TGA	Thermogravimetric Analysis

TG	Thermogravimetry
UNFCCC	United Nations Framework Convention on Climate Change
WEC	World Energy Council

CHAPTER 1. INTRODUCTION

1.1 World Energy and Policy

Energy is a vital requirement for the development of a nation, and has always been a significant and indispensable component for the economic growth of a nation. It is the controlling force of industrialization, as it drives the economic and social opportunities of a nation. It is established that no nation has been able to advance past a subsistence economy without ensuring at least minimum access to energy services for a wide section of its population [2].

There is a global challenge on energy security as the world's population continues to increase resulting in ever increasing demand for energy. The last quarter of the 20th century recorded increasing fluctuation in the price of crude oil that resulted in uncertainty for the world's economic projections. Currently, 85% of world energy demand is achieved from the combustion of fossil fuels, which are depleting [3]. The consumption of world energy is predicted to rise by 56% from 2010 to 2040 [3]. The high dependence on fossil fuels for energy is leading to rapid depletion of these resources but is also contributing greatly to environmental concerns. Burning fossil fuel to provide heat and power increases the emission of greenhouse gases, especially carbon dioxide (CO_2) into the atmosphere. CO_2 is one of the greenhouse gases that is responsible for global climate change and this has become a major environmental issue.

As the demand for sustainable heat and electricity generation continues to increase worldwide, developed nations are working towards sustainable energy for the future and also to reduce carbon emissions globally. World economic leaders and governments in several countries have set mandatory targets for a substantial percentage share of renewables in the energy generation market. There have been several directives, legislations, protocols and acts which outline an energy pathway that would limit the concentration of greenhouse gases in the atmosphere. The Kyoto Protocol was adopted in the United Nations Framework Convention on Climate Change (UNFCCC) in 1997 [4]. The Renewable Energy Directive 2009/28/EC ("the Directive") instituted a European framework for the promotion of renewable energy, setting mandatory national renewable energy targets for achieving a 20% share of renewable energy in the final energy consumption and a 10% share of energy from renewable sources in transport by

2020 [5]. The UK is bound by a legal framework to reduce greenhouse gas emissions by at least 80% below the 1990 levels by the year 2050 in accordance with the Climate Change Act 2008 [6]. The UK government also aims at shorter term emissions reduction targets in the form of the European Directive to produce 15% of its electricity from renewable sources by 2020 [7].

1.2 The Policy Drivers of Renewable Energy

The quest for increase in power generation from renewable energy (RE) is been policy-driven , as stated earlier, the aims are to protect the environment from the resultant climate change due to the combustion of fossil fuels, to improve energy security and finally to encourage economic development.

1.2.1 Environmental Concerns

Energy production and consumption through the use of fossil fuels are unsustainable. It causes emission of greenhouse gases including carbon dioxide (CO_2), methane (CH_4) nitrous oxide (N_2O), perfluorocarbons (PFCs), hydrofluorocarbons (HFCs), and sulphur hexafluoride (SF_6) resulting in climate change effect. Continuing with business as usual will increase the earth's global average temperature levels and this will have a detrimental effect on the population and some of the eco-systems.

Photochemical smog and acid rain are other problems associated with burning fossil fuels. For example, coal which contains relatively high sulphur and nitrogen contents will form oxides of nitrogen and sulphur respectively during combustion. Depending on the combustion system, about 95% of the oxides formed with nitrogen in the fuel during combustion is nitrous oxide (N_2O), which is a GHG and the remaining 5% is made up of nitric oxide (NO) and nitrogen dioxide (NO_2) [8]. The latter oxides react with atmospheric moisture to form acid rain which weathers buildings. Additionally, NO_2 is also known to cause inflammation of the lungs. The sulphur content in the fuel reacts with oxygen during combustion to form sulphur oxide. Sulphur oxide (SO_2) reacts with oxygen in the atmosphere to form sulphur trioxide (SO_3). SO_3 causes humans to cough and choke at concentrations as low as 1ppm (part per million) [9]. Acid rain is also formed when SO_3 reacts with water to form sulphuric acid (H_2SO_4). Oil pollution, oil spillage, soil erosion, contamination of underground water, destruction of land structure

and fertility as a result of mining are other environmental problems driving the need for the deployment of more renewable energy.

1.2.2 Energy Security

Due to the increasing demand in energy, the world cannot solely depend on fossil fuels as the primary source of energy. The fluctuation in the price of crude oil was a source of disequilibrium in the world's economic projections. Also the availability of these fossil fuels is rapidly decreasing and will be exhausted at some point. Increasing the share of renewable energy in the world's energy mix will increase energy security by offering greater diversity of supply, and, in many contexts, providing a less centralised and more modular supply that may be less prone to disruption [8].

1.2.3 Economic Development

High priority is often given to the deployment of renewable energy for more sustainable economic growth [10]. Countries can create more jobs by producing biofuels sustainably or by generating electricity using wind turbines and solar grids. According to United Nations Environment Programme (UNEP), renewable energy generates more jobs per unit of installed capacity, per unit of power generated and per dollar invested compared to fossil fuel power plants [8]. Job creation is another policy driver of renewable energy and is particularly appealing to policymakers or governments facing high and persistent unemployment [8]. Also the electricity generated via renewables can be sold or exported to other countries when not needed.

1.3 Overview of the Nigerian Energy

Nigeria with a population of about 180 million is endowed with enormous energy resources, such as, natural gas, petroleum, coal, nuclear, tar sands, and renewables; solar, wind, biomass and hydro power. However, development, exploitation and utilisation of such energy sources have been inclined towards petroleum, natural gas, and hydro only. With the discovery of oil in 1970 in Nigeria, a decade after obtaining her independence, the nation became highly dependent on crude oil and this has contributed about 70% of her revenue and about 25% of her gross domestic product (GDP).

Nigeria started the exploration of coal in 1916 and since then it is established that there are nearly three billion tonnes of coal reserves in seventeen identified coalfields with an average of over 600 million tonnes of proven reserves per coalfield [11]. However, at the end of the Nigerian civil war in 1967, many coal mines were abandoned and coal production has never completely recovered. This is evident as coal production in Nigeria dropped to less than 1% of the pre-war level in 1990 [12]. This decline in coal production was accelerated by the discovery of crude oil in commercial quantities in the late sixties.

According to the United State Energy Information Administration report [13], Nigeria is the largest oil producer in Africa. Nigeria holds the largest natural gas reserves in Africa and is the ninth largest holder of gas in the world. Nigeria produced about 1.2 billion cubic feet of dry natural gas between 2011 and 2012 as shown in Figure 1-1; there is a big gap between the production and consumption of natural gas in Nigeria. Presently in Nigeria, the production of natural gas is affected by the lack of infrastructure and poor distribution networks, thus leading to flaring of natural gas. Figure 1-2 shows the distribution of gas flaring around the world. From the figure, it is observed that Nigeria which flares the second largest amount of natural gas globally accounting for 10% of the total amount of gas flared, after Russia. According to the United State Energy Information Administration report [13], Gas flaring in Nigeria was reduced to about 515 billion cubic feet in 2011.

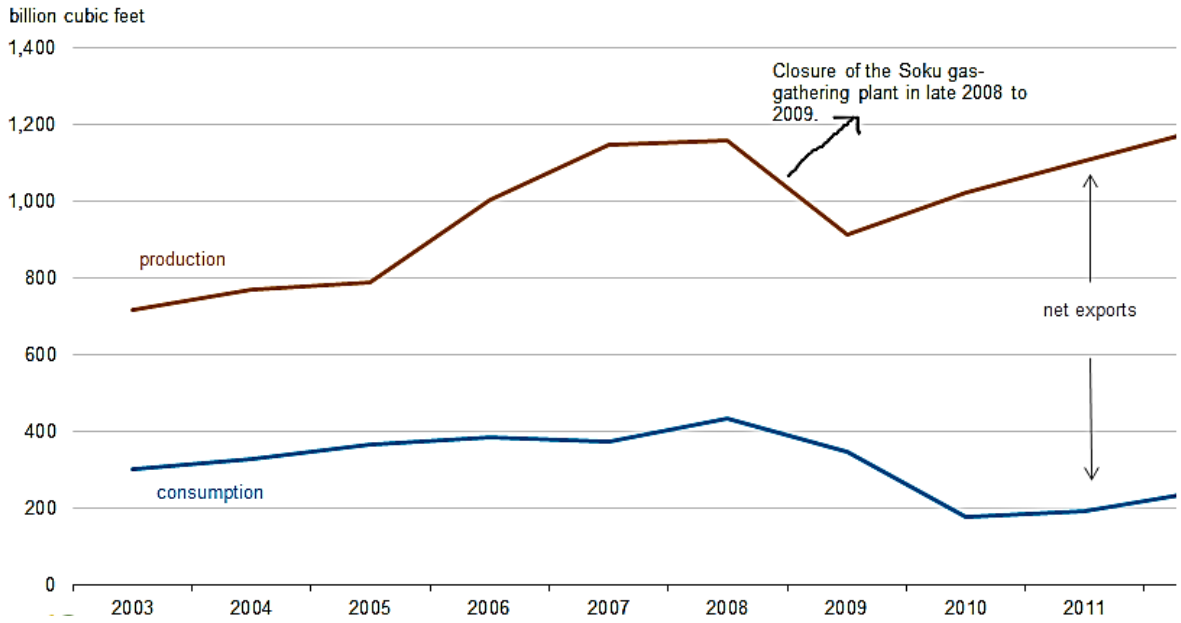

Figure 1-1: The trend for production and consumption of natural gas in Nigeria between 2003 and 2011 [14].

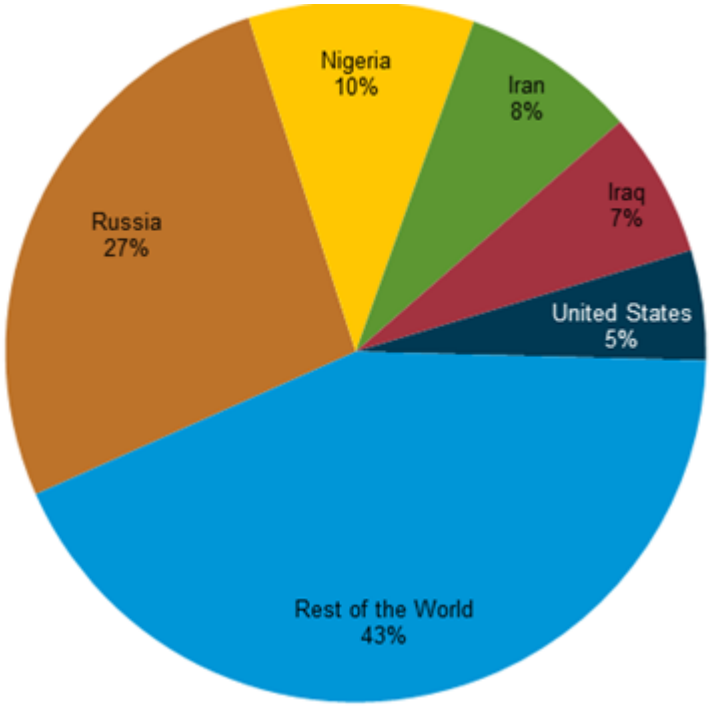

Figure 1-2: The top five natural gas flaring countries in the world, 2011 [14].

Nigeria is faced with heightened electricity problems, which continue to cripple her development despite the vast amount of natural resources in the country. Nigeria has one of the lowest net electricity generation per capita rates in the world [14]. The electricity demand surpasses the supply, resulting in load shedding, blackouts, and a reliance on private generators. In 2012, Nigeria's generation capacity was about 6,000 Megawatts (MW), with an energy mix of about 4,730 MW (79%) from fossil fuel sources and 1,270 MW (21%) was from hydro sources [14]. Nigeria plans to increase her generation capacity from fossil fuel and renewable sources to more than 20,000 MW by 2020.

According to the United State Energy Information Administration report [13], 83% of the total energy consumption in Nigeria in 2011, comes from renewables (biomass) i.e. firewood as shown in Figure 1-3. Firewood is used by most people in the rural areas for lighting, cooking and heating needs. There is the need for the utilisation of sustainable means of energy generation to meet the growing population of Nigeria as about 40% of households in Nigeria are connected to the national grid, 46% have access to electricity and only 2% of the rural households have access to electricity either by rural electrification actions initiated by the government or self-generation by private individuals [13].

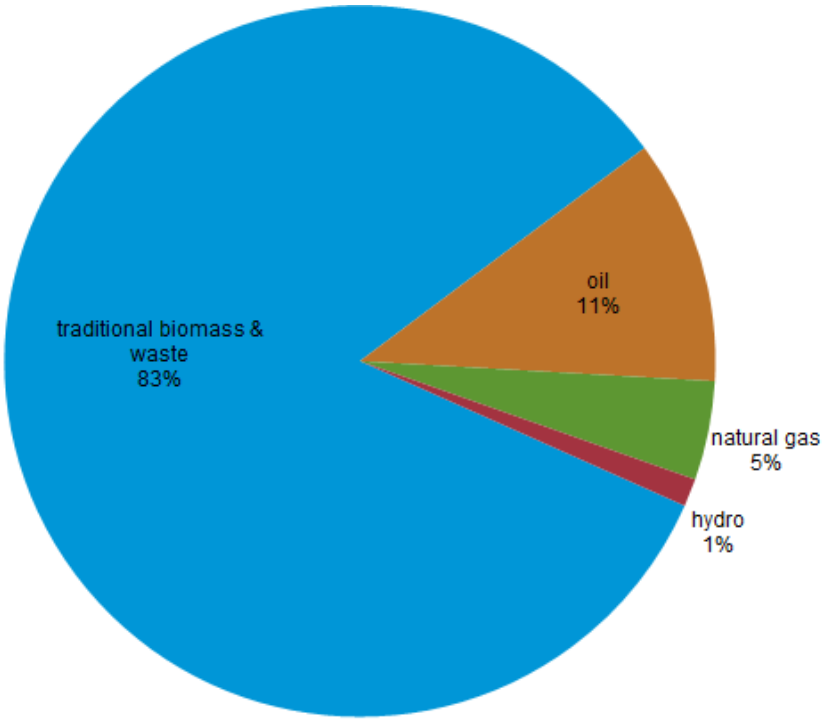

Figure 1-3: Primary Energy consumption in Nigeria, 2011 [13].

The Nigerian government privatised the operation of the nation's energy supplier i.e. Power Holding Company of Nigeria (PHCN) to private operators in 2013 in order to find lasting solutions to the erratic power supply in Nigeria. Policies and regulatory which includes off-grid electricity generation, encouragement of independent power projects, a legislative framework, rural electrification programmes, licensing arrangements for private-sector operators, design of further tax credits, capital incentives, preferential loan opportunities for renewable energy projects, Feed-in Tariffs and clarifying market rules for enabling environment are established to encourage development of the renewable energy sector. Presently in Nigeria, the establishment of off-grid electricity generation by the government is encouraging quite a number of operational independent power projects around the country.

1.4 The Nigerian Renewable Energy Plan

The Nigerian government plans set targets to ensure gradual transition from a fossil economy to one driven by an increasing share of renewable energy by 2025. It is expected that 75% of electricity generation in Nigeria will come from renewable energy by the end of 2025 [1]. This includes hydro, solar, wind and biomass.

1.5 Renewable Energy Sources in Nigeria

Nigeria has a huge reserve of different renewable energy sources which includes solar, hydro, wind, and biomass.

1.5.1 Hydropower

Nigeria is blessed with large rivers, dams and waterfalls, which offer high potential for hydroelectricity generation. Nigeria currently generates about 1,900MW of electricity from hydro and has a potential estimated at 14,750 MW [15]. Electricity generation from small HydroPower (SHP) plants has gained favourable attention in both the developed and developing economies of the world because of its intrinsic advantages [16]. SHP offers less geographical problems, reduced environmental impact, minimal civil works, and flood prevention.

1.5.2 Wind Energy

Generally, the wind speed in Nigeria is low due to her geographical location, except in the coastal regions and offshore. Oyedepo [17], reported that the Wind energy is available at annual average speeds of about 2.0 m/s in the coastal region and 4.0 m/s in the far northern region of the country. According to the Nigerian meteorological agency (NIMET), the most favorable sites for electricity generation from wind energy are the coastal areas, the offshore states (namely Lagos, Ondo, Delta, Rivers, Bayelsa and Akwa-Ibom), the inland hilly regions of the north and the mountain terrains in the middle belt regions of the country. The peak of the wind power is usually between April and August in most of the aforementioned sites, apart from offshore which have strong winds throughout the year. Wind energy contributions to the total energy consumption in Nigeria are insignificant.

1.5.3 Solar Energy

Nigeria is located along the equator, within a high sunshine belt for good solar radiation and thus has enormous solar energy potentials. Nigeria records minimum and maximum average radiations between 12 and 30 MJ/m^2/day for an average of six sunshine hours per day [16]. The lowest solar radiation is experienced for five months during the rainy season which is usually between May and October, while the highest level of solar radiation occurs for a period of six months; from November to April in the dry season. It is possible to generate about 1850 x103 GWh of solar electricity per year if solar collectors or modules were installed to cover 1% of Nigeria's land area of 923,773 km^2 [16].

1.5.4 Biomass

Biomass resources in Nigeria include woods, agricultural wastes, crop residues, sawdust, wood shavings, bird and animal litter and dung as well as industrial and municipal solid wastes [12]. As shown in Table 1-1, these were estimated in Mt as 39.1 fuel wood, 11.2 agricultural wastes, 1.8 sawdust, and 4.1 municipal solid wastes [12]. Tropical rain forest is the major source of timber supply and energy crops in Nigeria with high plant diversity of over 4,600 plant species. The forest covers 10% of the country's land area with over 560 tree species with range of about 30 to 70 species per hectare for trees ≥ 5 cm diameter at breast height (dbh) [18].

The highest quantities of crop residues in Nigeria are found in the guinea savannah in the north central region of Nigeria. Agricultural residues include cornstalks, rice husk, cassava peels, palm kernel shells, coconut shells and sugarcane bagasse.

At present, bio-energy sources are used by a significant number of people in rural areas to meet their basic energy needs (cooking, lighting and heating), but this is achieved in an inefficient way, with a negative impact on people's health as well as on the environment. It is therefore important to take adequate measures to modernize its supply, conversion and use in a sustainable way.

Nigeria is a member of the "non-Annex 1" countries who are signatories to the Kyoto protocol agreement. As such, Nigeria has no limit or emission restriction, but needs to initiate Clean Development Mechanism projects (CDM) in order to reduce emissions of greenhouse gases in the atmosphere. The success of CDM projects can earn Nigeria

carbon credits which can also be traded to other Annex 1 countries who are also trying to achieve their emission limits. The World Bank identified over 750 CDM projects in Nigeria, which, if implemented, could generate 100 million tonnes of carbon emission reductions annually [19]. As a consequence, the Federal government of Nigeria has initiated four CDM's, three of which concern gas flare reduction, recovery and processing, while the fourth is "Save 80 Fuel Wood Stoves" aimed at introducing the energy-saving and low polluting "Save 80" wood stove to the Nigerian Market.

According to World Energy Council (WEC) [2], the Federal government of Nigeria has also signed a Memorandum of Understanding (MoU) to develop forest carbon projects in the country, as well as to establish a carbon centre for the West African region. Several afforestation projects covering several thousand hectares in many States in Nigeria are completed. These have involved establishing seedling nurseries, and plantation management [20]. Woods in the plantations include *Gmelina, Terminalia*, teak, eucalyptus, and pine. Energy crops are currently cultivated primarily for the production of biofuels or generation of heat and electricity. Some notable examples of energy crops which are currently in production are corn (*Zea mays*), sugarcane (*Saccharum officinarum*), and short-rotation plantations of poplar (*Populus* spp.), physic nut, a member of the family Euphorbiaceae *(Jatropha curcas)*, and sycamore (*Platanus occidentalis*) [21].

Table 1-1: Estimated quantities for biomass resources in Nigeria [15].

Resources	**Quantity (Million tonnes)**	**Energy value ('000 MJ)**
Fuelwood	39.1	531.0
Agro-waste	11.2	147.7
Saw Dust	1.8	31.4
Municipal Solid Waste	4.1	-

Abila [22] reported that some of the drivers and incentives for the utilisation of bioenergy resources in Nigeria include price instability of fossil fuel, insecurity in the supply of fossil fuel, poor power distribution network, diversification of the economy, greenhouse gas emission control, climate change, poverty, unemployment, oil bunkering, militancy, deforestation, and abundance of sawmill products. These are grouped into four main headings of global and regional cooperation, energy, environmental and socio-economic concerns as shown in Figure 1-4.

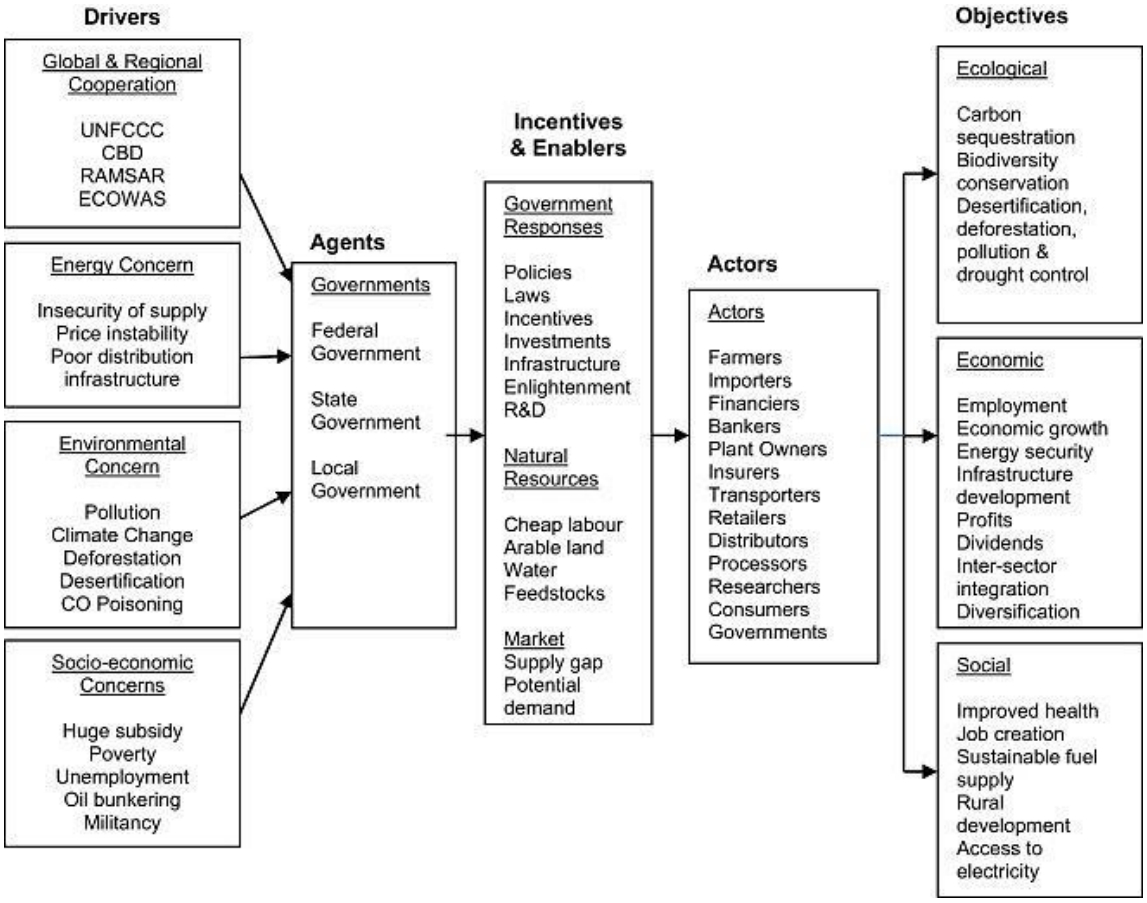

Figure 1-4: Conceptual framework of the drivers of biofuel utilization in Nigeria [22].

1.6 Thermochemical Processing of Biomass Energy

Thermochemical processing of biomass involves the use of heat and catalysts to transform plant polymers into fuels, chemicals, or electric power [23]. As shown in Figure 1-5, there are five different routes in thermochemical processing of biomass namely combustion, pyrolysis, gasification, hydrothermal processing and hydrolysis to sugars.

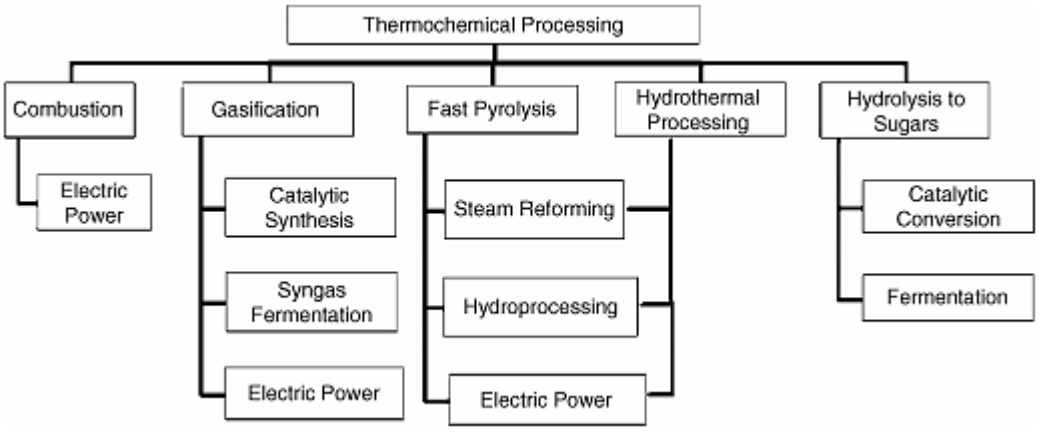

Figure 1-5: Thermochemical routes for production of fuels, chemicals and power [23].

1.6.1 Combustion

Combustion is the simplest thermal conversion of biomass and it involves burning of biomass in the presence of air or oxygen to release heat [24]. This process leads to the production of carbon dioxide, water vapour and trace amount of other components. There are four main stages in biomass combustion namely drying (evaporation of moisture), volatilization, devolatilisation and char burn out stage. The drying stage is the first phase in biomass combustion and is the phase where the moisture in the biomass is evaporated. Volatilisation is the next reaction or phase after the evaporation of moisture. This is where the biomass decomposes, and volatile gases are released leading to the formation of char. Devolatilisation is the phase that occur immediately after the release of volatile gases. In this phase, the volatile gases released are combusted above the fuel bed and this is characterised by yellow flames [23]. The final stage is the combustion of char. The solid char remaining after devolatilisation is combusted and its burning is characterized by small blue flames or glowing of the char pieces [23]. The temperatures of the flame can exceed 2000°C during biomass combustion, depending on the heating value and moisture content of the fuel, the mass ratio of air to fuel and the construction of the furnace [23]. It is important to have adequate air to fuel ratio to avoid incomplete combustion arising from the shortage of air; a situation that could potentially lead to large emissions of pollutants, formation of tars and raise environmental concerns [25]. Also when the air in the combustion chamber is too high, it lowers the combustion temperature and thermal efficiency. Different combustion methods are used to convert the chemical energy of biomass fuel

into high temperature exhaust gases, where the heat from the gases can be utilised for power generation [26], and can be seen in Table 1-2. The fluidised bed combustion system is the most recent development for biomass combustion in industrial applications.

Table 1-2: Combustion systems for biomass conversion [27].

Combustion method	Combustion type	Features
Fixed bed combustion	Horizontal/Inclined grate Water-cooling grate Dumping grate	Grate is level or sloping. Ignites and burns as surface combustion of biomass supplied to grate. Used in small-scale batch furnace for biomass containing little ash.
Moving bed combustion	Forward moving grate Reverse moving grate Step grate Louver grate	Grate moves gradually and is divided into combustion zone and after-combustion zone. Due to continuous ash discharge, grate load is large. The combustion obstruction caused by ash can be avoided. Can be applied to wide range of fuels from chip type to block type.
Fluidized bed combustion	Bubbling fluidized bed combustion Circulation fluidized bed combustion	Uses sand for bed material, keeps fuel and sand in furnace in boiling state with high-pressure combustion air, and burns through thermal storage and heat transmission effect of sand. Suitable for high moisture fuel or low grade fuel.
Rotary hearth furnace combustion	Kiln furnace	Used for combustion of high moisture fuel such as liquid organic sludge and food residue, or large waste etc. Restricted to fuel size on its fluidity.
Burner combustion	Burner	Burns wood powder and fine powder such as bagasse pith by burners, same as that for liquid fuel.

1.6.2 Pyrolysis

Pyrolysis is the thermal decomposition of biomass at high temperatures (500-900°C) in an inert environment to produce a solid char, liquid and non-condensable gases (for example, CO_2, H_2O, CO, C_2H_2, C_2H_4). The condensable phase which contains tar and reaction water (bio-oil) is the main interest in pyrolysis. It contains of mainly phenolic compounds and up to 20% water. The product of pyrolysis depends on the design of the pyrolyser, composition of biomass, and the reaction parameters i.e. heating rate, final temperature and residence time [28]. Slow pyrolysis i.e. at low heating rate, reaction temperature between 200-800°C and long residence times favour charcoal production. Therefore the amount of the char yield will be higher in slow pyrolysis. In contrast, fast pyrolysis i.e. at low temperatures (below 650°C) yields more vapours and condensable liquids while that at high temperatures (up to 1000°C) yields more gases [26]. Bio-oil

production is favoured by moderate temperatures (about 500°C), short reaction time (second), fast heating rate ($\geq 10^3$ Ks^{-1}) and rapid quenching.

1.6.3 Gasification

Gasification is a partial oxidation process (i.e. an endothermic reaction) at high temperatures (700-850°C) whereby carbonaceous fuels (e,g. biomass) is broken down into flammable gas mixtures known as producer gases [26]. The gas mixtures consist of carbon monoxide, hydrogen, methane, small amounts of nitrogen, carbon dioxide and higher hydrocarbons. Low temperature and high pressure gasification process (700-1000°C) favours the formation of methane, while high temperatures (above 1000°C) and low pressures favours the formation of carbon monoxide and hydrogen [26].

1.6.4 Hydrothermal Processing

Hydrothermal liquefaction is the decomposition of biomass in hot compressed water at a low temperature (300-350°C), pressure of 120-180 bar and at a reaction time between 5 to 20 mins to produce gas, liquid and solid. The process is suitable for very wet feedstocks i.e. biomass containing high moisture content, such as aquatic biomass; algae and organic sludge since the reaction takes place in water. Hydrothermal processing can be subdivided into two processing environments namely subcritical and supercritical [23]. The division is based on the critical temperature of water at 374°C and at 220.6 bar. The limit beyond which the water vapor phase can no longer be compressed to form a liquid phase is known as the critical temperature [23].

1.6.5 Thermal Hydrolysis to Sugar

Thermal hydrolysis involves the heating of the biomass at low temperatures (160-180°C) and high pressure. The long chain molecules which form hemicellulose and cellulose are separated in an aqueous media in order to obtain the constituent parts of the molecules [24]. The process is used in the production of ethanol or biogas from biomass. Lignin which is the binding agent in lignocellulosic biomass envelopes the cellulose to form a protective barrier and during fermentation the cellulose is transformed into sugars which are later used as a raw material for the production of ethanol and biogas [24].

1.7 Problems of Biomass as a Renewable Source of Energy

The potential of biomass for sustainable energy is widely recognised and many power stations have started retrofitting biomass burners into existing coal plants to meet their emission limits. Globally, biomass is considered to be one of the most promising renewable energy resources, with 3.7 million of TEP (total energy potential) coming from forests and 1.33 million of TEP per year coming from agricultural and urban wastes [29-31]. Despite the abundance of bioenergy resources in the form of wood, straw and waste, there are several problems associated with the utilisation of biomass. The supply chain cost of transportation and storage for biomass when compared to coal is higher as a result of the low energy density of biomass, which also reduces the thermal capacity in boilers when co-fired with coal [32]. Furthermore, the high content of moisture in biomass reduces the thermal efficiency for energy production. Also, in pulverized-fuel applications, the energy required for grinding of biomass, which is often required at the conversion chamber, is very high due to its tenacious and fibrous nature [33]. There are other risks associated with biomass storage, transportation and feeding. These include self-heating, off-gasing and dust explosions leading to various accidents, production loss, capital investments and even loss of life. Biomass ability to take up moisture from the environment during storage leads to deterioration and degradation. Self-heating is the term used to describe the reaction that initiates a spontaneous combustion. Long term storage of biomass can potentially lead to self-heating and explosion. Off-gasing occurs when emission of volatiles from biomass pellets along the supply chain is released into the environment. Emissions are released from volatiles (condensable gases such as ketones, aldehydes, low molecular carboxylic acids and terpenes) during high temperature drying and can potentially lead to further reactions during storage such as oxidation and hydrolysis. In addition to this, non-condensable gases such as carbon monoxide, carbon dioxide and methane are also released during storage. These gases are hazardous and can cause serious health problems if not well managed and controlled.

1.8 Biomass Pre-treatment Technologies

Many of the problems highlighted in Section 1.7 of this thesis can be solved using some pre-treatment processes. Prior to the utilization of biomass for energy conversion, the biomass feedstock is usually prepared in a way that favours the processes. This

method of preparation is called pre-treatment. Pre-treatment of biomass employs a number of scientific methods, which can alter the characteristics of the biomass or structure of the lignocellulose component of the biomass to increase its efficiency. There are a number of pre-treatment options that aim to tackle the problems associated with biomass utilization in order to increase the energy conversion efficiency. There is no general feedstock preparation (i.e. pre-treatment) that can be universally used at all production plants. Therefore, the choice of the pre-treatment to apply depends on the nature of the feedstock (softwoods, hardwoods, agricultural residues and herbaceous crops) being processed. Pre-treatments are commonly classified into four forms namely; mechanical, chemical, biological and thermal pre-treatment.

Mechanical pre-treatment involves reduction of the particle size of the biomass into smaller sizes. This includes chipping, milling, grinding and densification. The process is used in order to make feedstock handling, transportation and storage easier and to improve the energy efficiency.

Chemical pre-treatment is a form of pretreatment that is wholly initiated by chemical reactions to disrupt the biomass structure. Examples of chemical pre-treatment are (i) the use of mineral acids to breakdown lignin and hemicellulose in the biomass in order to access the cellulose, (ii) the use of calcium hydroxide (alkali) to force the breakdown of bonds that link hemicellulose to lignin.

An example of biological pre-treatment process is the use of enzymes from fungi, bacteria, and other microorganisms to break down the hemicellulose and lignin component of the biomass. Biological pre-treatment requires low energy, but needs longer residence since the rate of biological hydrolysis is generally very slow.

Thermal pre-treatment involves the use of heat within a temperature range to alter the properties of biomass before energy conversion e.g. drying, carbonization, hydrothermal carbonization (HTC) and torrefaction. Torrefaction is the topic of this research and is described extensively in Chapter 2.

1.9 Torrefaction

Torrefaction is a promising pre-treatment process that is currently receiving attention to solve many of the problems associated with biomass use. It has the potential to increase

the amount of biomass that could be fired in power plants [34-38]. It involves the use of relatively low temperature, ranging between 200 and 300^{o}C, in the absence of oxygen. The process causes the biomass to lose low molecular weight volatile compounds and gases due to the dehydration and decarboxylation reactions of the long polysaccharide chains [37]. About 70% of the initial biomass weight and about 90% of the original biomass energy is retained, resulting in energy densification [39, 40]. The properties of the solid product or torrefied wood changes and become more like low rank coal (lignite) in the Van Krevelen diagram, since biomass preferentially loses oxygen and hydrogen over carbon (this is shown in Chapter 5) [41].

According to the IEA [14], about 3.9 billion tons of world coal is being used annually to produce electricity (63% of annual world coal use). With increasing rules and regulations to use cleaner and renewable fuels in order to reduce GHG emissions and environmental concerns, torrefied fuels can be used to reduce the amount of coal being used for power generation. There has been a growing interest in the development of torrefaction plant around the world. There are few large scale units for torrefaction plants across the globe. For example, in 2011, Vattenfall (a power generating company) carried out large scale trials of co-firing 4300 tonnes of torrefied biomass with coal using different co-firing rates up to 50% in Reuter West coal-fired power plant, Berlin, while Topell, (Netherlands) produced 60,000 tonnes of the torrefied biomass used in the same power plant in 2012 [42]. Recently (on 6th March, 2014), in the US, Vega Biofuels and its partners, Agri-Tech Producers, LLC (ATP), entered into a joint venture agreement to build and operate a pilot torrefaction facility in South Carolina [43]. On the 25th of June, 2014, Vega Biofuels announced that they have received an order to ship 250,000 tons of torrefied fuels at a price of $230 per metric ton over the next five years to an European power company (ECEM Salzburg Energy and Environment Consulting, Austria) [43].

There are several processes that utilised torrefied biomass as feedstock other than cofiring the feedstock with coal. For example, torrefied fuels are can be used in entrained-flow gasification (EFG) and can also be used for pellet production. Figure 1-6 show a schematic description of a torrefaction plant and how the steam as well as the flue gas can be recycled in order to improve the plant efficiency.

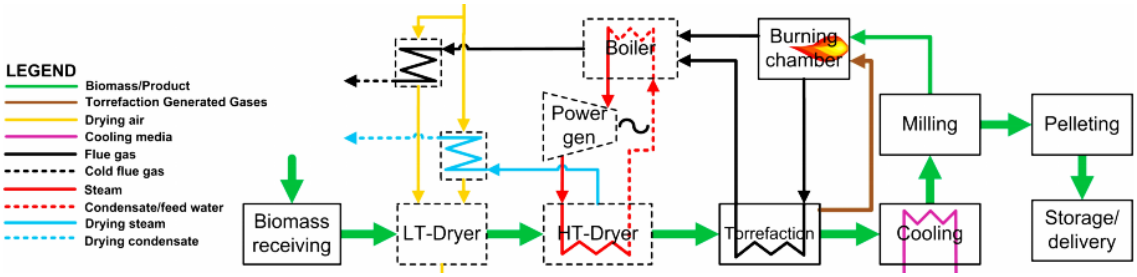

Figure 1-6: A schematic diagram of a torrefaction plant [44].

1.10 Project Overview

The potential of biomass for sustainable energy generation is increasing worldwide and biomass has assumed a pivotal role because it is considered to be "low carbon" and possesses infinite sustainability potential [45]. Globally, biomass is considered to be one of the most promising renewable energy resources and is seen as a feasible replacement for fossil fuels [46]. Recently, Nigeria joined other nations in the quest for harnessing biofuel potential by promoting and implementing the biofuels development and adoption programme. The Nigerian government set targets to ensure gradual transition from a fossil economy to one driven by an increasing share of renewable energy by 2020. It is expected that 75% of electricity generation in Nigeria will come from renewable energy by the end of 2025 [1].

Nigeria is blessed with a large amount of bioenergy resources and her forest industry for timber is well established. Wood residues from sawmills are under utilised. An estimate of 104 000 m^3 of forestry wastes is generated daily from logging and sizing operations [47]. The waste wood is currently being used for energy generation by large number of people in rural areas in Nigeria to meet their basic energy needs (coking, lighting and heating), but this is done in an inefficient way, with a negative impact on people's health as well as on the environment.

There are several problems associated with the use of biomass as a fuel and these drawbacks include low bulk densities, hydrophilic, heterogeneous and fibrous in nature. The supply chain cost of transportation and storage for biomass when compared to coal is higher as a result of the low energy density of biomass, which also reduces the thermal capacity in boilers when co-fired with coal [32]. Also, the high content of moisture in biomass reduces the thermal efficiency for energy production leading to poor combustion characteristics. In pulverized-fuel applications, the energy needed for

grinding of biomass is very high due to its tenacious and fibrous nature [33]. Furthermore, their ability to take up moisture leads to deterioration and degradation during storage. Torrefaction is an emerging and promising research area that is receiving attention to become a viable pretreatment technology to solve problems associated with biomass utilization in gasification and combustion applications [45].

This thesis evaluates the energy potential of Nigerian woods and a residue since there is very little information in the open literature concerning the fuel properties of these woods and energy crops. In particular, the benefits gained from torrefaction of these biomass will be investigated. In addition, an in-depth investigation into how raw and torrefied biomass fuels behave during pyrolysis and combustion are also covered. Finally, a comparison between the Nigerian and European biomass is also presented.

This research is partly funded by the EPSRC Energy Programme (Grant EP/H048839/1) and Niger Delta Development Commission (NDDC) overseas Scholarship Scheme. The Energy Programme is a Research Councils UK cross council initiative led by the Engineering and Physical Sciences Research Council (EPSRC) and contributed to by the Economic and Social Research Council (ESRC), National Environment Research Council (NERC), Biotechnology and Biological Sciences Research Council (BBSRC) and Science and Technology Facilities Council (STFC).

1.10.1 Group Project Aims and Objectives

The torrefaction project which involve collaboration between the bioenergy group of the University of Leeds and other interested parties such as Alstom Power Limited, have set objectives. Individuals are assigned either to carry out such objectives or to continue with the tasks that are yet to be completed from the project aims.

The group project aims are listed as follows:

- To study the feasibility of using coal milling technology for thermally pre-treated (torrefied) biomass.
- To give an initial assessment of the combustion properties of torrefied biomass.
- To develop and validate torrefaction model based on Functional Group Biomass (FG Biomass).

The group project objectives are:

- To prepare thermally treated biomass (torrefied fuel) from different size fractions.
- Characterisation of thermally treated fuels and to determine the extent of conversion in order to establish the maximum particle size that can be converted along with the operating conditions.
- To carry out a study on nitrogen partitioning in fuels.
- To characterise the treated material for the Hardgrove Grindability Index (HGI), density, and surface area.
- To produce and characterise the high heating rate chars of different size fractions obtained from a drop-tube furnace.
- To determine the reactivities of the chars from different size fractions obtained from the drop-tube furnace.

1.10.2 Research Aims and Objectives

This section outlines the aims and objectives that are set out for the development of this thesis.

The aims are:

1) To assess the energy potential of some of the biomass resources in Nigerian and see how they compare with European biomass.
2) To carry out torrefaction studies on some European and Nigerian biomass.
3) To study the effect of temperature, and residence time (torrefaction conditions) on the behaviour of biomass fuels when treated with torrefaction.
4) To examine the fate of nitrogen in the fuel during torrefaction as well as the behaviour of lignocellulosic component of the fuel upon torrefaction.
5) To investigate the products of torrefaction in terms of their composition, chemical and physical characteristics.
6) To understand the pyrolytic characteristics of thermally treated biomass.
7) To study the combustion behaviour of thermally treated biomass and also to assess the reactivities of the chars from torrefied fuels.

In order to achieve these aims, the following objectives are set:

a) To source and obtain some Nigerian woods and residue.

b) To characterise the untreated fuels using standard methods (proximate, ultimate, heating value, metals analysis, ash fusion tests), and compare these to some European biomass.
c) To determine the lignocellulose composition as well as the fouling and slagging indices for the untreated Nigerian fuels.
d) To characterise the untreated fuels using laboratory scale tests (TGA pyrolysis and combustion, grindability, pyrolysis-GC-MS, single particle combustion).
e) To prepare torrefied (thermally treated) fuels at low and high torrefaction conditions in order to determine the effect of increasing the severity of torrefaction on the biomass sample.
f) To determine the standard fuel characterisation of torrefied biomass fuels by carrying out proximate and ultimate analyses in order to determine their volatile, ash, moisture, fixed carbon, carbon, hydrogen, sulphur, oxygen and nitrogen contents. The calorific value, mass and energy yields, as well as the overall mass balance are also assessed using various analytical and laboratory methods.
g) To provide a relationship between the elemental composition of biomass fuels and energy yields with increase in severity of torrefaction.
h) To assess the behaviour of lignocellulosic component of the fuels upon torrefaction by monitoring the changes in the lignocellulosic fractions through analytical methods of determining ADL, ADF and NDF.
i) To show whether there is depletion or concentration of nitrogen during torrefaction by providing a mass balance for nitrogen and carbon in the fuel.
j) To examine the grindability behaviour of torrefied biomass fuels using the Hardgrove Grindability tests.
k) To determine a modified Hardgrove Grindability Index of torrefied biomass fuels in comparison to reference standard coals, as well as to provide their particle size distribution profiles in order to have a deeper understanding on their milling behaviour.
l) To identify the compounds, as well as the elemental compositions of the condensable fractions that are obtained during torrefaction using Pyrolysis GCMS and CHNS analysis.
m) To analyse the rate of decomposition of biomass fuels during torrefaction using TGA method.

n) To study the reactivity of torrefied fuels during pyrolysis using the peak maximum temperatures and kinetics data from TGA.

o) To determine the effect of temperature and residence time (torrefaction parameters) on the fuel reactivity.

p) To compare the fingerprint of the released volatiles during pyrolysis for the torrefied fuels to that of the raw fuels in order to see how torrefaction changes the volatile compositions using Pyrolysis GCMS analysis.

q) To carry out a comparison between the result obtained for determination of moisture, volatile and ash content using TGA analysis to those obtained using British standards procedures.

r) To carry out high heating rate combustion studies using single particle combustion test in order to simulate biomass (raw and torrefied fuels) combustion in a furnace.

s) To carried out low heating rate combustion studies of biomass under TGA in order to determine the ignition temperature and peak char combustion temperature.

t) To study the effects of temperature and residence time on the char reactivity of torrefied fuel.

u) To predict the rate of char combustion and kinetics parameters using data from TGA.

1.11 Thesis Outline

Chapter 1 This chapter briefly reviews the current world energy situation and the drivers for renewable energy globally. An overview of the Nigerian energy scene which includes the various renewable energy sources is also covered. In addition to this, biomass and some of the thermal conversion technologies are introduced in preparation for the next chapter.

Chapter 2 contains a literature review of the lignocellulosic component of biomass, thermal decomposition of biomass, torrefaction, pyrolysis and combustion characteristics of biomass.

Chapter 3 outlines the fuels analysed for these studies and the experimental methods employed for their analyses with the equipment used.

Chapter 4 presents results for characterisation of some Nigerian and European biomass for combustion and pyrolysis applications.

Chapter 5 presents an investigation into torrefaction and its effect on fuel properties. The organic composition of the tar fractions from the torrefaction process is also presented in this chapter.

Chapter 6 includes the results of studies on thermal decomposition of biomass (pyrolysis) and work related to thermal degradation kinetics.

Chapter 7 examines the effects of torrefaction on the combustion characteristic of biomass.

Chapter 8 presents the main conclusions for this research along with suggestions for further work.

CHAPTER 2. Literature Review

2.1 Characterisation of Biomass

The conversion efficiency of biomass to fuel or energy is dependent on its origin and the type of the biomass. Biomass are characterised by their physical and chemical properties and these properties have a strong influence on the thermal conversion of biomass to fuels and energy. The physical properties of biomass includes sizes, thermal conductivity, shapes, bulk density, specific heat capacity, grindability, and porosity while the chemical properties are characterised by ultimate and proximate analyses, inorganics, reaction rates and heating value. The ultimate analysis of biomass gives the elemental compositions of biomass in weight percentage and proximate analysis offers information about the percentage weight of moisture (M), volatile matter (VM), fixed carbon (FC), and ash that is present in the biomass. It is important to mention that the physical and chemical properties of biomass change with temperature during a period of time (residence time) in the boiler. Other chemical compositions that influence the conversion process of biomass are the lignocellulose component, lipids, proteins, simple sugars, starches etc. The differences in the chemical compositions are caused by various factors such as the growing conditions, species, type of plant tissue, and stage of growth [48].

2.2 Biomass Composition

Biomass is made up of lignocellulose (cellulose, hemicellulose and lignin), starch, triglycerides and other organic constituents such as resins and terpenes. However, from the listed components, lignocellulose is the most significant during biomass conversion to energy and fuels. It characterises the structure of plants according to two main sugar-based polymeric structures; cellulose and hemicellulose, and the phenolic polymer, lignin. The most abundant component found in plant is cellulose (40-50%), followed by hemicellulose (20-35%) and lignin (10-30%) [49]. Lignocellulose is the term used wholly to describe these three polymeric compositions of biomass and is mainly considered in most of the studies describing the decomposition mechanisms of woody and herbaceous biomass. It was suggested by Klass [24], that other compositions

(starch, triglycerides) and organic matters present in biomass are in relatively small quantities and therefore have little or negligible impact in any thermal reactions.

2.3 Cell Structure of Biomass (Lignocellulose)

In plant structures lignocellulose records the most dominant group of constituents on a mass basis. Its primary role is found in the cellular structure of plants and forms the establishment of cell walls and their mutual coherence. Lignocellulose offers mechanical strength and tenacity (toughness) to plant structures. A typical plant cell structured is show in Figure 2-1. The cell wall of a plant cell consists of primary and secondary cell walls. When one cell splits into two, a primary cell wall develops around each two new cells. The primary cell wall is laid down just outside the cell membrane, and is flexible, making way for the new cells to grow. This new cell wall is typically made of cellulose molecules, arranged into thin hair-like strands called microfibrils [24]. The microfibrils are structured in a meshwork pattern together with other components such as hemicellulose, glycans and pectins, link them together and help build up the cell wall [49, 50]. The secondary cell wall develops between the plasma membrane and the primary cell wall after the cell has finished growing. It is made by laying down successive layers of cellulose microfibrils and lignins. The second layer of the secondary wall which is the thickest is developed from vertically oriented macrofibrils. The macrofibril is from microfibrils, which mainly contain evenly oriented cellulose molecules of certain length [51]. The cellulose chains consist of unstructured but crystalline molecules connected together. The polymeric composition of the different walls and layers differs strongly and the tasks for each wall are different.

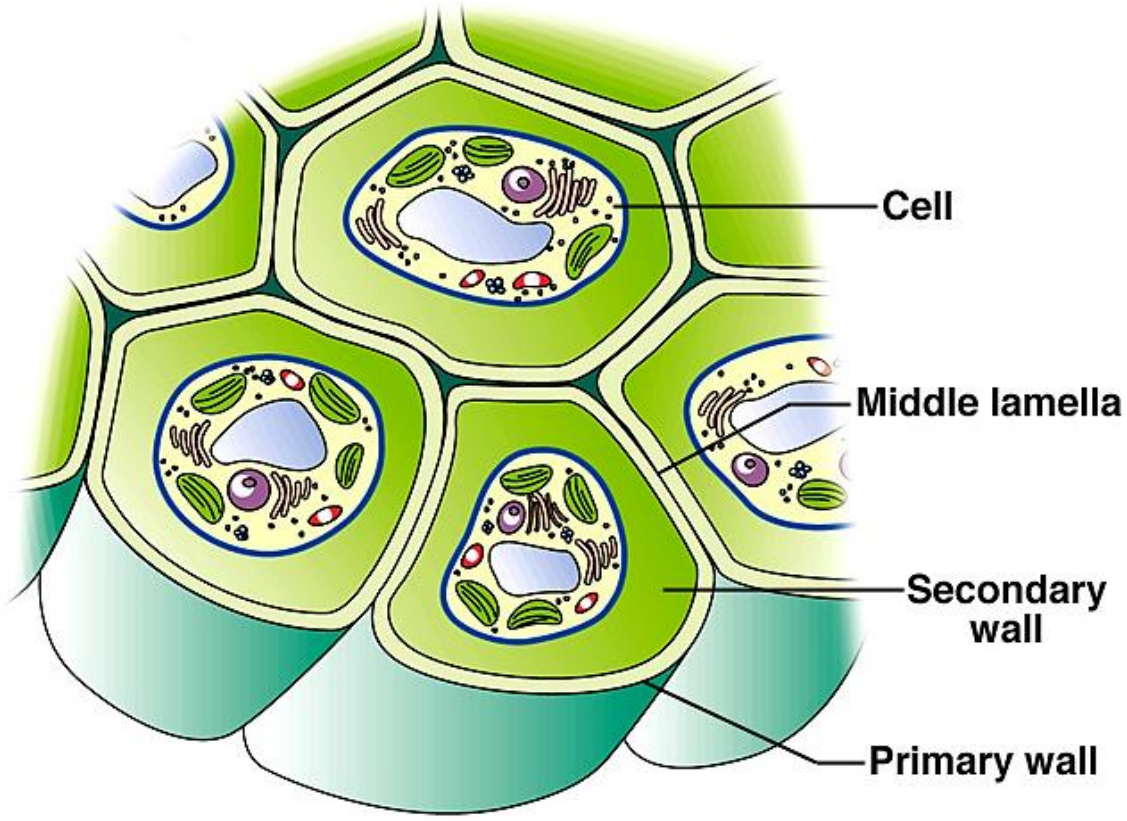

Figure 2-1: Typical plant cell structure [51].

Figure 2-2 depicts how the polymeric structure differs throughout the cell wall. The secondary cell wall is divided into three sub-layers i.e S1, S2 and S3 [52]. The three-layered secondary cell wall primarily consists of cellulose and is well structured by nature. The S2 layer is the thickest and contains macrofibrils comprised of the microfibrils of cellulose. The cellulose macrofibrils are embedded in a matrix of (disoriented) hemicellulose that bonds the macrofibrils structurally, through hydrogen bonding. The S1 and S3 layers contain hemicellulose and cellulose fibres positioned at right angles to the cell. The middle lamella is mainly lignin and acts as a binding agent, between the adjacent cells. The fraction of lignin decreases in the inward cell while the fraction of cellulose increases. The cell wall follows a repetitive pattern of hemicellulose binding the macrofibrils of a cell wall and lignin binding adjacent cells. The role of hemicellulose can be described as the role concrete plays in reinforcement [24]. Without concrete in reinforcement, iron rods lose their mutual coherence and orientation.

All the layers (three-layers) of the cell wall do not have same fibre orientation. The wood structure contains lots of these cellular units 'glued' together by the lignin-rich primary walls. The anisotropic and fibrous nature of wood is caused as a result of the differences in thickness and orientation of the different layers.

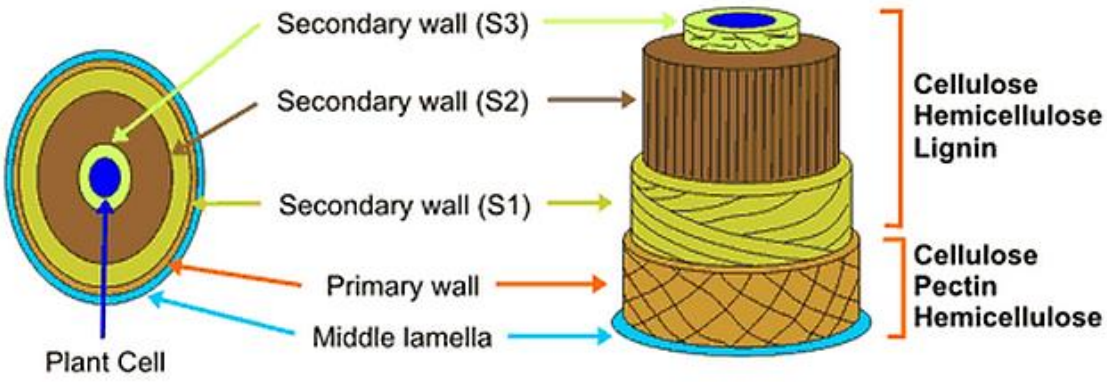

Figure 2-2: Distribution of lignocellulose within the three layered secondary wall [51].

2.3.1 Cellulose

Cellulose, is the major chemical component of fibre wall. It contributes about 40-50% of the wood's dry weight. Cellulose has high molecular weight and is the most abundant biopolymer. It is a homopolysaccharide, and is made up linear chains of D-glucose that are linked together by 1, 4 – glycosidic bonds without branches [49, 50]. Cellulose molecules are totally linear and they formed strong crystalline, fibrous structures resulting from the presence of hydrogen bonding which offer high thermal stability to the structure as illustrated in Figure 2-3.

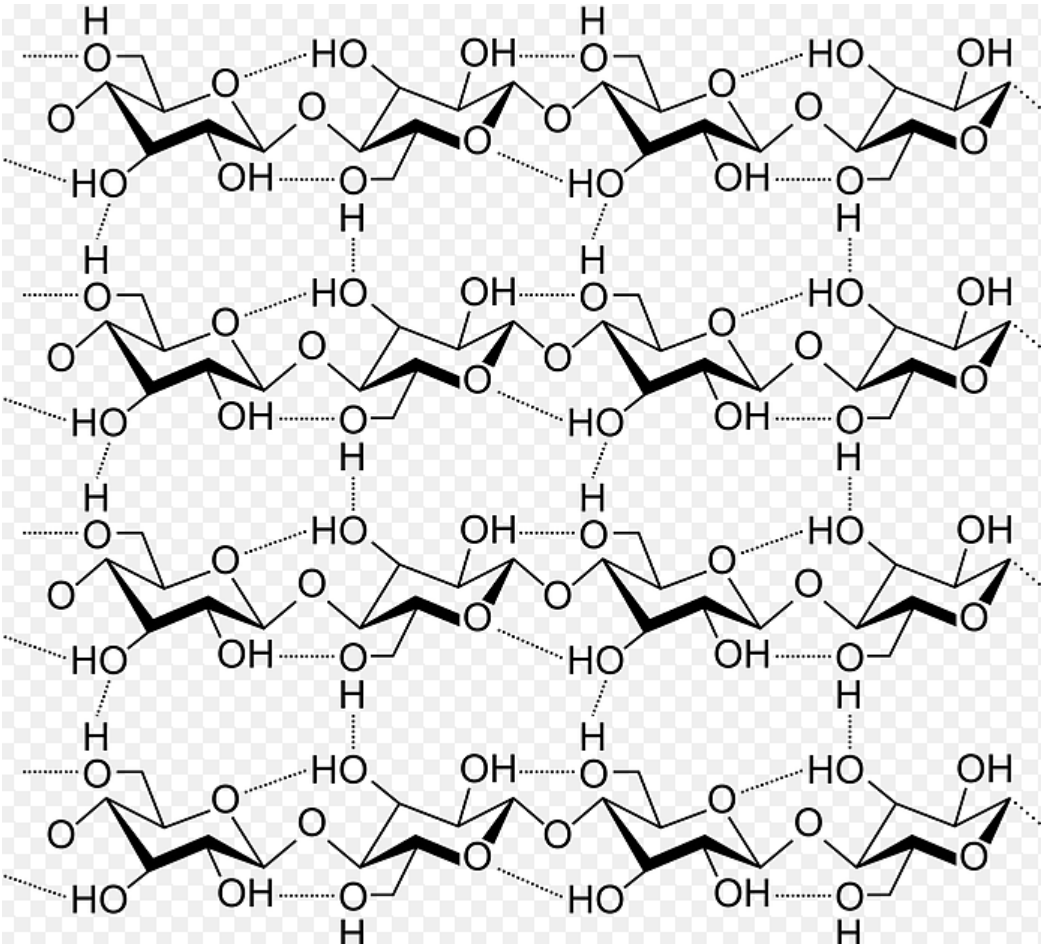

Figure 2-3: Structure of cellulose [53].

2.3.1 Hemicellulose

The word "hemicellulose" refers to the polysaccharide components of plant cell walls other than cellulose, or to polysaccharides in plant cell walls that are extractable by dilute alkaline solutions [54]. Hemicelluloses comprise almost one-third of the carbohydrates in woody plant tissue. It comprises various polymerized monosaccharides (e.g. glucose, mannose, galactose, xylose, arabinose, 4-O-methyl glucuronic acid and galacturonic acid residues). The chemical structure of hemicelluloses consists of long chains of variety of a pentoses, hexoses, and their corresponding uronic acids. The amount of hemicellulose in hardwood is higher compared to softwood [55]. The major hemicelluloses in softwoods are galactoglucomannans and arabinoglucuronoxylan, while glucuronoxylan is the predominant hemicelluloses in hardwood [55]. Hemicellulose accounts for 25 – 35 % of the dry wood mass [26].

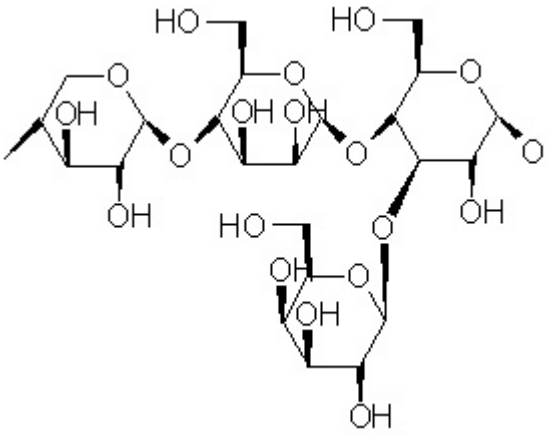

Figure 2-4: Illustrative chemical structure of hemicellulose [53].

2.3.2 Lignin

Lignins have high molecular weights, and polymers comprising phenylpropane units . Lignin is a polyphenolic cross – linked biopolymer, full of aromatic rings with various branches [49]. The chemical structure of lignin is complex and is based on three monomeric precursors namely; coniferyl alcohol, sinapyl alcohol, and p-coumaryl alcohol [56] as shown in Figure 2-5. Lignin acts as a primary binder for cellulose fibres. This organic substance binds the cells, fibres and vessels which constitute wood and the lignified elements of plants. It is the most abundant renewable carbon source on Earth after cellulose. Lignin performs three vital roles in plants that includes shielding of plants from pathogens and foraging animals, facilitating upward movement of water and minerals through the plant's vascular tissue and ensuring that plants grow upright as they compete for sunlight. Lignin also captures atmospheric carbon and thereby plays a vital role in the carbon cycle. In hardwoods, lignin is mostly made up of guaicyl- and syringylpropane units, while in softwoods, guaiacylpropane remain the main component of lignin[57-59]. It is difficult to define the precise structure of lignin as a chemical molecule as it shows a certain variation in their chemical composition [60]. Bridgeman *et al.*[61], mentioned that lignin is one of the most tenacious biological molecule and highly resistant to natural degradation.

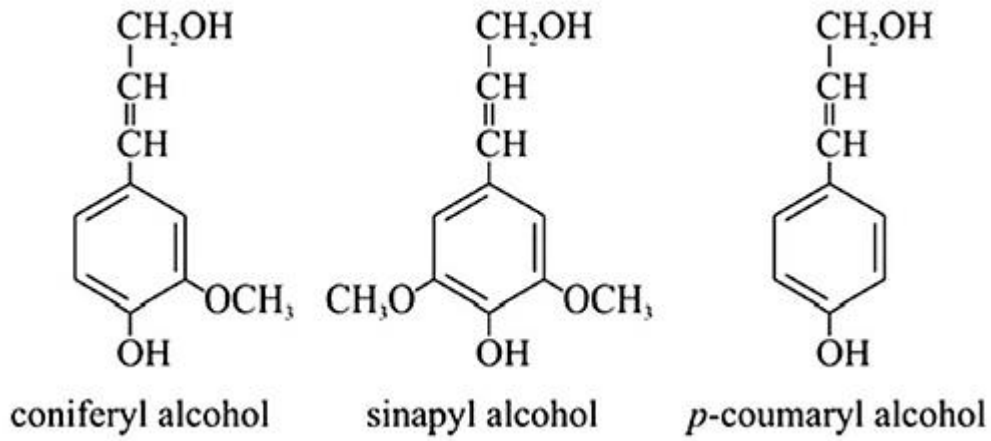

Figure 2-5: Chemical structures of main components of lignin[56].

2.4 The behaviour of lignocellulosic biomass to pyrolysis

The behavior of lignocellulosic materials primarily depends on its chemical composition and structure. The constituent polymers from lignocellulosic biomass react differently under pyrolysis conditions [49, 62]. During the pyrolysis of biomass, the main chemical components (hemicellulose, cellulose and lignin) undergo a series of transformations and the degree of crystallinity and polymerization of the starting materials are integral in defining their respective thermal degradation behaviour [54, 62-64]. A good understanding of how these constituents behave upon thermal treatment is vital for efficient conversion to fuel or energy.

In recent years, there has been an increasing interest in the behaviour of the lignocellulose components of biomass under pyrolytic conditions, in order to gain better understanding of the pyrolytic mechanism of the whole biomass system from the pyrolysis of individual components [54, 62, 64, 65]. From the morphological view of the plant cell-wall as discussed in Section 2.3, cellulose, hemicellulose and lignin comprise 40–50 wt. %, 20–35 wt.% and 10–30 wt.% of the plant material respectively, and would not function individually without the intrinsic interactions of the whole biomass system during pyrolysis [65, 66]. For example, hemicellulose, is the least stable and composed primarily of xylans and mannans but is considered to be cross-linked with cellulosic polymers, lignin and pectins, providing the structural support to the secondary cell wall in plant [67]. A common viewpoint shows that cellulose microfibrils

are coated with the hemicellulose in the primary cell wall of the plant, which hinders the flocculation of the cellulose microfibrils [62, 67].

In studies of decomposition behaviour of lignocellulose component, Gu *et al.*[68], investigated the thermal degradation of milkweed plant in a nitrogen atmosphere by using TGA-FTIR. They also studied the degradation of some commercial lignin, cellulose and different hemicelluloses. The comparison of the weight loss and the temperature of the maximum rate of weight loss, suggested a conclusion that hemicellulose is the least stable component in milkweed floss, while cellulose has a higher ignition and decomposition temperature, and that lignin starts to break down at a lower temperature than milkweed floss, but it degrades more slowly as the temperature rises [68]. The Fourier transform infrared (FTIR) spectra at 300^0C reported in their studies indicated that the main degradation products were H_2O and CO_2 and that the other organic volatile products were methanol, acetic acid and formic acid [68].

Yang *et al.*[49] indicated that the pyrolysis of the synthesized biomass samples containing two or three of the biomass components showed negligible interaction among the components. In their studies on the characteristics of hemicellulose, cellulose and lignin pyrolysis, firstly, they used a computational approach to predict the weight loss of a synthesized biomass from its composition in cellulose, hemicellulose and lignin, and then later predicted the proportions of the three components of a biomass experimentally. The results calculated by Yang *et al.*[49] in their studies for the weight loss of the synthesized biomass are comparable with the experimental results. Figure 2-6 shows the decomposition profiles of lignocellulose during pyrolysis with respect to mass and the rate of mass loss as reported by Yang *et al.*[49]. The figure indicates that hemicellulose begins to degrade at a temperature less than 200^0C and rapidly degrades from 220ºC to 315ºC. The rapid degradation of hemicellulose found during thermal analysis is because hemicellulose is made up of various saccharides such as xylose, mannose, glucose and galactose and has a less stable structure when compared to cellulose and lignin; hence becomes susceptible to break down easily [49]. Cellulose decomposition is also observed from this figure. This is evident with a significant mass loss and faster rate of decomposition than hemicellulose decomposition at temperatures

between 315-400ºC. The temperatures for cellulose degradation is higher because cellulose is made up of long polymer chains of glucose without branches, which gives it a very strong and stable structure and thus decomposes at higher temperatures than hemicellulose [49, 62]. Lignin which functions as a binding agent for the cellulose and hemicellulose fibres [49, 60, 62, 65, 69] is the most difficult to breakdown. It is made up of aromatic rings with various branches and cross-linkages which degrade slowly over a very wide range temperature range 150-900°C [49].

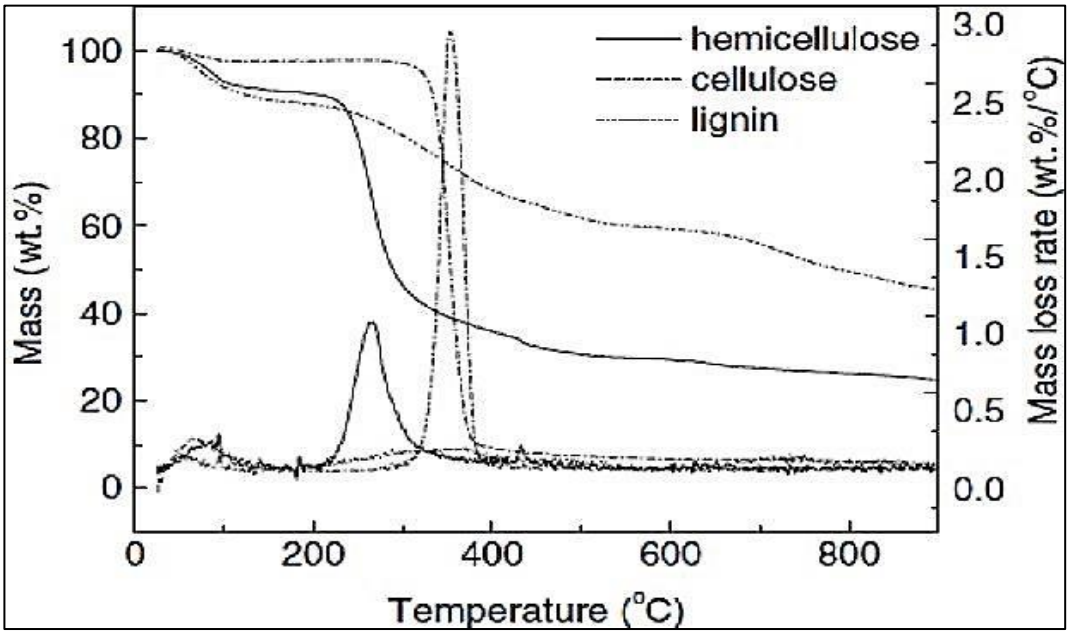

Figure 2-6: Profiles of mass losses and rates of mass loss for thermal decomposition of hemicellulose, cellulose and lignin under thermogravimetric analyser [49].

Yang *et al.*[49] also studied the decomposition products during pyrolysis i.e. volatile organic compounds and the main gaseous product. It was found that the main products are carbon dioxide, carbon monoxide, and methane and some organics (a mixture of acids, aldehydes, alkanes and ethers). These gases were observed to be released primarily at low temperatures from the decomposition of hemicellulose and to a lesser extent, cellulose [49].

A similar study was conducted by Stefanidis *et al.*[65], in order to understand the behaviour and decomposition pathways of cellulose, hemicellulose and lignin during pyrolysis. They carried out thermogravimetric analyses, along with thermal and catalytic fast pyrolysis experiments for cellulose, hemicellulose, lignin, and their mixtures in order to investigate their pyrolysis products and also to know whether the prediction of the pyrolysis behaviour of a certain lignocellulosic biomass feedstock is feasible, when its content in these three constituents is known.

Figure 2-7 shows the decomposition profiles (weight loss and derivative weight loss curves) of cellulose, xylan and lignin samples during pyrolysis as reported by Stefanidis *et al.*[65]. From this figure, it was observed that cellulose degradation occurred over a narrow temperature range, between 280 °C and 360 °C. They observed the highest rate of decomposition of cellulose at 339 °C and that the percentage of cellulose left at 500 °C and 800 °C is 10.7 and 7.4 wt.% respectively. It was established from their studies that the wide range of decomposition temperatures found during pyrolysis of cellulose is due to cellulose's very homogeneous unbranched crystalline structure of linked D-glucose units [65]. Xylan, a polysaccharide was observed to break down at a slower and wider temperature between 200 °C and 320 °C with two distinct peaks; one at 246 °C and one at 295 °C [65]. The lower decomposition temperature range of xylan is attributed its structure, which is amorphous with many branched units that have low activation energy[49]. The xylan residue at the two reference temperatures i.e. 500 °C and 800 °C was reported to be significantly higher than that of cellulose, presenting approximate values of 30 and 25 wt.% respectively. It was reported that the high residue found after the pyrolysis of xylan is partly due to the high ash content found in the commercial sample (xylan) that was used. The ash content of xylan, and lignin that was reported in their study on a dry basis, was 6.36 and 2.28 wt.% respectively and there was no ash found in cellulose. According to Patwardhan *et al.*[70], the higher solid residue left at the end of xylan pyrolysis (despite using an ash-free sample in their studies on product distribution from the fast pyrolysis of hemicelluloses extracted and purified from switchgrass) is due to the sugar differences in xylan's composition (pentoses and hexoses), which causes pyrolysis to progress through a different mechanism from that of cellulose, thus resulting into higher solid residue formation

[70]. Also from Figure 2-7, it was observed that lignin breaks down over a very wide temperature range, from 140 °C to 600 °C, with a very low-intensity peak around 380 °C [65]. The lignin residue at the two reference temperatures of 500 °C and 800 °C was about 53.4 wt.% and 41.2 wt.% respectively [65]. The high levels of residue left after pyrolysis of lignin is due to the complexity in the structure of lignin. It is made up of a complex network of cross-linked aromatic molecules which are difficult to break down and therefore have high thermal stability [49, 71].

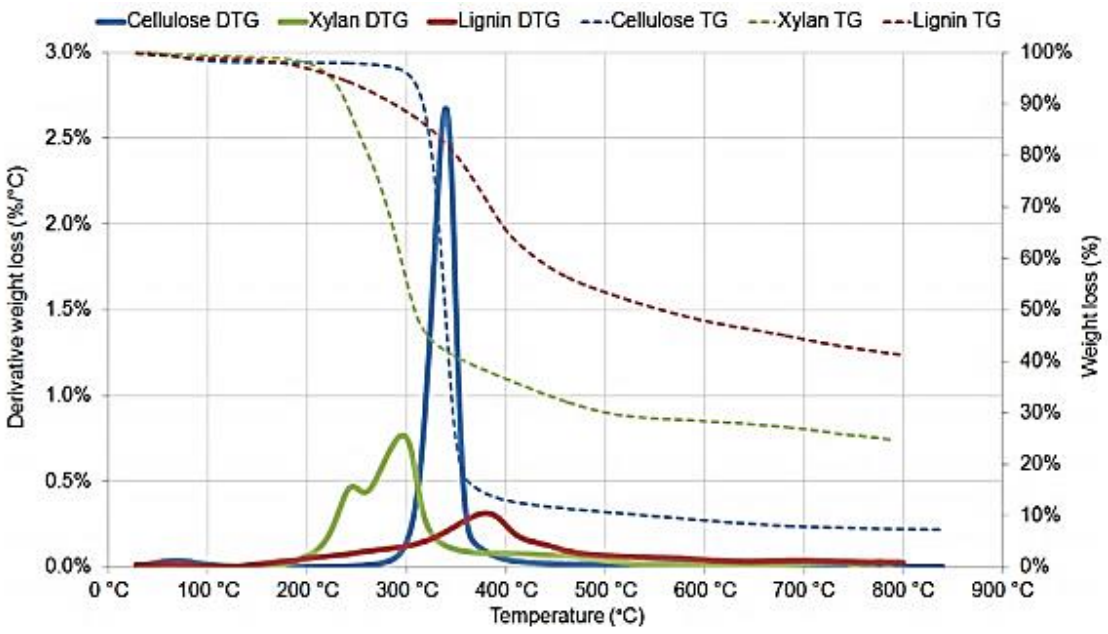

Figure 2-7: Weight loss and derivative weight loss curves for cellulose, xylan and lignin samples [65].

Furthermore, the presence of metals particularly potassium in biomass also affects the behaviour and the decomposition pathway of the lignocellulosic component of the fuel [48, 72-76].

Nowakowski and Jones [72], investigated the influence of potassium on the pyrolysis behaviour of cell-wall components under TGA. Hydrochloric acid was used as a treatment to remove salts and metals from the cellulose and lignin samples. The demineralised samples, as well as untreated xylan, levoglucosan, and chlorogenic acid were impregnated with potassium. The untreated samples, alongside the demineralised samples and the potassium impregnated samples were characterised under TGA. They

found that potassium catalysed the pyrolysis of the cell wall components and also impacted the char formation stage by increasing the char yields considerably. The peak maximum temperature of pyrolysis was reported to shift to lower temperature, and the char yield increases.

Nowakowski *et al.*[75], carried out further studies on potassium catalysis in the pyrolysis behaviour of short rotation willow coppice and a synthetic biomass i.e. a mixture of the main biomass components (cellulose, hemicellulose and lignin) in order to understand the effect of potassium on decomposition of biomass. In their studies, hydrochloric acid was used to remove salts and metals from the willow sample in order to obtain a demineralised sample. The demineralised sample was impregnated with potassium. They applied the same type of treatment to the synthetic biomass for comparative studies. The samples were then pyrolysed in a purge of nitrogen under TGA and the DTG profiles are reported in Figure 2-8. From Figure 2-8a, the DTG profile of raw willow sample presented two main unresolved peaks which denote the decomposition of hemicellulose and the initial stage of degradation of cellulose (peak between 230°C and 350°C, with the peak temperature at 333°C), while the second step is the degradation of lignin and the final degradation of cellulose (peak between 350°C and 430°C, with the peak temperature at 374°C). The DTG pyrolysis profile of demineralised willow (Figure 2-8a) showed that the hemicellulose peak is weak compare to that of raw willow, indicating some change in the hemicellulose content. The second main peak shifted to slightly higher temperature, and is as a result of the removal of some catalytic metals through acid washing. Also, the DTG pyrolysis profile of willow impregnated with potassium showed two clearly resolved peaks with lower peak maxima at 233°C and 313°C indicating a strong catalytic effect.

Figure 2-8(b) shows the DTG pyrolysis profiles of the raw and treated biomass cell-wall components samples. The figure showed a similar thermal decomposition profile to that of willow and can be used to describe the thermal decomposition characteristics of willow. DTG analysis indicated a two-step thermal degradation with the first step for both raw and HCl treated synthetic biomass samples, occuring at 300–350°C represent the decomposition of hemicellulose and the initial stage of degradation of cellulose,

while the second step at 350-425°C shows the degradation of lignin and the final degradation of cellulose respectively.

Nowakowski *et al.*[75], found that the catalytic effect on the degradation is greater for the willow than for synthetic biomass. Figure 2-8 showed that the peak of cellulose decomposition shifted from 374°C to 333°C for the synthetic biomass, and from 374°C to 313°C for the willow sample upon impregnated with potassium [75].

In the same studies, Nowakowski *et al.*[75] further quantified the yields for TGA pyrolysis of willow samples and synthetic biomass samples and the data are presented in Table 2-1. Form this table, it is observed that both samples with the HCl treatment gave more volatile yield and less char yield than their raw counterparts resulting from the removal of inorganic constituents that favours char formation [75]. Demineralised willow recorded the lowest char yield (yield decreased by 54% when compare to that of raw willow). They reported that the effect of demineralisation is more significant on willow compare to synthetic biomass since there is higher metal content in the fuel than the synthetic biomass [75]. They found out that potassium produced more effect on the char formation stage resulting into higher char yield, especially in the synthetic biomass as shown in Table 2-1. Generally, Nowakowski *et al.*[75] studies showed that potassium catalyses pyrolysis and the effect can be observed by a decrease in the peak maximum temperature in the DTG plots of willow and synthetic biomass samples (Figure 2-8).

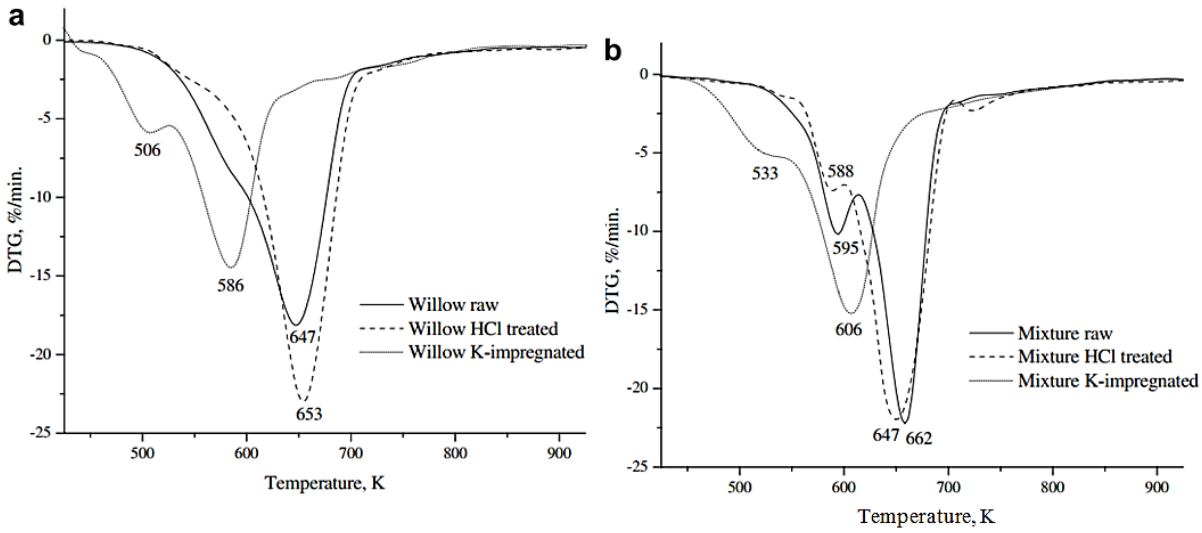

Figure 2-8: DTG pyrolysis profile for: a) willow and b) synthetic biomass samples [75].

Table 2-1: Pyrolysis yields for pyrolysis of willow and synthetic biomass samples [75].

Sample	Pyrolysis yields (%)	
	Volatiles	Char
Willow raw	87.7	12.3
Willow HCl treated	93.3	6.7
Willow K-impregnated	80.2	19.8
Mixture raw	81.7	18.3
Mixture HCl treated	83.1	16.9
Mixture K-impregnated	68.7	31.3

In the second part of Stefanidis *et al.*[65] studies, they examined to see if there are any synergistic effects between the lignocellulose components of biomass during pyrolysis. They carried out pyrolysis studies on two mechanically mixed samples called Mixture 1 and 2. “Mixture 1” contained ½ cellulose and ½ xylan , while the other sample “Mixture 2” contained ⅓ cellulose, ⅓ xylan and ⅓ lignin [65]. TG analysis was done for both mixed samples at the same conditions as the separate biomass components and the experimental TG and DTG curves were compared to calculated curves [65].

Figures 2-9 & 2-10 shows the experimental and calculated weight loss and derivative weight loss curves for Mixture 1 and 2 respectively [65]. From Figure 2-9, it can be

observed that the experimental and calculated weight loss curves agreed quite well for Mixture 1, but there were noticeable differences in the derivative weight loss curves. The xylan peaks, that were calculated at 247 °C and 302 °C, appeared as expected, with only a slight drop in intensity, but the cellulose peak is wider, had significantly lower intensity and shifted to a slightly higher temperature (349 °C instead of 339 °C) [65]. Figure 2-10 also shows that the experimental and calculated weight loss curves for Mixture 2 agreed quite well, but there were differences between the experimental and the calculated derivative weight loss curves. The experimental cellulose peak in Mixture 2 was wider than that calculated. The drop in the intensity and the shift in the temperature of the cellulose peak (the peak was expected at 339 °C but it turned out at 353 °C) were more noticeable in Mixture 2 [65]. Also, there was no visible lignin peak in the experimental derivative weight loss curve of Mixture 2, due to its low intensity and the overlapping cellulose peak[65]. Generally, the maximum weight loss rate of cellulose decreased considerably and shifted to a higher temperature in both mixed samples. Stefanidis *et al.*[65] reported that these observations show a limitation in the heat transfer from the heated plate of the TG instrument towards the cellulose particles, which appeared to decompose at higher temperatures and over a wider range due to the possible difference between the temperature that was recorded by the TG instrument and the actual temperature of the mixed biomass sample (that was in fact lower). The hemicellulose particles, which break down at lower temperatures, formed a charred film that wrapped around the cellulose particles and acted as a heat barrier [65]. Stefanidis *et al.*[65] concluded that the differences between the calculated and experimental DTG curves were due to the limitations of heat and mass transfer in the biomass mixtures.

Wang *et al.*[77] and Hosoya *et al.*[78] also reported the same observations about the charred hemicellulose forming around cellulose particles and suggested that it could limit mass transfer during the volatilization of the cellulose particles.

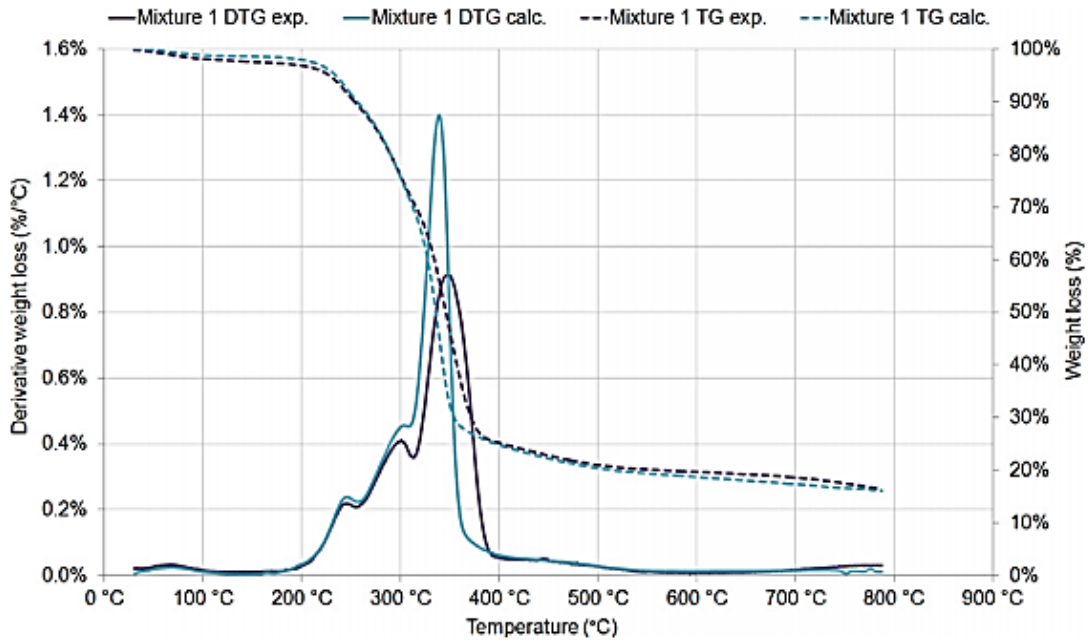

Figure 2-9: Experimental and calculated weight loss and derivative weight loss curves for Mixture 1[65].

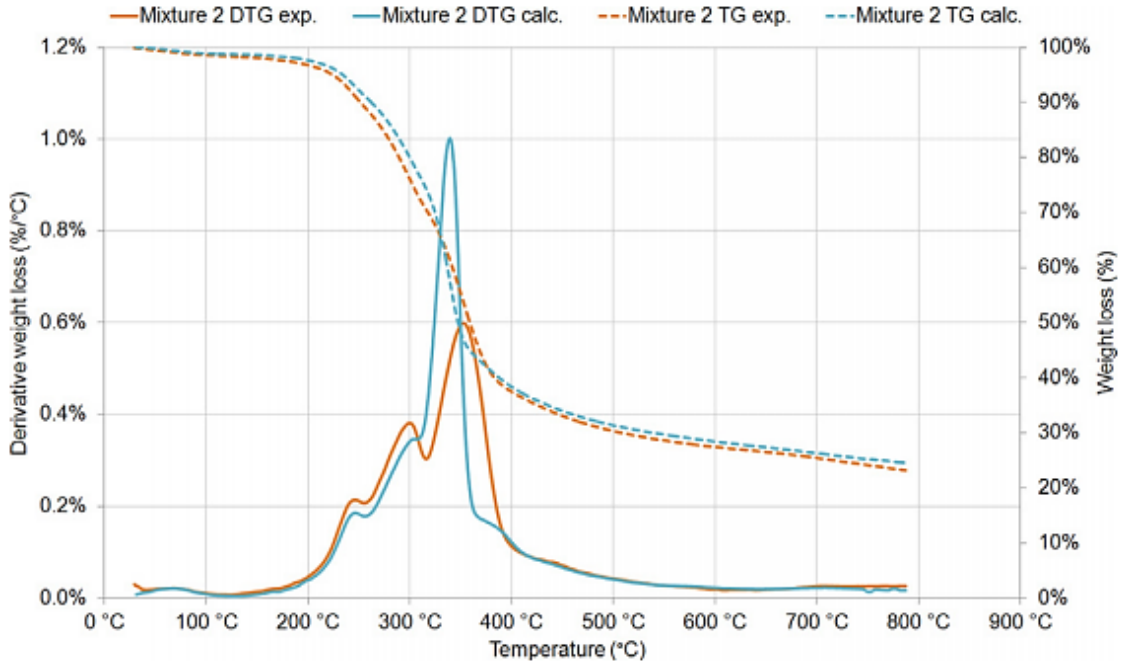

Figure 2-10: Experimental and calculated weight loss and derivative weight loss curves for Mixture 2 [65].

Shen *et al.*[62] concluded that the interactions among the chemical components of lignocellulosic biomass under pyrolytic conditions occur, and that the interactions among the components should be significantly investigated in order to have a better understanding of the pyrolysis of the biomass system. They mentioned that a good understanding of the intrinsic interaction mechanism between lignocellulose components in biomass is required to predict the pyrolytic behaviour of biomass and also to maximise the conversion process [62].

2.5 Kinetics of the Thermal Decomposition of Biomass

Thermal decomposition of biomass is highly complex in which several reactions occur simultaneously due to the heterogeneous nature of biomass composition. The biomass constituents i.e. hemicelluloses, cellulose and lignin, as mentioned earlier decompose at a range of temperatures and rates which makes the process complex. Furthermore, transport processes, such as inter- or intra-particle heat and mass transfer, could also affect the degrading process, and the exclusion of these phenomena would limit the prediction of thermolytic behavior and kinetic parameters[63].

There are many studies on pyrolysis of biomass under controlled heating rate (non-isothermal) conditions and isothermal (steady-state) conditions [62]. The advantage of determining kinetic parameters under non-isothermal conditions is that only a single sample is required to calculate the kinetics over an entire temperature range in a continuous manner and it has been established that multiple heating rates should be selected to improve the accuracy of the non-isothermal method [62].

Different kinetics are expected for different biomass, since the composition of lignin is not the same for hardwood and softwood [79-82], and the contents of catalytic metals, particularly potassium, differ[37]. Understanding of the kinetics of thermal decomposition of torrefied fuel is also vital in the modeling of both its combustion processes and reactor kinetics. The rate of release, quantity, and composition of the volatiles influence flame ignition, stability, and the temperature profile in the radiant part of the furnace [83]. Therefore, these elements are significant in reactor design in pulverized fuel power stations, where they impact on NO_x reduction mechanisms.

Similarly, in fast pyrolysis the relative rates of decomposition, cracking, and repolymerization/condensation reactions affect the quantity and quality of bio-oil produced as well as the thermal stability [83].

Several studies found in the literature used different approaches but simplified models to derive the kinetics parameters and the rate of decomposition; all of these models are based on the decomposition of the three lignocellulose constituent of biomass. Most models looked into kinetics of cellulose degradation since cellulose accounted for about 50% of biomass composition by weight. Van der Stelt [41] reported that the first model on kinetics of biomass decomposition was developed in 1960s by Broido to model the reaction involved in cellulose pyrolysis. The Broido method suggested that the decomposition of cellulose can be represented through two competing reactions as shown in Figure 2-11 [62]. The first step is vital at low temperatures, usually below 280^0C and slow heating rates, resulting into formation of anhydrocellulose. This reaction becomes more endothermic leading to formation of tars at about 280^0C. The third steps is an exothermic decomposition of anhydrocellulose to form char and gas.

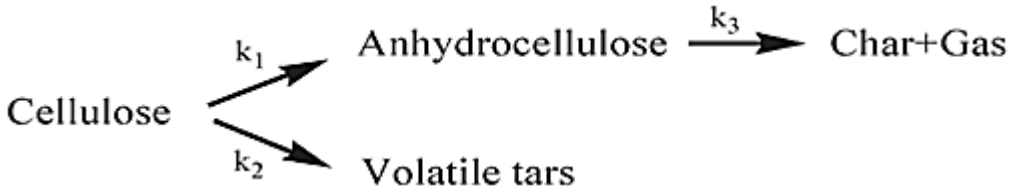

Figure 2-11: The kinetic model for cellulose pyrolysis proposed by Broido [62].

Shafizadeh[64] carried out a kinetic study of cellulose pyrolysis in 1979 and from this study, a chemical reaction model known as Broido-Shafizadeh model[84] for cellulose decomposition, as displayed in Figure 2-12 was proposed by Bradbury *et al*.[85]. This model used transitional steps to describe the pyrolysis kinetics of cellulose into intermediate (active cellulose) and final products (volatile tar, char and gas). The first step is characterised by an accelerating rate of weight loss which led to formation of ‘‘active cellulose’’ through the depolymerization reaction at low temperatures between 259 to 295°C [62]. The ‘‘active cellulose’’ then undergoes the two competitive

reactions to produce either char and gas or primary volatiles [62]. It is important to mention that Shafizadeh [64] didn't observe the accelerating rate of weight loss at high temperatures (above 295°C) in his studies and therefore, cellulose degradation process was said to follow two competitive first-order reactions, leading to formation of char voliatiles and formation of char and gas, thereby eliminating the formation of ''active cellulose''.

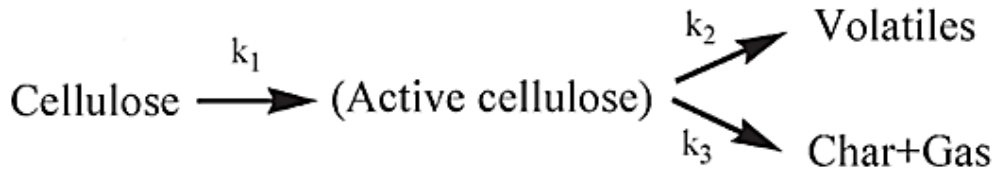

Figure 2-12: The kinetic model for cellulose pyrolysis proposed by Bradbury et al[85].

Figure 2-13 shows the model developed by Koufopanos *et al.*[86], to describe the pyrolysis of biomass. The kinetic scheme of the reaction is similar to the mechanism proposed by Shafizadeh (1979, 1982) for the pyrolysis of cellulose [86]. The model stipulates an initial reaction (k_1) which explains the overall results of the reactions prevailing at lower pyrolysis temperatures (below 200°C), leading to the transformation and modification of the biomass. This step is assumed to be of zero-order and is not associated with any weight-loss. Koufopanos *et al.*[86] then observed a weight loss at lower temperatures (200-250°C) which becomes significant compared to that observed at higher temperatures only for very long exposure times. However, the operating conditions in practice use high temperatures and rather short pyrolysis times, hence; they suggested the first step (intermediate) in the model to occur without associating it to any weight loss. The intermediate formed then degrades through two competitive reactions, i.e. to form volatile/ gaseous products (k_2) and to char (k_3). It was assumed that the three reactions follow the Arrhenius law[86].

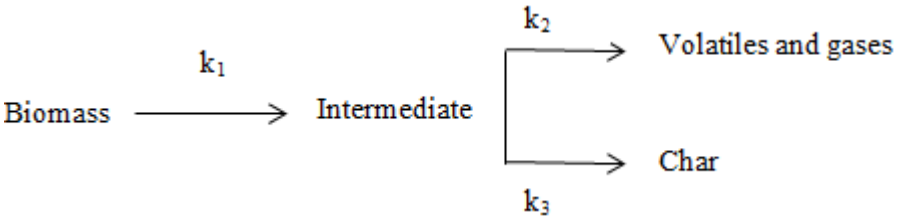

Figure 2-13: The kinetic model for cellulose pyrolysis proposed by Koufopanos *et al.*[86].

The studies on kinetics and models described in the literature were summarised by four different mechanisms by Prins *et al.*[87] and are shown in Figure 2-14. The mechanisms differ in number of intermediate steps and associating reactions, as well as the reaction constants (k_1, k_2, k_3, etc.).

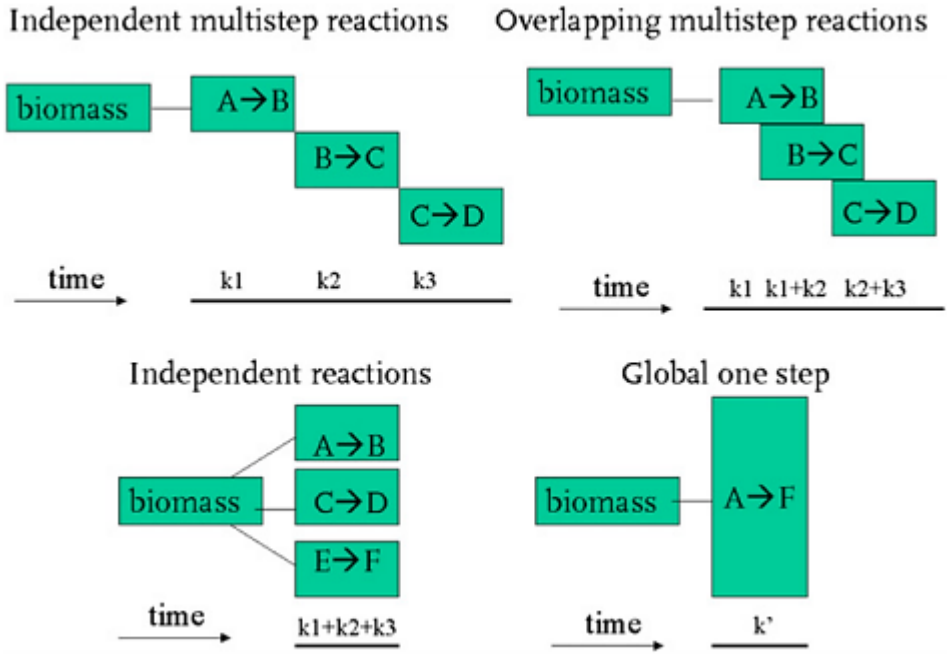

Figure 2-14: Kinetics models for biomass decomposition [87].

For emphasis, it is important to re-iterate that during the torrefaction process, mass loss mostly comes from the decomposition (devolatilisation) of hemicellulose and partly lignin. Generally, much of the available literature on kinetics and models deals with pyrolysis temperature range above 300°C during investigations on biomass decomposition.

Di Blasi and Lanzetta [88] investigated the decomposition of xylan at temperatures between 200-340°C in order to assess the isothermal rate kinetics. They modelled that decomposition via a two-step mechanism; the first step considered are the depolymerisation reactions which involve the rapid release of volatile and formation of a solid residue. The reaction progresses at a slower rate in the second step which leads to formation of chars, and more volatiles are also released.

Prins *et al.*[89] created a kinetic model for the torrefaction of willow using the two steps decomposition mechanism that was proposed by Di Blasi and Lanzetta [88]. The model is illustrated in Figure 2-15. Di Blasi and Lanzetta [88] described the rate kinetics using a combination of two-step decomposition mechanism with parallel reactions for the formations of solids and volatiles, where A is the hemicellulose decomposition, B is the intermediate product that has a reduced degree of depolymerisation (cellulose decomposition) and C is the torrefied sample. k_1, k_2, k_{v1} and k_{v2} are the four Arrhenius kinetic parameters that were used to determine the mass loss data experimentally[90].

A study was conducted by Prins *et al.*[89] to determine whether the weight loss kinetics for torrefaction of biomass follows the reaction pathways (two- step decomposition mechanism) that was proposed by Di Blasi and Lanzetta [88].

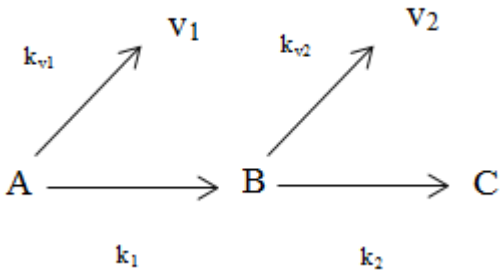

Figure 2-15: Two stage biomass decomposition mechanism by Di Blasi and Lanzetta [88].

They indicated that the char yields and kinetics parameters obtained for biomass would vary. Consequently, the reaction rates and char yields of the first and second step for

willow were compared to those for xylan that was previously studied in Di Blasi and Lanzetta [88] and they discovered that the first reaction step is faster (A to B + V_1) than the second step (B to C + V_2).

Figure 2-16 presents the modelling of the mass loss of willow which reveals that the first step was completed within 15-60 min and produced a mass loss of 16-30% at temperatures between 250-300°C, while the second step took longer time to complete and caused mass loss between 42-48%. Prins *et al.*[89] interpreted the initial mass loss recorded at the first stage resulting from hemicellulose decomposition, while the second stage is from decomposition of both cellulose and small fraction of lignin, as well as charring of the remaining hemicellulose at higher temperatures.

Figure 2-17 reveals the predicted char yields are comparable to the experimental data [89]. willow is observed to have a slower first reaction, as a result of its lower hemicellulose content than the xylan. The higher weight loss recorded in the second reaction is probably due to the decomposition of other reactions, including cellulose. The model was also examined for higher heating rates up to 100°C min^{-1} and the pattern of weight loss corresponded with the experimental results. They concluded that thermal pre-treatment should be carried out at a temperature below 300°C for the torrefaction process. This is because; at above 300-320°C, the reaction will become exothermic and causes fast thermal cracking of cellulose to produces tar.

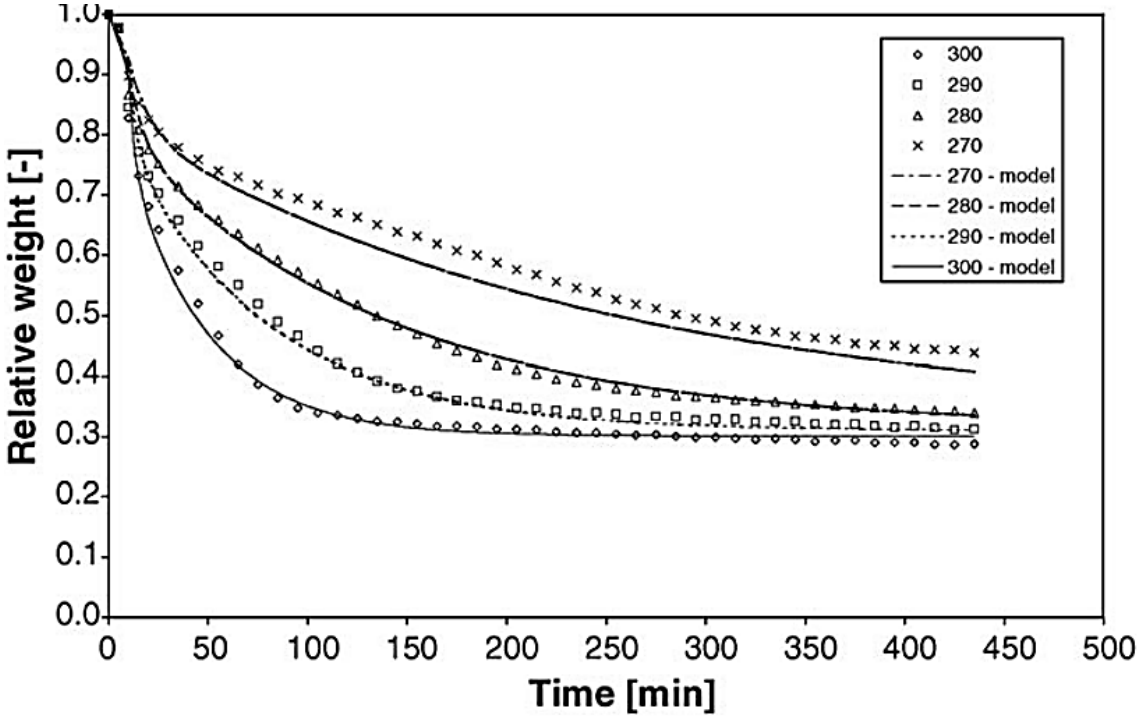

Figure 2-16: Correlation of experimental and modelled relative weight of willow upon torrefaction at 270°C, 280°C, 290°C and 300°C with a heating rate of 10°C min-1[89].

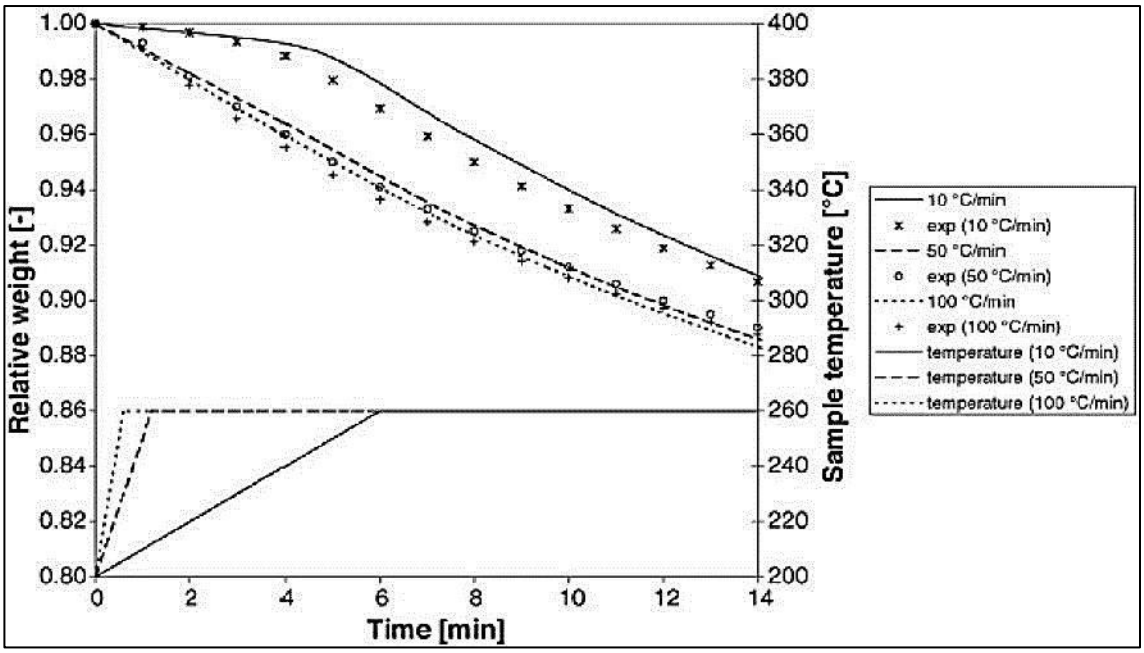

Figure 2-17: Correlation of experimental and modelled relative weight of willow upon torrefaction at 260°C with various heating rate of 10, 50 and 100°C min-1 [89].

2.5.1 Acquiring Kinetic Parameters from Experimental TGA Data.

Thermogravimetric analysis (TGA) is the most commonly applied thermal analytical technique in solid-phase thermal decomposition studies and is widely used to study the thermal behaviour of biomass by measuring the decrease in substrate mass caused by the release of volatiles, or devolatilisation, during thermal decomposition [82]. In TGA, the mass of a sample is heated at a certain rate and is recorded as a function of temperature or time. The rate of mass loss (derivative thermogravimetry DTG) is obtained by taking the first derivative of such thermogravimetric curves (TG) i.e. $-\mathrm{d}m/\mathrm{d}t$ curves. The development of a system in 1899 by Sir William Roberts-Austen that uses thermocouples to measure the temperature difference between a sample and an adjacent inert reference material subjected to an identical temperature alteration marked the discovery of differential thermal analysis (DTG) [82]. This technique is used to determine the rate of the pyrolysis and the rate of the char oxidation with a postulation that both reactions follow the Arrhenius law. In most cases, the reaction order n, is assumed to be equal to one and other parameters like the pre-exponential factor A and the apparent activation energy E are determined.

Saddawi *et al.*[83] studied kinetics of the thermal decomposition of willow using the four different mathematical methods available for extraction of the kinetic parameters. They carried out an investigation of the method of data analysis that is appropriate for extracting reliable kinetic data from TGA experiments and also conducted a review of previously published work on biomass and its polymeric components in order to ascertain the variation in kinetics, reasons for differences, and extrapolation to flame temperatures. They assessed the kinetic parameters for pyrolysis of willow using four different methods; the reaction rate constant method, temperature integral approximation by Murray and White, temperature integral approximation by Doyle and temperature integral approximation by Senum and Yang [82, 83, 91, 92]. The authors reported that out of the four methods studied, the Senum and Yang, Murray and White, and the reaction rate constant method are the methods that yielded kinetics which

represent the initial pyrolysis of willow more accurately, but which suggest a low activation energy is appropriate (less than 80 kJ/mol in this case). They concluded that the Senum-Yang approach, the Murray and White, and also the reaction rate constant method present apparent first-order kinetics with excellent predictions under conditions of low heating rate.

The reaction rate constant method is of interest since it is one of the three recommended by Saddawi *et al.*[83] for extracting kinetics data under conditions of low heating rate. It involves the assumption of a global first-order reaction and using the initial decomposition in the weight loss curve to assess the A and Ea from the TGA. This method was used by Saddawi *et al.*[46], in their studies on the effects of mineral content on torrefied fuel characteristics, to derive the activation energies of willow, eucalyptus, miscanthus and wheat straw torrefied at 290^{o}C for 60 minutes which gave values of 130kJ/mol, 141kJ/mol, 151kJ/mol and 90.4kJ/mol with pre-exponential factors, 19.4s^{-1}, 21.9s^{-1}, 23.6s^{-1} and 11.8s^{-1} respectively.

This method is assumed to follow Arrhenius function as seen in Equation 2.1:

$$k = A\ exp\left(-{Ea}/{RT}\right) \qquad \text{Equation 2-1.}$$

where k is the reaction rate constant, A is the pre-exponential factor (s^{-1}), Ea is the activation energy (KJ/mol), R is the gas constant (8.314J/mol K), and T is the temperature (K).

If the weight loss with time curve is assumed to be the result of one or more first-order reactions, then each reaction can be described by Equation 2.2:

$$kt = -\frac{1}{(m-m\infty)}\frac{dm}{dt} \qquad \text{Equation 2-2.}$$

Where *dm/dt is the* gradient of the tangent of the weight loss curve at time, *t , m is the* mass at time, *t*

m∞ is the terminal mass for that particular degradation. Evaluation of A and E can be done using Equation 3.3:

$$\ln k = \ln A - \left({}^{Ea}/_{RT}\right) \qquad \text{Equation 2-3.}$$

A and E can be obtained by the intercept and slope of a plot of *ln k* versus 1/T .

2.6 Torrefaction Overview

Torrefaction is a promising pre-treatment process that is currently receiving attention to solve many of the problems associated with biomass, and it has the potential to increase the amount of biomass that could be fired in power plants [34-38]. It originates from the French word *'torrefier'*, which means to roast coffee. According to Prins *et al.*[87], the earliest torrefaction study was in France in the 1930s where the potential of torrefaction was carried out for the generation of syngas and again in the 1980s, when a torrefaction plant was built in France by a French company, Pechiney , to produce 12000 ton/acre of torrefied woods which were to be used as charcoal substitute in metallurgic processing plant [35]. The project relapsed because the plant's efficiency was low and not economical viable (high cost of production) but was technically feasible. Since then, especially in the last decade, there has been a growing interest in torrefaction and several trials have been carried out ranging from bench scale laboratory tests to large scale industrial trials but up until now, there is no evidence of any commercial production of torrefied fuels.

The properties of the solid product or torrefied wood are changed and become more like low rank coal (lignite) in the van Krevelen diagram, since biomass loses oxygen and hydrogen preferentially over carbon [41]. Thus the net calorific value i.e lower heating value (LHV) is increased. In addition, torrefaction reduces the tenacity of biomass, and

it becomes more friable and easier to mill, resulting in lower energy consumption during milling. In fact, there is a significant improvement in the milling behaviour of the biomass leading to an increase in the amount of biomass throughput during co-milling with coal [93].

2.7 Chemistry of torrefaction

The torrefaction process involves the use of relatively low temperature ranging between 200^0C and 300^0C in the absence of oxygen. The process causes the biomass to lose low molecular weight volatile compounds and gases due to the dehydration and decarboxylation reactions of the long polysaccharide chains. Bridgeman *et al.*[37] reported that biomass exhibit different behaviour to thermal treatment owing to their types, origin and properties. Therefore, the process of biomass thermal degradation mainly depends on the type of biomass.

Figure 2-18 shows the different stages involved in the torrefaction process. *Bergman et al.*[35], presented the five primary stages of torrefaction as: initial heating, pre-drying, post-drying, intermediate heating, torrefaction and solid cooling. The process is initiated by heating the biomass to a point where evaporation takes place. The temperature is then taken to a point above 100°C, this allows the release of water content from the biomass at a constant rate during the pre-drying phase. The third phase ensures that biomass is free of moisture, although some mass loss is expected (due to loss of moisture and also from volatile of light organic compound such as extractives and oils). The biomass starts to torrefied when the temperature is increased above 200°C. Devolatilisation commences and continues during this heating period and finally stops at the period of cooling. At this stage, the biomass experiences degradation, as a result of destruction of hemicellulose, and minor loss from lignin and cellulose. Bergman *et al.*[35] and Van der Stelt *et al.*[41] stated that hemicellulose is the most reactive polymer, followed by lignin, and cellulose is the most thermally stable in torrefaction process. At a temperature in the range of 290^0C, the decomposition becomes exothermic and more vigorous and more mass loss is observed. Finally, the solid is allowed to cool to the desired temperature, to a point where there is no further mass loss. It is important to mention that there is a clear distinction between the actual time for torrefaction and

residence time of the biomass. Generally, biomass dwells longer in the reaction tube owing to the fact that it has to be pre-treated (drying of moisture) before the actual torrefaction takes places. For that reason, to know the actual torrefaction time, reaction time is used instead of (reactor) residence time. The reaction time is total time taken to heat the biomass from 200°C to the desired final (torrefaction) temperature and the time the biomass spends at the desired temperature [35].

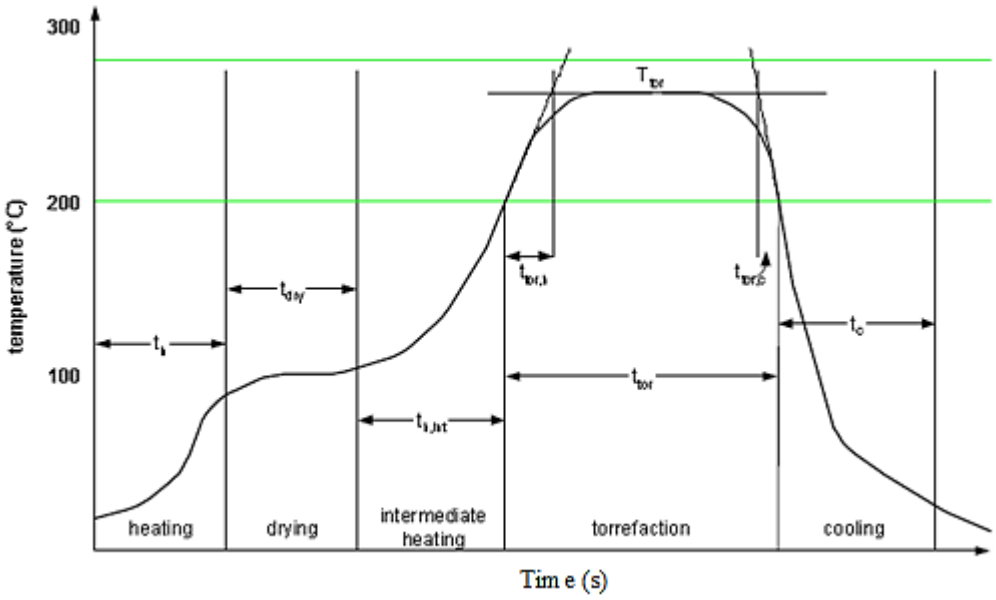

Figure 2-18: Stages involved in torrefaction process [35].

2.8 Decomposition mechanisms during torrefaction

Cellulose has gained most attention when discussing thermal decomposition of biomass, since is the largest fraction of the biomass composition. However, studies on thermal decomposition of cotton wood and its constituents from Shafizadeh and McGinnis [64], showed that cellulose decomposition is not the most relevant constituent in the temperature range of torrefaction (200 – 300 °C) and this is seen in Figure 2-19. From this figure, it can be observed that only small fraction of cellulose degrades at 300 °C leading to little mass loss. All other materials studied in Figure 2-19 experienced a significant mass loss at a temperature above 200 °C especially xylan, a model for hemicellulose.

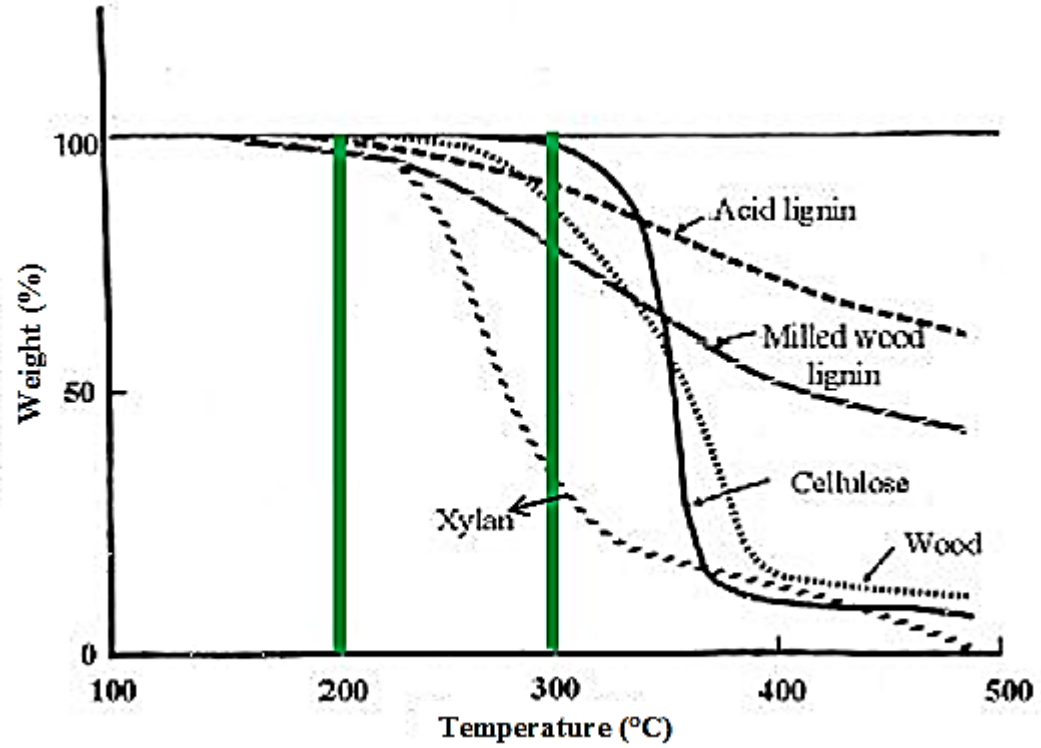

Figure 2-19: Thermogravimetry of cotton wood and its constituents [64].

Studies have shown that during torrefaction, mass loss mostly comes from the decomposition (devolatilisation) of hemicellulose and partly some of lignin [37, 87, 94]. Decomposition of Xylan-based hemicellulose starts at a temperature around 230°C to 280°C. Lignin which is the binding agent in woody biomass decompose at a slower rate, but shows a steady increase of decomposition starting from temperatures of about 200 °C or even lower.

Shafizadeh *et al*[64] show that depolymerisation of wood occurs at significant rates at 150 °C. Also from the same report, they further mentioned that the rate of depolymerisation is already occurring readily at 190 °C.

Di Blasi and Lanzetta [88] found a two-step mechanism that can be used to describe hemicellulose decomposition. Depolymerisation reactions which is the first reactions that usually takes place at a temperature below 250°C, thus altering and rearranging the

polysugar structures. Thermal degradation of these oligosaccharides and monosaccharaides at higher temperatures usually between 250-300°C result in formation of chars, CO, CO_2 and water. The fragmentation of the carbon skeleton accounted for the formation of light volatiles like carbonyl compounds.

Gaur and Reed [95] mentioned that cellulose decomposition resulting in mass loss starts at 250°C. Several gases, condensable liquids and char are formed during this process.

Chen *et al.*[96] studied torrefaction of seven lignocellulosic samples namely hemicellulose, cellulose, lignin, xylan, dextran, xylose and glucose at three different temperatures namely 230, 260, and 290ºC for an hour, followed by pyrolysis at a final temperature of 800ºC using TGA. They carried out this study in order to investigate the thermal degradation characteristics of the tested samples and to obtain useful insights into torrefaction mechanism. The TGA plots obtained from their study are shown in Figure 2-20a. Generally, at a reaction temperature of 230 °C, hemicellulose starts to degrade slightly, leading to release of some moisture and light volatiles from the tested samples When the temperature was increased to 260 °C, hemicellulose was partly decomposed, while cellulose and lignin were barely affected. Further increase in temperature to 290 °C caused a large portion of hemicellulose and cellulose to be destroyed. Figure 2-20b) shows the DTG peaks that were obtained from the TGA experiments. The DTG peak for hemicellulose at 230ºC showed that it was less affected and presented the slowest rate of mass loss when compare with DTG peaks for hemicellulose at 260 and 290ºC. The DTG peak for cellulose at 230ºC is relatively small, since only 1.05 wt% of cellulose is degraded at this temperature. However the DTG peaks for cellulose is higher when the temperature was increased to 260 and 290ºC, leading to a significant rate of degradation, of about 4.43 and 44.82 wt% of cellulose respectively. Lignin appeared to be relatively less affected by torrefaction, its decomposition occurred gradually over a wide range of temperature up to about 800ºC and at a very low mass loss rate during pyrolysis. The DTG peaks for lignin are much smaller than those of hemicellulose and cellulose in Figure 2-20b). The mass loss of lignin at 230, 260 and 290ºC is 1.45, 3.12 and 6.97 wt% respectively.

Chen *et al.*[96] also carried out co-torrefaction of lignocellulose materials. The blended hemicelluloses, cellulose and lignin together and a mixture containing the three constituents was torrefied at the three torrefaction temperatures to investigate the synergistic effect of co-torrefaction (reference). The TGA and DTG plots in Figure 2-21 shows that the reaction of individual component in the mixture does not depend on the other and there is no cross-link interaction among the three constituents during torrefaction. Therefore, it was established that the weight loss of lignocellulosic materials during torrefaction could be predicted from the linear superposition of the weight losses of the individual constituents [96] and this is in agreement with earlier work from this laboratory [75].

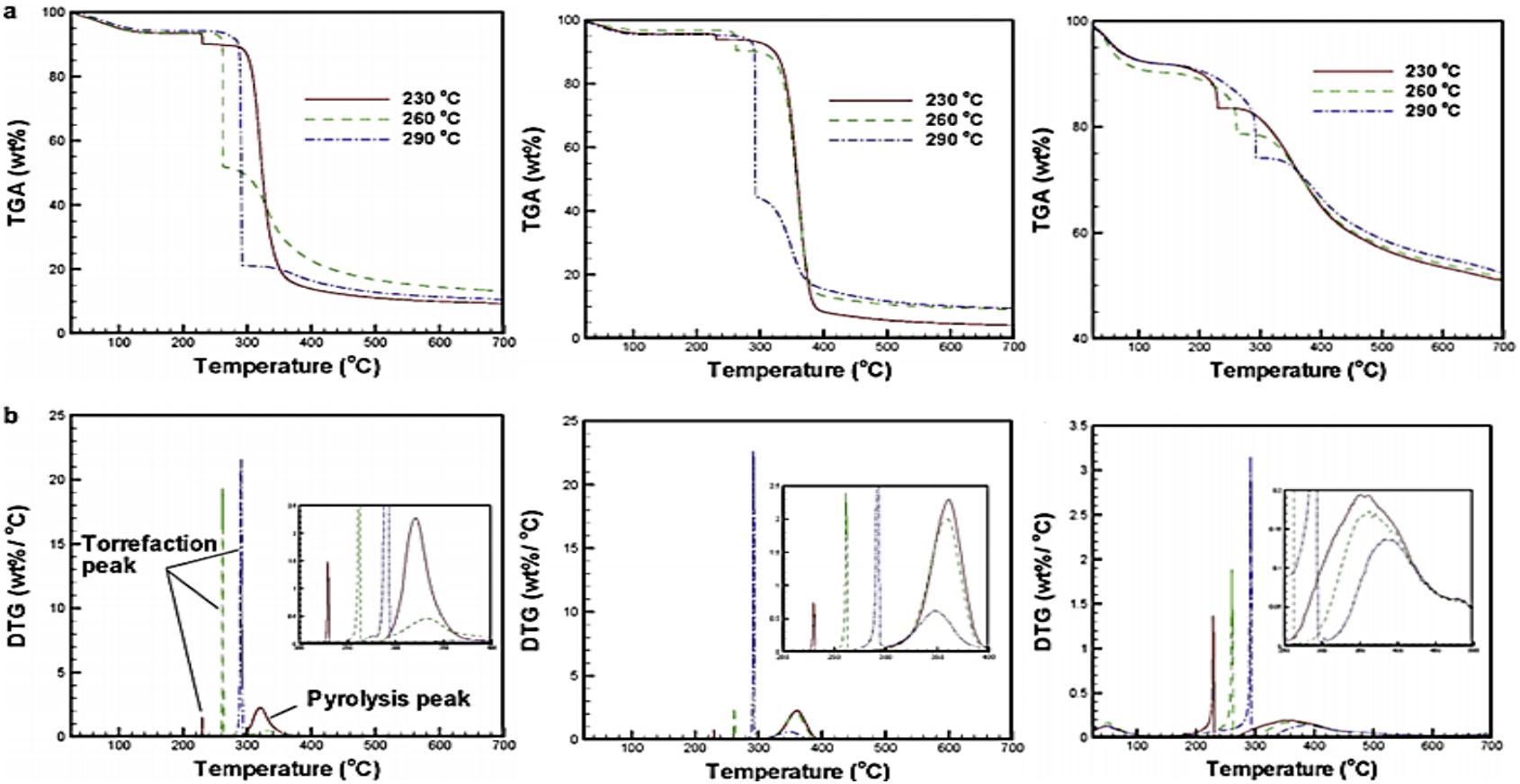

Figure 2-20: a) TGA and b) DTG plots of hemicellulose (left), cellulose (middle) and lignin (right) at three torrefaction temperatures (230, 260 and 290ºC with a residence time of an hour) [96].

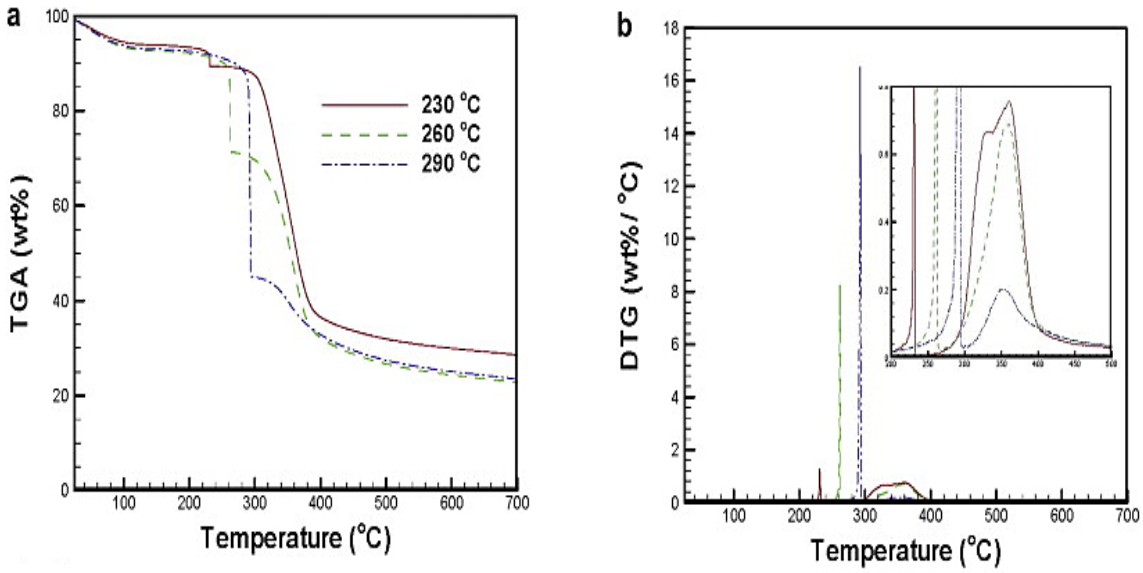

Figure 2-21: a) TGA and b) DTG plots from co-torrefaction of hemicellulose, cellulose and lignin blend at three different torrefaction temperatures (230, 260 and 290 °C for an hour and composition ratio for hemicellulose: cellulose: lignin = 1:1:1) [96].

Bergman *et al.*[35] illustrated the stages of decomposition of the polymers of biomass during torrefaction with Figure 2-22. From the figure, it can be observed that hemicellulose is the most reactive component, responsiblefor the majority of the mass loss during this process. The stage marked A is the drying period, where evaporation of moisture occurs. The stage marked B only happens in lignin and at this stage, the softening of lignin occurs. In stage C, the temperature is increased, thereby causing partial decomposition of hemicellulose, prompting the release of low molecular weight volatiles. Also, at this stage, lignin and cellulose may suffer degradation, but the effect on the mass loss is minimal. In stage D, devolatilisation and carbonisation of the polymers formed in C occur. This is where a further increase in temperature happens. At temperature above 250ºC, there is further devolatisation and carbonisation to the hemicellulose while cellulose and lignin continue to undergo slower decomposition over a wider temperature range than hemicellulose. Thermal softening of lignin has been observed at a temperature below 200°C resulting into a small amount of weight loss. Char formation and the release of volatiles are obtained from a devolatilisation process in the temperature region of 230-300°C.

Overall, the resultant product of the hemicellulose degradation gives rise to a percentage of products which fall in the proportions of approximately 70–90% solids, 6–35% liquid, and 1–10% gas (on a mass basis). About 70% of the initial biomass weight and about 90% of the original biomass energy is retained, resulting in energy densification [39, 40]. However, the solid product called “torrified biomass” or “char” is usually the quantity of interest. The solid fraction compose mainly of unreacted cellulose, unreacted lignin as well as non-volatile byproducts of hemicellulose degradation (depending on the reaction temperature). This, alongside other reasons has limited the conclusive characterisation of torrified biomass.

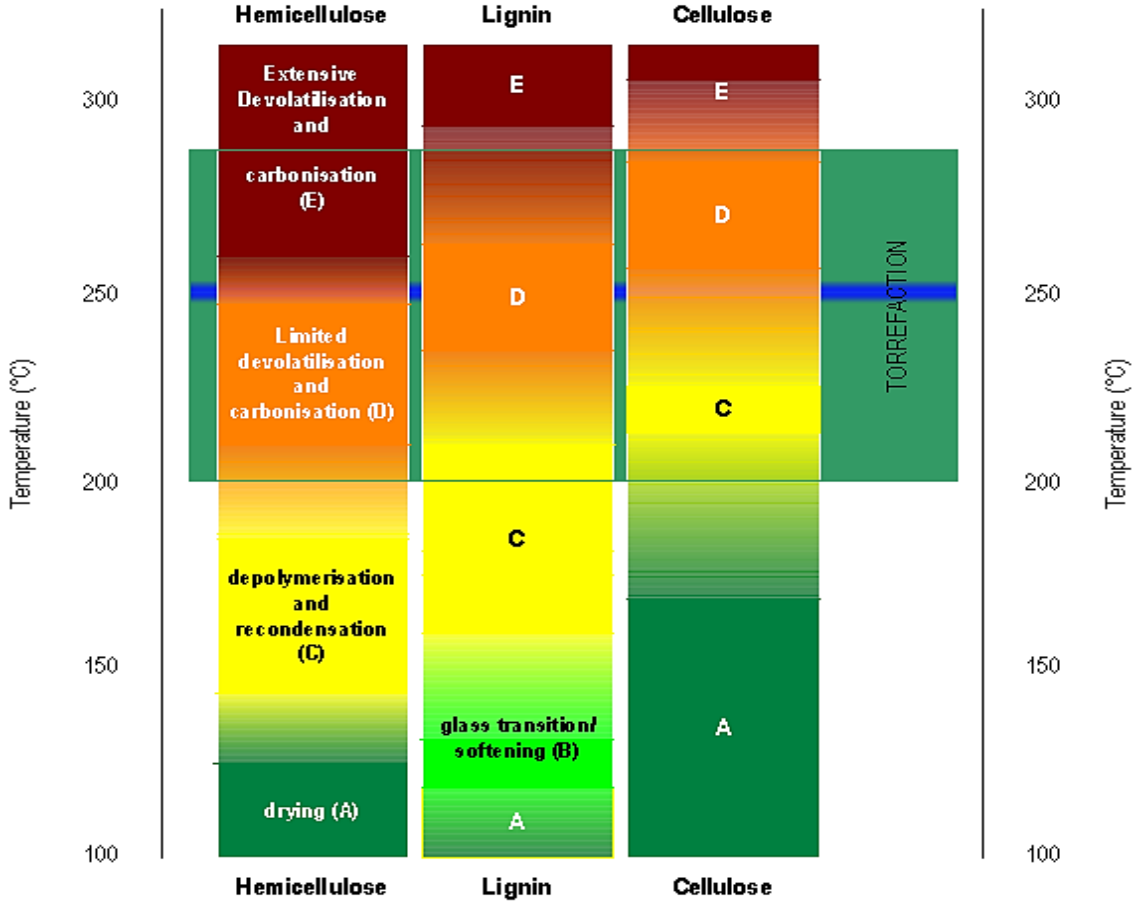

Figure 2-22: Decomposition mechanism of biomass [35].

2.9 Mass and Energy Balance

During torrefaction process, roughly 70% of the initial biomass weight and about 90% of the original biomass's energy (resulting into energy densification [39, 40]) is retained, while about 30% of the mass is converted to gas and 10% of the energy content is in the gases. The mass and energy balances in torrefaction are assessed using the mass and energy yields in Eq. 4 and Eq. 5:

$$\text{Mass yield, } \text{ŊM} = \left(\frac{Mchar}{Mfeed}\right)_{\text{daf}} \qquad \text{Equation 2-4.}$$

$$\text{Energy yield, } \text{ŊE} = \text{ŊM}\left(\frac{HHVchar}{HHVfeed}\right)_{\text{daf}} \qquad \text{Equation 2-5.}$$

Where M_{char} is the mass of treated sample on a dry ash free basis (daf), M_{feed} is the mass of raw biomass sample on a dry ash free basis, HHV_{char} is the high heating value of the treated sample on a dry ash free basis, and HHV_{feed} is the high heating value of the raw biomass, on a dry ash free basis.

Dhungana studied torrefaction of Pine sawdust at 280^0C for 60 mins in a muffle furnace and reported the mass and energy balance for the products' yield in the chart shown in Figure 2-23. They stated that the process produced about 22% of the original mass (untreated sawdust) as condensable volatiles, whilst approximately 6% of the original sample mass is converted to non-condensable gas and 67% of the original sample mass is retained as the solid product of torrefaction. The chart also showed that most of the energy (94%) is retained in the torrefied biomass, despite losing a large percentage of its mass during the torrefaction process.

Ferro *et al.*[97] also reported the solid's energy yield of 92% and mass yields of 88.1%, 8.5%, 2.9% for solid, liquid and gas respectively in similar tests.

Similarly, Pach *et al.*[98] reported mass yield of 77.3%, 19.6%, and 2.1% for solids, 77.3% solids, condensable volatiles and gases respectively, in their study on torrefaction of Pine, at 280˚C for 60minutes.

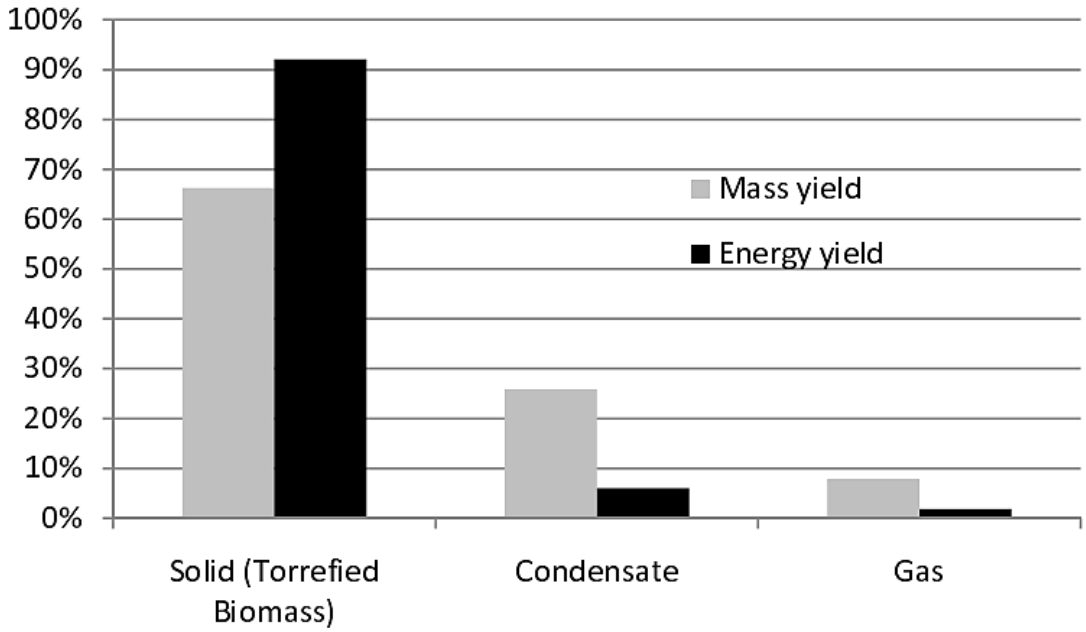

Figure 2-23: Mass and Energy balance on torrefaction of sawdust [98].

Chew and Doshi [99], complied data in the literature on mass yield and energy yield of different biomass subjected to the torrefaction process which are listed in Table 2-2. From the table, it is observed that the mass yields for woody biomass vary from 52-95.1% of its original weight upon torrefaction at different temperatures between 220-300^{o}C and at residence time 0.5-1 hour. The conversion rate of non-woody biomass is relatively higher than woody biomass due to its higher hemicelluloses content, consequently resulting in lower mass yield between 24-95% for different biomass when torrefied at different temperatures (250–300^{0}C) and residence times (30 or 60 minutes). Studies found that the polymeric structure of the feedstock influences the reactivity of torrefaction reaction and higher content of xylan, which is the main constituent in hemicelluloses fraction, will increase the rate of reaction [99].

Also from Table 2-2, it can be observed that the energy yield for woody biomass exposed to torrefaction temperatures below 250 °C is over 95% except for Lucerne wood (88%). Increasing the torrefaction temperature to above 250 °C, reduces the energy yield [99]. Generally, non-woody biomass presented a wider spread in energy yield compared to woody biomass, ranging from 29% to 98%, due to the higher variation in volatile matter and hemicelluloses fraction[99].

Torrefaction processes are usually operated at mass yields of 70-90% with the corresponding energy yields of 70–95%. The effect of reaction time is seen to be less significant compared to temperature and the ideal operating condition is either at a lower temperature regime or higher torrefaction temperature coupled with shorter duration to minimize energy loss [99, 100].

Table 2-2: Mass yield and energy yield of different biomass at different torrefaction temperatures and residence times **[99]**.

Biomass	*t* (h)	*T* (°C)	MY (wt.%)	EY (wt.%)	HHV (MJ/kg)	Biomass	*t* (h)	*T* (°C)	MY (wt.%)	EY (wt.%)	HHV (MJ/kg)
Woody biomass											
Birch	1.0	250	85.50	97.93	18.83	Empty fruit bunches (oil palm)	1.0	220	43.16	43.54	17.17
Logging residue chip	0.5	225	88.00	92.68	19.79		1.0	250	36.98	38.39	17.67
	0.5	250	81.00	91.43	21.21		1.0	300	24.18	29.00	20.41
	0.5	275	70.00	82.07	22.03	Kernel shell (oil palm)	1.0	220	77.44	73.80	18.85
	0.5	300	52.00	73.09	26.41		1.0	250	73.83	71.18	19.07
Leucaena	0.5	200	91.00	94.14	21.00		1.0	300	71.27	78.12	21.68
	0.5	225	86.50	90.33	21.20	Lucerne	1.0	230	87.00	88.28	18.69
	0.5	250	73.00	76.24	21.20		1.0	250	81.60	83.06	18.75
	0.5	275	54.50	61.21	22.80		1.0	280	71.60	77.31	19.89
Pine	0.5	225	89.00	93.92	19.48	Mesocarp (oil palm)	1.0	220	63.08	61.21	19.03
	0.5	250	82.00	89.20	20.08		1.0	250	60.04	58.91	19.24
	0.5	275	73.00	86.29	21.82		1.0	300	52.45	59.30	22.17
	0.5	300	52.00	71.49	25.38	Peanut husk	1.0	250	72.50	81.02	16.35
Pine	1.0	230	92.40	96.51	18.07		1.0	270	67.00	85.18	18.60
	1.0	250	88.20	94.37	18.51		1.0	300	55.75	72.25	18.96
	1.0	280	78.10	93.90	20.80	Rape stalk	0.5	200	63.29	65.82	19.50
Willow	0.5	230	95.10	96.05	20.20		0.5	250	38.26	41.01	20.10
	0.5	250	89.60	92.29	20.60		0.5	300	25.30	29.13	21.59
	0.5	270	79.80	85.39	21.40	Reed canary grass	0.5	250	83.00	85.13	20.00
	0.5	290	72.00	78.84	21.90		0.5	270	72.00	76.80	20.80
Wood briquette	0.5	220	94.00	95.91	20.43		0.5	290	61.50	68.75	21.80
	0.5	250	74.00	78.39	21.21	Rice straw	0.5	200	59.84	59.98	17.16
	0.5	270	56.00	63.70	22.77		0.5	250	40.32	42.46	18.03
Wood briquette	1.0	220	90.00	94.36	20.99		0.5	300	36.57	39.90	18.68
	1.0	250	65.00	71.63	22.06	Sawdust	1.0	250	67.25	72.48	19.55
	1.0	270	54.00	61.99	22.98		1.0	270	59.50	67.14	20.47
Non-woody biomass							1.0	300	42.00	55.10	23.80
Bagasse (sugarcane)	1.0	230	87.50	96.42	17.08	Straw pellets	1.0	230	95.00	95.53	17.90
	1.0	250	78.90	92.03	18.08		1.0	250	90.00	92.07	18.21
	1.0	280	68.60	82.90	18.73		1.0	280	79.90	89.87	20.02
Cotton stalk	0.5	200	63.89	83.44	23.94	Wheat straw	0.5	200	47.56	56.02	19.84
	0.5	250	33.80	45.30	24.57		0.5	250	41.24	51.05	20.85
	0.5	300	30.04	41.02	25.03		0.5	300	31.61	40.67	21.67

t: time; T: temperature; MY: mass yield; EY: energy yield; HHV: higher heating value.

Figure 2-24 shows that the mass yield is significantly influenced by the hemicellulose content of the biomass. The lignocellulosic biomass with lower hemicellulose composition gives higher mass yield. For example, willow, which has the least hemicellulose content of 14% compared to 30% with that of reed canary grass and 31% with that of wheat straw, records the highest mass yield [37].

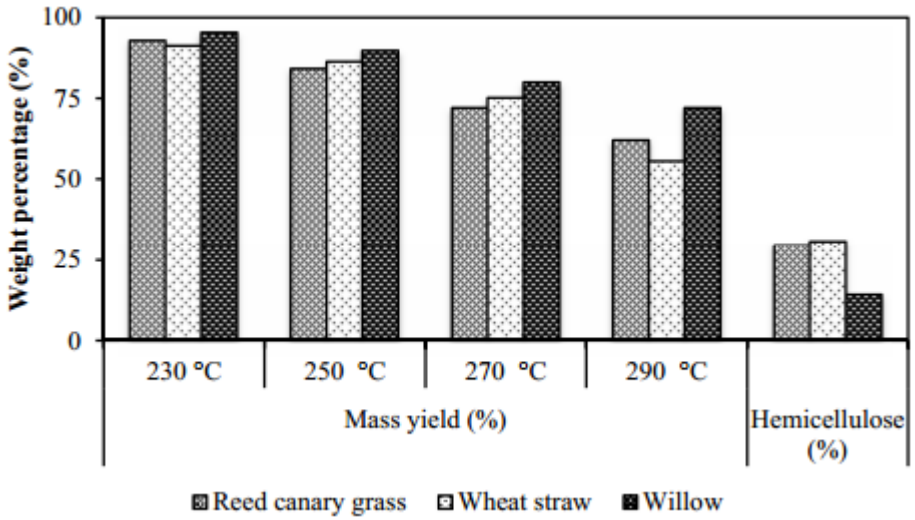

Figure 2-24: Mass Yield from the Torrefaction of reed canary grass, willow and wheat straw (At different temperature and residence time of 30 minutes) alongside with the hemicellulose content in the fuels [37].

2.10 The effect of torrefaction on the fuel properties.

The torrefaction process has major effects on the properties of the biomass such as the colour, particle size, particle shape, mass loss, proximate analyses, ultimate analyses, heating values, grindability, and hydrophobicity of the sample. These are discussed in the following sub-sections.

2.10.1 Colour

The first noticeable transformation in a torrefied biomass is the colour, which changes from brown to darker brown or black, as the torrefaction temperature and residence time is increased [93, 101]. The changes in colour upon torrefaction are mainly due to hydrolysis and oxidation reactions [102]. Aydemir *et al.*[103] studied the influence of thermal treatment on colour changes of six different wood samples at three

different temperatures of 160, 180, and 200°C and at a residence times of 3, 5, and 7 hours. They concluded that the change in colour of wood upon thermal treatment is influenced by the extractive compositions in the wood. The dark colour characteristics of thermally treated woods is caused by the changes and the transformation of the hemicellulose and lignin under the thermal degradation which is significantly influenced by the reaction temperature, reaction time, pH level and the type of species [104]. The change in colour from light brown to dark brown, black, or red-orange depends on the type of phenolic compounds that form during torrefaction [105]. Therefore, depending on the reaction time and temperature of torrefaction process, the colour of the solid product changes from light brown to dark brown or black [103, 105]. Figure 2-25 shows the changes in colour for willow at various conditions.

Figure 2-25: Images of willow: a) untreated; b) low temperature, short residence time; c) low temperature, long residence time; d) high temperature; short residence time; e) high temperature, long residence time [93].

2.10.2 Particle size and shape

The size and shape of the biomass particles are also observed to change upon torrefaction. Arias *et al.*[106], examined these transformations using an optical microscope to have a good understanding of the structural changes of eucalyptus upon torrefaction at 240°C and 280°C and at residence time of 3 hours. Figure 2-26 indicates that the untreated biomass fuel which is very fibrous in nature, turn out to be simpler and less fibrous particle upon torrefaction. The particle sizes of the untreated biomass fuels were also observed to decrease with increasing severity of conditions (temperature and residence time). Arias *et al.*[106] postulated there is transformation in the hemicellulose structure of the torrefied biomass fuel, which causes reduction in the particle sizes and the shape becomes more spherical. These changes are observed when

a sieving process was carried out, and a large number of small particles were found to pass through the sieves. Repellin *et al.*[107] established that torrefaction causes the lignocellulosic material to shrink, and consequently, creates stress in the wood fibres with the crack, leading to depolymerisation. An examination of the raw and torrefied Eucalyptus Saligna (E.Saligna) structure using Scanning Electron Microscope (SEM) was carried out by Almeida *et al.*[108] and presented in Figure 2-27. The results showed significant damage to the structure of the torrefied E.Saligna samples with several fractures occurring in the most fragile tissues, compared to the raw E.Saligna which was observed to be fibrous and intact.

Figure 2-26: SEM images of raw eucalyptus (RE), torrefied eucalyptus (TRE) at 240°C and 280°C respectively [90].

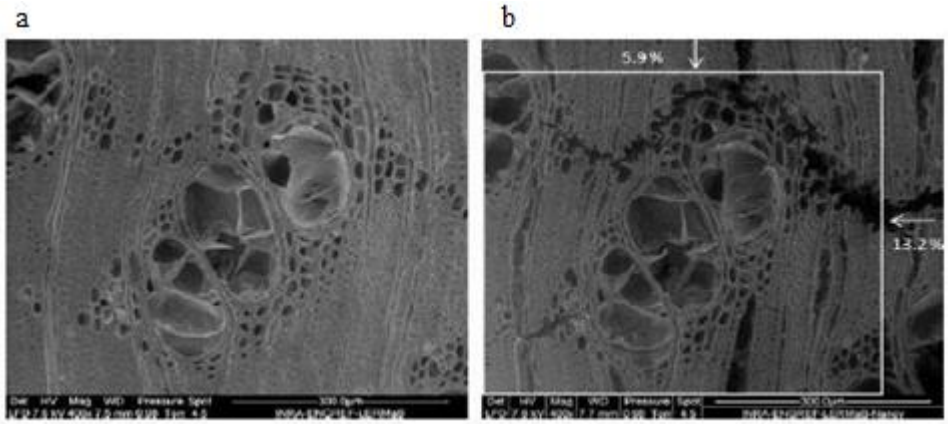

Figure 2-27: SEM images of *E.Saligna*: a) untreated and b) torrefied at 280ºC with a residence time of 5 hrs [108].

2.10.3 Mass loss

The mass of solid products (torrefied fuels) reduces when compared to the mass of the untreated biomass fuels that goes into the reactor originally. Bridgeman *et al.*[37]

reported similar reduction in the percentage mass of reed canary grass (RCG) with increasing temperature, from 230 to 290°C using the chart shown in Figure 2-28. This change resulted from loss of moisture during the drying stage, release of reaction water vapour and the release of volatiles. The latter is due to the decomposition of hemicellulose and slight decomposition of cellulose during torrefaction.

Mass loss is also reported to be higher during torrefaction of smaller particles (size varies from 0.23 to 0.81 mm) and is lower for larger particles resulting from the higher heat transfer rate in small particles [104]. For instance, Medic *et al.*[109] reported a higher mass loss in the 'ground' corn stover than that of the whole stover. Similar studies conducted by Kokko *et al*.[104] in a bubbling bed reactor showed a higher mass loss in the smaller particle compared to that of the bigger particles. Wang *et al.*[77] observed a similar trend of higher mass loss of finer particle size in a microwave-assisted torrefaction process. They reported mass reduction ratios of 65%, 69%, and 72%, when the particle sizes were in the range of 0.149-0.297mm, 0.149-0.074 mm, and < 0.074 mm, respectively. The greater intra-particle effect and the heat transfer area in the fine particles causes a higher reaction temperature, enhancing the devolatilization reactions [104]. The transfer of heat in the torrefaction process mainly depends on the size, shape, and biomass properties, and these parameters influence both the convective and the conductive heat transfer rate from the reactor to the biomass and within the biomass, respectively [104]. There is reduction in the convective heat transfer rate in larger pieces of biomass particle with the surface area per unit volume or mass being lower.

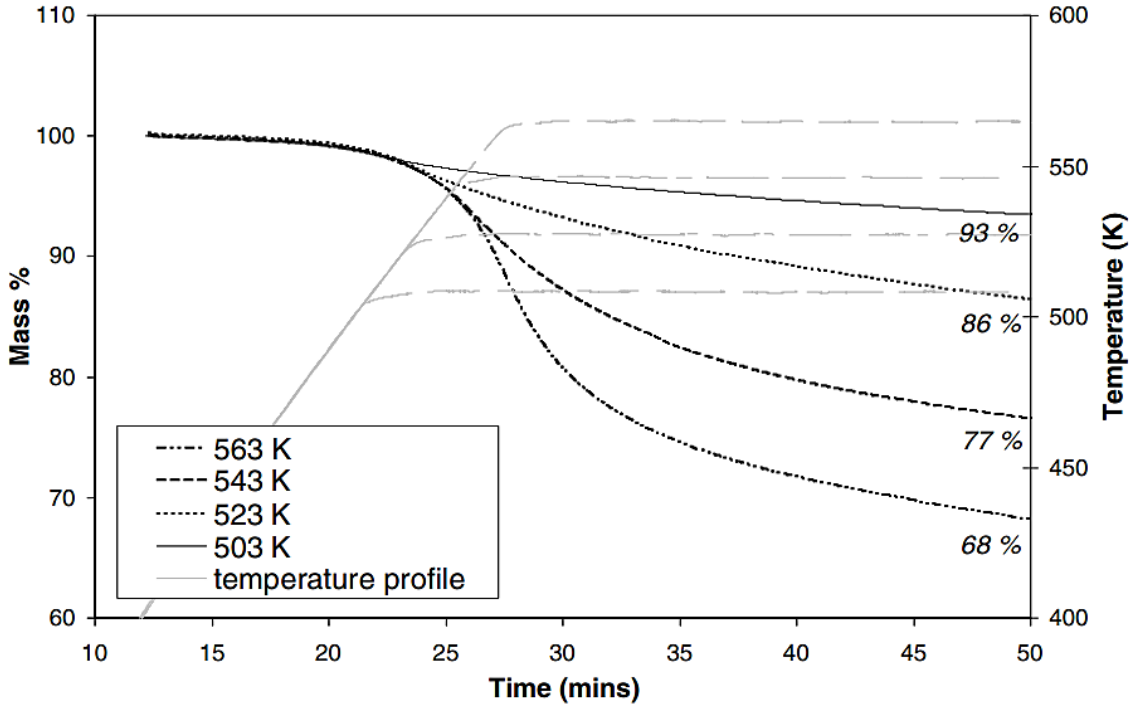

Figure 2-28: Mass loss reported by Bridgeman *et al.* [37], during torrefaction of reed canary grass at different temperatures.

2.10.4 Proximate, ultimate, high heating value, and Van Krevelen diagram.

The changes in the moisture, volatile matter, ash and fixed carbon content of torrefied biomass can be determined from proximate analysis. A considerable amount of literature has been published on characterization of torrefied fuels. Generally, these studies show that the moisture content and volatiles content reduce with increasing torrefaction conditions, while ash and fixed carbon content of the torrefied biomass increases. Moisture loss occurs during drying and also in the conversion of complex polymers of biomass into the smaller monomers, and then the conversion of smaller monomers into condensable and non-condensable volatile gases. This transformation will cause the torrefied fuels to have a proximate and ultimate composition different from that of the untreated biomass. Torrefaction removes some low organic volatile matter from the parent biomass due to the decomposition and devolatilization reactions [37, 40, 41, 45, 89, 98, 100, 104], thus making the fixed carbon and the ash content to become concentrated. The ash which is the noncombustible material in the biomass increases because none of it is driven away during the torrefaction process [104]. The

increasing trend observed in the ash content and the reducing trend is found in both the moisture and volatile content during characterization of torrefied rice husks (the fuel was torrefied at three different temperatures and residence times) are shown in Figure 2-29. From this figure, the moisture content and volatiles were found to reduce from 4.0 to 2.5% and 55 to 30% respectively, while the ash content appeared to increase from 20 to 32% when the temperature increased from 250 to 300ºC with a residence time of an hour. As shown in Figure 2-29, temperature is observed to significantly affect the properties of torrefied rice rusk than residence time. The effect of longer residence time is seen to cause minor changes in volatile and ash contents, while the moisture content continued to decrease. However, a longer residence time is observed to release more volatiles gases and consequently, in some cases, it causes the evolution of secondary volatile gases, which has a higher energy value relative to the first stage volatiles [104]. Similar observations were made by Bates and Ghoniem [110], and they discovered that the first stage volatiles in the two-step torrefaction kinetics had a heating value of only 4.4 MJ/kg compared to 16 MJ/kg in the second stage volatiles.

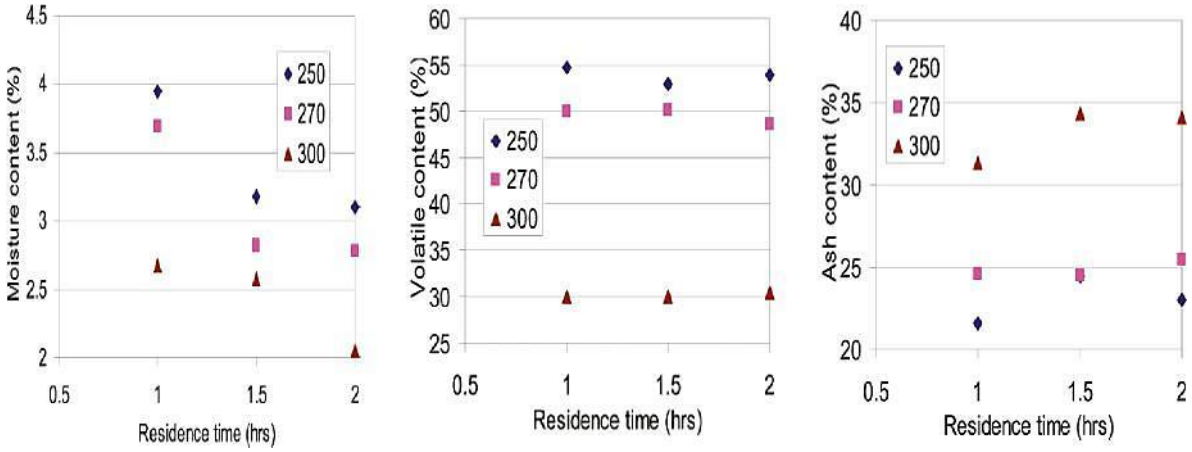

Figure 2-29: The change in the moisture, volatile and ash contents of torrefied rice husks [111].

A considerable amount of literature has been published on water loss during torrefaction at different temperatures and residence times [37, 97, 112-116]. In contrast, fewer researchers have focused on nitrogen loss during the pretreatment process [81, 111, 117-119]. With the growing use of biomass in combustion applications, the reduction of the associated NOx emissions, and thus the contribution from fuel nitrogen, becomes of

great interest [120-123]. The first study recorded on loss of nitrogen during torrefaction was reported by Tumuluru [81] in 2001 which stated that torrefaction results in a decrease in nitrogen, hydrogen and oxygen content resulting in decreased H/C and O/C ratios. Recent studies conducted by Tumuluru *et al.*[124], concluded that there is depletion of nitrogen upon torrefaction and this is dependent on the type of fuels and the process conditions. The researchers reported a marginal nitrogen loss during torrefaction of miscanthus at 250°C for 30 minutes; and a further reduction in nitrogen by 14.28%, which was observed when the severity of the process conditions were increased to 350 °C with a residence time of 120 minutes. Also from the same report [124], a study on torrefaction of white oak sawdust at 270°C for 30 min showed that moisture, volatiles, and hydrogen decreased with increased torrefaction temperatures. However, nitrogen contents changed very little from 0.17% to 0.16%, while the carbon content value increased from 50.28% to 53.10% under the same conditions.

Arias *et al.*[106] carried out torrefaction of eucalyptus wood at 280 °C for 3 hours and observed about 26% reduction in the oxygen and 24 % increment of carbon content in the torrefied eucalyptus fuel. Similarly, Chen *et al.*[125] found about 45% reduction in the oxygen and 44% increment of carbon content of torrefied Lauan samples after it is torrefied at 280 °C in 2 hours. Bridgeman *et al.*[37] carried out torrefaction of Reed canary grass, willow and wheat straw at four different temperatures 230, 250, 270 and 290ºC and observed changes in the chemical composition of the torrefied fuels. Figure 2-30 shows the effect of temperature on the carbon, hydrogen and oxygen content of the three biomass fuels. The content of hydrogen and oxygen reduces and the carbon content increases in the torrefied biomass fuels when the severity of the condition is increased, thus leading to higher heating value (HHV). In this instance, the calorific value of untreated willow which was 20 MJ kg^{-1} was found to be 20.2 MJ kg^{-1} and 21.9MJ kg^{-1} upon torrefaction at two different temperatures of 250ºC and 290ºC.

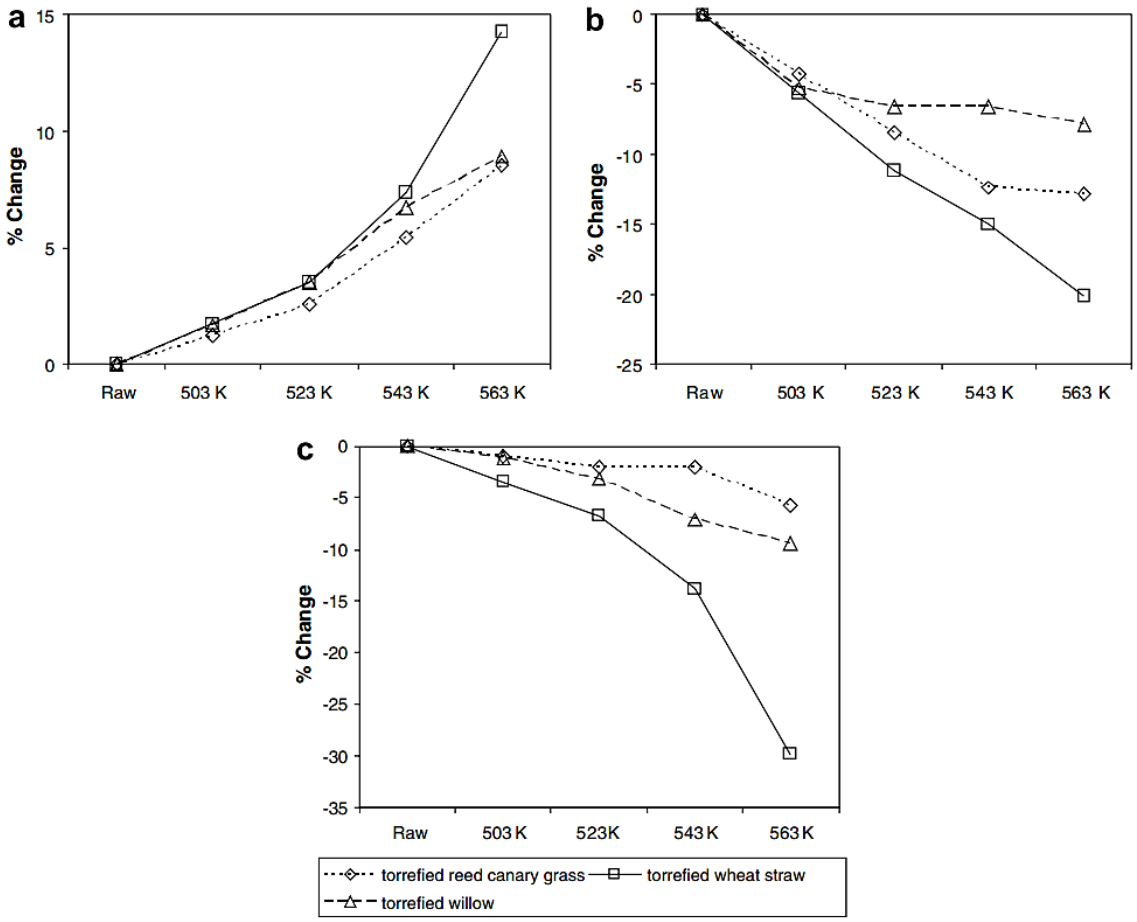

Figure 2-30: Changes in a) carbon, b) hydrogen and c) oxygen upon torrefaction at increasing temperatures [37].

The heating value of the torrefied fuels increases because, the carbon becomes more concentrated due to the formation of more C-C and C-H bonds, thus offers the properties to release more energy than O-H and C-O bonds in the raw biomass [104, 110]. The preferential loss in the hydrogen and oxygen reduces the O/C and the H/C ratios of biomass [41]. This makes the properties of torrefied biomass to become more like low rank coal (lignite) in the van Krevelen diagram, shown in Figure 2-31 [93]. The plot of van Krevelen shows that increasing the severity of torrefaction conditions causes more reduction of the O/C and H/C ratios and moves the torrefied fuels properties close to that of coal. It is important to mention that consideration needs to be given to energy yield, even though the torrefaction process at a more severe condition produces solid fuel that has similar characteristics to those of coals. This is because energy yield is observed to decrease when the severity of the torrefaction

condition, (particularly temperature) increases [104]. In addition to this, literature suggests that the formation of CO_2 and H_2O increases when the temperature and residence time increases due to the release of oxygen from biomass [104].

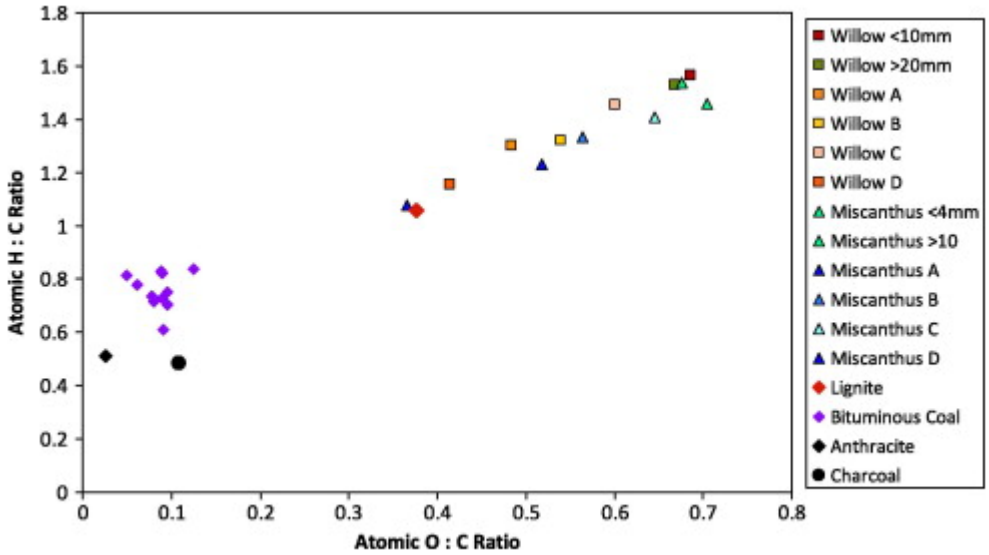

Figure 2-31: Van Krevelen diagram showing properties of coals, raw and torrefied fuels, where A-D are the four torrefaction conditions that were applied to the treated fuels [93].

2.10.5 Hydrophobicity

The moisture content in raw biomass fuels is generally very high and this remains a problem during thermal conversion for energy purposes. Lignocellulose biomass is susceptible to moisture absorption because of the presence of hydroxyl groups. Torrefaction is said to improve the hydrophobic nature of a biomass because the process decomposes the hydroxyl groups that take up moisture [126]. In addition to this, the decomposition of hydroxyl groups causes formation of new molecules and condensed tar which can possibly block the pores, thus preventing the uptake of water vapour and subsequent condensation [127]. This ability to resist moisture is described as hydrophobicity [128, 129].

Bergman [36] investigated the hydrophobic nature of biomass by immersing raw and torrefied pellets fuels in water for 15 hours. The results show raw pellet fuel soaked in more water and quickly disintegrated into original particles while torrefied biomass absorbed about 7-20% moisture by its weight. Increasing the severity of the torrefaction

conditions also has a favorable and positive influence on the hydrophobicity of biomass [104].

2.10.6 Grindability

Lignocellulose biomass is difficult to grind because of its fibrous and tenacious nature [107]. Hardgrove Grindability Index (HGI) is used to assess the level of difficulty in the grinding of solid coal samples into the powder, and the higher the value of HGI, the easier a coal fuel can be reduced to fine powder [130, 131]. Some studies have used a modified HGI test to evaluate the grindability of torrefied biomass including earlier work from this laboratory [93, 128]. Literature suggests that torrefaction improves the grindability of biomass and the value of HGI of the torrefied biomass increases with the residence time and the torrefaction temperature [93, 107, 128, 131]. Torrefied fuels becomes brittle due to degradation of hemicellulose and the depolymerization of different molecules during the thermal treatment [131].This reduces the power consumption during milling [35], leading to increase of biomass utilization for heat and electricity generation in power stations [93].

Arias *et al.*[106] investigated the influence of torrefaction on the grindability of eucalyptus and reported that there is significant improvement in the grindability of torrefied eucalyptus and reduction in the particle size especially, when the torrefaction condition is more severe. Similarly, Phanphanich and Mani [101] torrefied pine chips and pine logging residue chips at four different temperatures of 225, 250, 275 and 300ºC and reported that there is a reduction in the power consumption during grinding. This is shown in Figure 2-32. The figure shows that torrefaction at 300ºC reduced the fuels' power consumption during grinding by six times and ten times for logging residues and pine chips respectively in comparison to when they are untreated. For instance, an investigation carried out by Bergman *et al.*[35] on the grindability behaviour of both untreated and torrefied treated willow, larch and beech, and their respective power consumption during grinding [35], is shown in Figure 2-33. From this figure, it can be seen that the power consumption needed to break torrefied willow (torrefied at 230ºC for 30 minutes) to particle size of about 0.2 mm was reduced by 50%, compared to the power needed to grind untreated willow to the same particle

size. The power consumption for grinding torrefied willow (torrefied for 30 minutes at 259ºC and 270ºC) to the same particle size reduced further.

Bridgeman *et al.*[93] compared the grindability behaviour of untreated and torrefied miscanthus with that of reference standard coals (32, 49, 66 & 92) using an adapted grindability test, HGI. HGI is commonly used to determine the grindability behaviour of coals in power plants. The details for the experimental method of the modified HGI version by Bridgeman *et al.*[93] was used to assess the grindability behaviour of torrefied fuels studied in this thesis and can be found in Section 3.11.1 and 3.11.2. Figure 2-34 shows the changes in the particle distribution curves of miscanthus samples, compared to those of the four standard reference coals. This figure presents miscanthus "D" to have a grindability behaviour closest to coal of known HGI value, 92. The HGI value of miscanthus "D" was approximately 80. Bridgeman *et al.*[93] concluded that the grindability of a fuel will improve better with increasing torrefaction condition. Therefore fuels torrefied at higher temperature will have better grindability behaviour.

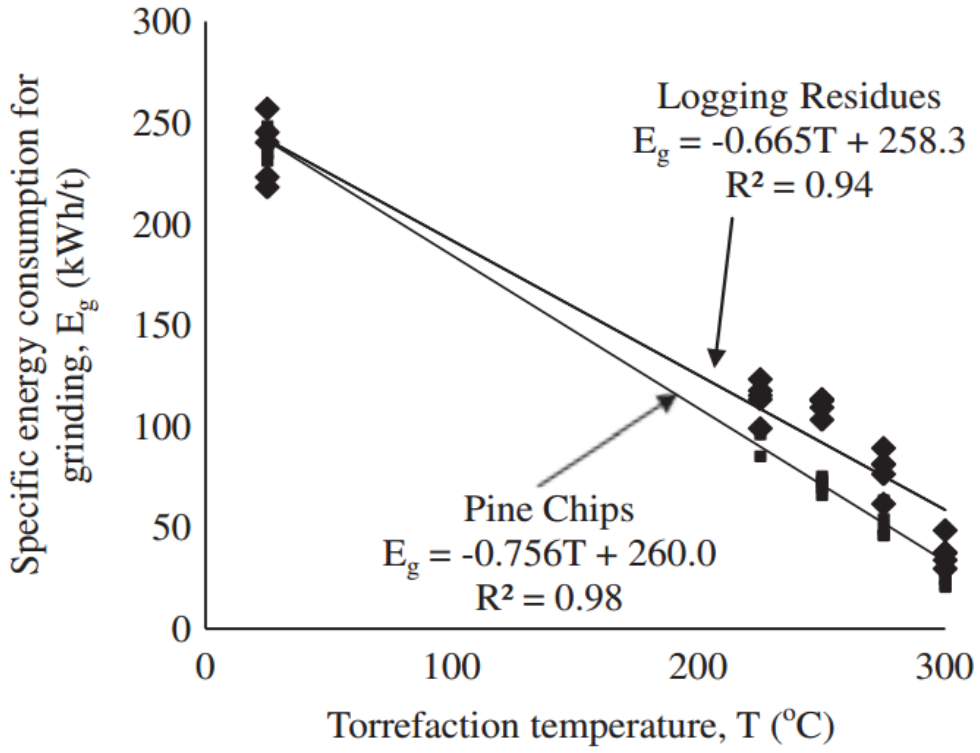

Figure 2-32: Specific energy consumption for grinding of raw and torrefied pine chips and logging residues [101].

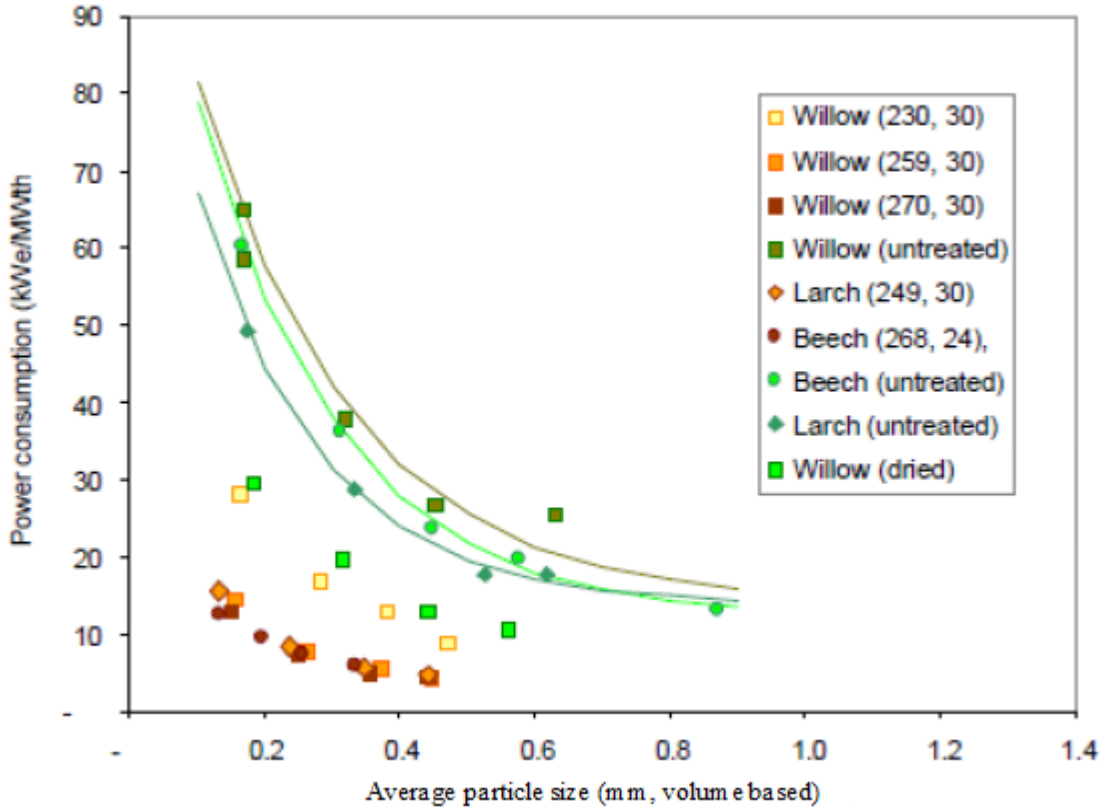

Figure 2-33: Power consumption during grinding of raw and treated fuels (willow, larch and beech) into different particle sizes. Fuels were torrefied at different temperatures between 230-268°C and residence time between 24-30 minutes [35].

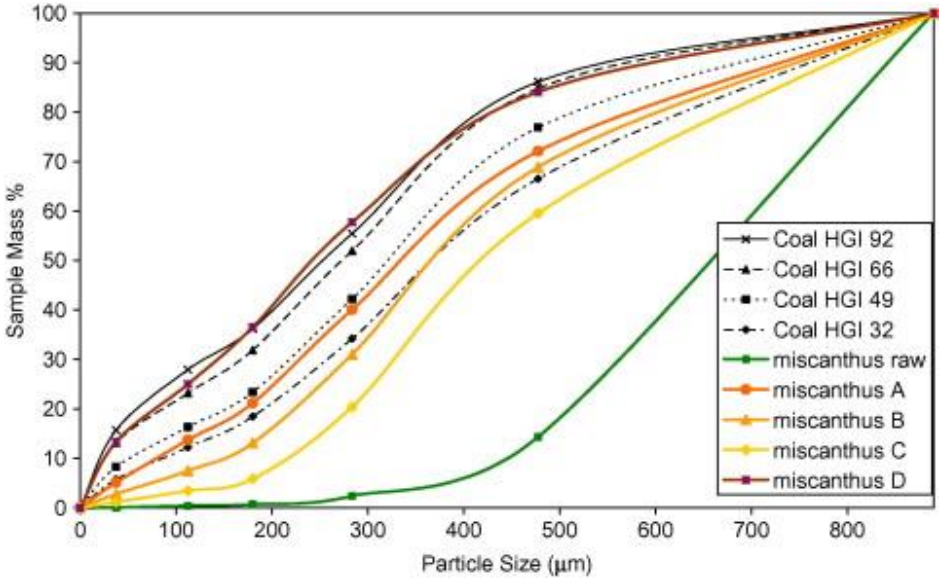

Figure 2-34: Particle size distribution curve for untreated and torrefied miscanthus (A-D), where A was treated at 290ºC with a residence time of 10 mins, B at 240ºC with a residence time of 60 mins, C at 240ºC with a residence time of 10 mins and D at 290ºC with a residence time of 60 mins, alongside four standard reference coals of HGI 32, 49, 66 and 92 [93].

2.11 Condensables and non-condensable products of torrefaction

The products released during torrefaction are divided into two categories namely condensable gas or liquid and permanent gases (non-condensable). The two main liquid products in the condensable phase are acetic acid and water, with smaller quantities of lactic acid, methanol, furfural, formic acid, toluene, benzene hydroxyl acetone and traces of phenol [89]. These products originate from the decomposition of hemicellulose. The release of water occurs during drying phase and also during dehydration reactions between organic molecules [37]. Acetic acid and methanol are respectively formed from acetoxy and methoxy groups attached to hemicellulose sugar monomers and lignin, while other compounds are produced at higher temperatures during the polymerisation reactions [36, 89, 109].

The non-condensable products are mainly CO_2, and CO. In addition to this, traces of H_2, and low molecular weight hydrocarbons such as CH_4, can also be seen [55], as

shown in Figure 2-35. The release of carbon dioxide is caused by decarboxylation reaction of acid groups that were attached to hemicellulose [36, 37, 89, 109].

Bergman *et al.* [36] suggested that the heat of torrefaction could be produced from the combustible products that were released, as this will increase the efficiency of the process. Therefore, it is important to analyse these products to assess the feasibility of generating heat in torrefaction.

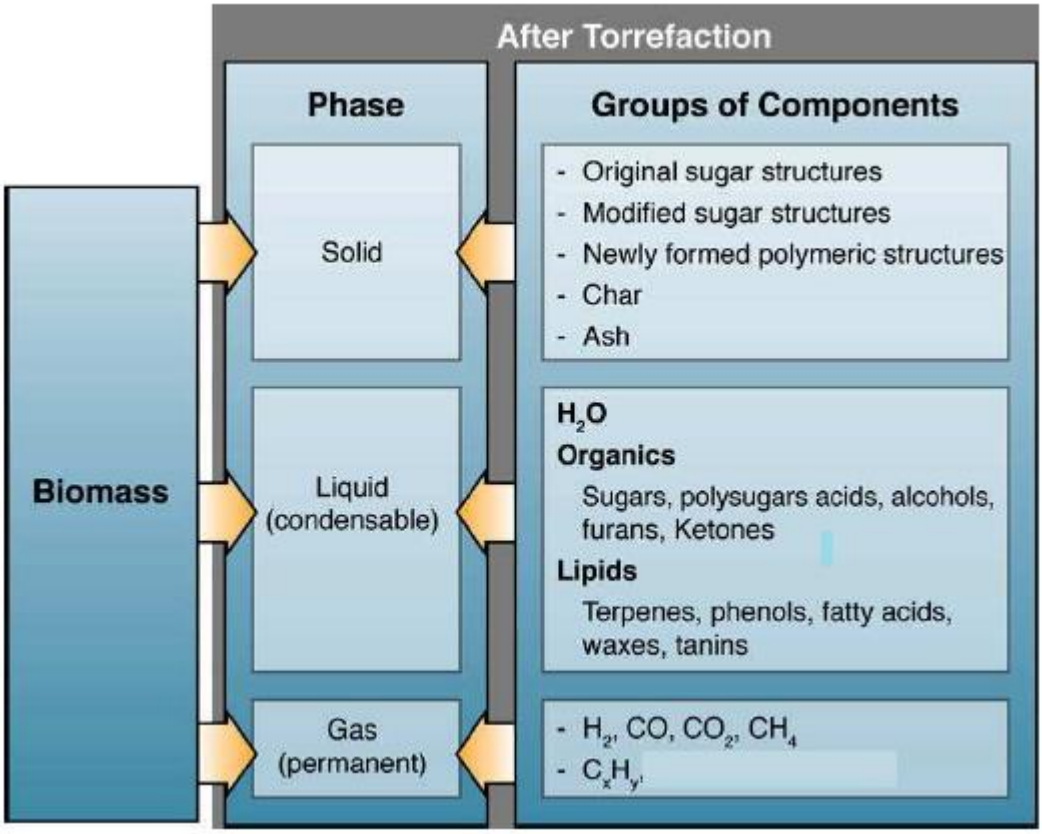

Figure 2-35: Formation of different products during torrefaction of biomass [132].

2.12 Studies into the combustion behaviour of raw and torrefied biomass

Raw biomass is said to be thermally less stable than torrefied biomass, and it produces a lower heat of reactions during combustion [37]. The heat released during combustion of torrefied fuels is higher and this increases with the severity of the torrefaction conditions. This is due to the loss of some volatile matter from the

original biomass upon torrefaction, which causes the treated fuels to develop a highly porous char material that enables increased oxygen diffusion during combustion. Chen *et al.*[125] stated that torrefied fuels have lower burnout rate due to the low volatile content in the torrefied biomass. They stated that torrefied fuels have a longer burn out duration than that of the raw biomass but is shorter when compared with that of coal [125].

Bridgeman *et al.*[37] carried out combustion studies of raw and torrefied willow with particles sizes of about 2-4 mm in length in a methane flame using a Meker burner. A fixed biomass particle of willow was held by a needle and attached to an R-type thermocouple in a ceramic housing. A Photo-Sonics Phantom V7 high-speed video recorder was used to record the images of the combusting particles upon exposure to the methane flame. The images recorded were analysed to obtain information on the combustion behaviour of the fuels and also to determine duration for volatile and char combustion. Figure 2-36 a) and b) depicts the duration of volatile and char combustion of raw and torrefied willow respectively. The results showed that volatile combustion is shorter and char combustion is longer for torrefied willow compared to that of raw willow. Bridgeman *et al.*[37] reported that generally, the overall duration for complete combustion of torrefied willow upon exposure to the methane flame is higher and this is mainly due to the longer char combustion duration.

Arias *et al.*[106] carried out non-isothermal thermogravimetric analysis of raw and torrefied eucalyptus in air. Figure 2-37 shows the DTG mass loss curves of the raw and torrefied eucalyptus. The DTG curves of the torrefied biomass samples revealed two-well defined peaks, which mainly corresponded to the combustion of cellulose and lignite, while the raw eucalyptus also showed similar peaks with an hemicellulose shoulder peak. The shoulder peak is not found in the DTG peaks of torrefied eucalyptus because of the volatile loss upon torrefaction. The mass loss during the release and combustion of volatile (first stage) decreases with the severity of the torrefaction conditions. However the mass loss increases during char combustion stage (second stage). They also assessed the kinetic parameters of the torrefied samples for both reaction stages and found that the activation energy of the second stage remained

practically unaltered due to the relatively low torrefaction temperatures employed, which prevented the thermal decomposition of the less reactive components of the lignocellulosic biomass [104, 106]. Torrefied fuels are less reactive [133], and researchers suggested that the decrease in reactivity of the torrefied fuels is caused by the accumulation of ash over the char surface which reduces the direct contact of the oxidation media with the carbon and consequently increases the combustion time [134]. However, Fisher *et al.*[135] stated that char reactivity can be affected by how the volatile is removed from the original raw biomass. They suggested that the two major factors controlling char reactivity are volatile matter and porosity. This is in agreement with the work carried out in this is laboratory by Jones *et al.*[133], on the comparison of torrefied biomass combustion to coal.

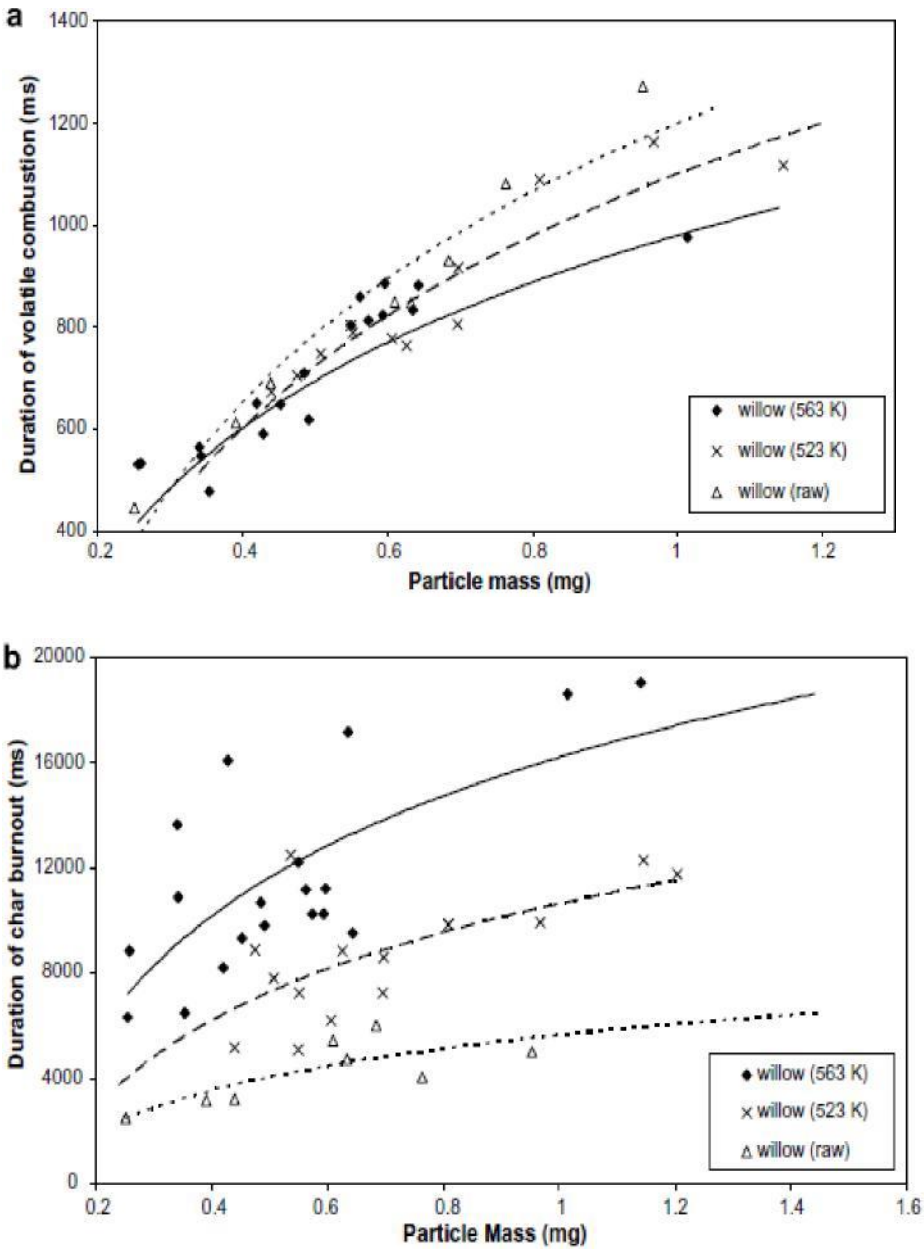

Figure 2-36: Duration of a) volatile combustion and b) char burnout of raw and torrefied willow particles (250 and 290°C) [37].

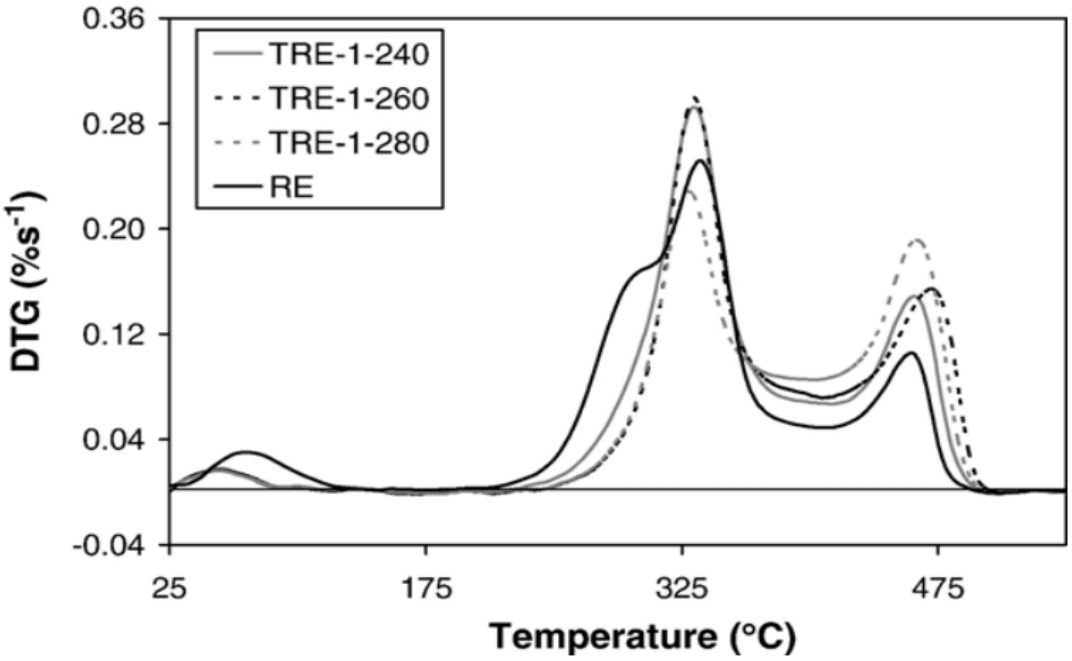

Figure 2-37: DTG curves for combustion of raw and torrefied eucalyptus (torrefied at three different temperatures of 240,260, and 280°C for an hour) samples [106].

2.13 Conclusions

Torrefaction is a promising technology which offers to increase the amount of biomass throughput for energy uses. This chapter shows possible areas where there are research gaps in the torrefaction process and highlights the need for further research in those areas.

Most of the literature focuses on lignocellulose analysis of the untreated biomass samples before torrefaction but fails to track these changes after torrefaction. Different kinetics are expected for different biomass, since the composition of lignin for hardwood, softwood and agricultural residues is not the same, and the content of catalytic metals, particularly potassium, differ. The solid fraction (torrefied fuel) is composed mainly of unreacted cellulose, unreacted lignin as well the as non-volatile byproducts of hemicellulose degradation. Discrete amounts of degradation may occurion the cellulose or lignin during torrefaction, and this has also limited the conclusive characterization of torrified biomass. Thus the solid product, called “torrefied biomass” or “char”, is always the quantity of interest. Also, during

torrefaction, the mass loss mostly results from the decomposition of hemicellulose and the partial decomposition of lignin which mostly depends on torrefaction conditions. Therefore, to optimised the mass and energy balance, there is need to understand how the reaction conditions affects the quality and quantity of products yielded during torrefaction.

Upon torrefaction, the treated fuels become soft and easier to grind depending on the severity of the conditions applied. The effect of torrefaction on the milling behaviour of the fuels is investigated in this project in order to evaluate the performance of grindability behaviour of a biomass fuel since this is one of the factors that determine the amount of biomass that is utilized in power stations. In this thesis, Hardgrove Grindability Index (HGI), was modified and adapted to predict the performance of the grindability behaviour of the untreated and torrefied biomass and also to show the particle size distribution of the fuels after milling. Also, correlations between the HGI_{equiv} and mass yields and energy yields, and the carbon content have been produced.

Condensable and non-condensable products from the torrefaction reaction have been studied in the literature but only a few studies describe how it can be achieved or obtained. This thesis however describes the laboratory methods involved in the collection of liquids. The condensable liquids were characterized to identify various compounds they contained.

Finally, combustion characteristics of the torrefied fuels have been compared to their raw and untreated counterparts. Studies on the combustion behaviour of torrefied biomass in comparison to the raw biomass and coal are emerging in the literature, although most authors focus on the physical and chemical characteristics of the thermally treated biomass. During combustion, raw biomass produces smoke, and can reduce thermal efficiency due to its high moisture content. When substituting coal with biomass, the impact on NOx production during combustion is generally good (i.e. lower), because of the lower nitrogen content in the fuel. However, changes in flame shape, flame temperature, and the gaseous environment in the near and far burner regions, also impact on NOx. Therefore understanding the combustion behaviour and properties of biomass is very important in order to enhance its performance in the

combustion chamber. This will also help in identifying the environmental issues surrounding the burning of torrefied biomass as a potential substitute for fossil fuels.

CHAPTER 3. MATERIALS, EXPERIMENTAL METHODS AND EQUIPMENT

3.1 Introduction

This chapter describes the biomass materials that have been characterised for their different fuel properties along with the methods and equipment used.

3.2 Biomass Samples

The planting of fast growing tree species in Nigeria started in 1913 with the tropical rain forest being the major source of timber supply and energy crops in Nigeria [136]. This rainforest covers 10% of the country's land area with high plant diversity of over 4,600 plant species, and over 560 tree species with a range of 30 to 70 species per hectare for trees ≥ 5 cm diameter at breast height (dbh) [18].

The feedstock studied are four selected Nigerian woods namely G*melina arborea, Terminalia superba, Lophira alata, Nauclea diderrichii and* one abundant agricultural residue; Palm kernel expeller (pke respectively), along with two UK fuels; wheat straw and Miscanthus. The Nigerian fuels were obtained from local sawmaills and supplied by Quintas Renewable Energy Solutions Limited, in chip form with average dimensions of 2.5cm x 2.2cm x 1.1cm as shown in Figure 3-1 while wheat straw and Miscanthus were obtained from farms all around Yorkshire and were of different particle sizes. The Nigerian woody samples were oven-dried at a temperature of 60°C for over two weeks in order to reduce the moisture content to about 12% which prevented biological degradation. The samples were weighed and sealed in a polythene bags to prevent them reabsorbing moisture from the atmosphere prior to the experiments. Figure 3-2 displays PKE and the UK fuels studied.

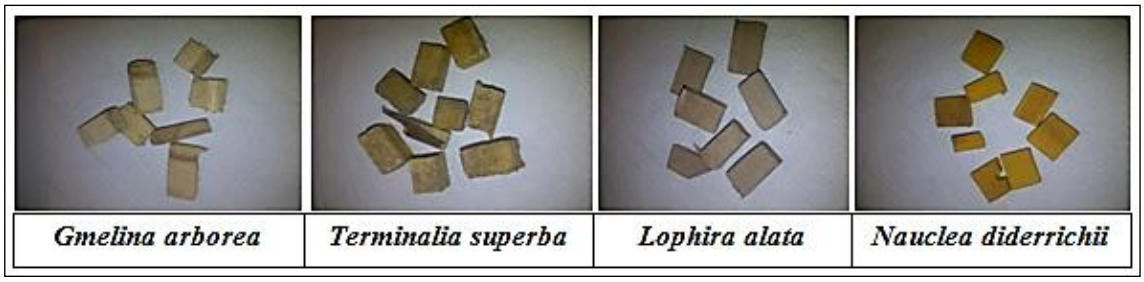

Figure 3-1: The four selected Nigerian wood.

Figure 3-2: The Nigerian agricultural residue and UK fuels.

3.2.1 Gmelina Arborea

Gmelina Arborea belongs to the verbenaceae family and has various common names; Gmelina, Yemane, Kashmir tree, and white teak.

3.2.1.1 Description

Gmelina Arborea which is shown in Figure 3-3 is mostly found in the tropical rain forest in Nigeria, and is a short rotation coppice deciduous, medium-sized tree that grows up to a height of about 30-40m tall. It has a cylindrical bole that is slightly bent to about 80-140cm in diameters and without a support. Its plane, corky or rough bark has a grey to yellowish grey or pale brown colour with many branches [18]. It's grows to a harvestable timber size of 5.8m – 8.3m with a diameter of 10cm – 15cm in about three years. Gmelina has a life span of 30 to 50 years and may exceed $30m^3$ per hectare production every year with good soil conditions, proper care and maintenance. It has high biomass yield, ranging from 83.2 oven dry tonnes ha^{-1} (5 years) to 394.9 oven dry

tonnes ha^{-1} (21 years) and a mean annual biomass increment varied from 16.2 to 20.9 t ha^{-1} yr^{-1} [4]. Its leaves of 10cm – 20cm long, 7cm – 13cm wide are opposite and seasonal. Gmelina has been considered to be highly favoured in plantations due to its adaptability to a wide range of soil and climatic conditions. The extensive range of site and environmental conditions that Gmelina tolerates, together with its fast growth rate, ease of propagation from seeds and cuttings, good coppicing and short rotation, has contributed to its success in plantations[137, 138]. The wood of Gmelina arborea has a specific gravity of 0.42–0.64 and a relative high heating value [4].

3.2.1.2 Uses

Gmelina is manly used for pulpwood production due to its high yield of craft pulp and low chlorine yield. Its wood is used in making musical instruments and for boat decking, general carpentry, woodwork, furniture, and other household products. Its wood is also used as fuelwood and charcoal with an energy yield of 18-20 MJ/kg [138]. Its seeds, bark, leaves, and fruits are medicinal and can also be used to cure fever, wounds, ulcer, leprosy, blood diseases, etc.[138].

3.2.1.3 Distribution

Gmelina Arborea is originally from India and Burma, and has a natural distribution extending from the Himalayan in Pakistan to Nepal, Cambodia, Thailand, Vietnam, and southern provinces of China [139]. Plantation of Gmelina is found in tropical areas of Africa, Asia and America. It is planted in many tropical Africa countries such as Senegal, Gambia, Sierra Leone, Côte d'Ivoire, Mali, Burkina Faso, Ghana, Nigeria, Cameroon and Malawi with an area estimate of 130,000 ha [140]. In Nigeria, *Gmelina arborea* can be found in Oke-Awon (south-west) between latitude 09°07'N and longitude 04°55'E [138].

Figure 3-3: SEM images of *Gmelina arborea* showing (a) 3-yr old (b) wood in transverse section [140].

3.2.2 Terminalia Superba

The common names of Terminalia Superba are Limba, white afara, shinglewood, white mukonja, and Congo walnut and the tree belongs to the combretaceae family.

3.2.2.1 Description

Terminalia Superba as shown in Figure 3-4 is a deciduous, medium-sized tree that grows up to an average height of about 45-50 m tall. The tree has a branchless bole whose height is 30 – 35m. It is typically straight and cylindrical, up to 120–150 cm in diameter, with large, fairly thick, long flat supports up to 5–8m high. The bole diameter could possibly reach 50cm in 20 years. Its bark is characterised with a smooth surface and its leaves are normally plain, opposite and deciduous, leaving scars on twigs when shed. The petiole which is the stalk attaching the leaf blade to the stem is 3-7cm long. It also has a shallow root system and its taproot often disappears with age. It has sessile, small and greenish-white flowers, which are usually associated with 7-18cm long spikes. Its fruit is described as small, transversely winged, sessile, golden-brown smooth nut, 1.5-2.5 x 4-7 cm (including the wings). The average density of the wood is 480-650 kg/m^3 at about 12% moisture content [141].

3.2.2.2 Uses

The wood is generally used for interior joinery, doors, mouldings, furniture, office-fittings, crates, matches, veneer and plywood, light construction, light flooring, ship

building, interior trim, vehicle bodies, sporting goods, toys, novelties, musical instruments, food containers, vats, turnery, hardboard, particle board and pulpwood. In the rural part of Nigeria, the wood is also used as firewood and for charcoal production. The bark of the tree is identified with a yellow dye which is used to dye fibres for matting and basketry. The bark of the tree is among the trees in Nigeria that are used for traditional medicine to treat wounds, sores, haemorrhoids, diarrhoea, dysentery, malaria, vomiting, gingivitis, bronchitis, aphthae, swellings and ovarian troubles, and as an expectorant and anodyne.

3.2.2.3 Distribution

Terminalia Superba grows well on rich, well-drained alluvial soils, and is widely distributed across many countries such as Angola, Benin, Cameroon, Central African Republic, Congo, Cote d'Ivoire, Democratic Republic of Congo, Equatorial Guinea, Gabon, Ghana, Guinea, Liberia, Nigeria, Sierra Leone, Togo, Argentina, Bolivia, Brazil, Burkina Faso, Chile, Colombia, Costa Rica, Ecuador, Fiji, French Guiana, Guatemala, Guyana, Honduras, Indonesia, Kenya, Malaysia, Mexico, Nicaragua, Niger, Panama, Paraguay, Peru, Philippines, Solomon Islands, Surinam, Tanzania, Uganda, Uruguay, US, Venezuela, Zimbabwe [141]. In Nigeria, it can be found in Gambari Forest Reserve (7° 23'N, 3°33'E) in Oyo State of south-western Nigeria [142]. *Terminalia* seed is easily collected between July and September in Nigeria. Direct sowing of *Terminalia superba* is not effective, as common practice involves raising nursery stock.

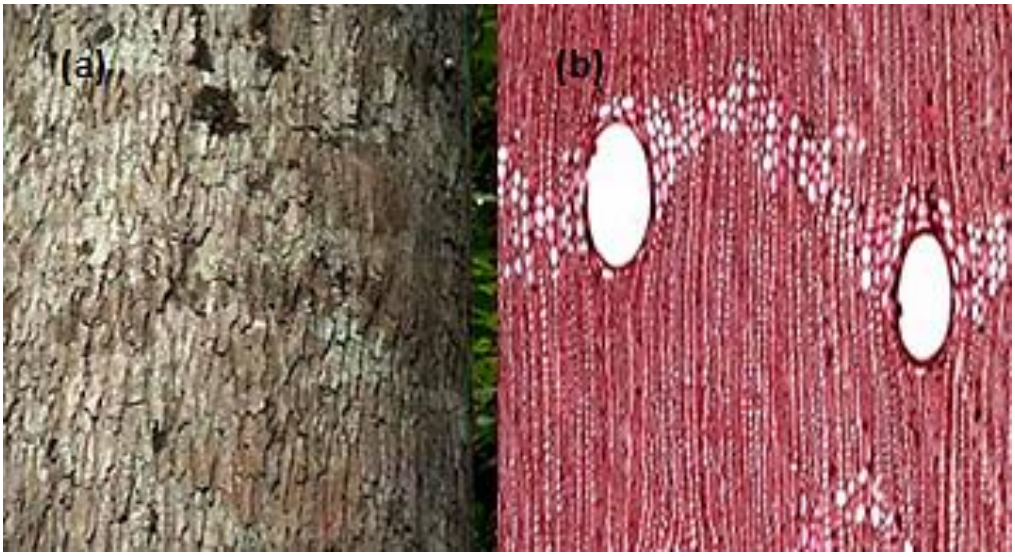

Figure 3-4: Photographic and SEM images of *Terminalia superba* showing (a) the bark (b) the wood in transverse section[141]**.**

3.2.3 Lophira Alata

Lopira Alata belongs to the ochnaceae family and has various common names; Azobé, Ekki, and Red ironwood [141].

3.2.3.1 Description

Lophira Alata shown in Figure 3-5 is a deciduous tree found in the freshwater forest and grows up to a height of about 36-46m with a branch-free trunk of 21m and a diameter of up to 1.8m [143]. The tree has swollen, superficial and spreading roots which are visible for several metres. Its leaves clustered at the ends of its branches with a petiole of 0.5–2.5 cm long. Lophira is considered to be a vulnerable and endangered species [144] and has a strongly scented flowers. The wood is assessed to be very heavy and hard with a density of 1010–1150 kg/m^3 at 12% moisture content [145].

3.2.3.2 Uses

The wood is used for underwater constructions, heavy construction work, bridges, heavy-duty flooring, fuel wood and it produces an excellent charcoal. It is used in Africa as a medicine for treatment of snake bite, leprosy, cough, fever, jaundice, sleeplessness, respiratory diseases, yellow fever, dysentery, amongst others [145].

3.2.3.3 Distribution

It is widely distributed in the freshwater forest of Sierra Leone, Liberia, Ivory Coast, Ghana, Nigeria, Cameroon, Angola and Congo. It is found in the Niger delta flood plain of large coastal rivers of Nigeria i.e. at the coast of Osun, Ogun and Osse rivers [143].

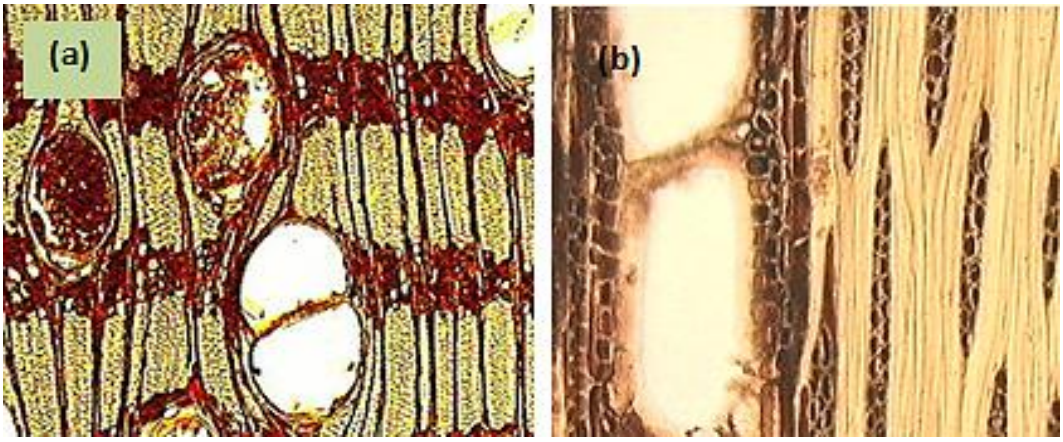

Figure 3-5: SEM images of Lophira alata showing (a) transverse section (b) tangential section [146].

3.2.4 Nauclea Diderrichii

Nauclea diderrichii belongs to the Rubiaceae family with common names; Brimstone tree and African peach.

3.2.4.1 Description

Nauclea diderrichii as shown in Figure 3-6 is a deciduous, evergreen tree with a mean tree diameter at breast height (dbh), total height and stand bole volume ranged from 9.6 to 29.3 cm; 9.0 to 23.6 m and 23.27 to 535.52 m^3/ha, respectively while total above ground biomass varied from 32.5 to 287.5 t/ha between 5 and 30 years [147]. Its bole is identified to be slim, straight, cylindrical, and branchless, an average between 20-30 m and a broad spherical crown with thick foliage. The shiny leaves are about 15 cm in length, and longer when young. Its flowers are branded as small, green-white-yellow and tubular with a width of 3 cm, while its stalks are just about a centimetre.

3.2.4.2 Uses

The wood is used in Africa for carving mortars, mine props, furniture, drums, poles, doors, tools, heavy construction, heavy flooring, joinery, interior trim, boat building, vehicle bodies, railway sleepers, sporting goods, toys, novelties, agricultural implements, draining boards, turnery and sliced veneer. In Nigeria, it is used as fuelwood and also for charcoal production. It is also used for medicinal purposes [148].

3.2.4.3 Distribution

The tree can be found in the humid tropical rainforest of Nigeria is one of the known trees in the early stage of forestry practice in Nigeria. It is one of the few indigenous trees that were successful under plantation management. Forest commission of Nigeria [20], considered *Nauclea* to be vulnerable and endangered. They stated that the continued existences of this tree species were threatened due to exploitation since the 19^{th} century. In order to ensure regeneration of this species, attention has been directed towards plantation of this tree species recently and large success is recorded in Oluwa and Omo forest reserves, with establishment of about 1,354ha plantations of *Nauclea* [147]. It can also be found growing in Angola, Benin, Cameroon, Central African Republic, Chad, Congo, Cote d'Ivoire, Democratic Republic of Congo, Gabon, Ghana, Liberia, Sierra Leone, Togo and Uganda [147].

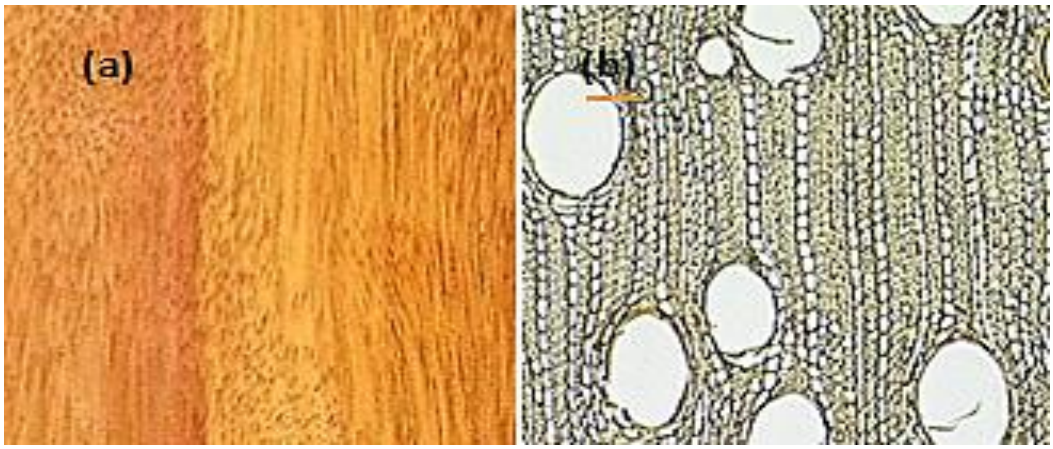

Figure 3-6: SEM images of *Nauclea Diderrichii* showing (a) wood surface (b) transverse section [148].

3.2.5 Palm Kernel Expeller (PKE)

PKE also known as palm kernel shell (pks) as shown in Figure 3-7 is the hard endocarp of palm kernel fruit that surround the palm kernel seed of the oil palm tree (*Elaeis guineensis*). PKE is the by-product produced when crushing of the kernel is done to remove the palm seed after the production of palm kernel oil. During the extraction of oil from palm, several by-products such as, solid residues and liquid wastes are produced. The by-products include fronds, trunks, empty fruit bunches (EFB), mesocarp fiber and PKEs as shown in the process flow diagram for a palm oil mill in Figure 3-8 [149].

3.2.5.1 Description

The oil palm is a perennial crop that originated from West Africa. Presently the world's largest producer and exporter of palm oil is Malaysia replacing Nigeria as the main producer since 1971 [150]. It flourishes to about 9 metres in height and is usually identified with a crown of feathery leaves that are up to 5 mm long [151]. Flowering is characterised with the growth of cluster of egg-shaped red, orange or yellowish fruits, each about 3 cm long. Oil palm cultivates in the lowlands of the humid tropics within 15°N and 15°S where there is abundant of rainfall (1,800-5,000 mm/year). The plantation acclimatises to soil conditions with a low pH, but equally sensitive to high pH (>7.5) and to non-flowing water It requires a climatic condition with relative humidity of not less than 75% and a temperature range of between 17 to 28°C [152].

3.2.5.2 Uses

The by-products and residues of the oil palm are of high economical potential. PKE is highly rich in protein and fibre content. Also, it has high energy value which makes it suitable for both an animal feed and for energy purposes. Most of the palm residues that have been co-fired in the UK are imported from Malaysia and Indonesia (UK Biomass Strategy, May 2007). The PKE studied here which is shown in Figure 3-2 was supplied by RWE npower in a pulverised form.

Figure 3-7: Palm kernel expeller [149].

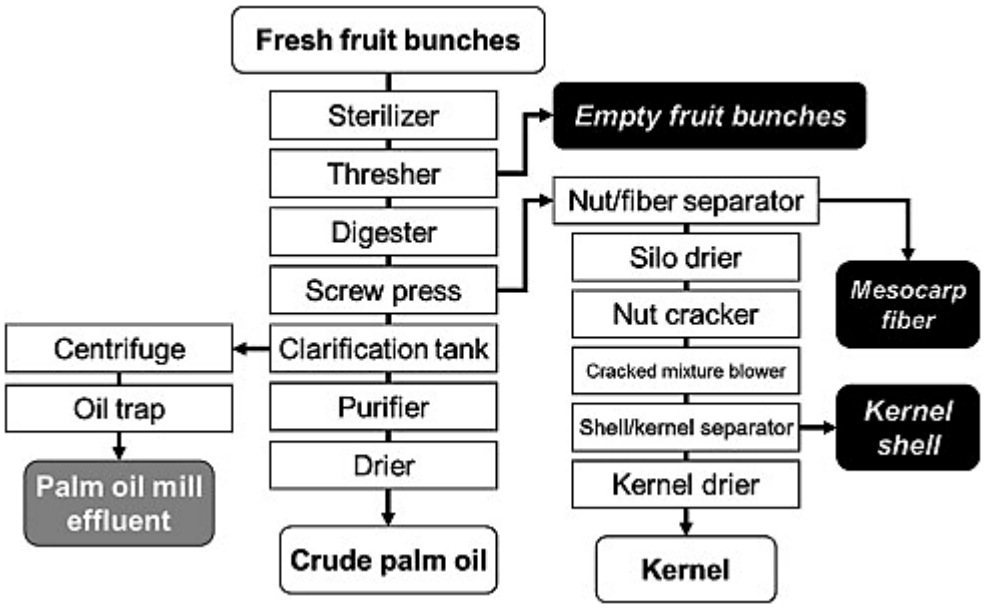

Figure 3-8: Process flow for palm oil mill [149].

3.2.6 Miscanthus

Miscanthus x giganteous species as shown in Figure 3-9 are woody, perennial and rhizomatous grasses that originated from from Asia, and have the potential for rapid rates of growth. *Miscanthus* is grown in spring and once planted, is able to remain in the ground for at least fifteen to twenty years. New shoots develop around March each year and develop rapidly in June/July producing bamboo like canes. During the autumn/winter season, *Miscanthus* withers, the leaves shrivel, and this organic matter serves as nutrients to the soil. This leads to the harvest of its canes in winter or early

spring of the following year. This growth pattern is cycled every year for the lifetime of the crop, which is about 15 to 20 years [153].

Miscanthus grows well on different type of soil but with optimum yields from soil having pH value between 5.5 - 7.5 [153]. Its growth rate also depends on the amount of sunshine, temperature and water available and changes in the climatic conditions affect the annual yields of the crop.

Figure 3-9: Mature stand of *Miscanthus* [153].

3.2.6.1 Uses

Miscanthus is used in the European Union as a commercial energy crop, as a source of heat and electricity, or processed into biofuel products. Research trials are conducted all around the world and are making progress on the use of *Miscanthus* as a source of biomass for the production of energy in cofiring activities or conversion for biofuel production.

3.2.7 Wheat straw

Wheat Straw as shown in Figure 3-10 is the agricultural waste that remains after the wheat grains and chaff are extracted from the crops. It is usually collected and stored in a straw bale which is a bundle of straw tightly fastened with twine or wire. Straw accounted for about half of the yield of cereal crops such as barley, oats, rice, and wheat. It is used for production of biofuels, livestock bedding and fodders, thatching and basket-making.

Figure 3-10: Wheat Straw

3.3 Sample Preparation and Sizes

The samples were reduced to smaller size fraction using a Retsch Cutting Mill SM100 (Figure 3-11a) and milled further using the Retsch PM100 planetary ball mill (Figure 3-11b) with stainless steel milling cup and balls (Figure 3-11d). The milled fractions were sieved using a stack of sieves and using a Retsch mechanical sieve shaker AS 200 Basic (Figure 3-11c). Different particle sizes ranging from < 53µm to < 1180 µm were collected and stored.

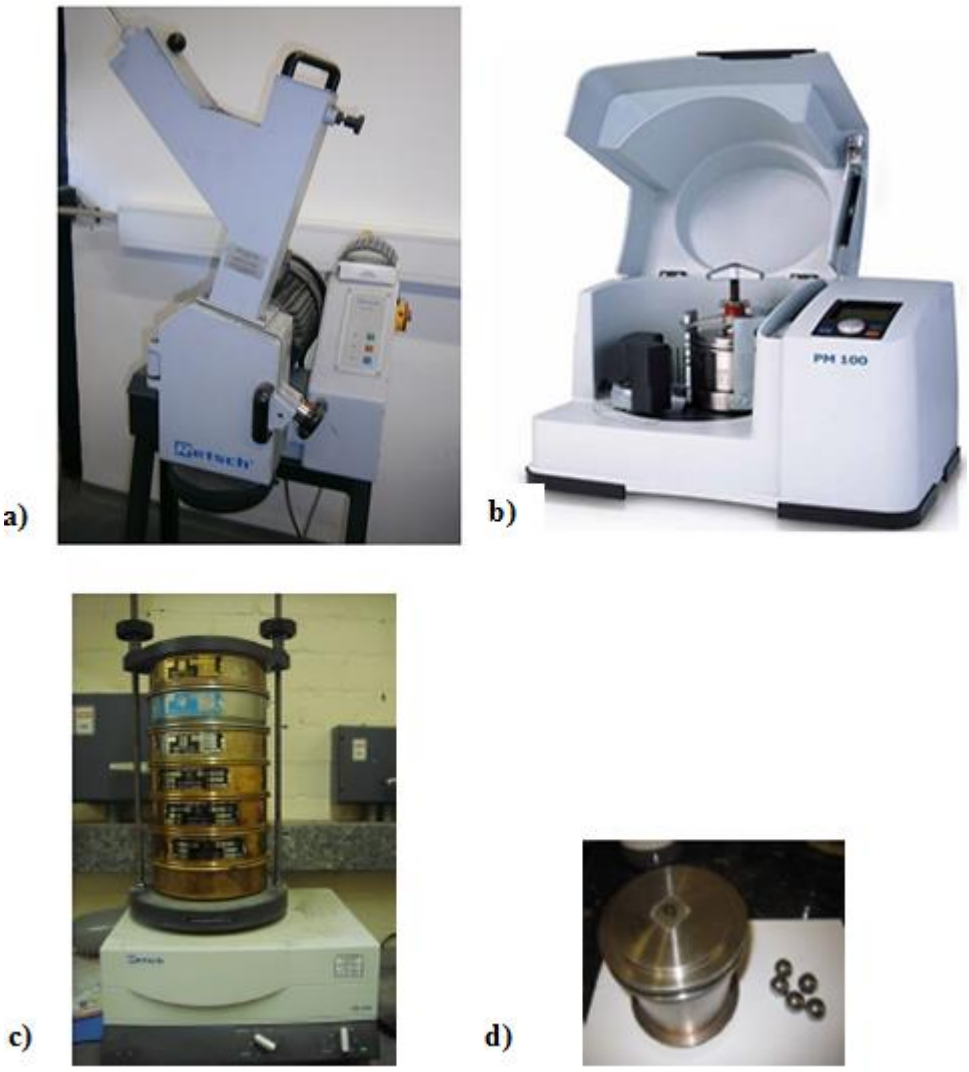

Figure 3-11: Retsch cutting mill SM 100, b) Retsch PM 100 ball mill, with 250 mL & 500 mL milling cups, c) Stack of sieves of 600, 355, 212, 150, 75 and 53 µm meshes on an Retsch Mechanical Sieve Shaker AS 200 Basic for particle size distribution experiment and d) Stainless steel milling cup and steel balls.

3.4 Proximate Analysis using British Standard Methods

The determination of moisture, volatile matter and ash content were carried out using British standards BS EN 14774-1:2009 for moisture, BS EN 14775:2009 for ash and BS EN 15148:2009 for volatiles. The reproducibility for the proximate analyses was ≤0.2%. Approximately 1g of each sample (particle size < 600 µm) was used for each analysis and was carried out in duplicate. The mean values were taken for further analysis. Determination of moisture was carried out in a Carbolite MFS oven, volatile matter

determination was carried out in a Carbolite VMF (+PID/CHIM) furnace and ash content determination was carried out using a Carbolite OAF 10/1 furnace.

3.4.1 Moisture Content Analysis, M_{ad}

Approximately 1 g of sample with particle size less than 600µm was added into a weighing dish in an even layer and this was then weighed together with its lid to the nearest 0.1 mg. The dish (uncovered) with the lid was heated separately in the Carbolite MFS oven, at (105± 2) ℃ for 3 hours. Immediately after drying, the lid was replaced while the dish is still in the oven. The dish plus residue with the lid on was transferred into the desiccator to allow cooling at the room temperature and then reweighed.

M_{ad} is expressed as percentage by mass and calculated using the formula equated below:

$$\mathbf{M_{ad}} = \frac{(m_2 - m_3)}{(m_2 - m_1)} * 100\ \% \qquad \text{Equation 3-1.}$$

Where,

m_3 is the mass of the dish plus lid and sample after drying,

m_2 is the mass of the dish plus lid and sample before drying and

m_1 is the mass of the empty dish and the lid.

3.4.2 Volatile Matter Content, V_d

Approximately 1 g of sample with particle size less than 600µm was added into a crucible in an even layer and this was weighed with its lid to the nearest 0.1mg. The covered crucible was then heated in a Carbolite VMF (+PID/CHIM) furnace at (900±10) ℃ for seven minutes. The dish plus residue with the lid was transferred into the desiccator to allow cooling at the room temperature and then reweighed.

$\mathbf{V_d}$ is expressed as percentage by mass on a dry basis and calculated using Equation 3-2: below:

$$\mathbf{V_d} = \left[\frac{100\,(\boldsymbol{m_2} - \boldsymbol{m_3}) - M_{ad}}{(\boldsymbol{m_2} - \boldsymbol{m_1})}\right] * \left(\frac{100}{100 - M_{ad}}\right) \qquad \text{Equation 3-2}$$

Where,

m_3 is the mass of the dish crucible plus lid and sample after heating

m_2 is the mass of the crucible plus lid and sample before heating

m_1 is the mass of the empty crucible plus lid and

M_{ad} is expressed as the percentage moisture content of the test sample used for determination.

3.4.3 Ash Content, A_d

Approximately 1 g of ground sample with particle size less than 600 µm was added into a crucible in an even layer and this was weighed to the nearest 0.1mg. The crucible was then heated in a Carbolite OAF 10/1 furnace at 250 ℃ for 60 minutes and raised to (550± 10) ℃ for another 2 to 3 hours. At the end, the crucible is allowed to cool and then weighed.

$\mathbf{A_d}$ *is* expressed as percentage by mass on a dry basis and calculated using Equation 3-3 below:

$$\boldsymbol{A_d} = \left|\frac{(m3 - m1)}{(m2 - m1)}\right| \times 100 \times \left|\frac{100}{(100 - M_{ad})}\right| \qquad \text{Equation 3-3.}$$

Where,

m_3 is the mass of the dish and sample after ashing

m_2 is the mass of the dish plus sample before ashing

m_1 is the mass of the empty dish and

$\mathbf{M_{ad}}$ is expressed as the percentage moisture content of the test sample used for determination.

3.4.4 Fixed Carbon Content, *FCC*

The fixed carbon content was calculated on a dry basis, by subtracting the sum of the ash and volatile matter contents (both on a dry basis) from 100% using Equation 3-4 below:

$$\% \, FCC = 100\ \% - (\%\ A_d + \%\ V_d) \qquad \text{Equation 3-4.}$$

3.5 Proximate analysis using the Thermogravimetric Analyser (TGA)

The determination of moisture, volatile matter and ash content was also obtained from pyrolysis and combustion tests using a TGA Q5000 analyser (Figure 3-12) by heating the sample (less than 53 µm) from room temperature to a final temperature of 900 ℃ at 10 ℃ min^{-1} under nitrogen with a holding time of 10 min. After which, the gas was switched to air in order to obtain the ash content. Figure 3-13 shows how data for moisture, volatile, fixed carbon and ash contents can be assessed and obtained from the analysis.

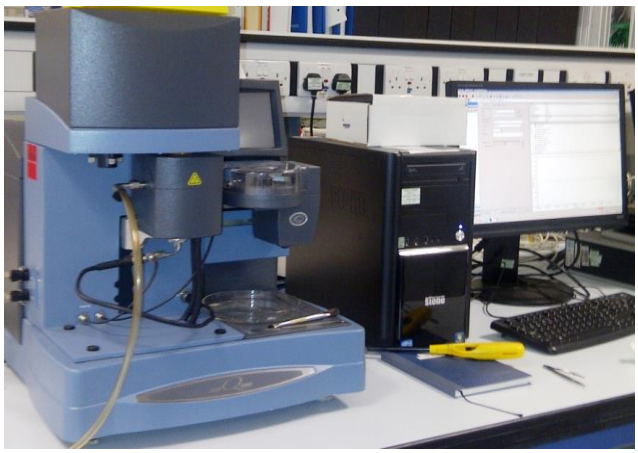

Figure 3-12: TA Instruments TGA Q5000.

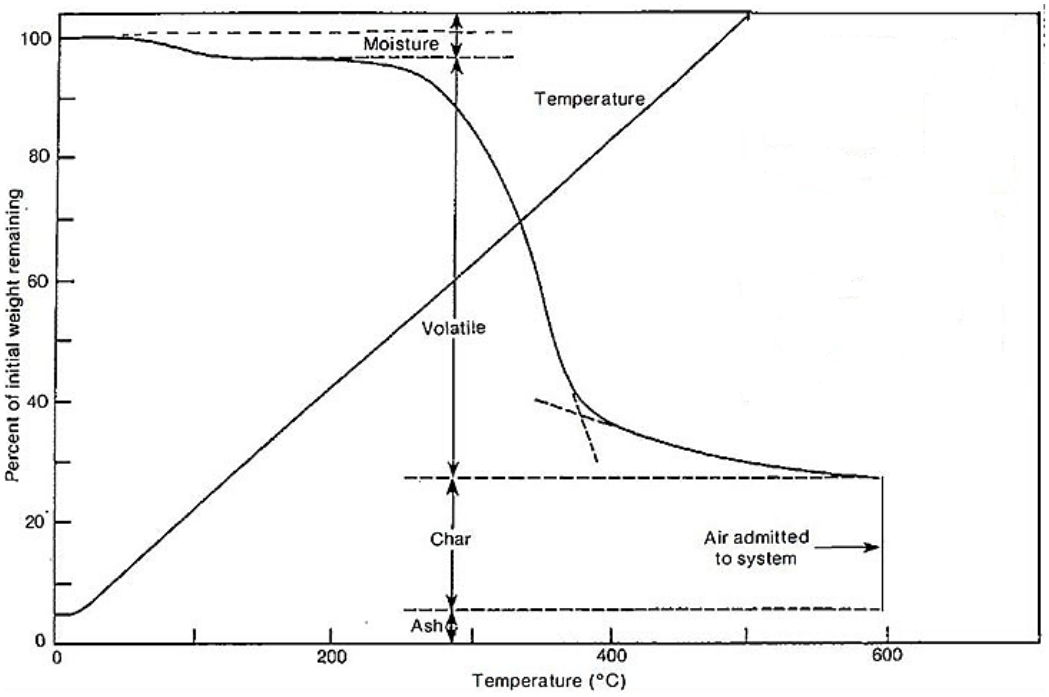

Figure 3-13: A typical diagram of a thermogravimetric analysis of a biomass **[154]**.

3.6 Ultimate Analysis

The elemental composition, C, H and N contents of the samples were measured using a CE Instruments Flash EA 1112 Series elemental analyser as shown in Figure 3-14. Approximately 3-4mg of Samples with particle size < 600 µm was wrapped in tin capsules and dropped into the chamber inside the analyser. The sample was combusted in the chamber to produce CO_2, water vapour and nitrogen, and separated into a chromatography column. Each quantity was detected using a thermal conductivity detector and compared with standards to determine the percentage of carbon, hydrogen and nitrogen. The standards used in this project were 2, 5 – (Bis (5-tert-butyl-2-benzo-oxazol-2-yl) thiophene (BBOT) and Oatmeal. The measurements were performed in duplicate and the mean values are reported. The weight percentage of measured elements (C, H, N,) were recalculated on a dry ash free basis Wt_{daf}% using Equation 3-5, and weight percentage of oxygen was calculated by difference (on a dry ash free basis) in Equation (3-6).

$$Wt_{daf}\,\%\ \text{element} = \frac{\text{measured,wt\% element}}{100 - ash,wt\ \% - M_{ad}\ \%} \times 100 \qquad \text{Equation 3-5.}$$

$$Wt_{daf}\ \%\ \mathrm{O} = 100\ \% - (\ \mathrm{wt\%\ C} + \mathrm{wt\%\ H} + \mathrm{wt\%\ N}) \qquad \text{Equation 3-6.}$$

The relative error for the analysis of C was in the range of 0.1−1.8%, but for H and N, the relative error was ≤0.2%.

Figure 3-14: CE Instruments Flash EA 1112 Series elemental analyser.

3.7 Calorific Value

Friedl *et al* [155] used a data containing 154 grouped of biomass samples to develop a correlation between heating values of biomass and elemental composition. They described calorific value of a biomass as the heat released by complete combustion of unit mass of fuel. The determination of C, H, N, S, Cl, ash and high heating values (HHV) were carried out as suggested by Friedl *et al.*[155]

A method using two equations to estimate HHV (dry basis) based on C, H and N contents were then produced: an ordinary least squares regression (OLS) and a particle least squares regression (PLS) method as displayed in Equations (3-7) and (3-8) respectively:

$$HHV\ (OLS) = 1.87C^2 - 144C - 2802H + 63.8CH + 129N + 20147 \quad \text{Equation 3-7.}$$

$$HHV\ (PLS) = 5.22C^2 - 319C - 1647H + 38.6CH + 133N + 21028 \quad \text{Equation 3-8.}$$

C, H and N contents were expressed on a dry basis in terms of wt % and the units were in KJ /Kg. The results indicated that the use of both models for assessing HHV gave nearly the same performance. Hence, the average of both HHV was used to create a final model for the determination of the calorific value of a biomass, as equated in Equation (3-9):

$$HHV = 3.55C^2 - 232C - 2230H + 51.2C \times H + 131N + 20{,}600 \quad \text{Equation 3-9.}$$

The standard error of calibration for this model was 337 kJ kg^{-1} and the linear correlation coefficient R^2 is 0.943. Bridgeman *et al.*[93] used this correlation for torrefied willow and found that small inaccuracies could occur due to the high carbon content of the torrefied fuel. Therefore, in their study, HHV values were further measured using the bomb calorimetry analysis to validate the estimated values. This generated the need for further validation of torrefied fuels with carbon contents greater than 50.5% (dry basis) and the measurements were comparable with differences between the values of 300 to 600 kJ kg-1 (Table 3-1).

Table 3-1: Calculated and measured HHV for different conditions of torrefied willow [93].

Sample	Condition		% Carbon content	HHV kJ kg^{-1} (dry basis)		
	T (°C)	t (min)	(daf basis)	Calculated	Measured	Differences
Willow A	290	10	56.5	22400	21800	600
Willow B	230-250	60	54.3	21400	21000	400
Willow D	290	60	60.3	23900	23600	300

Here, high heating values (HHV) of raw and torrefied biomass fuels were assessed using the formula suggested by Friedl *et al.*[155], using Equation (3-9), and were also determined experimentally using bomb calorimeter.

3.8 Ash Metal Analysis

Ash analysis was done at TES Bretby Ltd, UK. The ashes were prepared according to the British standard method described in Section 3.2.3. Approximately 0.25g of the ash was dissolved in nitric acid in a digestion tube. The solution was whirl mixed and kept at room temperature for 2 hours before being placed in a heating block and incubated overnight. Following acid digestion, 5ml of 25% hydrochloric acid was then added and the sample was heated to 80^{o}C before analysing it using inductively coupled plasma spectrometry (ICP) with mass spectrometric detection. The metal contents determined were converted to theoretical weight percent oxides.

3.9 Ash Fusion Test

An ash fusion test was carried out in a Carbolite digital ash fusion furnace (Figure 3-15) with a camera (black and white) fixed on it to capture the different phases of the ash when being heated up under a controlled heating rate in an oxidizing environment. Ash was prepared repeatedly to obtain sufficient quantity of ash using the British standard method described in Section 3.4.3. The ash was then ground in an agate mortar to ensure homogeneity of ash samples. About 2-3 drops of deionised water was added to the ash to make an ash paste. The ash paste was then pressed into an upright petroleum jelly coated cylindrical stainless steel mould for easy removal of the moulded ash. The test pieces were removed from the mould after drying for at least an hour. Extra measures were taken to ensure that the edges and top of the test pieces were not damaged. The test pieces were then covered and left overnight to dry. The furnace was heated to 550 ^{o}C the next day and the test pieces were supported and moved in to the furnace inch by inch in order to prevent thermal shock. The ash test pieces were then heated to 1500 °C at 7 °C/min heating rate and at a gas flow rate of 50ml/min. Images were collected by the camera at every degree of temperature rise between 550 °C and 1500 °C. The images captured at different temperature were analysed to determine key phase temperatures i.e. shrinkage starting temperature (SST), deformation temperature

(DT), hemisphere temperature (HT) and flow temperature (FT) as shown in Figure 3-16 using British standards DD CEN/TS 15370-1:2006.

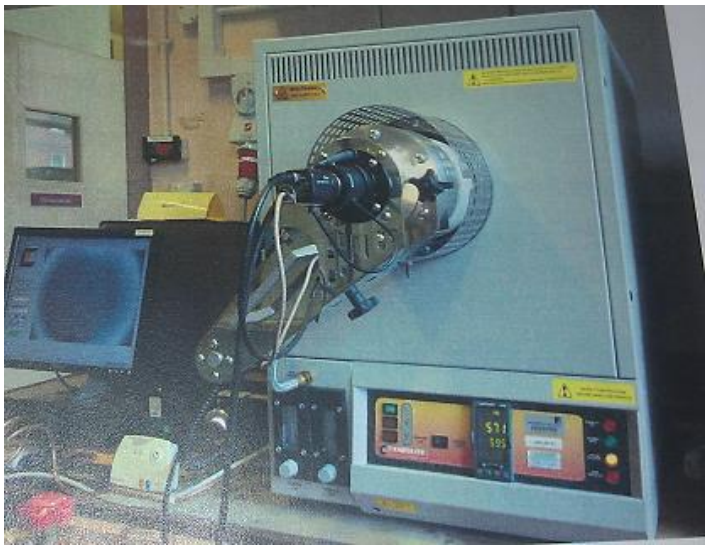

Figure 3-15: Carbolite Digital Ash Fusion Furnace

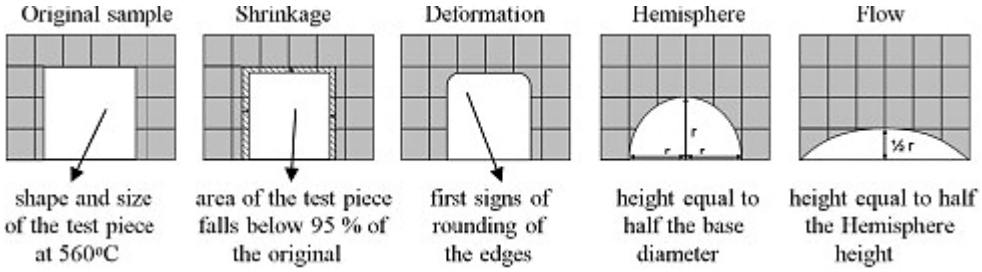

Figure 3-16: Phases in the ash melting process.

3.10 Biochemical Composition

The biochemical composition of the biomass samples were determined using wet chemical methods as in Section 3.10.1.

3.10.1 Analytical Determination of ADL, ADF and NDF

Determination of lignocellulosic fractions of the fuels was carried out at IBERS Analytical Chemistry Laboratory at the University of Aberystwyth, UK. The

gravimetric measurements of Neutral Detergent Fibre (NDF), Acid Detergent Fibre (ADF) and Acid detergent Lignin (ADL) were made using refined versions of Van Soest's methods [156] using the Gerhardt fibrecap system. In summary, the NDF, which is taken as the total cell wall, is the residue, corrected for ash, left after refluxing for 1 h in a neutral buffered detergent solution. ADF, is the ash corrected residue remaining after refluxing the samples in a solution of Cetyl Ammonium Bromide (CTAB) in 2 M sulphuric acid and is a measure of cellulose and lignin only. ADL was assessed by treating ADF with 72% sulphuric acid to disolve the cellulose to determine crude lignin. Ash was assessed in the samples after heating at 600°C in a muffle furnace for at least 4 h. The concentration of hemicelluloses and cellulose were calculated according to Equations (3-10) and (3-11) respectively.

$$\% \text{ Hemicellulose} = \% \text{ NDF} - \% \text{ ADF} \qquad \text{Equation 3-10.}$$

$$\% \text{ Cellulose} = \% \text{ ADF} - \% \text{ ADL} \qquad \text{Equation 3-11.}$$

3.11 Grindability Test

The British Standard for Hardgrove Grindability Index (HGI) BS 1016-112:1995 is usually used to determine the milling behaviour of coal but not biomass. In order to be able to compare the grindability properties of the biomass with coal, a modified version of the Hardgrove Grindability Index (HGI) was used, as described in Bridgeman *et al.*[93]. The method was modified to give an "Equivalent HGI", HGI_{equiv}. The modified method entails using a fixed volume of biomass or coal sample (50 cm^3) instead of having a fixed weight (50g) [93].

3.11.1 Calibration of Retsch PM 100 Ball Mill using the 250 mL Stainless Steel Milling Cup

The grinding of the fuels was accomplished using a Retsch PM100 ball mill which is shown in Figure 3-11b. In order to establish the optimum operating conditions for the fuels, preliminary milling tests were carried out using standard reference coals of HGI 26, 49, 69 and 94, and biomass (raw and torrefied). The mill was then re-calibrated with the coals to allow a comparison between the fuels as described in Bridgeman *et al.*[93].

The operating procedure involved using the Retsch cutting mill SM 100 (Figure 3-11a) that had a 4 mm screen mesh for milling each of the standard reference coals.

The coal was then separated into different size fractions using a stack of 1180µm and 600µm sieve meshes using a Retsch mechanical Sieve Shaker AS 200 Basic (Figure 3-11c) at amplitude of 90 for 5 min. After which a measuring cylinder was then used to measure out a volume of 50 cm^3 with an accuracy of ± 0.1 cm^3 of the coal collected on the 600 µm sieve, and transferred to a 250 mL stainless steel milling cup containing 15 numbers of stainless steel ball (the diameter of the steel ball is 20mm), and then ground for 2 minutes at a speed of 165rpm. The coal was then removed from the milling cup and sieved again using a 75 µm sieve and shaken at the same operational settings (amplitude and time) on the sieve shaker. The process was repeated for the rest of the coal and biomass studies, and also the amplitude setting on the sieve shaker and the time taken to sieve during this experiment were uniform for comparison purposes. The mass of sample, *m that* passed through 75µm sieve was calculated using Equation 3-12.

$$m = m_v - m_1 \qquad \text{Equation 3-12.}$$

where m_v is the original mass of 50cm^3 coal or biomass sample and m_1 is the mass of coal or biomass sample retained in the 75µm sieve.

This experiment was repeated twice for each sample, or more (if mass loss was assessed to be over 0.5g), depending on the consistency of the results and an average and standard error were calculated from the results. The mass percentage of sample that passed through a 75µm sieve is plotted against the HGI values for the four reference coals and is shown in Figure 3-17.

The linear fit was then used to assess the equivalent HGI of the samples and is interpreted in Equation (3-13) below as:

$$HGI_{equiv} = \frac{(m - y\ intercept\ of\ the\ calibration\ curve)}{slope\ of\ the\ calibration\ curve} \qquad \text{Equation 3-13.}$$

The plot showed a good correlation coefficient R^2 value of 0.97 and from the equation of a straight line, y = 0.1746x - 0.8258 which was also derived from the plot, the HGIequiv of all samples were obtained using the equation (3-14) below:

$$HGI_{equiv} = \frac{m+0.8258}{0.1746} \qquad \text{Equation 3-14.}$$

Where m is the amount (in %) of sample that passed through 75 micron sieve.

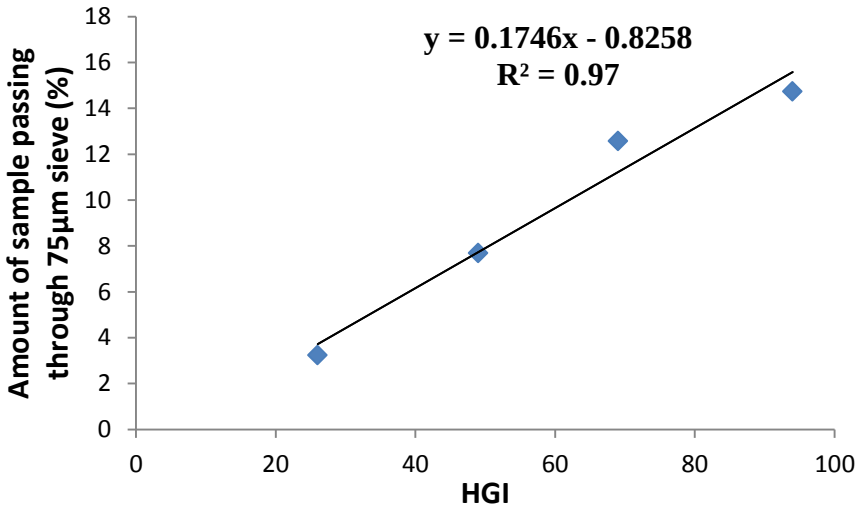

Figure 3-17: Calibration curve from four standard reference coals of HGI 26, 49, 69 and 94 for a Retsch PM100 ball mill.

3.11.2 Particle Size Distribution

The particle size distribution profiles for the biomass samples were compared with the reference coals to have a deeper understanding into their grindability behaviour, using the method described in Bridgeman *et al.*[93]. The procedure is almost similar to the one described in Section 3.11.1. Here a volume of 50cm^3 of the sample which was collect on the 600µm sieve is weighed out and transferred into a 250ml stainless steel milling cup containing 15 stainless steel balls of 20mm in diameter and then ground for 2 minutes at a speed of 165rpm. The sample was emptied from the milling cup and separated using a series of sieves of different mesh sizes 600, 355, 212, 150, 75 and 53µm using a sieve shaker for 5 minutes as stacked in Figure (3-11c). Finally, the mass

of sample retained in each sieve was measured and calculated as a percentage of the original sample mass, also using average particle size of the sample collected on each sieve as the mid-point between two consecutive sieves, a plot of the particle size distribution was obtained. This was then plotted together with the four reference standard coals for comparison purposes.

3.12 Thermogravimetric Analysis (TGA) and Burning Profile

3.12.1 TGA Pyrolysis and Combustion Studies

The slow pyrolysis and combustion of samples were carried out using a TA Instruments TGA Q500 which is shown in Figure 3-12. Approximately 2-3mg of each sample was placed in the microbalance and heated at a rate of 10ºC/min from room temperature to 700ºC in a purge of nitrogen at a flow rate of 50 ml/min. The pyrolysed sample was allowed to cool to a temperature ~40°C before heating up again at 10°C min^{-1} to 900ºC under a constant flow of air (50 ml/min) to obtain the char burning profile. The TA Instruments TGA Q500 was connected to a PC which stores data from the experiment. Differential thermogravimetric analysis (DTG) was assessed by plotting the rate of decomposition of a sample against temperature and the maximum peak temperatures for pyrolysis and combustion were obtained.

3.12.1.1 Pyrolysis Kinetics

The kinetics for pyrolysed samples were assessed in order to obtain the reaction mechanism using data obtained from the TGA in Section 3.12.1. The reaction was assumed to follow first order reaction mode, hence the Arrhenius function as shown in Equation 3-15 was used to assess the pre-exponential factors, A (s^{-1}) and activation energies, Ea (kJ/mol).

$$k = \text{A} \exp\left(-{}^{Ea}/_{RT}\right) \qquad \text{Equation 3-15.}$$

Where k is the reaction rate constant; Ais the pre-exponential factor (s^{-1}); Ea is the activation energy (kJ/mol); R is the gas constant (8.314J/mol K) and T is the temperature in kelvin (K).

The weight loss with time curve is assumed to be the result of one or more first-order reactions and the reaction is described by equation (3-16).

$$k_t = - \frac{1}{m - m\infty} \frac{dm}{dt} \qquad \text{Equation 3-16.}$$

dm/dt is the gradient of the tangent of the weight loss curve at time *t*, *m* is the mass at time *t and m*∞ is the final mass. Therefore equation 3-17 can be used to determine the values of A and Ea.

$$ln\ k = ln\ A - (^{Ea}/_{RT}) \qquad \text{Equation 3-17.}$$

A and Ea was obtained from the intercept and slope of a plot of *ln k* versus 1/T and can be seen in Figure 3-18.

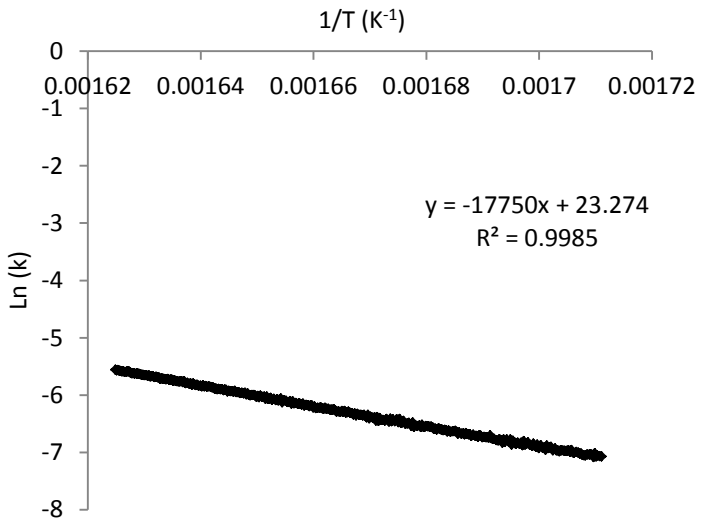

Figure 3-18: Arrhenius plot for sample L270-30.

3.13 Pyrolysis-Gas Chromatography-Mass Spectrometry (Py-GC-MS)

Py-GC-MS analyses were carried out on the samples using a CDS 1000 pyroprobe . The probe was attached to a HP 5890 series II Gas Chromatograph and fitted with a Rtx 1701 60 m capillary column (0.25 id and 0.25µm film thickness). The oven was held at a temperature of 70°C for 120 seconds and then programmed at 20°C min^{-1} to a final temperature of 250°C, and held for 15 min. Approximately 2-3 mg of sample were

placed in a 20 mm silica tube between two plugs of quartz wool. The sample was then pyrolysed at a maximum temperature of 600°C with a nominal ramp rate of 20°C min^{-1} and a final dwell time of 20s. Products were characterised using mass spectral detection (NIST 05A MS library) and by comparisons with literature [157].

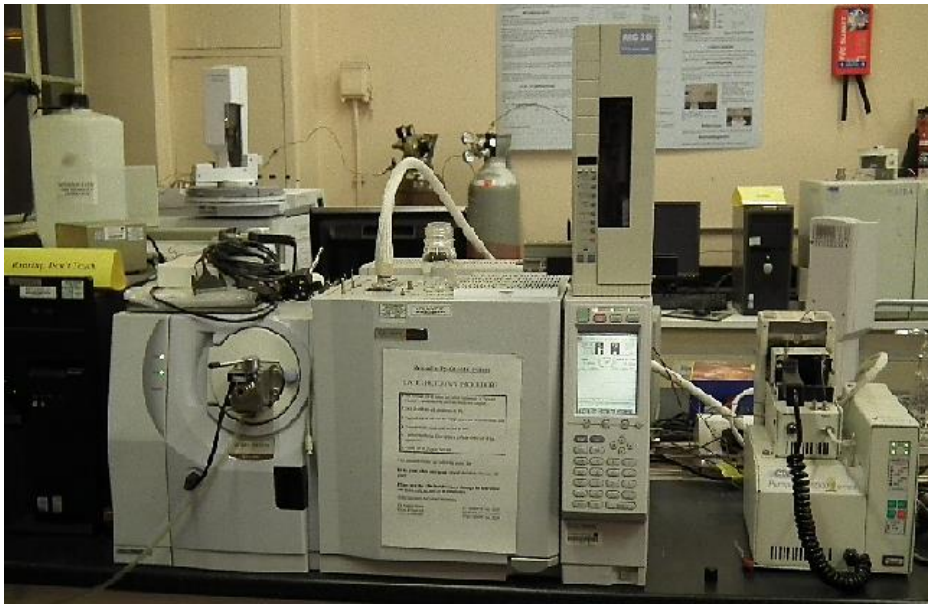

Figure 3-19: A CDS 1000 Pyroprobe with HP 5890 series II Gas Chromatograph.

3.14 Single particle combustion

In order to obtain an insight into the combustion behaviour of the samples in flames, single biomass particles were combusted in a methane-air flame. The experiment involved suspending cubed shaped fuel particles (2x2x2mm) on a steel needle in a natural gas flame from a Meker type-burner, at a temperature of ~1200^{o}C and oxygen concentration of 10.3 mol %. Prior to combustion, each particle was weighed and held in place on a steel needle adjacent to an R-type thermocouple in a ceramic housing. The needle was then covered by a protective water-cooled sheath and was centrally positioned above the burner before the flame was lit. When the flame was lit, the protective sheath was retracted to expose the fuel particle to the methane-air flame. Upon complete combustion, the flame was extinguished, the needle with fuel ash were discarded. The set-up for the experiment can be seen in Figure 3-20. For video interrogation, a Photron FASTCAM SA5 camera was employed to record the images of

the burning particles during the experiment at a frame speed of 125 frames per second (fps). The videos were stored on a computer and analysed using PFV (Photron FASTCAM Viewer) Version 3.20 software.

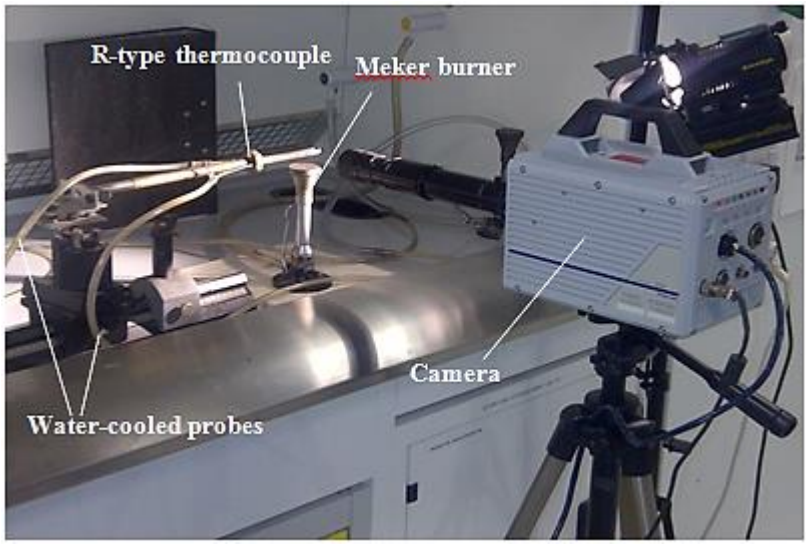

Figure 3-20: Single Particle Experiment setup.

3.15 Torrefaction Experiments

3.15.1 Torrefaction using the bench scale reactor

Torrefaction experiments were carried out using a bench scale reactor and are reported in Chapter 5. The Nigerian samples alongside wheat straw were treated in the rig as shown in Figure 3-21. The reactor is equipped with a three zone horizontal furnace with an internal diameter of about 75 and 750mm long and also it has a reactor tube, with an internal diameter of 60 mm and 800 mm in length. The schematic diagram for the reactor is shown in Figure 3-22. Approximately 100 g of biomass was housed inside the reactor tube and positioned between two glass wool plugs as shown in Figure 3-23. There were three thermocouples in the reactor tube that provided the temperature profile of the process at three different locations. The thermocouples were separated at a distance of about 20cm from each other inside the reactor tube and this can be seen in Figure 3-24. The figure reveals the positions of three thermocouples at about 20 cm intervals inside the reactor tube, aiming at recording the inlet gas temperature, bed

temperature and outlet gas temperatures. A value and flow-meter were attached to the rig to control the flow of nitrogen supply to the reactor tube. Nitrogen was supplied at a rate of 1.2l/min to the reactor in order to ensure a continuous inert environment throughout the experiment. While the sample was in the tube furnace, the temperature was elevated to 150^{o}C from room temperature at a heating rate of 10^{o}C/min and was held at this temperature for an hour in order to remove inherent moisture. After drying, the reactor temperature was further raised to a final temperature and was also held at this temperature for a certain period of time, which is known as the residence time. (see Table 3-2). The type of treatment, the reaction (final) temperatures, the residence times and the interpretation of the treatment that were applied are listed in Table 3-2. Also, details of sample nomenclature are presented in Table 3-3. It is important to mention that the residence time in this context is referred to as the time at which the treatment remains at the maximum reaction temperature, after which the samples were quickly quenched under nitrogen flow to stop further reaction. It was observed that the time taken for the reaction to cool down to a temperature below 200ºC is significant and also varies for each sample. Hence, cooling duration is sample dependency and consequently, residence times were about 10-20 minutes longer than planned. Also, temperature in the centre of the bed were seen to be higher than the set temperature (up to 20°C higher), and this suggested that torrefaction process can be an exothermic reaction.

The treated solid remaining after the process which is usually referred to as torrefied fuel was weighed and the mass yield, η_M was calculated as a function of the percentage of the original mass sample in Equation (3-18) below:

$$\text{Mass yield, } \eta_M = \left(\frac{Mchar}{Mfeed}\right)_{daf} * 100 \qquad \text{Equation 3-18a.}$$

$$\text{Energy yield, } h_E = \eta_M *. \left(\frac{HHVchar}{HHVfeed}\right) \qquad \text{Equation 3-19b.}$$

where *Mchar* is the mass of the torrefied fuel on a dry ash free basis (daf) and *Mfeed* is the mass of the untreated (raw) sample that was fed into the reactor on a dry ash free

basis (daf), HHV_{char} is the higher heating value of the torrefied biomass and HHV_{feed} is the higher heating value of the raw biomass, both also on a dry ash free basis (daf).

Figure 3-21: Torrefaction rig with a three temperature zone.

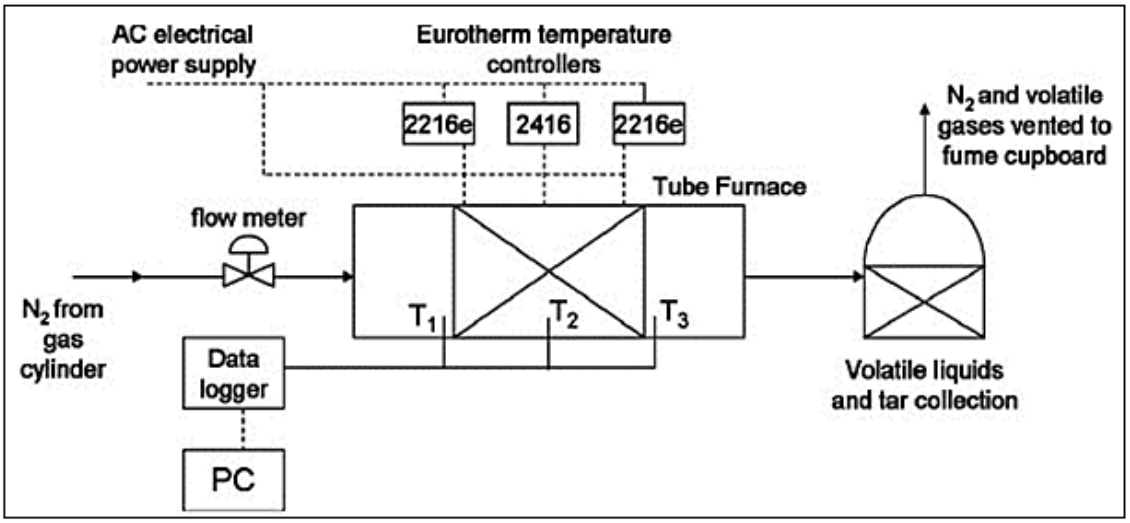

Figure 3-22: Schematic diagram of borosilicate reactor tube [93].

Figure 3-23: Image showing the positioning of the sample inside the reactor tube.

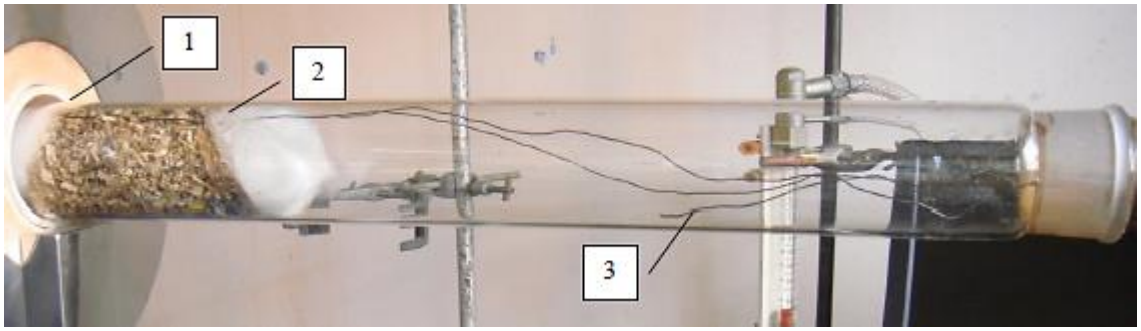

Figure 3-24: Image showing the arrangement of the three thermocouples in the tube. The location of the the first (1) thermocouple is nearer to the glass wool on the left, the 2nd thermocouple (2) stays in the middle of the sample bed and the 3rd thermocouple (3) is usually about 20cm away from the 2nd as indicated in the figure.

Table 3-2: Pre-treatment conditions used in this study.

Condition type	**Temp. (^{0}C)**	**Residence time (min)**	**Interpretation**
Low	270	30	High temperature with longer residence time
Mild	270	60	High temperature with shorter residence time
Critical	290	30	Very high temperature with longer residence time

Table 3-3: Sample designation, material and torrefaction conditions for the samples.

Sample designation	**Material and torrefaction condition**
G270-30	*Gmelina arborea* torrefied at 270° C for 30 minutes.
G270-60	*Gmelina arborea* torrefied at 270° C for 60 minutes.
T270-30	*Terminalia superba* torrefied at 270° C for 30 minutes.
T270-60	*Terminalia superba* torrefied at 270° C for 60 minutes.
L270-30	*Lophira alata* torrefied at 270° C for 30 minutes.
L270-60	*Lophira alata* torrefied at 270° C for 60 minutes.
N270-30	*Nauclea diderrichii* torrefied at 270° C for 30 minutes.
N270-60	*Nauclea diderrichii* torrefied at 270° C for 60 minutes.
P270-30	*Palm kernel expeller* torrefied at 270° C for 30 minutes.
P270-60	*Palm kernel expeller* torrefied at 270° C for 60 minutes.
P290-30	*Palm kernel expeller* torrefied at 290° C for 30 minutes.

The overall mass and energy balances for the torrefaction process for each sample were investigated in this study. Nitrogen and volatile gases were expelled to the fume hood, while condensable volatiles and tar were collected in a flask immersed in a dry ice and acetone bath (see Figure 3-25); a way of preventing the evaporation of the acetone. Also non condensable gases were fed into the gas chromatogram (GC) for further analysis. The set up for the traps used in collection of liquid products is presented in Figure 3-25, and the trap connection to the GC (Perkin Elmer Autosystem XL GC) can also be seen in Figure 3-26. The permanent gases that were detected include CH_4, CO_2 and CO. A condenser as shown in Figure 3-25 was connected to the chiller (temperature was set to 0°C), and then connected to the three traps. The traps were partitioned to three different sections to confine water, tars, and volatiles that could block the GC line. The last trap (line) was connected to the GC at about 5min before the end of the drying period and the GC became operational at this time. The GC was calibrated using a mixture of gases of known concentrations (methane: 1000 ppm, carbon monoxide: 5000 ppm, carbon dioxide: 5000 ppm and nitrogen: Balance), and was used to quantify the permanent gases that were detected during torrefaction.

The three round bottom flasks for the first, second and third traps were each weighed, together with their respective stoppers before and after torrefaction. In order to ensure full compliance of health and safety regulations, the next process which involved liquids phase extraction was done in the fume cupboard. After weighing, liquid contents were transferred into a 100 ml separating funnel. 10 ml of dichloromethane (DCM) was used to rinse the flask and poured into the funnel to completely remove deposit in the flask. DCM was also used to flush out the tars deposits in the condenser, and then poured into the same funnel. The mixtures in the funnel were stirred actively for a while and left for 24hours to allow phase separation into two layers. The lower layer of the separation is the organic phase while the upper layer is the aqueous fraction. The organic phase mixture was transferred into a 100 ml beaker of known mass. The weight of the beaker plus the mixture was recorded. The aqueous fraction at the top layer of the funnel was also transferred into a weighed glass vial.

Both the beaker and the vial were placed in the fume cupboard for about 3-4 days in order to ensure complete evaporation of DCM from the separated samples. Beakers and vials were weighed on a daily basis until the weights appeared constant. It is also important to mention that during this process, low organic volatiles may be lost during evaporation of DCM from the mixtures. The liquids were further analysed in Section 3.15.2, and the flow diagram showing the products of torrefaction in this study can be seen in Figure 3-27. In order to assess the overall mass balances of torrefaction of biomass, mass yields of the torrefied products are calculated as:

$$\text{Solid yield}_{\text{(as received)}} = \frac{X}{A} * 100\ \% \qquad \text{Equation 3-20.}$$

Where **A** is the mass of untreated sample and **X** is the mass of treated biomass and are calculated as received.

$$\text{Total Liquid yield} = \frac{Y}{A} * 100\ \% \qquad \text{Equation 3-21.}$$

where **Y** is the total mass of liquid yield that comprised the organic (tar) phase, $\mathbf{Y_o}$ and the reaction water phase, $\mathbf{Y_1}$ contents of the liquid.

The mass yields of organic and the reaction water phases can be expressed as follows:

$$\mathbf{Y_o} = \frac{P}{A} * 100\ \% \qquad \text{Equation 3-22.}$$

$$\mathbf{Y_1} = \frac{Q}{A} * 100\ \% \qquad \text{Equation 3-23}$$

where **P** and **Q** are masses of collected organic and water phases respectively.

$$\text{Gas yield} = \frac{A-X-Y}{A} * 100\ \% \qquad \text{Equation 3-24.}$$

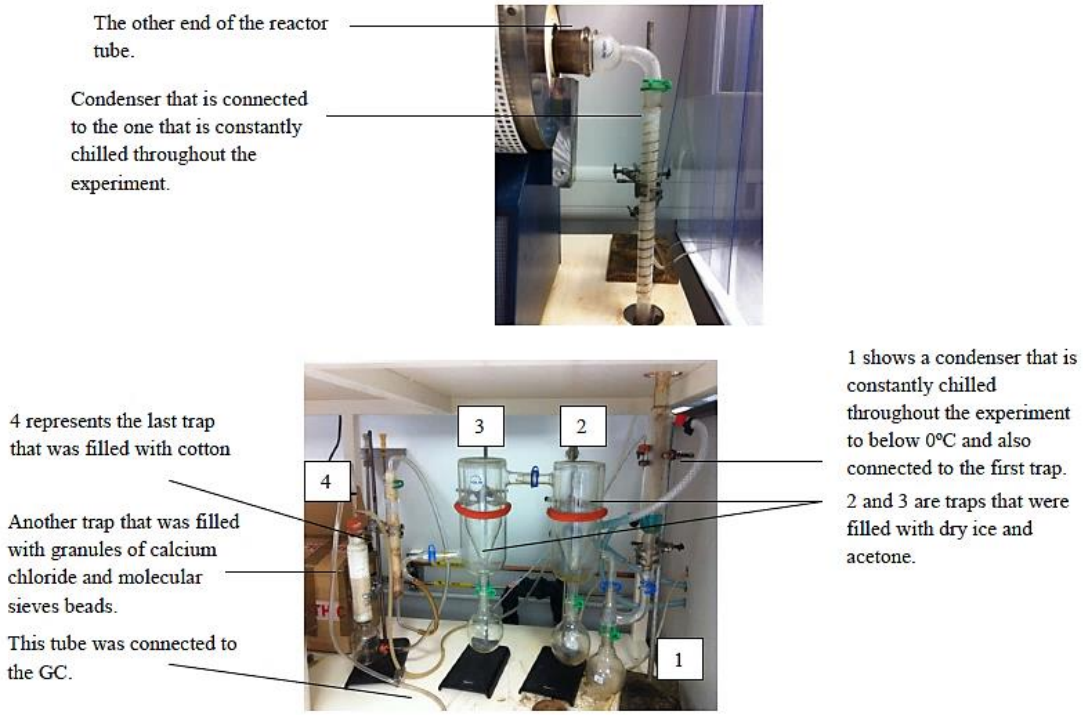

Figure 3-25: Torrefaction setup for collection of liquid products **[90]**.

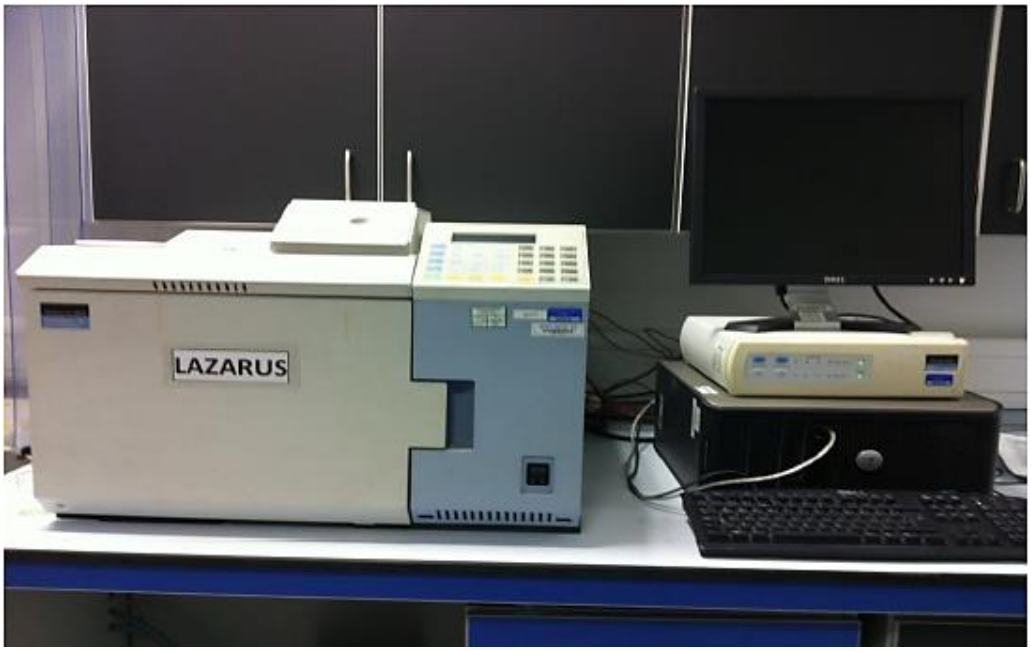

Figure 3-26: Perkin Elmer Autosystem XL GC that was used to detect and quantify the permanent gases during torrefaction.

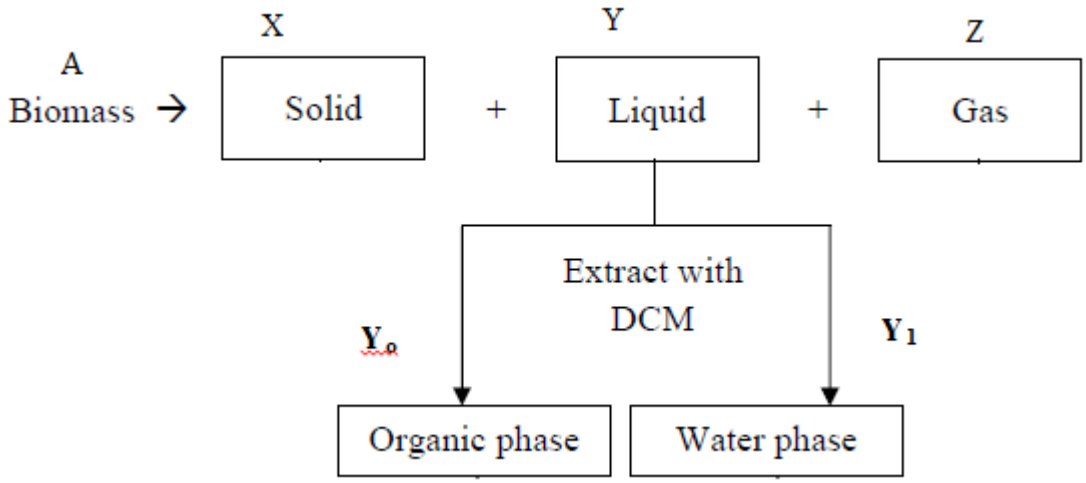

Figure 3-27: Flow diagram of the different types of products that were obtained from torrefaction process, where **A** is the mass of the sample that was fed into the reactor, **X**, **Y**, and **Z** represent the mass of the solid liquid and gas yields respectively.

3.15.2 Analysis of Tars

The tar products that were collected during torrefaction were only analysed using GC-MS and CHNS

3.15.2.1 Liquid-GC-MS

The components in the organic liquid products that were obtained from torrefaction were analysed using an Agilent 7683 series auto sampler. Approximately 1.5ml of each sample was placed in vials and mixed with DCM. The mixture was shaken together to ensure that the organic liquid completely dissolved in the DCM. The vial was placed on the sample carrier and automatically injected on to the Agilent Technologies 6890N Gas Chromatograph, containing the same column and operating under the same oven heating conditions described in Section 3.13 and analysed with the Agilent Technologies 5975 Inert XL Mass Selective Detector as shown in Figure 3-28.

Figure 3-28: Agilent 7683 series auto sampler with Agilent 6890N Gas Chromatograph and Agilent 5975 Inert XL Mass Selective Detector.

CHAPTER 4. CHARACTERISATION OF SELECTED NIGERIAN BIOMASS FOR COMBUSTION AND PYROLYSIS APPLICATIONS

4.1 Introduction

Biomass is the most utilised form of renewable energy, especially in developing nations, and is a possible replacement for fossil fuel in power generation. The most commonly used method for recovering energy from biomass is combustion. Many countries are exploring the utilisation of energy crops and indigenous residues to deliver sustainable sources of biomass. Biomass resources in Nigeria include woods, agricultural wastes, crop residues, sawdust, wood shavings, bird and animal litter and dung as well as industrial and municipal solid wastes [12]. These were estimated in million tonne (Mt) as 39.1 fuel wood, 11.2 agricultural wastes, 1.8 sawdust, and 4.1 municipal solid wastes [12]. The highest quantity of woody biomass is found in the rain forest in southern Nigeria, and the highest quantities of crop residues is from the guinea savannah in the north central region of Nigeria. Agricultural residues include cornstalks, rice husk, cassava peels, palm kernel shells, coconut shells and sugarcane bagasse. Clearly, these resources are currently under-utilised, it is therefore important to consider adequate and environmental friendly measures to modernize its supply, conversion and use in a sustainable way. For these bio-resources, detailed characterisation of the fuel properties is essential in order to optimise the combustion processes. There is very little information in the open literature concerning the fuel properties of woods and energy crops in Nigeria and this chapter aims to characterise some of the plantation and timber species (*Terminalia superba*, *Nauclea diderrichil*, *Gmelina arborea*, *Lophira alata*) alongside one agricultural residue (palm kernel expeller (PKE), for their fuel, pyrolysis and combustion characteristics. Results are compared with some typical UK energy crops and residue that are listed in Chapter 3, namely willow Eucalyptus, miscanthus and wheat straw respectively.

4.2 Materials and Experimental Methods

4.2.1 Sample Preparation

The samples studied are detailed in Sections 3.2.1 to 3.2.7. The samples were prepared and milled to particle sizes ranging from < 53μm to < 1180 μm according to the procedures stated in Section 3.3.

4.2.2 Experimental Methods

The details for all the experiments conducted in this chapter are found in Section 3.4.1 to 3.4.12.

4.3 Results and Discussion

4.3.1 Proximate Analysis and Fixed Carbon Content

The results from the proximate analysis of the selected Nigerian fuels are listed in Table 4-1 and compared to some selected UK energy crops and a residue, wheat straw. The moisture content of the Nigerian fuels appeared high, especially for *Gmelina* and *Nauclea,* which were over 39% and, consequently, there was a need for air drying. For this reason, the samples were oven-dried in batches at a temperature of 60^{o}C for over 72 hr in order to prevent biological deterioration and also to ensure that the water content in the sample is reduced to a low level. The moisture content was measured after drying to about 12% and reported as $MC_{(ad)}$. *Terminalia*, *Nauclea*, and *Gmelina* have volatile content of 80.2%, 80.6% and 80.9% (dry basis) respectively and are comparable to that of Eucalyptus (79.9%). The amount of volatile in PKE (76.1%) and *Lophira* (78.1%) is similar to that of willow (77.6%). PKE and *Gmelina* also appeared to contain the least and highest amount of volatile respectively. Overall, miscanthus and wheat straw recorded the highest and lowest volatile content respectively, with respective values of 82.9% and 74.1%. The results also showed that the selected Nigerian woods have lower ash contents than the UK fuels in this study. *Nauclea* and *Gmelina* have particularly low ash presented value of 0.7 and 1.0 (%) respectively. *Lophira*'s ash content is 1.6% while *Terminalia* and PKE have ash contents of 2.2 and 2.9 (%) respectively and is similar to the ash values obtained from the UK fuels (except straw). The fixed carbon contents of the selected Nigerian woods are comparable to the UK woods. *Lophira* has a

similar value for fixed carbon content with short rotation willow coppice, i.e. 20.3 and 19.8 wt% respectively, while *Terminalia* (17.4wt %) is comparable to eucalyptus and wheat straw (17.6wt %). PKE and miscanthus present the highest and lowest value for fixed carbon content respectively (21 & 14.7wt %).

Table 4-1: Proximate analysis of the fuels studied.

Sample	**Moisture (wt %)^{ar}**	**Moisture (wt %)^{ad}**	**Volatiles (wt %)^{db}**	**Ash (wt %)^{db}**	**Fixed Carbon (wt %) $^{db}_{a}$**
PKE	9.6	8.9	76.1	2.9	21.0
Lophira	13.9	12	78.1	1.6	20.3
willow (SRC)	9.8	n/a	77.6	2.6	19.8
Nauclea	42.0	4.2	80.6	0.7	18.8
Gmelina	39.9	4.9	80.9	1.0	18.1
Eucalyptus	23.7	6.1	79.9	2.6	17.6
wheat straw	6.1	n/a	74.1	8.3	17.6
Terminalia	17.4	5.2	80.2	2.4	17.4
miscanthus	7.2	n/a	82.9	2.5	14.7

ar: as received, ad: after air drying at 60^{o}C, db: dry basis, n/a: not applicable and ^{a}: is calculated by difference.

A direct relationship between biomass elemental composition and heating value has been established using Equation 3-9 [48, 155]. Table 4-2 presents the ultimate analysis and the respective heating values HHV on a dry basis for the fuels. The C content of the Nigerian fuels is comparable to that of willow and it is >50 wt %, except for *Terminalia*. PKE and *Nauclea* record the highest C contents (>53 wt %). The higher than average C contents of the Nigerian fuels were confirmed by their corresponding relatively higher experimental HHVs obtained, which were in the range 19.4−21.1 MJ kg^{-1}. The experimental HHVs are also listed in Table 4-2, and were in good agreement with the calculated values (<4% error). The H content in miscanthus and wheat straw is low (<5 wt %), while the nitrogen content of the fuels is <1%, and range from 0.2 to 0.7%. The fuels with the highest nitrogen contents are *Nauclea* and willow (0.6−0.7%). The

contents of sulphur and chlorine in all the fuels were below the detection limits, except for miscanthus and wheat straw, which resulted in a chlorine content of 0.31 and 0.42 wt %, respectively. Also from Table 4-2 is the oxygen contents for the fuels. The oxygen content in the fuels is between 40.6 - 51.38 wt%, with *Nauclea* and wheat straw having the lowest and highest content of oxygen respectively.

Table 4-2: Ultimate analysis and estimated CV of fuels.

Sample	**C (wt.%)**	**H (wt.%)**	**N (wt.%)**	**Cl (wt.%)**	**O (wt.%)** [a]	**HHV (MJ/Kg)**[b]	**HHV (MJ/Kg)**[c]
Nauclea	53.1	5.7	0.6	N.D.	40.6	21.2	20.9
PKE	53.6	5.1	0.5	N.D.	40.8	21.0	21.0
Gmelina	51.4	5.7	0.2	N.D.	42.7	20.4	20.8
Lophira	51.8	5.0	0.3	N.D.	42.9	20.3	21.1
willow	51.1	5.3	0.7	N.D.	42.9	20.2	-
Terminalia	48.9	5.2	0.3	N.D.	45.5	19.2	19.4
Eucalyptus	46.3	5.1	0.5	N.D.	48.1	18.3	-
miscanthus	46.1	4.9	0.2	0.31	48.5	18.1	-
wheat straw	42.8	4.9	0.5	0.42	51.38	17.6	-

db: dry basis, [a]: is calculated by difference, [*]: is less than 0.01%, [b]: is calculated according to Equation. (3-9), [c]: determined experimentally, N.D: not detected and -: not determined.

4.3.2 Lignocelluloses analysis

The main component of biomass is the lignocellulosic cell wall, and knowledge of these components will help maximize conversion yields, as well as optimising the process design. The lignocellulose compositions of the selected Nigerian fuels are reported as received and are shown in Figure 4-1. Hemicellulose composition was obtained from the difference between *neutral detergent fiber*, NDF% and acid *detergent fiber*, ADF%, cellulose was derived from the difference between ADF% and acid *detergent* lignin, ADL%, while ADL is the lignin concentration. The lignocellulose composition in the

fuels do not add up to 100%; the difference is accounted to be the cell wall intrinsic moisture, together with some hydroxycinnamic acids, some ash, proteins and the remains of other cell components. The percentage of cellulose in all the fuels is over 50 wt%, except for *Terminalia* and PKE which contains the least percentage of cellulose content (46.9 wt% and 39.1 wt% respectively). *Gmelina* has the highest percentage of cellulose composition (56.1 wt%). As expected, hemicellulose is the lowest fraction of the lignocellusic component in the fuels, and is between 7 - 11 wt%. The hemicellulose content in *Nauclea* and *Lophira* are slightly less than 82 wt% are seen to be the lowest among the fuels and the values are similar. This is expected since they are both hardwood and therefore contain lower amount of hemicellulose when compared to softwood. The content of hemicellulose in *Gmelina* and *Terminalia* (both are softwood) are about 10 wt% and contain more than *Nauclea* and *Lophira*. Overall, *Nauclea* (7 wt%) and PKE (11 wt%) have the lowest and highest hemicellulose composition respectively. There has been a major complexity in analysing the role of lignin in cell-wall digestibility due to the fact that a definitive molecular structure cannot be drawn for lignin and all lignin concentration estimates are simply empirical, based on the particular method of analysis chosen [44]. Consequently, lignin concentration estimates vary widely among methods. Klason lignin is the traditional method of analyzing wood which have been criticised for possible contamination with protein [156, 158]. Thus, the acid detergent lignin (ADL) which is the commonly used method for lignin determination was developed as an alternative to Klason lignin [156] and is performed on the ADF residue. The two methods of assessing lignin in the fuels were used in this studies. The content of acid detergent lignin in the fuels is between 21.6 and 33 wt%, with PKE and *Nauclea* having the least and most composition respectively. The results from Klason lignin are significantly different from those obtained from ADL. Klason lignin presents the concentration of lignin in the fuels as 34.7, 30.4, 33.1, 43.2 & 38.8 wt% for *Lophira*, *Terminalia, Gmelina*, PKE and *Nauclea* respectively. As expected, the concentrations of Klason lignin in the fuels are higher than the ADL estimation. Literature suggest that Klason lignin gives higher lignin concentrations in fuels [156, 158] and is a more accurate method of measuring lignin concentration in fuels [44, 159]. Also the ADL method underestimates lignin concentration due to loss of acid soluble lignin in the acid detergent step of the procedure [160, 161].

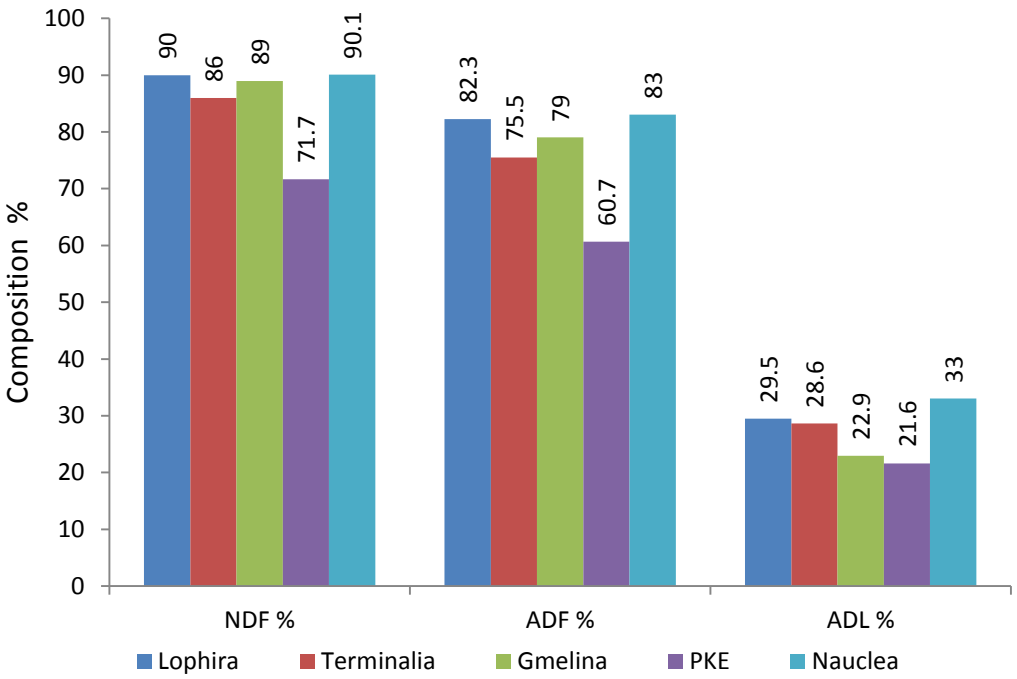

Figure 4-1: Lignocellulosic composition of the fuels.

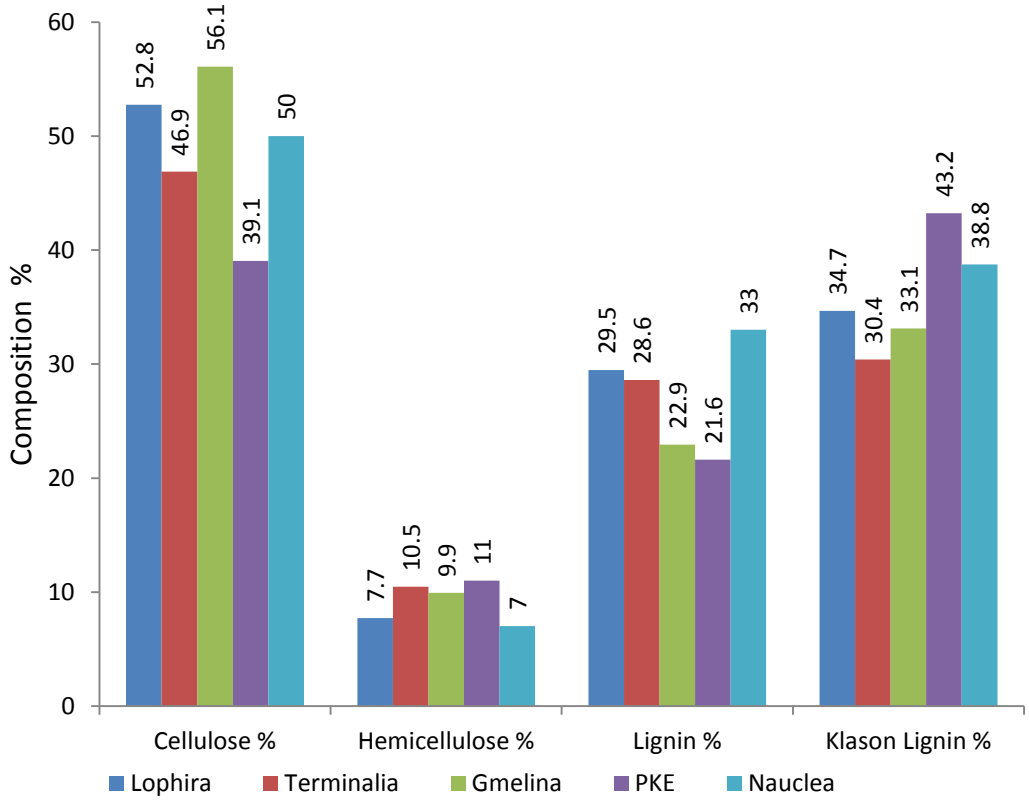

Figure 4-2: Lignocellulosic composition of the fuels (cont'd).

4.3.3 Ash Composition, Slagging and Fouling Indices

Slagging and fouling are two critical problems encountered in the boiler. Slagging is the term used to describe the deposition which appears in the boiler area where radiant heat transfer is at maximum, while fouling is evident in the convective heat transfer section. Slagging develops in the main flame zone as well as the burners, the boiler water-walls and the bottom hopper. It is known that the occurrence of alkali and alkaline earth metals in the fuel causes slagging and other forms of fireside deposits [48]. The metal salts in biomass will combine with oxygen to form metal oxides in the ash during combustion, together with chlorides, sulfates, and phosphates. Depending upon the ash characteristics, it might form hard deposits on the heat exchanger surfaces and boiler walls. K and Na, together with SiO_2 form low melting point ash mixtures. Thus, high alkali content in fuels causes severe slagging on the boiler grate or in the bed and because of its volatility, also results in fouling of convection heat transfer surfaces [48, 162]. The main components of the fuels ash is listed in Table 4-3. The total ash composition of some of the fuels does not add up to 100 because the ash composition is estimated only in the form of oxides. In reality, carbonates, hydrogen carbonates and sulphates are present [163]. *Terminalia* and *Lophira* have high CaO content, whereas the most abundant component in the *Gmelina* and *Nauclea* ash is K_2O. Therefore, these two pairs of woody biomass are expected to have very different ash melting behavior. In the case of PKE, silica is the main ash component.

The alkali index and base-to-acid ratio are used as a threshold pointer for determining fouling and slagging tendencies of a fuel respectively. The alkali index (AI) presents the quantity of alkali oxide in the fuel per unit of fuel energy (kg alkali GJ^{-1}) and is calculated using the formula equated below[48]:

$$AI = kg\ (K_2O + Na_2O) / GJ. \qquad \text{Equation 4-1}$$

The alkali index has a lower threshold value of 0.17 kg alkali/GJ above which fouling can probably occur and an upper threshold value 0.34 kg alkali/GJ above which fouling is definitely expected to occur [48, 164].

The base to acid ratio ($R_{b/a}$) index is normally used to predict the slagging tendency of a fuel [163] and is defined as the ratio of the basic metal oxides (CaO, MgO, K_2O, Na_2O and Fe_2O_3) to the acidic oxides (Al_2O_3, TiO_2, SiO_2 and P_2O_5) in the ash, as presented in Equation 4-2 [165].

$$\boldsymbol{R_{b/a}} = \frac{(\boldsymbol{Fe_2O_3 + CaO + K_2O + Na_2O})}{(\boldsymbol{SiO_2 + TiO_2 + Al_2O_3 + P_2O_5})} \qquad \text{Equation 4-2}$$

The base to acid ratios and base percentage calculated for the Nigerian fuels are also shown in Table 4-3, together with the alkali indices. Generally, the intrinsic mineral matter contained in biomass is lower than in coal, although this can be considerably higher in some species of grasses and agricultural residues [48]. The ash content of the Nigerian fuels are lower or at least comparable to those from the U.K. energy crops listed in Table 4-1, and are much lower than wheat straw. Also from Table 4-3, it is observed that the alkali index for all the fuels is below the 0.34 kg/GJ threshold value and hence these fuels are not predicted to cause severe fouling problems. *Gmelina* is expected to be the most problematic, however its alkali index is still below the "fouling probable" indicator. Furthermore, from the $R_{b/a}$ in Table 4-3, it is observe that *Terminalia*, *Gmelina*, and *Lophira* can be expected to have a higher tendency to form ash deposits in the combustion chamber than *Nauclea* and PKE. However, the Nigerian PKE presented a lower value for $R_{b/a}$ in comparison to the value reported for the imported PKE in Darvell *et al.*[165], which was calculated at 2.93.

Table 4-3: Ash composition of the fuels including slagging and fouling indices.

Elemental oxide	***Terminalia***	***Gmelina***	**PKE**	***Nauclea***	***Lophira***
SiO_2	1.7	8.9	57.1	9.5	10.5
Al_2O_3	0.3	1.0	11.0	0.9	0.3
Fe_2O_3	0.1	0.6	6.0	0.9	0.2
TiO_2	<0.1	<0.1	0.6	0.4	<0.1
CaO	41.7	19.6	5.8	9.3	41.0
MgO	1.0	2.8	1.8	3.0	2.7
Na_2O	0.1	0.3	0.4	0.3	0.4
K_2O	8.4	29.9	2.5	32.0	8.2
Mn_3O_4	<0.1	<0.1	0.2	0.2	0.4
P_2O_5	0.7	0.5	0.7	6.4	2.2
SO_3	1.5	1.7	1.5	4.14	3.5
Parameter	***Terminalia***	***Gmelina***	**PKE**	***Nauclea***	***Lophira***
Alkali Index (kg alkali/GJ)[a]	0.10	0.15	0.04	0.11	0.07
Base to acid ratio (including P_2O_5)[b]	19.00	5.12	0.24	2.65	4.04
Base Percentage (%)	51.3	53.2	16.5	45.5	52.5

[a,b] Calculated using Equations. (4-1) and (4-2) respectively.

4.3.4 Ash fusion test

Ash fusion tests (AFT) were carried out using the method described in Section 3.9 using a Carbolite digital ash fusion furnace at a controlled heating rate in an oxidizing environment. The four ash melting characteristic temperatures, shrinkage starting temperature (SST), deformation temperature (DT), hemisphere temperature (HT) and flow temperature (FT) were assessed for the Nigerian and UK fuels according to British standards (DD CEN/TS 15370 – 1:2006) and are listed in Table 4-4. It is to be noted that these temperatures are determined visually; therefore, there is an inherent error in

their estimations. In the case of the estimation of the shrinkage temperature, this error may be larger, because the contrast of the images collected at lower temperatures is poor. The standard error for deformation, hemisphere, flow and shrinkage temperature, is between 0 and 18°C, 0 and 14°C, 0 and 18°C, and 0 and 28°C respectively. Descriptions of the melting behaviour of the test pieces are also included in Table 4-4. As reported in Table 4-4, it was observed that the ashes from both PKE and miscanthus shrink then swell during the deformation stage, this is followed by bubbling and then melting. *Nauclea* ash was also observed to swell upon deformation (before melting). Further comparison of the deformation temperature can be made with values found in the literature [162, 163].

The deformation temperatures of lignites and a number of biomass are seen to pass through a minimum (parabolic curve) when plotted against base percentage; the minimum being in the range 35−55% basic oxides in the ash. Figure 4-4 shows the results compiled by Bryers [162] for some coal and biomass ash fusion tests. For comparison with Bryers [162] data for lignites, sub-bituminous coals, bituminous coal and a variety of biomass, as well as the hemisphere temperatures of the Nigerian biomass under an oxidising atmosphere are also plotted on Figure 4-4. It is important to mention that the compiled data by Bryers [162] was obtained in a reducing atmosphere and the values could be higher under oxidising conditions. For the base percentages reported in Table 4-3, ash melting temperatures could be lower than 1100^{o}C, since hemisphere temperatures of above 1100°C is expected for biomass with base percentages below ~30% and above ~ 60% according to the compiled data shown in Figure 4-4 [162, 163]. It is seen that the Nigerian biomass have comparable ash softening temperatures to lignites, and sub-bituminous coals ashes. The base percentage of the Nigerian woods also falls within the range 35−55% basic oxides (see Table 4-3) and thus it can be assumed that, like many other woods and biomass fuels, deposition will require careful monitoring and control if these fuels are utilized in high temperature combustion systems. However, it is also important to note that the values reported in this paper represent an average composition of the wood fuels, including the bark component. Clean white wood fuels have much lower ash contents and different ash compositions than those with bark [166, 167], furthermore, there is variability in ash

composition depending on the type of fiber (heartwood, branch wood, top branches, etc.) [166]. Thus, good fuel quality management is used by most power companies to help alleviate potential fuel deposition problems [5, 168-170] and, based on these results, similar fuel quality management is recommended for the Nigerian energy crops and woods.

Table 4-4: Ash Fusion Test (AFT) characteristic temperatures (^{o}C)

Fuel	Shrinkage Temp.	Deformation Temp.	Hemisphere Temp.	Flow Temp.	Comments
wheat straw	950	980	1095	1140	Shrinks, swell at deformation and later melts.
miscanthus	960	1000	1300	1325	Shrinks, swell at deformation, bubbles and later melts.
Willow	990	1075	1520	1525	Shrinks, and later melts.
PKE	1080	1130	1365	1380	Shrinks, swell at deformation, bubbles and later melts.
Gmelina	1030	1185	1490	1505	Shrinks, and later melts.
Terminalia	1065	1265	1510	1520	Shrinks, and later melts.
Nauclea	1070	1375	1480	1505	Shrinks, swell at deformation then melts.
Eucalyptus	950	1430	1445	1455	Shrinks and later melts.
Lophira	1110	1430	1455	1475	Shrinks, and later melts.

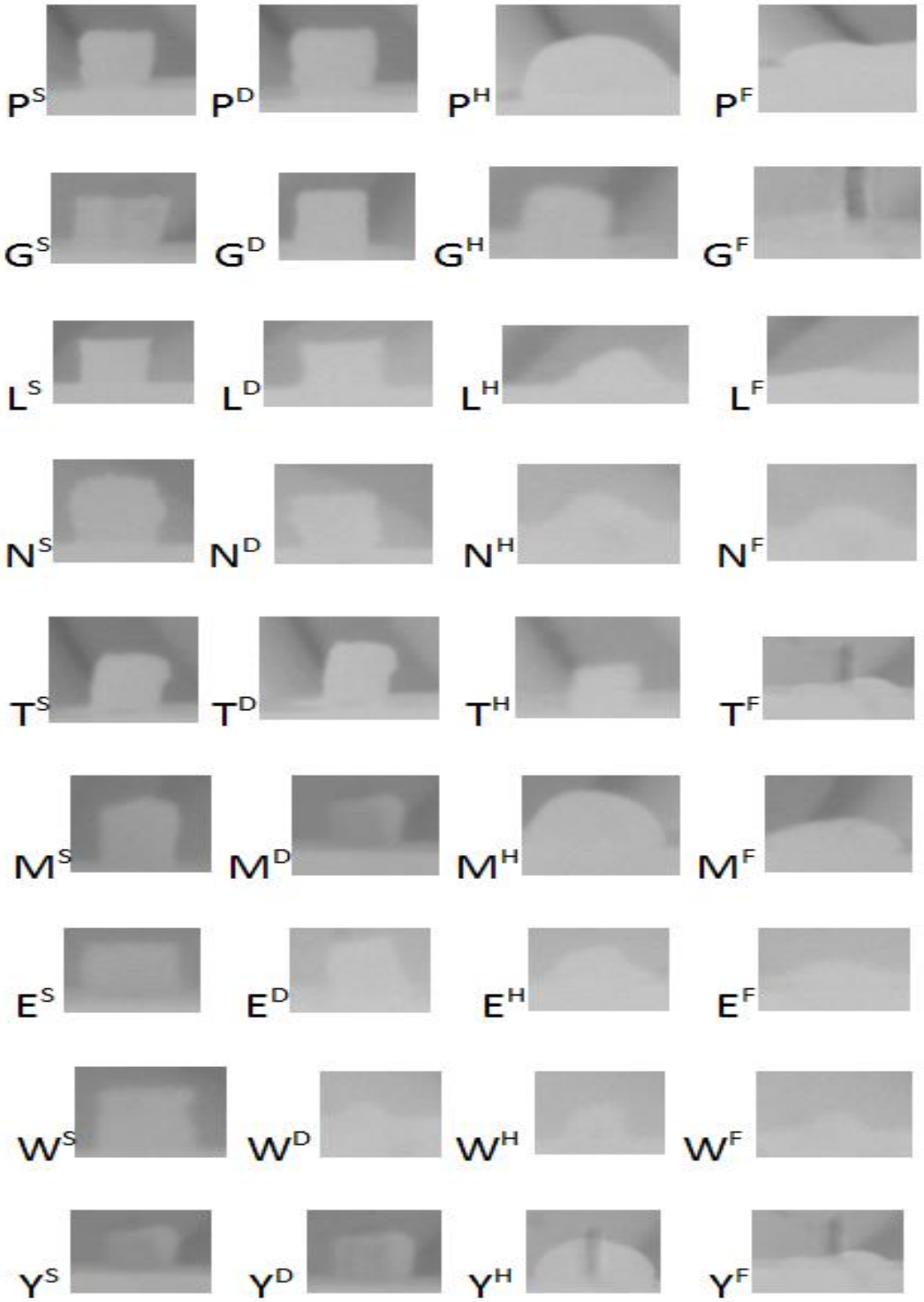

Figure 4-3: Ash melting images of the selected fuels for the characteristic temperatures.
P:PKE, G: *Gmelina*, L: *Lophira*, N: *Nauclea*, T: *Terminalia*, M: miscanthus, E: Eucalyptus, W: willow, Y: wheat straw, ^{S}: Shrinkage, ^{D}: Deformation, ^{H}: Hemisphere and ^{F}: Flow temperature respectively.

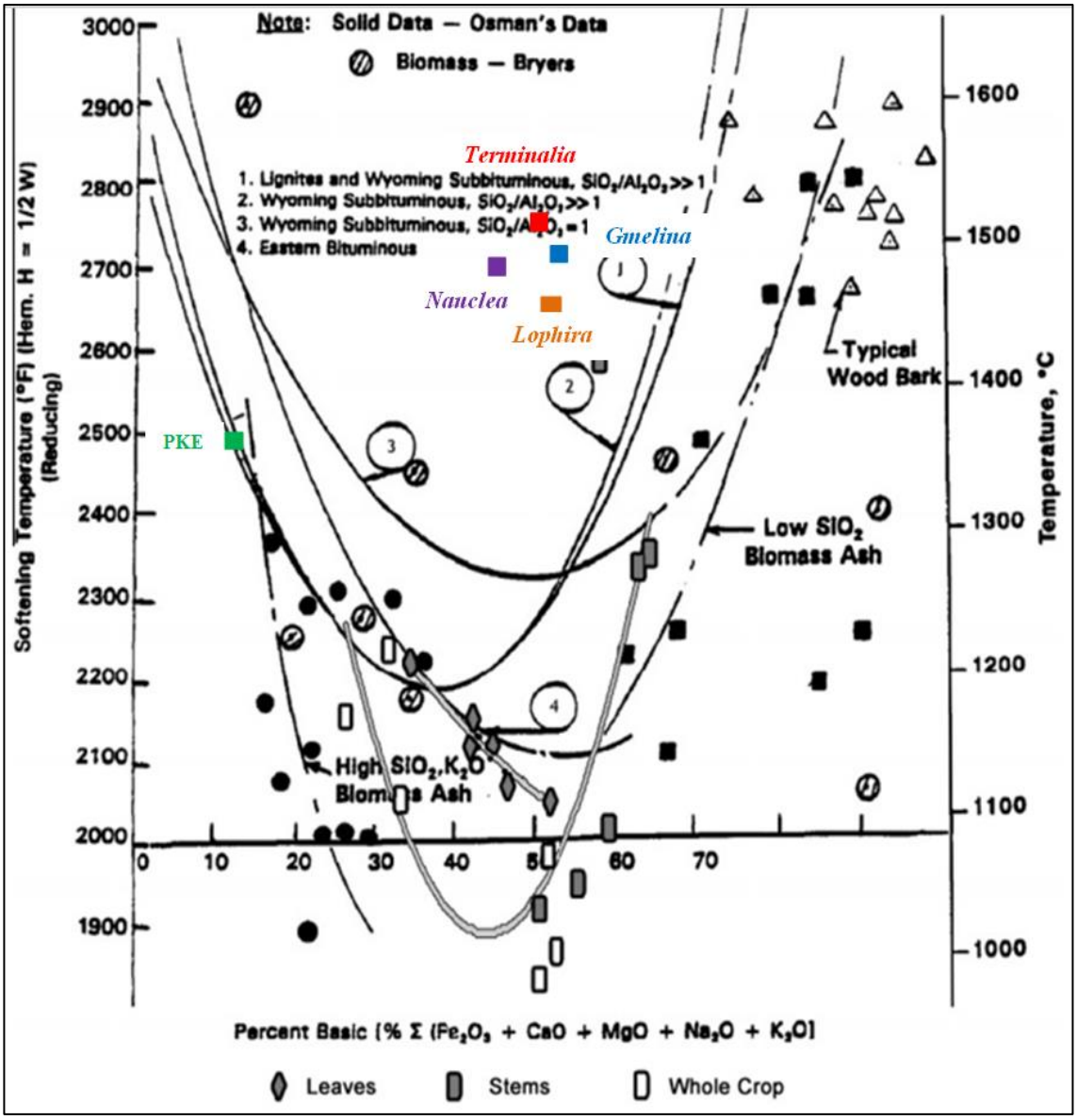

Figure 4-4: Hemisphere temperatures and base percentages of the Nigerian Biomass plotted with Bryers data [162].

4.3.5 Pyrolysis and Combustion Studies

4.3.5.1 Thermogravimetric Analysis (TGA), Differential Thermogravimetric Analysis (DTG)

TGA, DTG and pyrolysis kinetics analysis were carried out using the methods discussed in Section 3.12. The mass loss curve of pyrolysis followed by combustion for the fuels are shown in Figure 4-5 and plots of the derivative of the mass loss curve with time

(DTG) obtained during the temperature programmed pyrolysis and char combustion of the fuels in a thermogravimetric analyzer are shown in Figure 4-6 to 4-8. The temperature at which pyrolysis commences is indicated as T^o while the peak maximum temperature of pyrolysis (temperature for the maximum rate of pyrolysis) is indicated as T^p_{max}. There is a very small peak observed at a temperature <100 °C on the devolatilisation profile, which is due to moisture evaporation, whereas the second (main) peak between 200 and 400 °C is due to volatile release. The pyrolysis reaction continues slowly after the maximum peak temperature and finishes at a temperature which marks the end of volatile loss. This temperature is normally close to the final programmed temperature of 700^{o}C. The residual mass that is left after this temperature is the char and the ash content of the sample. The lower curves in Figure 4-6 to 4-8 illustrate the third stage of the reaction where the residual mass obtained after pyrolysis is cooled and then subjected to temperature programmed combustion to give ash, at a final temperature of 900^{o}C. Two key temperatures are also obtained during char combustion; the temperature T^i which denotes the start of combustion (often referred to as the char ignition temperature) and the temperature T^c_{max} which is the temperature for the maximum rate of combustion.

The four reference temperatures (T^o, T^p_{max}, T^i and T^c_{max}) obtained during pyrolysis and combustion of the fuels are seen in the Figure 4-9. The figure shows that *Gmelina* commenced pyrolysis at the lowest temperature T_o (247 ^{o}C) when compared to other fuels in this study, followed by PKE, *Nauclea* and miscanthus which started pyrolysis at a similar temperature but at 1 ^{o}C interval, i.e. 251, 252 and 253 ^{o}C respectively. Also, the start of pyrolysis is at a temperature of 256 ^{o}C for wheat straw, while *Terminalia* and *Lophira* commenced began pyrolysis at a much higher temperature of 261 and 264 ^{o}C respectively.

During pyrolysis, the lignocellulosic components decompose at different rates. Often, two peaks are seen corresponding to hemicellulose followed by cellulose decomposition over a narrow temperature window, as can be observed in the PKE plot (Figure 4-6). The DTG curves of *Terminalia* and *Lophira* (Figure 4-7) show a main peak with a shoulder at lower temperatures, which is normally considered to arise from

hemicellulose decomposition due to its less stable structure, while the main peak is considered to be mainly due to the degradation of cellulose. In contrast, only one peak can be observed for the devolatilisation of *Gmelina*, *Nauclea* and wheat straw (after drying) as shown in Figure 4-8. These observations are consistent with the comparative amounts of hemicellulose found in the fuels (as reported in Figure 4-1, in the lignocellulosic composition of the Nigerian fuels). It can be observed that the fuels with higher hemicellulose content, e.g. PKE and *Terminalia* resulted in a more pronounced shoulder/ peak due to hemicellulose decomposition (see Figure 4-6 and 4-7). Lignin decomposition occurs over a wide temperature range because of its cross-linked structure and aromatic nature, resulting in a much broader peak [34].

Figure 4-9 also shows the peak maximum temperature of pyrolysis (denoted by T^{p}_{max}) obtained from the DTG plots for the fuels. The T^{p}_{max} for wheat straw is 310^{o}C while *Nauclea* and *Gmelina* have same T^{p}_{max} (325 ^{o}C). The T^{p}_{max} for miscanthus, *Terminalia*, *Lophira* and PKE is 336, 343, 345, and 352 ^{o}C respectively. The devolatilisation and char combustion peak temperatures are often used as indicators of fuel reactivity; the lower the peak temperature, the more reactive the fuel is [35]. Generally, as expected wheat straw, a residue, has the lowest T^{p}_{max} and therefore is the most reactive fuel. The respective peak temperatures for the devolatilisation of *Gmelina* and *Nauclea* are lower compared to the rest of the Nigerian fuels, suggesting that these fuels would be the most reactive. Their tendency to pyrolyse faster than the other fuels is likely due to their relatively high potassium content, because it is known to catalyze pyrolysis reactions [23, 35]. Previous work has shown that the peak temperature for volatile combustion decreases as the potassium content of the fuel increases [23, 35, 36], however, potassium remains a problem in biomass ash as it causes slagging and fouling issues in the combustion chamber.

A very small peak can be observed in the DTG plots for *Lophira* and *Terminali*a at a temperature range 460−620°C (see Figure 4-7). These peaks can be attributed to the decomposition of calcium present in the fuels. An investigation was carried out by pyrolysing the mixture of the fuels and Calcium Oxalate (CaC_2O_4) under TGA (discussed fully in Chapter 6). which confirmed that the occurrence of these peaks in the

DTG curves for *Terminalia* and *Lophira* result from the decomposition of Calcium carbonate ($CaCO_3$), which accounts for ~41% of their ash as shown in Figure 4-3. The mass remaining after pyrolysis is the char, which was cooled down before being heated up in air to obtain the corresponding char burning profile.

The fuels reacts differently as ignition temperature varies for the fuels. The ignition temperature T^i is 314, 341, 345, 360, 390 ^oC for wheat straw, *Gmelina, Terminalia, Nauclea,* and *Lophira* respectively and 390 ^oC for both miscanthus and PKE, as shown in Figure 4-9. The char burning profiles have also been plotted in Figure 4-6 to 4-8 for the fuels studied. The DTG plots for the char combustion stage showed a single peak at temperatures ~300−500 °C except for wheat straw which has two double peaks. The double peaks found in the DTG plot of wheat straw during combustion stage could probably due to the presence of two different types of chars which could have occurred from the different parts of the original fuels, similarly, this has been previously reported by Gudka [171], and Kastanaki and Vamvuka [172].

Figure 4-9 also showed that the peak maximum temperature of char combustion for the fuels are found at temperatures between 397 and 485^oC with wheat straw (397^oC) and *Gmelina* (398^oC) having the lowest and highest T^c_{max} respectively. The T^c_{max} for *Nauclea*, miscanthus, *Terminalia*, *Lophira* and PKE are 428, 451, 403, 425 and 485^oC respectively. At the end of char combustion, is the fuel ash which was left on the sample after the TGA runs. wheat straw gave the most quantity of ash, while the fuels with the least ash quantity are *Nauclea* and *Gmelina*. The amount of ash left for each fuel is similar and consistence to the ash value reported in proximate analysis.

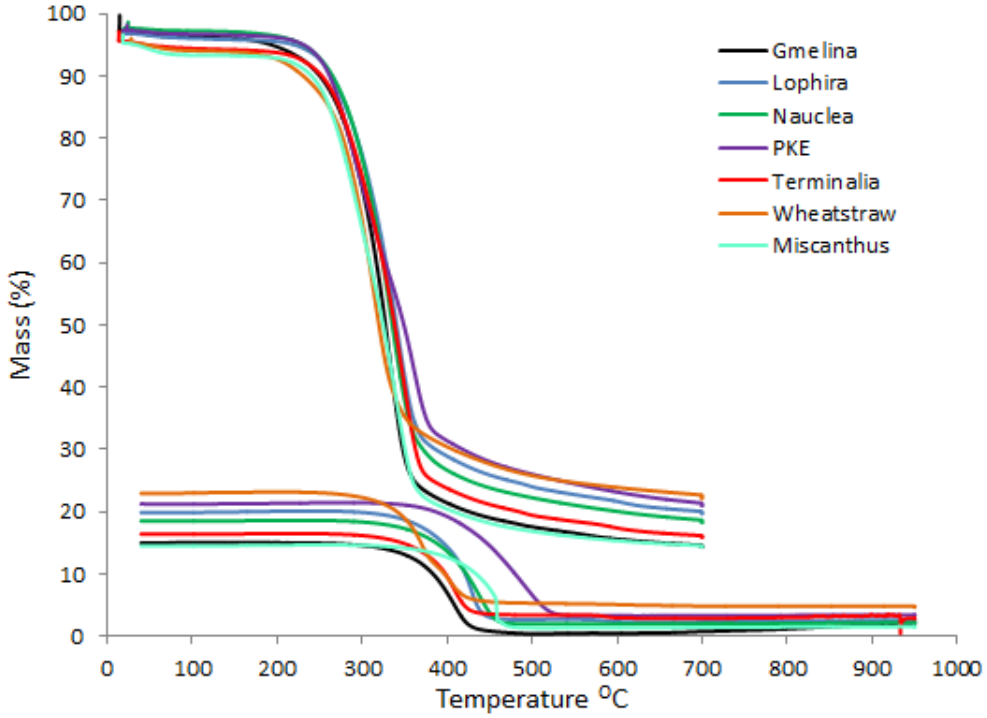

Figure 4-5: Mass loss curves against temperature for the fuels from TGA pyrolysis and combustion studies.

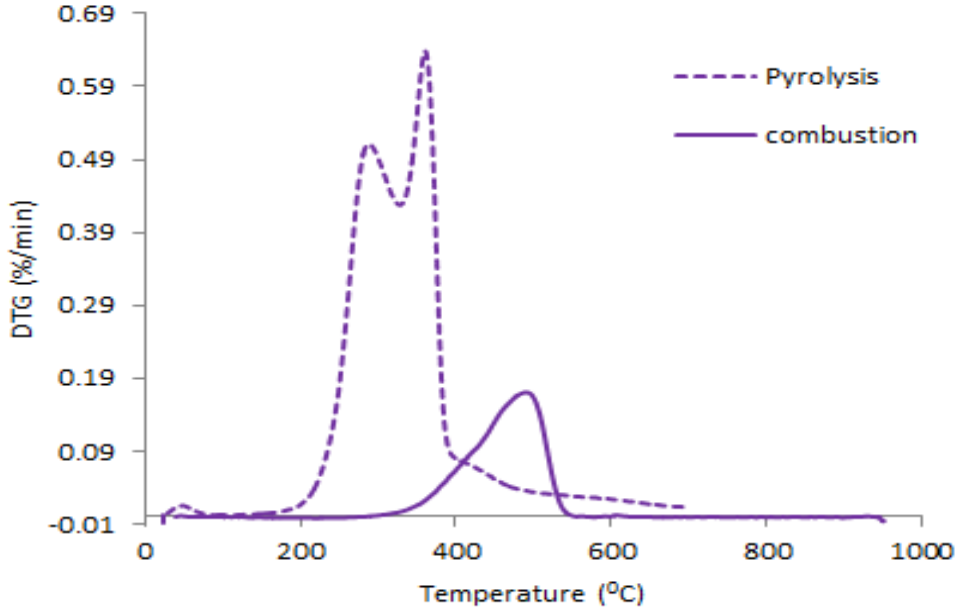

Figure 4-6: Derivative of mass loss (DTG) curves against temperature for PKE from TGA pyrolysis and combustion studies.

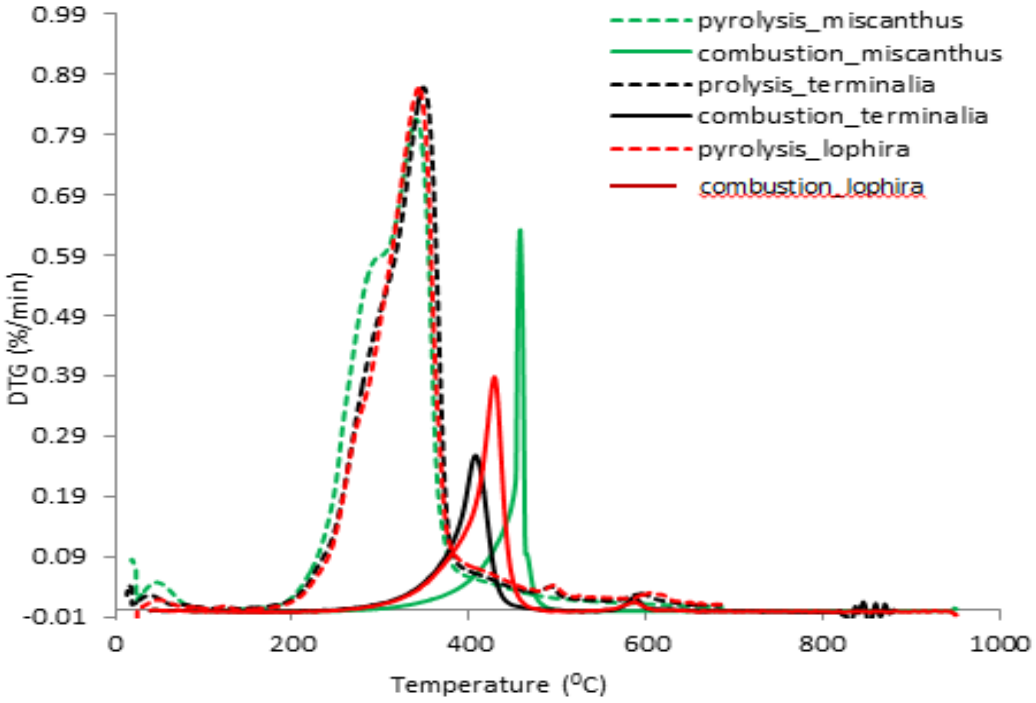

Figure 4-7: Derivative of mass loss (DTG) curves against temperature from TGA pyrolysis and combustion studies for miscanthus, *Terminalia* and *Lophira*.

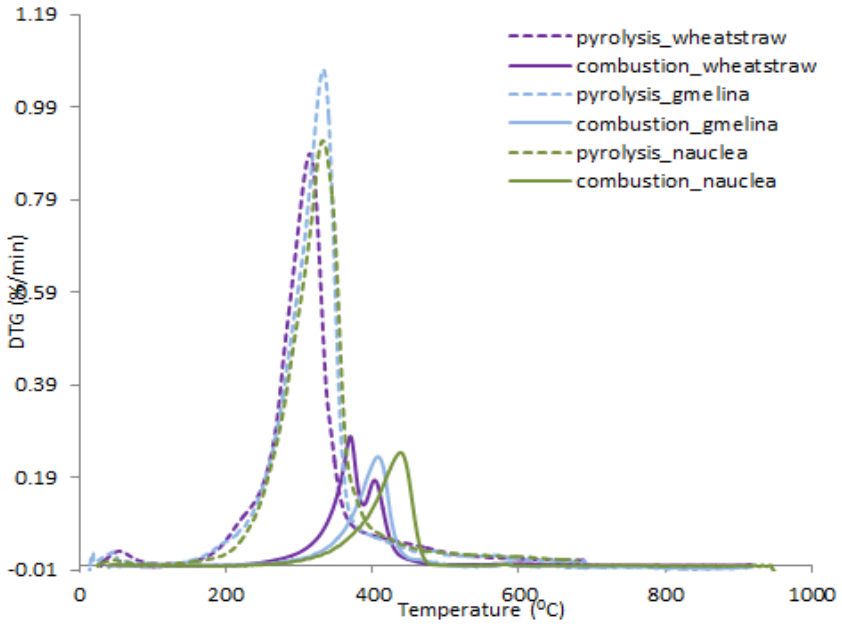

Figure 4-8: Derivative of mass loss (DTG) curves against temperature from TGA pyrolysis and combustion studies for wheat straw, *Gmelina* and *Nauclea*.

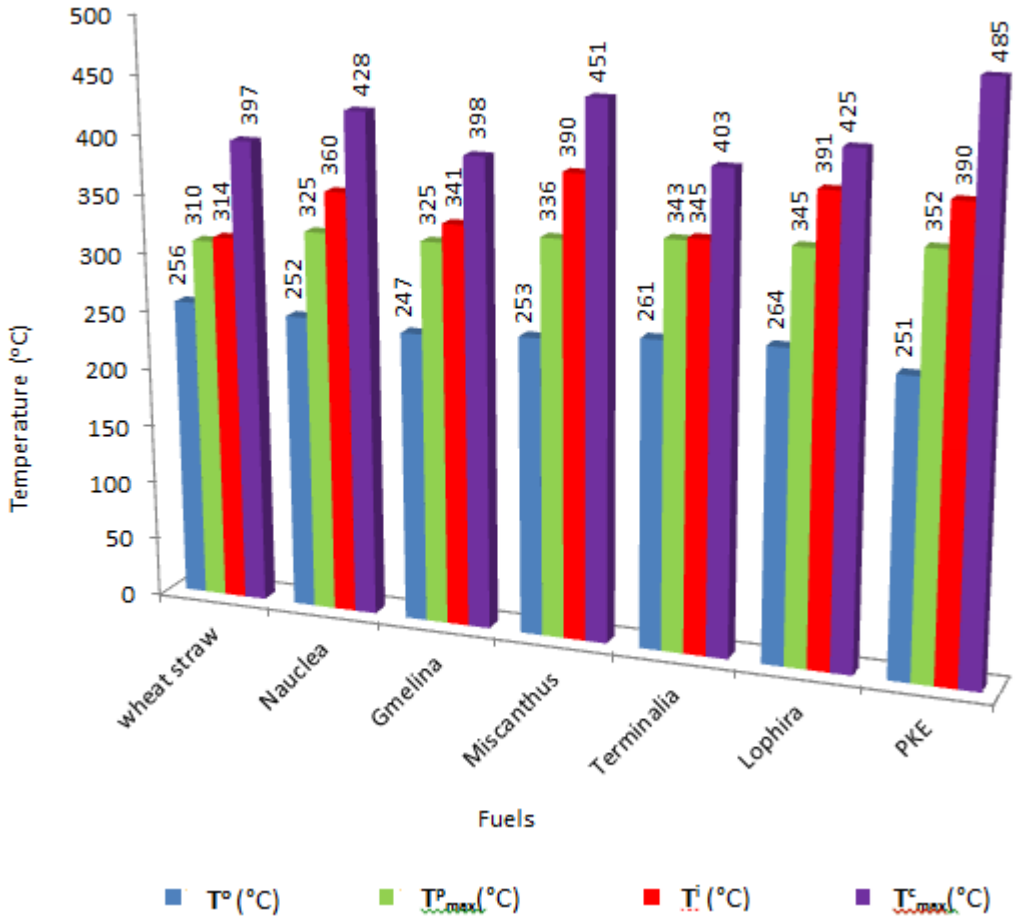

Figure 4-9: Pyrolysis and combustion temperature characteristics of the fuels.

4.3.5.2 Apparent First Order Kinetics

The kinetic parameters for the pyrolysis of the fuels were estimated from the TGA mass loss curves obtained using the methods described in Section 3.12.1.1 and are listed in Table 4-5. For this purpose, an apparent global first-order reaction rate was assumed [63, 79, 83, 173-175]. The rate of breakdown of the chemical constituents in the fuels to form the volatile molecules which then diffuse out of the particle is usually modelled on the much simplified assumption of a single step, first order Arrhenius reaction and is described using Equation (3-15). The pre-exponential factors A (s^{-1}) and activation energies Ea (kJ/mol) were calculated according to the reaction rate constant method [46, 83, 133]. The values of ln A, Ea (kJ/mol), and the correlation co-efficient, R^2 are presented in Table 4-5. The activation energies are approximately 78, 79, 95, 100, 110, 107, and 112 kJ mol^{-1} for *Nauclea*, *Gmelina*, wheat straw, miscanthus, *Terminalia*, PKE

and *Lophira* respectively and with respective pre-exponential factors (ln A) of 9.9, 10, 13.9, 13.9, 14.5, 15.6 and 15.9s^{-1}. The ranking of the Ea follows the same order with the rate of reactivity using DTG peak pyrolysis temperature except for PKE, which showed the highest peak temperature but resulted in slightly lower activation energy than both *Terminalia* and *Lophira*. For comparison purposes, the pyrolysis reactivities of the fuels were estimated at 573 K (k_{573}), using the kinetic parameters obtained, and these are also listed in Table 4-5. The higher the value of k at the reference temperature, the more reactive the fuel is [83, 133, 176]. From the data in Table 4-5, it is predicted that at k_{573} *Nauclea* and *Gmelina* would pyrolyse faster than *Terminalia* and *Lophira*, and that PKE would be the least reactive fuel. As expected, the same order of reactivity is obtained when comparing the peak temperatures for devolatilisation.

Table 4-5: Kinetics parameters of fuels as obtained from TGA pyrolysis

Fuel	Ln A (S^{-1})	Ea (kJ mol^{-1})	k_{573} (S^{-1})	R^2
wheat straw	13.95	94.52	0.00276	0.9904
Nauclea	9.88	77.81	0.00157	0.9953
Gmelina	10.03	78.77	0.0015	0.9947
miscanthus	13.88	99.55	0.0009	0.9761
Terminalia	15.57	110.24	0.00052	0.9982
Lophira	15.93	111.98	0.00051	0.9801
PKE	14.53	107.48	0.00033	0.9985

4.3.5.3 Single particle combustion

Single particle combustion experiment was carried out using the method described in Section 3.14. The video images recorded from the single particle combustion in a methane flame experiments were analysed to gain an insight into the combustion behaviour of the fuels at high heating rates/high temperature, and the following stages could be clearly identified from these images: ignition, volatile combustion, and char combustion. Consequently, the visual analysis of the images allowed the estimation of the ignition delay, and of the duration of the volatile and char combustion stages. In this work, the ignition of a fuel particle was assumed once flaming combustion was visible, after exposure to the flame.

The parameters that were used to assess the combustion properties of the fuels; i.e. ignition delay (sec), volatile combustion / duration of devolatilization (sec) and char combustion / duration of char burn-out (sec) were plotted against the dry mass of the sample (mg), and were established by referencing the following:

- The frame or time of the exposure of the particle to the flame (*a*).
- The frame or time when the particle became ignited (*b*).
- The frame or time at which the flame on the particle ends (*c*).
- The frame or time at which char combustion was completed (*d*).

The following calculations were further assessed:

- Ignition delay (sec) = b – a.
- Duration of devolatilisation / flame combustion (sec) = c – b.
- Duration of char combustion / burn-out (sec) = d – c.

When the biomass particle is exposed to the flame, it goes through the process of heating-up, moisture evaporation and then ignition [177, 178]. For the particle size studied here, the ratio of heat convected to the surroundings to heat conducted to the surface, i.e. the Biot number, which affects the heating-up process and the ignition delay, can be significantly influenced by the moisture content. However, in these experiments, the biomass was oven-dried (∼5−12% moisture). Ignition usually marks the beginning of volatile combustion and the end of moisture release. In combustion processes, the moisture content in the fuel particle is important because the requirement to dry the particles in the flame before they heat up and ignite causes a delay in the ignition process and can result in lifted or unstable pulverized fuel flames [179]. It is important to mention that the lignocellulosic constituents of the fuels differ, and softwoods *(Terminalia and Gmelina)* contain a smaller fraction of hemicellulose and a higher fraction of lignin when compared to hardwoods. Hemicellulose is considered to ignite faster, at the lowest temperature, when compared to cellulose and lignin [180]. A

plot of the ignition delay against original dry mass of the fuel particle can be found in Figure 4-10.

The differences in the ignition delay of the selected Nigerian fuels can be observed in Figure 4-10. From Figure 4-10, it can be observed that there were differences in the ignition delay of the studied Nigerian fuels. The ignition delay for *Nauclea* and *Gmelina* show a smaller dependence on particle mass than *Terminalia* and *Lophira*. However, in this case, this is probably due to the chemical composition of *Nauclea* and *Gmelina* and both fuels having significantly low moisture contents when compared with *Lophira*. Density and thermal conductivity differences of the woods will also influence moisture and volatile diffusion rates as well as heating rates. The ignition delay of *Nauclea*, *Terminalia*, *Lophira*, and *Gmelina* ranged from 0.03−0.05, 0.04−0.10, 0.03−0.11, and 0.04−0.06 s respectively, with error ≤ ± 0.008 s due to video frame speed. The spread in ignition delay arises in part from the difficulty in cutting particles to exactly the same size and also, in part, to the homogeneity of moisture content in individual particles. On average, *Nauclea* and *Gmelina* ignite faster, indicating that these fuels may be more reactive. As discussed in Section 4.3.5.1, the temperature of maximum volatile production rate is ∼20 °C lower for *Nauclea* and *Gmelina* compared to *Terminalia* and *Lophira* (see Figure 4-9).

Video analysis of the combustion of single particles revealed overlap of volatile (flaming) combustion and char (glowing) combustion in some cases, where char combustion proceeded at the bottom of the particle while volatile release and combustion occurred from the top of the particle. Even so, the combustion processes were analyzed as independent steps, which are discussed in this section. Volatile combustion was observed as the first stage following ignition, where the particles pyrolyzed and volatile organic compounds were released. Figure 4-11 shows the duration of volatile combustion plotted against the particles' initial dry mass. During this stage, the particles were seen to undergo devolatilisation and the volatile materials released were combusted resulting in a flame. The volatile content, and therefore its rate of release, differ for all the fuels due to their composition (see Table 4-1), and also due to the differences in mass. This accounted for the variation in the duration of

devolatilisation/volatile combustion of the fuels. The duration of flame combustion is comparable for all the fuels, except for *Nauclea*, as shown in Figure 4-11. There is quite a clear distinction between *Nauclea* and the other fuels, as similar sized particles are heavier in mass when compared to the other fuels. This resulted in a relatively longer volatile combustion stage (3.37−5.26 s). The flame duration for *Terminalia, Lophira,* and *Gmelina* ranged from 2.38−3.53, 3.22−4.21 and 2.02−3.74 s, respectively (error ≤ ±0.008 s). *Lophira* also had slightly longer flame duration than *Terminalia* and *Gmelina,* possibly due to slower release of volatile matter and also to variations in wood density. After flaming combustion, when all volatiles have been released, the volatile flame extinguishes, and oxygen can reach the residual char particle and heterogeneous char combustion commences. This process continues until the char is eventually reduced to a small mass of ash. It was also observed that shortly after devolatilization, the particle started to shrink and then shrinks more rapidly toward the end of the combustion reaction until the residual ash was left attached to the supporting needle, i.e., the video evidence is consistent with a "shrinking sphere" model for char combustion (Zone II or III) where there is a contribution to the observed combustion rate from diffusion processes. For this work, the duration of char burnout was estimated from the end of volatile combustion until complete char burnout was evident. Figure 4-12 shows the plot of char burnout duration versus dry mass for the fuels. From Figure 4-12, it can be seen that the duration for char burnout for *Terminalia,* and *Gmelina* were comparable, and ranged from 7.7 to 11.9 s (error ≤ ±0.008s), whereas the *Lophira* and *Nauclea* particles showed distinctly longer char burnout stages (9.7−19.1 and 21.6−39.5s, respectively). The major factors controlling char burnout are (i) the mass of char remaining after devolatilisation, (ii) the chemical factors determining the amount of high-temperature volatiles produced and on the development of char porosity, (iii) the amount of catalytic metals present in the char, (iv) the chemical reaction rate of the char combustion, and (v) the diffusion rates. *Lophira* and *Nauclea* have higher fixed carbon contents and higher heating values than the other fuels, which could have resulted in a larger mass of char and therefore longer char burnout. Variations in the density of the raw material, the elemental carbon content of the resultant char and porosity may also contribute to differences in char combustion rates. *Terminalia,* which has an average wood density of 550 kg m^{-3} and *Gmelina,* with average wood density of 530 kg m^{-3}, are

classified as medium density woods, whereas *Nauclea* (760 kg m^{-3} average wood density) and *Lophira* (with 940 kg m^{-3} average wood density) are classified as high-density woods. The higher mass per unit volume as well as possible depletion of amount of catalytic metals present in the resultant chars of could be responsible for the longer burn out rate of *Lophira* and *Nauclea*'s chars when compared with those of *Terminalia* and *Gmelina*; further work will establish the porosity development during devolatilisation and provide added insight into the observed differences in burnout rates. The slightly higher burnout times observed in *Nauclea* compared to *Lophira* could be due to *Nauclea*'s relatively higher elemental carbon content (see Table 4-2).

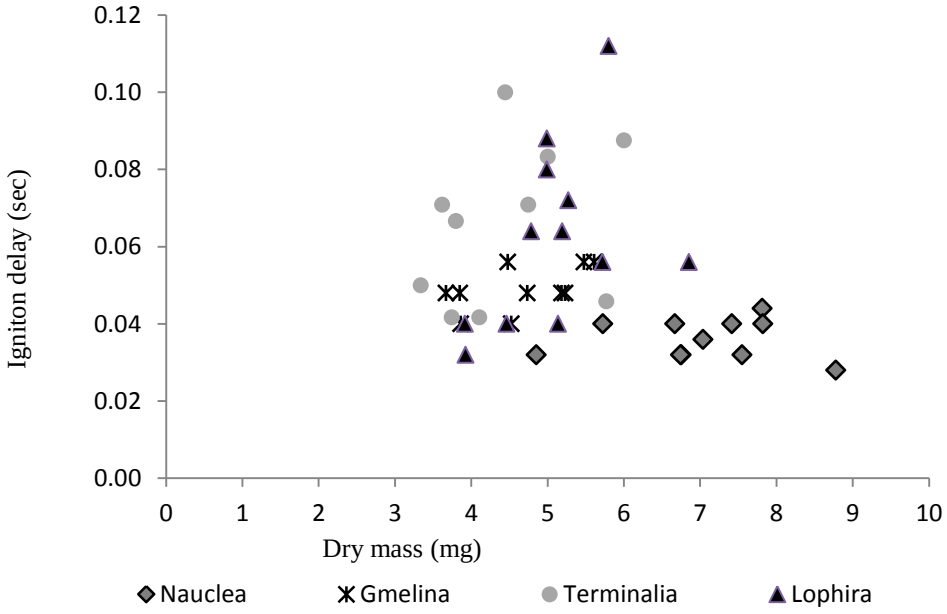

Figure 4-10: Plot of the ignition delay against particle mass.

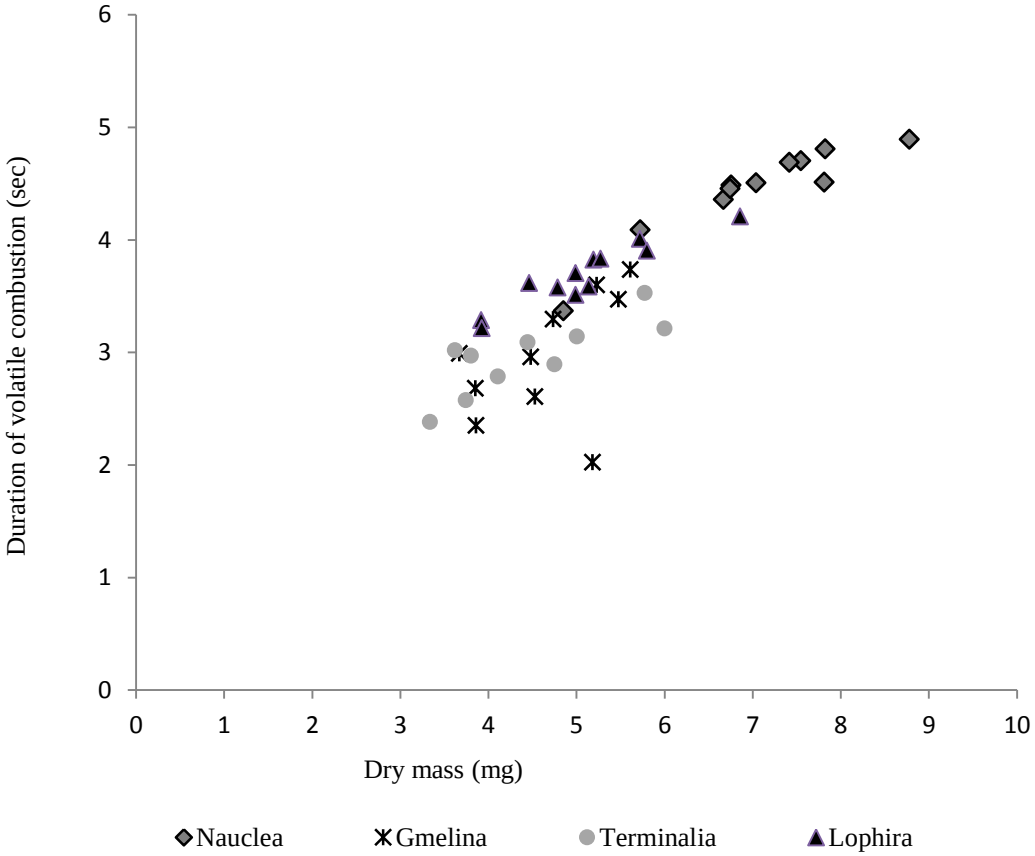

Figure 4-11: Flame duration versus dry particle mass of the fuels.

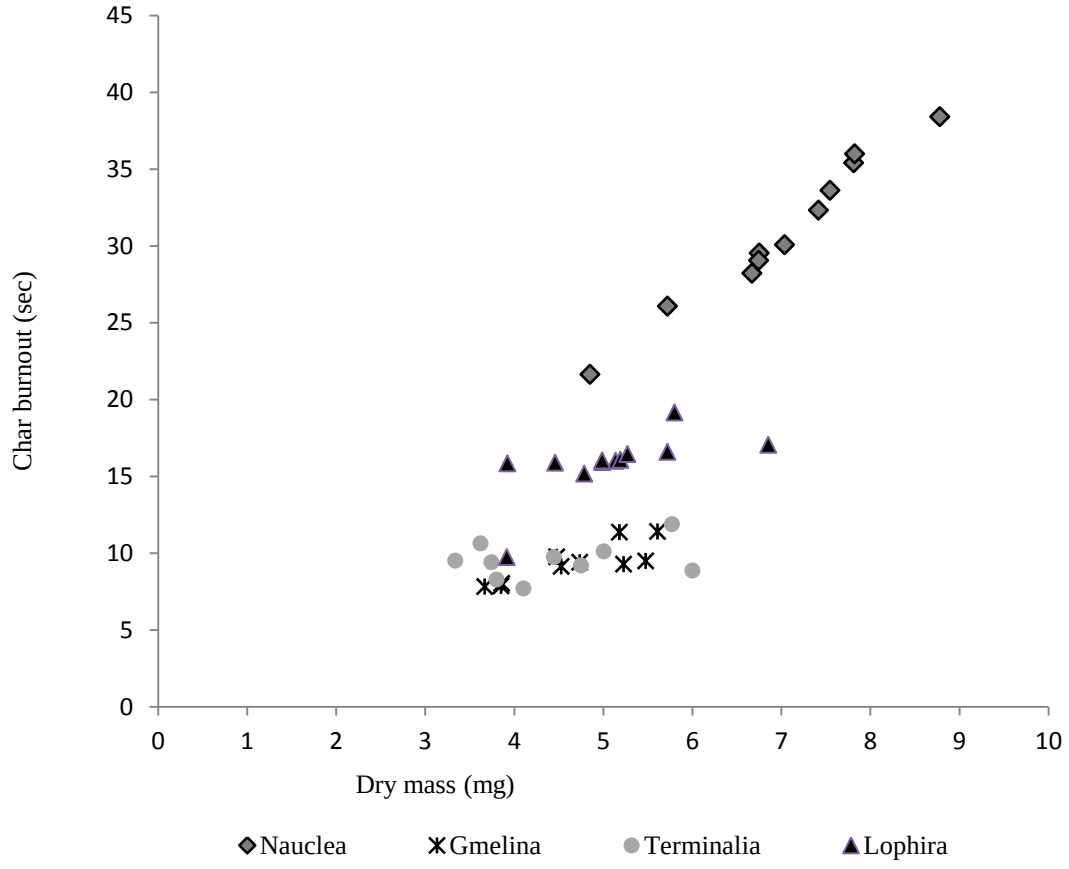

Figure 4-12: Char burnout duration versus dry particle mass of the fuels.

4.3.5.4 Pyrolysis-Gas Chromatography-Mass Spectrometry (Py-GC-MS)

Pyrolysis−Gas Chromatography−Mass Spectrometry (Py−GC−MS) was used to investigate the different organic groups in the volatiles released. The technique involves rapid heating of the fuels, which results in the release of volatile organic compounds and other volatile components from cellulose, hemicellulose, and lignin in a similar way to flash pyrolysis [181]. The analysis highlights the differences in biomass composition and structure of the fuels. The released products differ, depending on the amount and nature of the polymers found in the feedstock, but is also influenced by metal components, especially potassium [75]. To provide a semi-quantitative analysis some of the identified products were reported as a function of their peak area percentage. The experiment was conducted twice for each fuel to check the reproducibility of this analytical process. The average values of the peak area and peak area percentage were calculated and used for discussion for each of the identified product.

Table 4-6 shows the selected marker compounds for oil and lignocellulosic fractions in the Nigerian fuels, including PKE. The chromatograms obtained from the Py−GC−MS of the Nigerian fuels (with assignments to the main peaks) are presented in Figures 4-13 to 4-19. The main peaks were assigned from the mass spectral detection NIST05A MS library and also from the literature [120, 157]. A wide variation of decomposition products from lignocellulose and also products from oil components in the fuel, including long chain fatty acids, are observed in the chromatograms. Figure 4-20 to 4-21 shows a comparison of the decomposition products from the Py−GC−MS analyses for the fuels studied against their dry weight percentage. The peak area percentages were calculated from the chromatograms and normalized per mg of volatile products as detailed in Nowakowski *et al.*[157]. The decomposition products are also grouped into their various lignocellulosic components in Table 4-6. The peak area percentages were calculated from the chromatograms and quantified as a percentage of the fuel sample dry weight, which are listed in Table 4-7. The main products from their pyrolysis are methoxyphenols, originating from the degradation of their lignin fraction in the temperature ranges from 200-500°C [182-184]. Lignin is seen as a complex, heterogeneous polymer that is formed by the polymerization of three phenyl propane monomers, namely syringyl (3,5-dimethoxy-4-hydroxyphenyl), guaiacyl (4-hydroxy-3-methoxyphenyl), and p-hydroxyphenyl units [184]. The main pyrolysis of lignin commences with thermal softening at temperatures usually around 200 °C, and at higher temperatures. The fast pyrolysis of the lignin fraction resulted in monomeric phenolic compounds and oligomers with different degrees of polymerization; these lignin-derived products are primarily responsible for the highmolecular weight and viscosity of bio-oils [181]. The conversion process and resultant products in fast pyrolysis depend on several operating parameters [185]. The most important parameters are the pyrolysis temperatures and heating rates, which determine the final yields of products obtained: bio-oil, noncondensable gases, or char [69, 73, 181, 185, 186]. The mineral content in biomass also affects the quantity and quality of the products yields [69]. The literature suggests that high contents of monovalent potassium and divalent calcium in fuels are responsible for the lower organic volatile yield and may promote dehydration of holocellulose and demethoxylation of lignin units during pyrolysis [69, 72, 73, 181, 185-187]. This is consistent with the findings in this studies as Terminalia, which has the

highest CaO content (41.7 wt %) records the highest peak area % for lignin products especially for methoxy-phenols and phenols (see Figure 4-21). Depolymerization is the main process responsible for the decomposition of holocellulose during fast pyrolysis [72]. Qiang *et al.*[187] reported that the depolymerisation process results in the formation of various anhydrosugars (mainly levoglucosan), furans and other products, although the high content of CaO in the fuel reduces the formation of levoglucosan. The presence of calcium promotes glucose fragmentation instead of cellulose depolymerization. [72]. Levoglucosan, is often the main product formed from the depolymerisation reaction of cellulose [72]. Further cellulose degradation also leads to formation of furan and acids. During the pyrolysis of PKE, most of the furan compounds are from the dehydration of carbohydrates [188].

Table 4-7 shows the relative percentages of the volatile products that originate from the decomposition of the different lignocellulosic fractions and extractives. It can be observed that miscanthus, PKE and *Gmelina* are the only fuels that present extractive (oily compounds) in their volatile fraction. Since, the GC column used detects mostly the light to medium volatile products coming off from the pyrolysis of the fuels many of the cracked products are not being detected. Also some of the fuels studied have high contents of catalytic metals (e.g. Potassium) that are well known to crack holocellulose into lighter compounds, which are very likely to be missed by the column. Finally, the volatile yields from the Py-GC−MS experiments (Table 4-7) are slightly higher than the measured volatile content (Table 4-1). This is expected, since the pyroprobe is a flash pyrolysis technique that involves the rapid heating of samples and faster heating rates are known to favor higher volatile yields than slow pyrolysis.

Table 4-6: Classification of pyrolysis products into lignocellulosic groups [75, 157, 183].

Lignocellulosic component	Degradation temperature	Evolved compounds
Hemicellulose	150-350^{o}C	1,3-Pentadiene, 3-Methyl-1,2-cyclopentanedione, 1-methyl-4-(1-methylethenyl)-cyclohexanol, hydroxyl-2-Cyclopenten-1-one, Acetic acid.
Cellulose	275-350^{o}C	Furan, 2-methyl furfural, 1,2-Cyclopentanedione, Furanmethanol, 2(5H)-Furanone, Vinylfuran.
Lignin	250-550^{o}C	2-methoxylphenol; 2-methoxy-4-methylphenol; 4-methylphenol; 4-ethyl-2-methoxyphenol; 2-Methoxy-4-vinylphenol; Eugenol; 2,6-dimethoxyphenol, 2-methoxy-4-(prop-1-enyl) phenol, 1,2,4-Trimethoxybenzene; 1-(4-hydroxy-3-methoxyphenyl)-ethanone 3',5'-Dimethoxyacetophenone 1-(4-hydroxy-3-methoxyphenyl)-2-propanone 2,6-dimethoxy-4-(prop-2-en-1-yl) phenol, Methylparaben, Vanillin, Phenol.
Extractives	250-550^{o}C	Decanoic acid Desaspidinol Hexadecanoic acid 6-Octadecenoic acid 2,2-diethyl-3-methyl- Oxazolidine.

Table 4-7: Quantification of volatile yields into lignocellulosic groups (Peak area %)

Sample	Hemicellulose	Cellulose	Lignin	Oil	High-heating rate volatile yields
Lophira	2.8	<1	97.2	<1	87.1
Terminalia	11.1	<1	88.9	<1	82.5
Gmelina	<1	<1	87.5	12.5	84.2
PKE	<1	11.7	85.6	2.7	79.6
Nauclea	13.6	<1	86.4	<1	83.9
miscanthus	15.7	27.4	39.4	17.5	74.4
wheat straw	36.6	22.0	41.4	<1	87.8

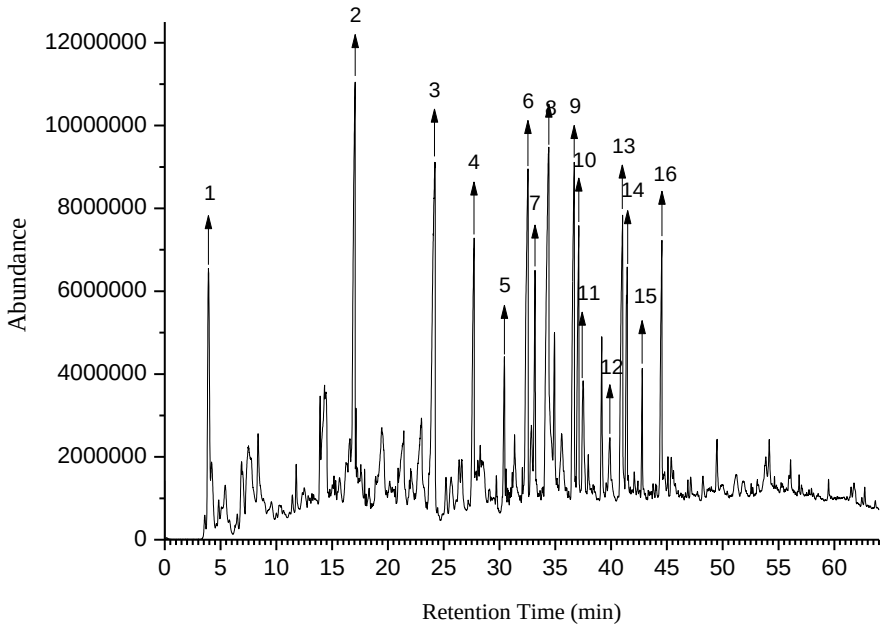

Figure 4-13: Py GC-MS chromatogram of *Nauclea* showing assigned peaks.

The main peaks are assigned as follows: 1: 1,3-pentadiene, 2: cyclohexanol, 1-methyl-4-(1-methylethenyl)-, acetate; 3: 2-methoxyphenol; 4: 2-methoxy-4-methylphenol; 5: 4-ethyl-2-methoxyphenol; 6: 2-methoxy-4-vinylphenol; 7: eugenol; 8: 2,6-dimethoxyphenol; 9: 2-methoxy-4-(1-propenyl) phenol -; 10: 1,2,4-trimethoxybenzene; 11: vanillin; 12: ethanone, 1-(4-hydroxy-3-methoxyphenyl); 13: 3',5'-dimethoxyacetophenone; 14&15: 2,6-dimethoxy-4-(2-propenyl)phenol.

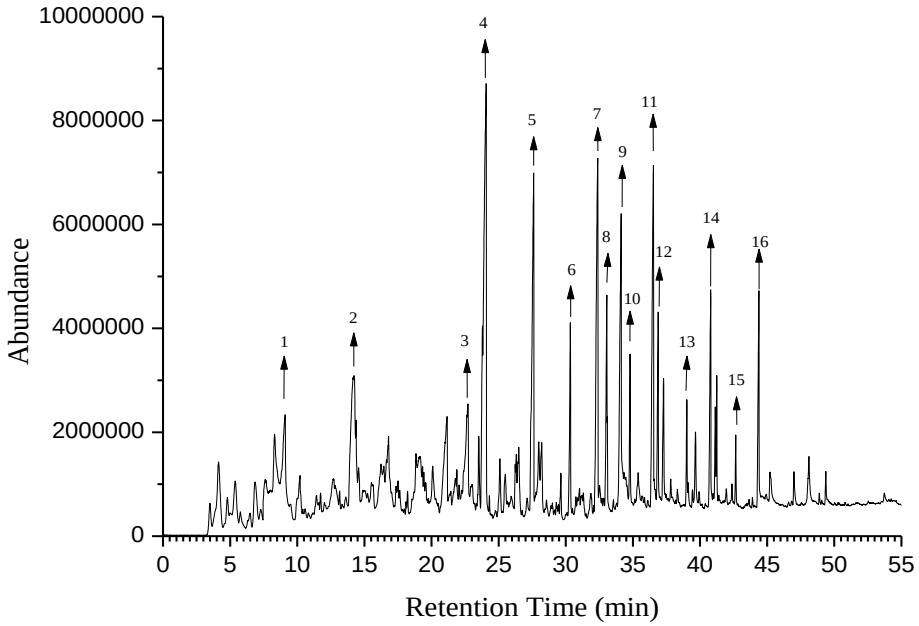

Figure 4-14: Py GC-MS chromatogram of *Terminalia* showing assigned peaks.

The main peaks are assigned as follows: 1:1,3-pentadiene, 2: cyclohexanol, 1-methyl-4-(1-methylethenyl)-, acetate; 3: 1,2-cyclopentanedione, 3-methyl; 4: phenol; 5: 2-methoxyphenol; 6: 2-methoxy-4-methylphenol; 7: 4-ethyl-2-methoxyphenol; 8: 2-methoxy-4-vinylphenol; 9: eugenol; 10: 2,6-dimethoxyphenol; 11: 2-methoxy-4-(1-propenyl)-phenol; 12: 1,2,4-trimethoxybenzene; 13: vanillin; 14: ethanone, 1-(4-hydroxy-3-methoxyphenyl); 15: 3',5'-dimethoxyacetophenone; 16: 2,6-dimethoxy-4-(2-propenyl)phenol.

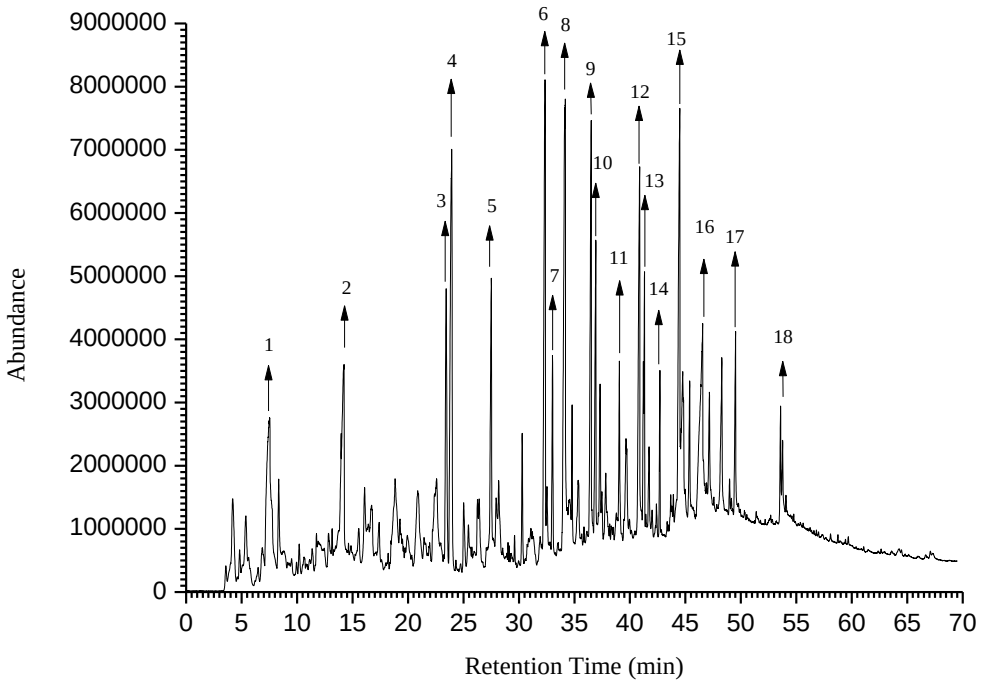

Figure 4-15: Py GC-MS chromatogram of PKE showing assigned peaks.

The main peaks are assigned as follows: 1: furan, 2-methyl-; 2: furfural; 3: phenol; 4: 2-methoxyphenol; 5: 2-methylphenol; 6: 4-methylphenol; 7: 2-methoxy-4-methylphenol; 8: 4-ethyl-2-methoxyphenol; 9: 2-methoxy-4-vinylphenol; 10: 2-methoxy-3-(2-propenyl)phenol; 11: 2,6-dimethoxy-phenol; 12: 2-methoxy-4-(1-propenyl)-phenol; 13: 1,2,4-trimethoxybenzene; 14: vanillin; 15: 3',5'-dimethoxyacetophenone; 16: 2,6-dimethoxy-4-(2-propenyl)-phenol; 17: n-hexadecanoic acid; 18: 6-octadecenoic acid.

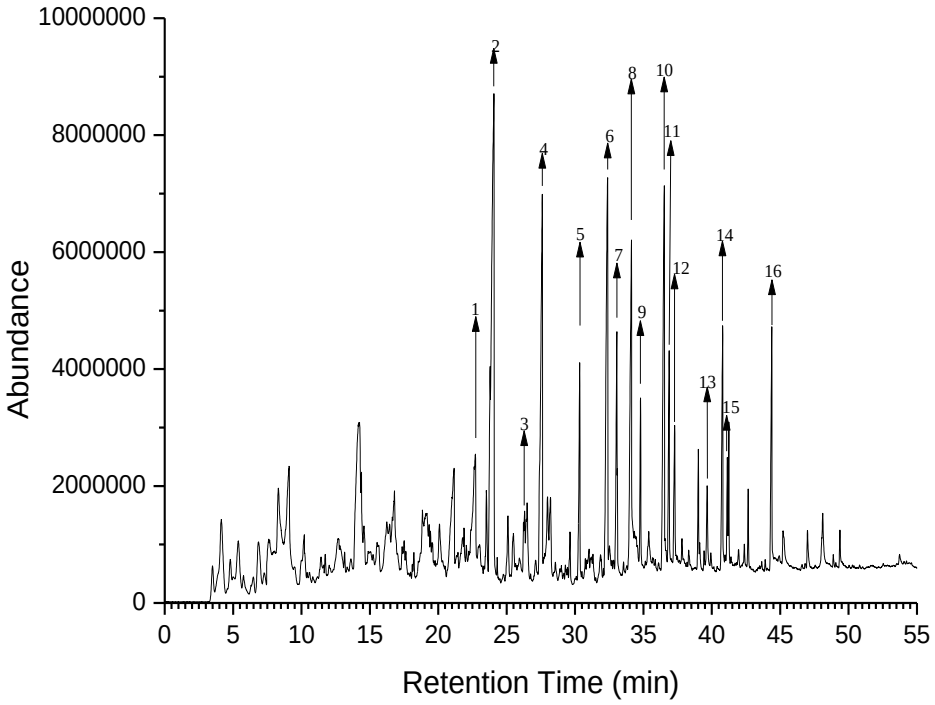

Figure 4-16: Py GC-MS chromatogram of *Lophira* showing assigned peaks.

The main peaks are assigned as follows: 1: 1,2-Cyclopentanedione, 3-methyl; 2: 2-methoxyphenol; 3: 2-methoxy-3-methylphenol; 4: 2-methoxy-4-methylphenol; 5: 4-ethyl-2-methoxyphenol; 6: 2-Methoxy-4-vinylphenol; 7: eugenol; 8: 2,6-dimethoxyphenol; 9: 2-methoxy-4-(1-propenyl)phenol; 10: 1,2,4-trimethoxybenzene; 11: vanillin; 12: ethanone, 1-(4-hydroxy-3-methoxyphenyl)-; 13: 3',5'-dimethoxyacetophenone; 14: 2-propanone, 1-(4-hydroxy-3-methoxyphenyl)-; 15: 2,6-dimethoxy-4-(2-propenyl)phenol; 16: 2,4-hexadienedioic acid, 3,4-diethyl-dimethyl ester.

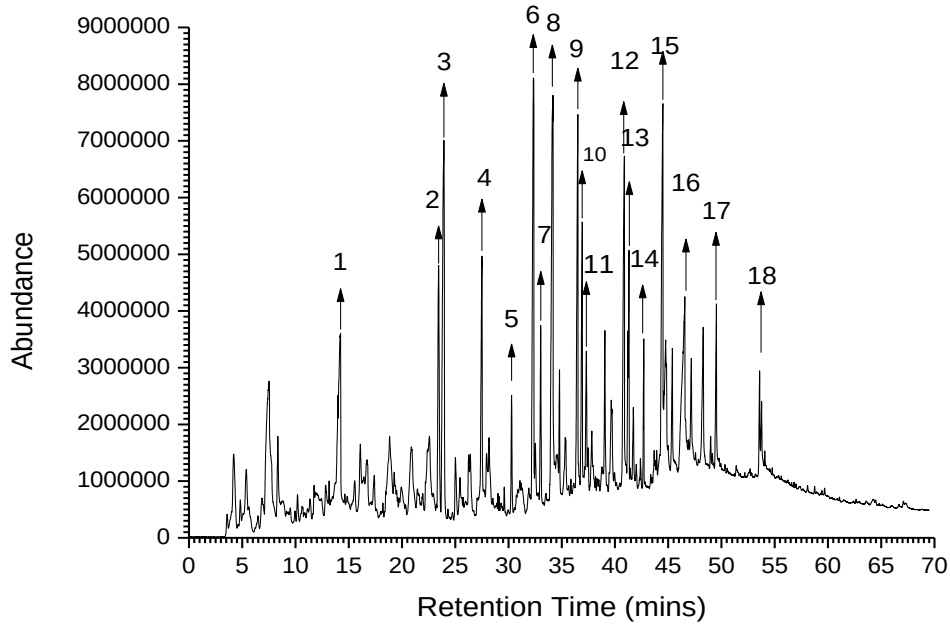

Figure 4-17: Py GC-MS chromatograms of *Gmelina* showing assigned peaks.

The main peaks are assigned as follows: 1: 3,5-dimethylpyrazole-1-methanol; 2: phenol; 3: 2-methoxyphenol; 4: 2-methoxy-4-methylphenol; 5: 4-ethyl-2-methoxyphenol; 6: 2-methoxy-4-vinylphenol; 7: eugenol; 8: 2,6-dimethoxyphenol; 9: 2-methoxy-4-(1-propenyl)phenol; 10: 1,2,4-trimethoxybenzene; 11: vanillin; 12: 3',5'-dimethoxyacetophenone; 13: 2,6-dimethoxy-4-(2-propenyl)-phenol; 14: methylparaben; 15: decanoic acid; 16: desaspidinol; 17: hexadecanoic acid; 18: 6-octadecenoic acid.

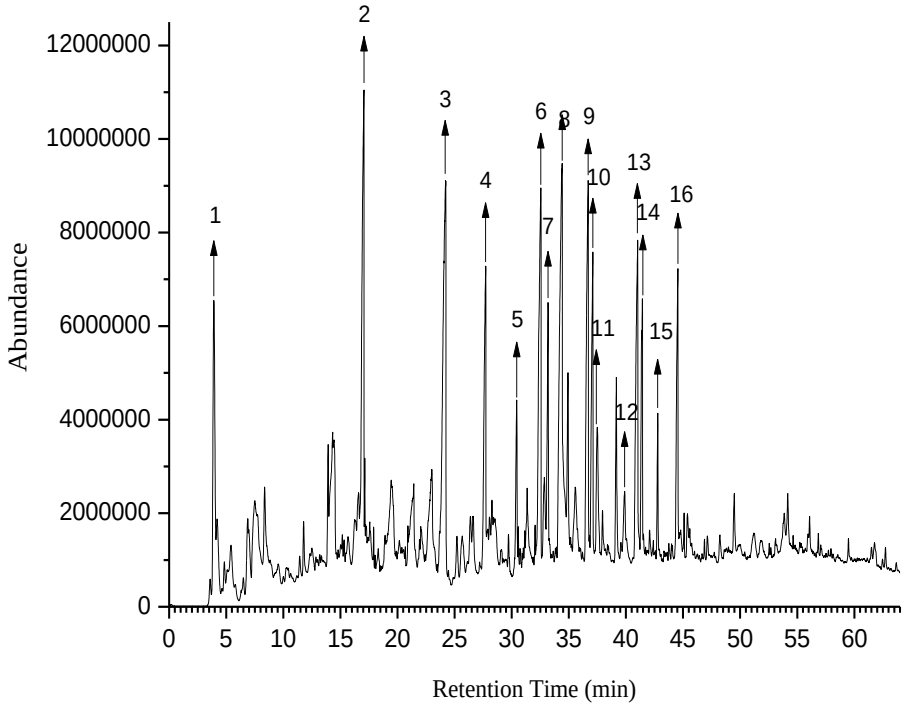

Figure 4-18: Py GC-MS chromatogram of miscanthus showing assigned peaks.

The main peaks are assigned as follows: 1: Acetic acid; 2: hydroxy-2-Cyclopenten-1-one; 3: methoxyphenol; 4: 4-methylphenol; 5: 4-ethyl-2-methoxyphenol; 6: 2-methoxy-4-vinylphenol; 7: eugenol; 8: 1,2-Cyclopentanedione; 9: Furanmethanol; 10: Furan, 2-methyl-; 11: Vinylfuran; 12: Furfural; 13&14: 2(5H)-Furanone; 15: 1,2-Cyclopentanedione 16: Oxazolidine, 2,2-diethyl-3-methyl-.

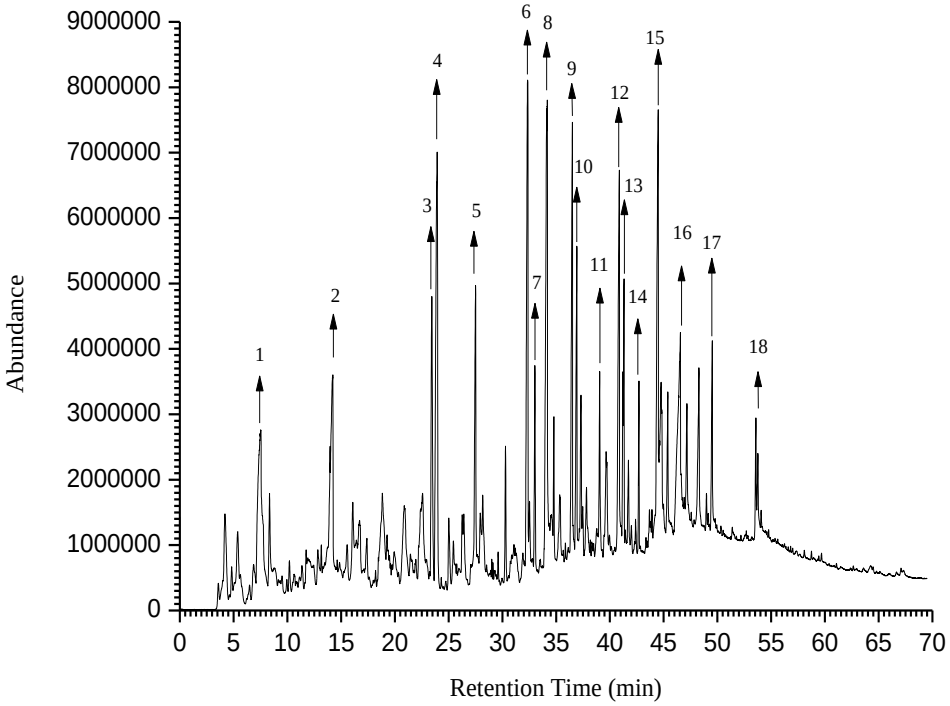

Figure 4-19: Py GC-MS chromatogram of *wheat straw* showing assigned peaks.

The main peaks are assigned as follows: 1: 1,3-pentadiene, 2: Acetic acid; 3: Fufural; 4: 2-Furanmethanol; 5: 3,4-Furandimethanol; 6: 1,2-Cyclopentanedione, 3-methyl-; 7: Vinylfuran; 8&9: Phenol, 2-methoxy-; 10&11: Phenol, 2-methyl-; 12: 2-Cyclopenten-1-one, 3-ethyl-2-hydroxy-; 13&14: Phenol, 2-methoxy-4-methyl-; 15&16: Phenol, 4-ethyl-2-methoxy-; 17&18: 2-Methoxy-4-vinylphenol.

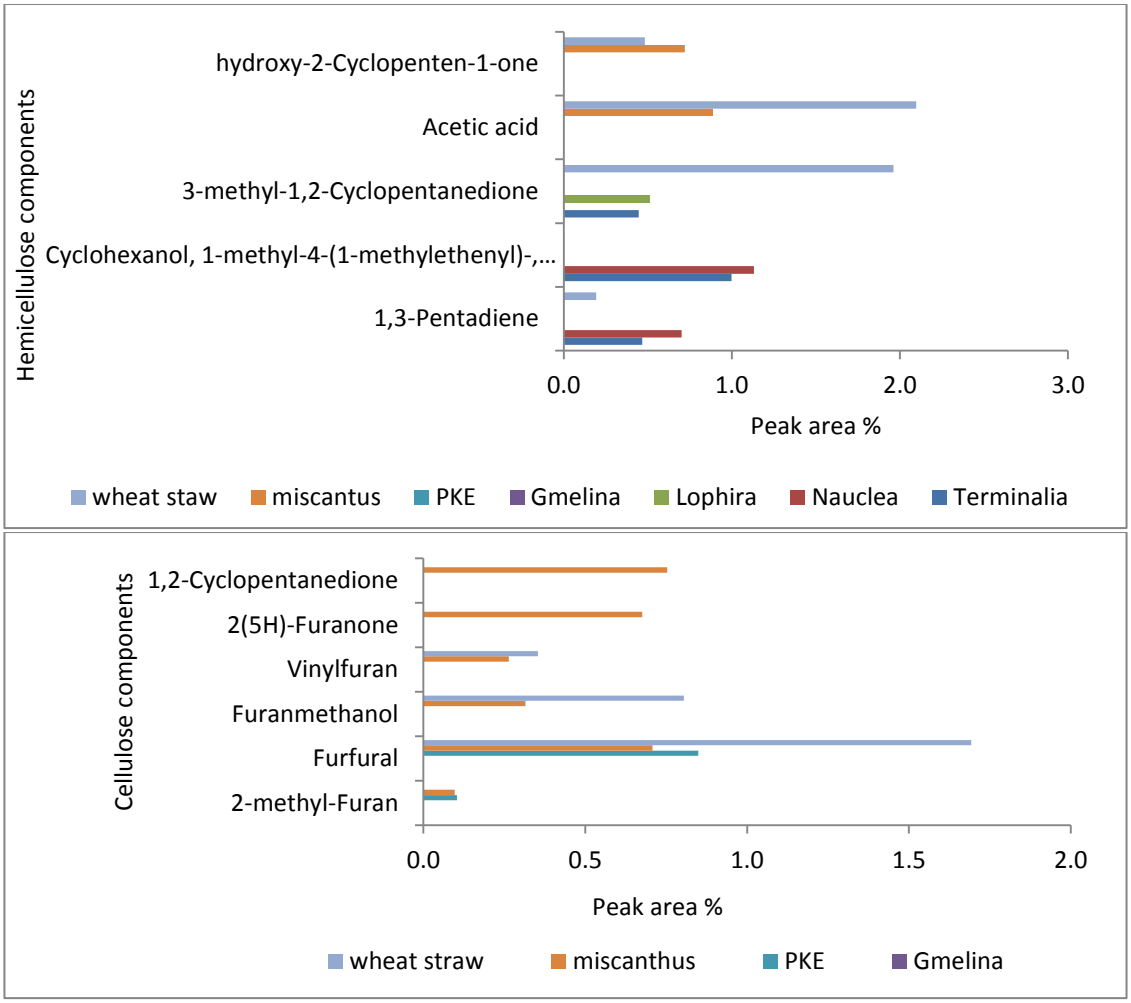

Figure 4-20: Key markers from the Py-GC-MS analysis of the Nigerian fuels.

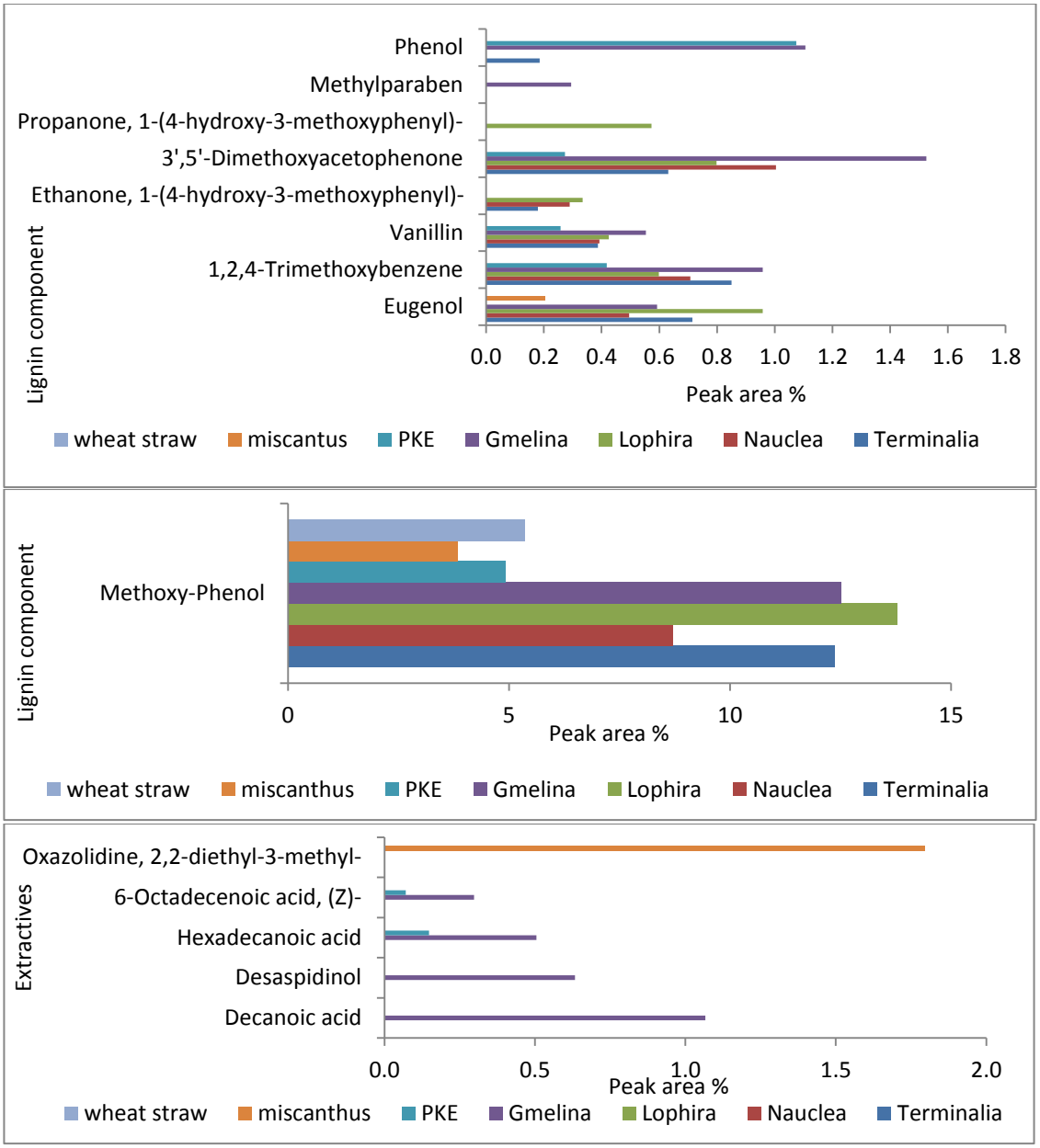

Figure 4-21: Key markers from the Py-GC-MS analysis of the Nigerian fuels (cont'd).

4.4 Conclusion

In this study, five selected Nigerian biomass (*Gmelina*, *Lophira*, *Terminalia*, and *Nauclea* and a residue- PKE) and UK fuels (miscanthus and wheat straw) have been characterised and then studied for their pyrolysis and combustion properties. Standard characterisation procedures such as proximate and ultimate analyses, metals analysis, and ash fusion tests were engaged for this purpose and the results were compared to the selected UK fuels. In addition, pyrolysis and char burning profiles of the fuels were

assessed by thermogravimetric analysis in order to understand their combustion properties, and the ash fouling and slagging propensity of the fuels were also predicted, High temperature combustion studies were carried out by suspending single biomass particles in a methane flame to gain information about the reactivity and combustion characteristics of the feedstock. Finally, pyrolysis coupled to GC-MS was also utilized to gain insight into the nature of the volatiles from the Nigerian woods compared to the other fuels.

The study showed that the selected Nigerian fuels have higher carbon contents (49-53% dry basis) when compared to the UK fuels and this resulted in the relatively high (for woody biomass) HHV value (19-21% dry basis). Chlorine and Sulphur content in the Nigerian fuels are below detection limit (0.01%). The content of ash in the feedstock are typical for woody biomass and were between 0.7 to 2.2 wt.% (dry basis). The ash components of the fuels are mainly potassium oxide, calcium oxide, and silica, particularly in the case of *Nauclea and Gmelina,* however, since they have low ash contents, therefore these fuels are not predicted for unusual fouling behavior or to create any major problems in boilers. The base percentages fall in the range 16.5-53%, which is the expected threshold for low melting ashes, even though results from the ash fusion test under oxidizing environments indicate that these ashes start to deform at temperatures above 1200^{o}C (except for PKE and Gmelina- at 1130 & 1185 ^{o}C respectively). Because of this it is recommended that careful management of feedstock quality (such as debarking) and boiler operation would be suitable for high temperature combustion applications.

Thermogravimetric analysis revealed differences in the combustion characteristics of these fuels. The potassium content in *Gmelina* is high and it seems to affect the combustion properties of the fuel, as the peak temperature for volatile combustion is lower when compared with all other fuels (except wheat straw, which is even higher in potassium), suggesting that the fuel is more reactive. Py-GC-MS analysis highlights the differences in biomass composition and structure of the fuels. The released products differ, depending on the amount and nature of the polymers found in the feedstock, but is also influenced by metal components, especially potassium. Furthermore, Py-GC-MS

analysis showed that methoxy-phenol is the main product from pyrolysis and that *Gmelina* and miscanthus contain considerable amount of extractive/oil. Finally the results from the single particle combustion experiments indicated that *Lophira* and *Nauclea* have significant longer char burnouts than *Gmelina* and *Terminalia,* probably due to the differences in wood density.

CHAPTER 5. TORREFACTION AND ITS EFFECT ON FUEL PROPERTIES

5.1 Introduction

Some of the drawbacks in the utilisation of biomass as feedstocks in power stations is their heterogeneous nature and high moisture content at first harvest, its hydroscopic and hydrophilic nature which makes them susceptible to bacterial degradation during storage. In addition, their fibrous nature makes them very difficult to grind, and their low heating value reduces their competitiveness in the energy generation market. Biomass feedstocks can differ noticeably in terms of morphological, physical, and chemical properties. The problems associated with the characteristics of biomass thus increase the processing cost across the supply chain, especially during feedstock preparation, handling, and transportation.

A feasible solution to solve the problems associated with solid biomass is to pre-treat the fuels using some of the methods that were described in Chapter 1. One of the pre-treatment solutions which is of great interest in the last decade is torrefaction. An investigation was carried out of how this thermochemical treatment affects the physical and chemical properties of biomass thereby presenting a more premium fuel.

Several studies on torrefaction have been described in Chapter 3 and were conducted at different temperatures between 200 to 300^{o}C and residence time between 30- 300 minutes [28, 38, 41, 96, 106, 108, 109, 115, 126, 128, 189], and it is established that increasing the severity of the torrefaction condition improves the quality of the premium fuel that is produced (torrefied fuel). However, the mass loss arising from the solid fuel during torrefaction should be kept as low as possible in order to maintain a balance between the mass yield and the energy yield [113, 118, 190]. Consequently, determining an optimum operating condition is important, since different types of biomass have different properties or lignocellulosic contents (particularly hemicellulose) and are expected to behave differently during pre-treatment. Hence there is a need to ensure that the solid products (torrefied fuels) obtained after torrefaction

retain an acceptable mass i.e. about 70% of the original feedstock dry weight, and about 80-90% of the feedstock's initial energy content [39].

Recently, the solid product (torrified fuels or char) has been the material of interest and a number of research have focused on characterisation of torrefied fuels using standard fuel analysis techniques, mass and energy balance [28, 37, 40, 87, 89, 100, 108, 114, 116, 126, 189, 191-193] and some have considered studying the effect of torrefaction on the milling behaviour of biomass [38, 93, 96, 100, 101, 106, 107, 115, 128, 189]. Also very few research focus on the loss of nitrogen in raw biomass upon torrefaction, as well as the morphology, physical and chemical characteristics. Therefore this chapter investigates the torrefaction of the samples described in Section 3.2 using a bench scale reactor as detailed in Section 3.15.1. The effect of torrefaction on the properties of biomass is also discussed.

5.2 Materials and Experimental Methods

5.2.1 Sample Preparation

The samples studied are in chips form (except for wheat straw) as detailed in Sections 3.2.1 to 3.2.5 and 3.2.7.

5.2.2 Experimental Methods

Biomass samples were torrefied using the method described in Section 3.15. Upon torrefaction, torrefied fuels were prepared and milled to particle sizes ranging from < 53µm to < 1180 µm according to the procedures stated in Section 3.3. The fuels were further subjected to a range of characterisation techniques as described in Section 3.4.1 - 3.4.4, 3.4.6 - 3.4.7, 3.10.1 and 3.11, which include proximate and ultimate analyses, determination of HHV using bomb calorimeter, grindability, and changes to lignocellulose composition of the fuels upon torrefaction, as well as determining the fate of the nitrogen in fuels upon torrefaction. The tars are also analysed using the methods described in Section 3.15.2.

The reaction conditions (temperature and residence time) that were applied during the torrefaction process and the details of sample nomenclature are listed in Table 5-1.

Three conditions were applied, (1) 270 ^{o}C -30mins,(2) 270 ^{o}C -60mins and (3) 290 ^{o}C -30mins.

Table 5-1: Sample designation, material and torrefaction conditions for the samples

Condition type	Sample designation	Material and torrefaction condition
1	G270-30	*Gmelina* torrefied at 270° C for 30 minutes.
2	G270-60	*Gmelina* torrefied at 270° C for 60 minutes.
1	T270-30	*Terminalia* torrefied at 270° C for 30 minutes.
2	T270-60	*Terminalia* torrefied at 270° C for 60 minutes.
1	L270-30	*Lophira* torrefied at 270° C for 30 minutes.
2	L270-60	*Lophira* torrefied at 270° C for 60 minutes.
1	N270-30	*Nauclea* torrefied at 270° C for 30 minutes.
2	N270-60	*Nauclea* torrefied at 270° C for 60 minutes.
1	P270-30	*PKE* torrefied at 270° C for 30 minutes.
2	P270-60	*PKE* torrefied at 270° C for 60 minutes.
3	P290-30	*PKE* torrefied at 290° C for 30 minutes.
1	W270-30	wheatstraw torrefied at *270* C for 30 minutes.
2	W270-60	wheatstraw torrefied at 270° C for 60 minutes.

5.3 Results and Discussion

5.3.1 Temperature Profile

The typical temperature profiles of torrefaction of the selected Nigerian biomass for the three conditions which were applied are shown in Figure 5-1. Two conditions were applied to the woody samples (270°C, 30 minutes and 270°C, 60 minutes) and a third condition which was applied for torrefaction of PKE (and 290°C, 30 minutes). This becomes necessary after seeing little improvements in the grindability of the end product "torrefied PKE" (this will be discussed in details in the later part of this chapter). From Figure 5-1, it can be seen that the process began with a drying stage at 150°C and was held for a period of 3600 secs (60 mins), subsequently programmed to a final desired temperature (270°C or 290°C) and then held for another 1800-3600secs (30 or 60 mins).

There were three thermocouples which were positioned at three different locations in the reactor in order to monitor the temperature zones in the reactor and biomass. These thermocouples were spaced 200mm from each other inside the reactor tube. Thermocouple 2 (T2) is positioned in the middle of the bed to measure the temperature of the biomass, while thermocouples 1 and 3 (T1 and T3) are positioned just before and after the sample to take the temperature differences in the zones. Also from Figure 5-1, it can be seen that in some cases, the temperature recorded profile for T1 is slightly lower than that of T2 and T3. The analysis is that the temperature detected in the sample bed is higher than the temperature of the reactor. This occurs because the particle sizes of the samples used in this study are in the form of chips and are large, with average dimensions of 2.5cm x 2.2cm x 1.1cm, and torrefaction mainly occur within the interior of the samples [28, 194]. Generally, the heat is transferred from the hot gas to the surface of the particle by convection and then into the interior (core) by conduction, thereby causing a temperature gradient [194]. The biomass core temperature gradually rises as it receives heat from the reactor and continues until the temperature rises above that of the reactor. At this point, the process (rate of torrefaction) becomes faster and is said to be an exothermic reaction [28].

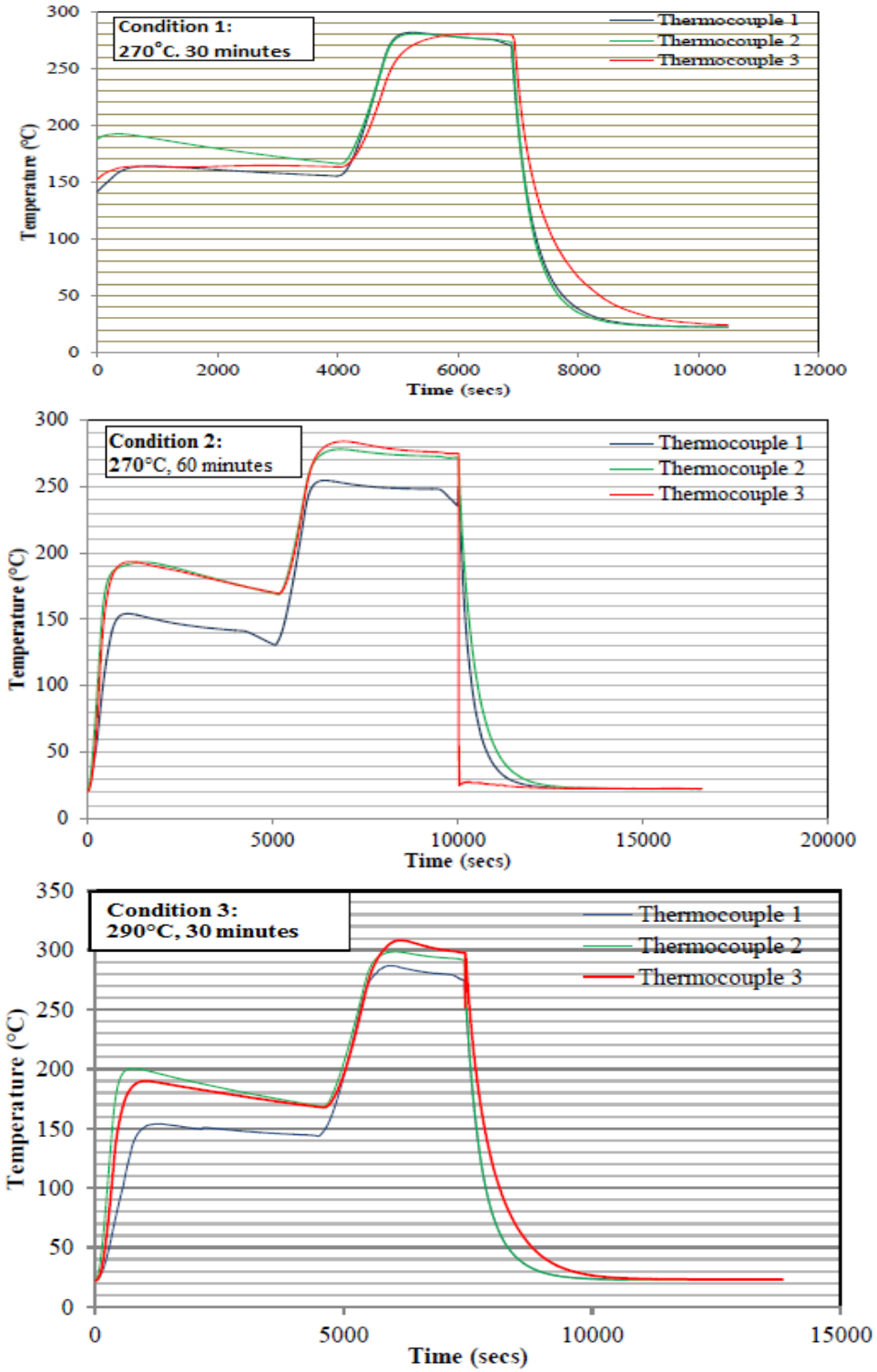

Figure 5-1: Temperature profiles of torrefaction of PKE at conditions 1, 2 (270°C with a residence time of 30 and 60 minutes respectively) and 3 (290°C with a residence time of 30 minutes).

5.3.2 Mass and Energy Yields

Figure 5-2 shows the mass and energy yields of all torrefied samples and were calculated using Equations 3-18(a, b). The mass yields of all torrefied samples ranged from 69.90% to 92.7% except for W270-60, W270-30 and N270-30 which recorded mass yields of 57.9%, 65.4% and 65.6% respectively, while energy yield for all the fuels ranged from 70.6% to 93.3%. Also, the mass and energy yields follow a decreasing trend as the torrefaction condition changes to become more severe except for PKE which recorded a lower mass yield for a less critical to a more critical condition. Torrefaction of PKE at a longer residence time t, produces lower mass yield than torrefying at a higher temperature T, as reported in the mass yield plot for PKE in Figure 5-2. This is possibly due to the difference in the lignocellulose composition of the raw feedstock [36, 93]. For samples torrefied using the least severe condition (condition 1), *PKE* had the highest mass and energy yield (92.7% and 93.3% respectively), while wheat straw had the least mass yield and energy yield (65.4% & 75.9% respectively), although the mass yield of W270-60 is almost the same N270-60 (both presenting yields of about 65%). Generally, comparing the mass and energy balance for conditions 1, 2 & 3 for the fuels; wheat straw produced the lowest mass yield and energy yield (57.9% & 70.6% respectively). This scenario is expected for wheat straw since the fuel is very reactive; therefore substantial mass loss was recorded when compared with other fuels using any of the three conditions.

In practice, acceptable mass and energy yield is 70% and 90% respectively, but this may differ, depending on individual interest. Similarly, Chew *et al.*[99] also mentioned that the yields for different feedstocks vary and is a function of its lignocellulose compositions, reaction temperatures and the residence times. Therefore the variation in the yields that were obtained during torrefaction of the Nigerian fuels and wheat straw is similar to the study of Chew *et al.*[99] and can be mainly attributed to the differences in their lignocellulose content. The energy yields of the torrefied fuels are also comparable to those obtained by Bridgeman *et al.*[37], from the torrefaction of willow and miscanthus which were torrefied at 230^{o}C, 250^{o}C & 290^{o}C for 10 minutes and 60 minutes each which varied between 76.0% to 96.8%. Furthermore, it is also similar to the yields obtained by Phanphanich *et al.*[101], from the torrefaction of pine wood chips

and residue chip at four different temperatures of 255^{o}C, 250^{o}C, 270^{o}C and 300^{o}C and at a single residence time of 30 minutes which ranged from 71% to 94%.

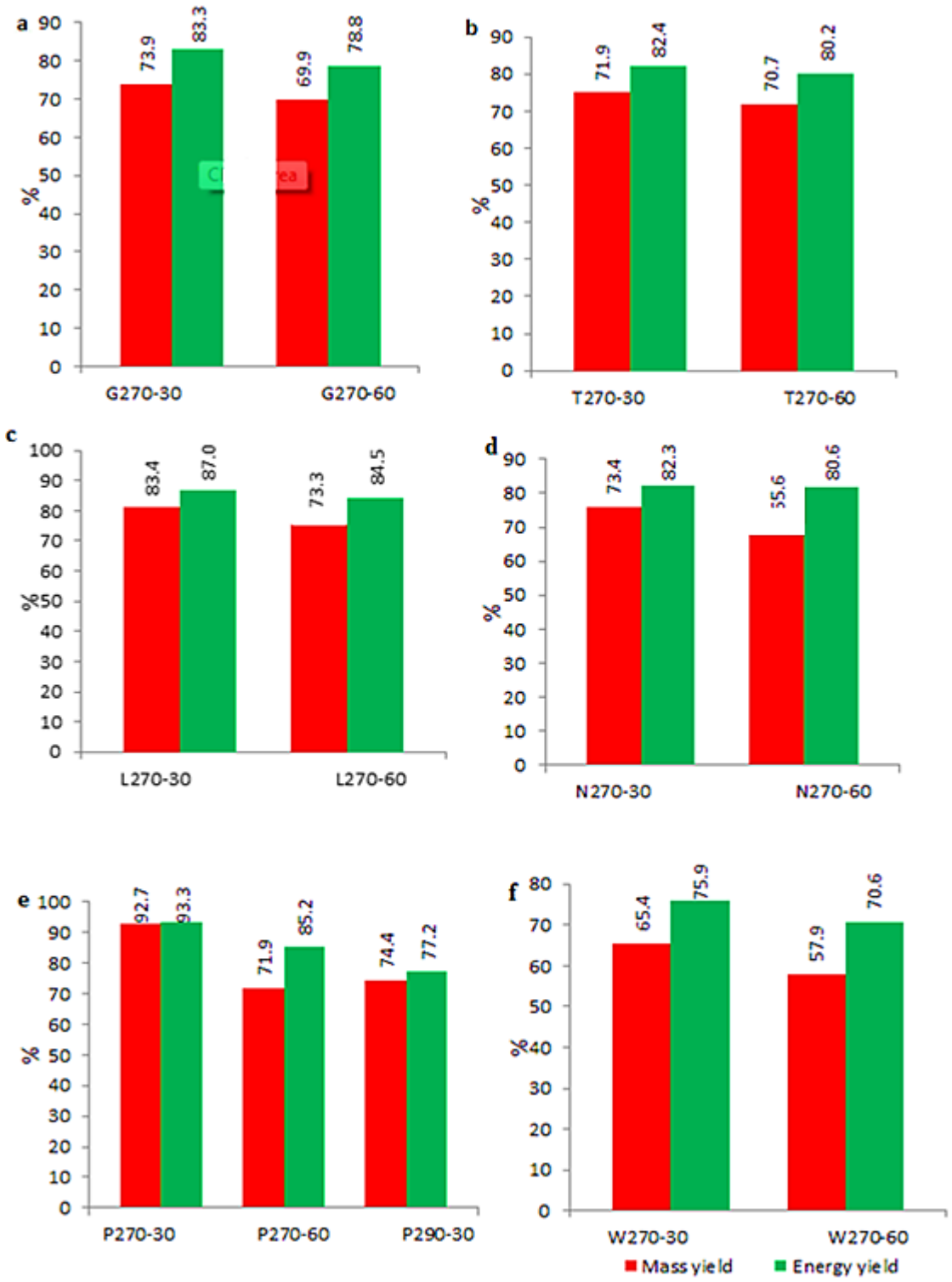

Figure 5-2: Mass and energy yields of torrefied a) *Gmelina*, b) *Terminalia*, c) *Lophira*, d) *Nauclea*, e) PKE and f) wheat straw.

5.3.3 Overall Mass Balance

Figure 5-3 reveals the overall mass balance of the selected Nigerian fuels. This was achieved by comparing what comes out with what goes in. The yields are mainly from solid fractions (torrefied fuels), followed by condensables (including aqueous and organic liquids) and permanent gases (methane, carbon dioxide and carbon monoxide). The yields have been corrected for moisture content and reported on a dry basis. It is important to mention that some of the condensed volatiles were lost during torrefaction due to evaporation or recovery, which gave room for experimental errors during weighing.

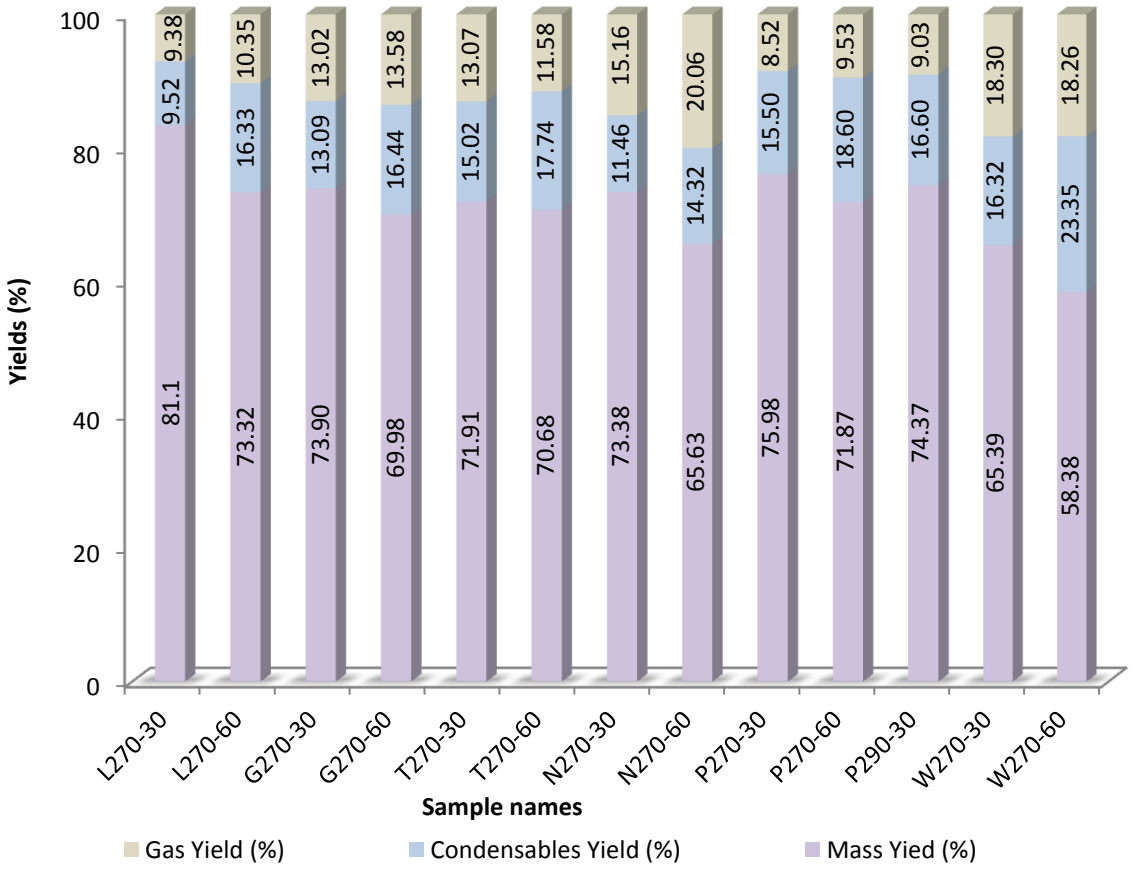

Figure 5-3: Overall mass balance of torrefaction of the fuels treated at 270ºC & 290ºC with a residence time of 30 & 60 minutes.

5.3.4 Fuel Characteristics

5.3.4.1 Proximate and Ultimate Analyses

Proximate and ultimate analyses were carried out on the solids fraction obtained from torrefaction, and the results, alongside with the corresponding heating values are reported in Table 5-2. The effect of using different torrefaction conditions is noticeable on the characteristics of the treated fuels and is compared to the untreated samples in Table 5-2. It can be observed from this table that pre-treated samples (torrefied fuels) have lower moisture contents than the raw biomass. This happened because a significant amount of water is lost during the two different phases of torrefaction i.e. at the drying phase (before torrefaction) and during the dehydration phase [37, 87, 109]. However, the moisture content of torrefied fuel cannot be related to the torrefaction temperature since there is re-absorption of small amounts of extrinsic moisture during the storage of the samples [93]. The re-absorption is minimal since torrefied fuels are hydrophobic in nature and this makes them lose their characteristics to form hydrogen bonds with water due to the destruction of its OH groups during dehydration reactions and the formation of non-polar unsaturated structures [36, 128].

Table 5-2: Proximate analysis (db), ultimate analysis (daf), & HHV (db) of raw and torrefied samples.

Samples	MC (%)	VM (%)	AC (%)	FC (%)	C (wt%)	H (wt%)	N (wt%)	O[a] (wt%)	HHV[b] (kJ/kg)	HHV[c] (kJ/kg)
Gmelina	4.9	80.9	1.0	18.1	51.9	5.7	0.16	42.2	20,400	20,800
G270-30	2.4	73.7	1.7	24.6	58.1	5.8	0.14	36.0	22,900	22, 700
G270-60	2.1	69.8	1.8	28.5	58.7	5.5	0.14	35.7	23,000	23,100
Terminalia	5.2	80.2	2.2	17.4	50.1	5.3	0.33	44.3	19,200	19,400
T270-30	1.5	72.9	4.4	22.8	56.1	5.5	0.34	38.0	21,200	21,000
T270-60	1.5	68.3	6.3	25.4	58.7	5.3	0.35	35.7	21,500	21,500
Lophira	12	78.1	1.6	20.3	52.6	5.0	0.24	42.1	20,200	21,100
L270-30	2.6	70.8	2.0	27.2	57.4	5.2	0.26	37.0	22,200	22,500
L270-60	2.6	67.6	2.2	30.2	58.1	5.5	0.27	36.1	22,600	23,000
Nauclea	4.2	80.6	0.7	18.8	53. 4	5.8	0.60	40.2	21,200	20,900
N270-30	2.5	66.0	1.0	33.0	59.3	5.5	0.70	34.5	23,200	23,400
N270-60	1.6	62.3	1.4	36.3	60.6	5.6	0.70	33.2	24,600	24,500
PKE	8.9	76.1	2.9	21.0	55.2	5.2	0.42	39.2	21,000	21,000
P270-30	3.5	70.4	5	24.6	58.0	5.4	0.46	36.1	21,700	21,500
P270-60	2.8	57.5	7.9	34.6	68.7	5.8	0.53	25.0	25,600	25,500
P290-30	3.4	65.7	5.2	29.1	60.4	5.2	0.50	33.9	22,400	22,600
wheat straw	6.1	74.1	8.3	17.6	46.7	6.1	0.50	46.6	17,100	17,000
W270-30	3.5	61.5	13.2	25.4	58.2	5.6	0.70	35.4	19,600	19,800
W270-60	3.1	52.8	17.1	30.1	64.5	5.6	0.67	29.1	20,600	20,600

db = dry basis; daf = dry ash free; HHV = Higher Heating Value; MC = moisture content; VM=volatile matter; AC=ash content; FC=fixed carbon; a = assessed by difference; b: calculated using Equation 3-9;
c: determined experimentally; Sulphur in the fuels is below detection limit of 0.01%.

Table 5-2 also shows a trend of decreasing volatile content and increasing fixed carbon content as the torrefaction conditions (temperature and residence time) becomes more severe. The volatile content in Table 5-2 ranges between 52.8% to 80.9% and this is comparable to that study undertaken by Ohliger *et al.*[115] in the torrefaction of beechwood at different torrefaction temperatures of 270^{o}C, 280^{o}C, 290^{o}C and 300^{o}C and residence times of 15, 20, 40 and 60 (minutes) which recorded volatile contents ranging from 56.8% to 83.4%. The ash content in torrefied fuels is seen to be concentrated and more concentrated by increasing the severity of the torrefaction condition [101]. The increasing trend in fixed carbon content occurred because during torrefaction H/C and O/C bonds are broken down (dehydration reactions between organic constituents), leading to an increase in carbon content at the expense of oxygen and hydrogen [97] thus, causing alterations in the chemical composition of the fuels.

Also in Table 5-2 is the ultimate analysis of the fuels. It is necessary to mention that the contents of oxygen and hydrogen in the ultimate analysis have been corrected for the hydrogen and oxygen in the moisture, as suggested by Basu *et al.*[28], since hydrogen and oxygen are the contents of the water vapour lost from the dehydration reactions between organic constituents and evolution of volatiles (that are rich in hydrogen and oxygen). The consequence of the changing C, H and O contents in the chemical composition of the fuels is the increase in higher heating values. Generally, the carbon content in some of the Nigerian raw fuels and their torrefied counterparts is relatively high. The high carbon content found in these fuels were confirmed by their corresponding relatively higher experimental HHVs obtained which are also listed in Table 5-2, and were found to be in good agreement with the calculated values with error of <4%. The HHV of all samples showed an increasing trend from raw to torrefied and also from a lower torrefaction condition to a higher one. Contrary to the trend of increasing HHV as torrefaction condition increases, are P270-30, P270-60, and P290-30 which had HHV value of 21,700kJ/kg, 25,600kJ/kg and 22,400kJ/kg respectively. This shows that PKE becomes more torrefied at a longer residence time at a temperature of 270^{o}C than at a shorter residence time at a critical temperature of 290^{o}C. Hydrogen and nitrogen contents presented in Table 5-2 did not show clear trends. Similarly an unclear

trend of nitrogen is reported in the torrefaction of beechwood by Ohliger *et al.*[115]. The sulphur content in the fuels that were studied is below the detection limit.

The results obtained from elemental analysis were used to illustrate the changes in the chemical composition of the raw and torrefied fuels as shown in the Van Krevelen diagram in Figure 5-4. The figure shows the plot of atomic ratios of hydrogen to carbon against oxygen to carbon for raw and torrefied samples, alongside various grades and types of coal. This offers an understanding about their carbon, hydrogen and oxygen compositions. The raw fuels and the coals appear to have the highest atomic H/C and O/C ratios and lowest atomic H/C and O/C ratios respectively, while torrefied fuels have intermediate values, showing a transition towards coal with increasing torrefaction condition. The samples which were torrefied at higher conditions (torrefaction temperature and residence time) tends to behave like low rank coal and had properties that are comparable to that of lignite. These findings are shown in Figure 5-4 which is comparable to those done by Bridgeman *et al*.[37].

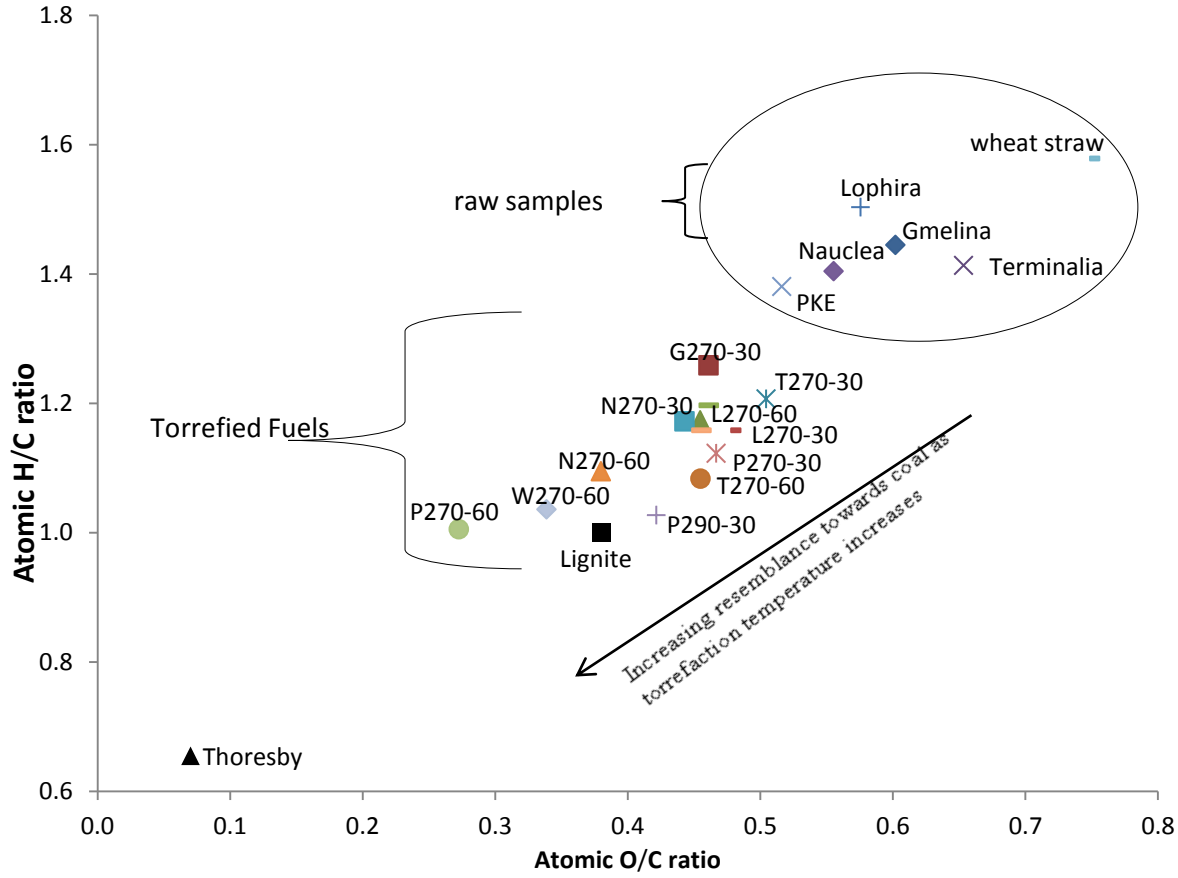

Figure 5-4: Van Krevelen Diagram showing properties of raw and torrefied fuels alongside Thoresby coal and lignite.

5.3.5 The fate of Nitrogen in the Fuel during the Torrefaction Process

The balance of nitrogen and carbon during torrefaction can be found in Table 5-3. There are noticeable and major changes in the content of nitrogen upon torrefaction as shown in Table 5-3. Between 6 to 42% (standard error ≤ 0.006) of nitrogen is lost and the loss increases with increased residence time for all fuels studied except for *Terminalia*. As the process conditions become more severe, the loss of nitrogen increases between 20 to 57% (standard error ≤ 0.013). This indicates that the release of nitrogen may be fuel dependent. While N is concentrated in the majority of the torrefied fuels (exception is *Gmelina*) such that weight percent N increases, the N partitioning indicates a loss of N during torrefaction, as shown in Table 5-3. Furthermore, if we compare the N/C atomic ratios (also listed in Table 5-3) of the raw fuel to torrefied fuel;

it is evident that nitrogen is released at the same rate as carbon (atom per atom), as in general there is little change on these ratios. However, when comparing the mass of Nitrogen in fuel per unit energy (kg/GJ) as shown in Table 5-3, generally, it is evident that in most cases N reduces on an energy basis with torrefaction (except T270-60, P270-30, P290-30, W270-30 and W270-60).

Table 5-3: Mass balance for nitrogen and carbon of the selected fuels.

Sample	$N_{wt\ \%\ raw}$	$N_{wt\ \%\ Tor}$	N_{loss} %	$C_{wt\ \%\ raw}$	$C_{wt\%\ Tor}$	C_{loss} %	N/C raw	N/C Tor	$N_{kg/GJ\ raw}$	$N_{kg/GJ\ Tor}$
G270-30	0.16	0.14	36	48.86	55.69	19.87	0.0027	0.0022	0.078	0.061
G270-60	0.16	0.14	42	48.86	56.43	23.12	0.0027	0.0020	0.078	0.061
T270-30	0.30	0.34	23	46.30	52.88	22.09	0.0056	0.0055	0.17	0.16
T270-60	0.30	0.35	23	46.30	54.18	21.56	0.0056	0.0055	0.17	0.16
L270-30	0.24	0.26	22	45.51	54.86	11.47	0.0045	0.0040	0.13	0.12
L270-60	0.24	0.27	29	45.51	55.37	21.47	0.0045	0.0041	0.13	0.12
N270-30	0.60	0.70	16	50.87	57.25	20.85	0.0101	0.0100	0.29	0.29
N270-60	0.60	0.70	24	50.87	58.82	27.25	0.0101	0.0102	0.29	0.28
P270-30	0.42	0.46	6.3	48.78	53.17	8.00	0.0070	0.0068	0.21	0.22
P270-60	0.42	0.53	17	48.78	61.55	17.45	0.0070	0.0076	0.21	0.21
P290-30	0.42	0.50	18	48.78	55.23	23.35	0.0070	0.0078	0.21	0.24
W270-30	0.50	0.70	9.2	40.20	48.77	25.50	0.011	0.012	0.29	0.37
W270-60	0.50	0.67	22	40.20	51.78	29.39	0.011	0.011	0.29	0.33

5.3.6 The Behaviour of Lignocellulose Component of the Fuels upon Torrefaction.

The chemical properties of wood changes when they are exposed to different temperatures. During the drying stage, at a temperature of about 100^{o}C, the wood begins to undergo depolymerization reactions, a situation that reduces the strength of the wood. At a temperature above 105°C, thermal degradation and transformation occurs inside the hemicelluloses cellulose, and lignin polymers. In the torrefaction process, the biomass polymers reacts differently to thermal conditions and undergo several but distinctive changes that can be quantified using the analytical methods described in Section 3.10.1. These methods were used for assessing the chemical

composition of the biomass before and after torrefaction and the results are presented in Table 5-3 as received. Hemicellulose composition was assessed from the difference between neutral detergent fiber, NDF% and acid detergent fiber, ADF%, cellulose was obtained from the difference between ADF% and acid detergent lignin, ADL%, while ADL is the lignin concentration. It is worth noting that the lignocellulose composition in the fuels does not add up to 100%, the difference is considered to be the cell wall intrinsic moisture and some extractives and ash. Hemicellulose is the most reactive to heat treatment; the results from Table 5-3 show that during torrefaction process at a temperature of 270^{o}C, almost all the hemicellulose content of the fuels have gone especially at the longer residence time of 60 minutes. For example, in Table 5-3, the hemicellulose content for *Terminalia* (10.47%), *Gmelina* (9.93%), PKE (11.01%) and *Nauclea* (7.03%) were reduced to 0.05%, 2.04%, 5.99% & 4.02% respectively upon torrefaction at a temperature of 270^{o}C for 30 minutes except for *Lophira* (7.72%) where all the hemicellulose content appeared to be lost at this torrefaction condition. The effect of increased residence time of 60 minutes was seen as the hemicellulose content in the fuels was further reduced to zero except for *Nauclea* which has 2.24% of hemicellulose content left. PKE which appeared to have lost all its hemicellulose content when torrefied at 270^{o}C for 60 minutes tends to retain 2.15% of its hemicellulose content at a more critical temperature (290^{o}C) and at a residence time of 30 minutes.

The cellulose content decreases from 52.76% to 48.89%, 46.89% to 46.02%, 56.1% to 52.04%, 39.05% to 33.62% and 50.01% to 42.01% for *Lophira, Terminalia, Gmelina*, PKE and *Nauclea* respectively when torrefied at 270^{o}C for 30 minutes. A further reduction in the cellulose content is observed when the fuels are torrefied at the same temperature for longer residence time of 60 minutes as shown in Table 5-3. Upon torrefaction at this condition, the content of cellulose found in the fuels is 46.48, 45.17, 50.36, 28.65 and 41.37(%) for *Lophira, Terminalia, Gmelina*, PKE and *Nauclea* respectively. PKE also showed to have retained more of its polymer content (cellulose) when torrefied at 290^{o}C for 30 minutes than when torrefied at 270 ^{o}C for 60 minutes.

In addition, two methods for lignin determination were used in this chapter namely acid detergent lignin (ADL) and Klason lignin (see Section 3.4.7.1). The two methods of

assessing lignin in the fuels have been compared and possible reasons for their differences were mentioned in Section 4.3.2. From Table 5-3, the lignin content in the fuels (assessed from ADL and Klason methods) becomes concentrated (higher) upon torrefaction at a mild condition and increases more and more when the torrefaction condition becomes more critical. ADL content increases from 29.49% to 40.97, 28.62% to 41.38%, 22.93% to 32.02%, 21.62% to 24.77% and 33.03% to 44.12% when torrefied at 270^{o}C for 30 minutes for *Lophira, Terminalia, Gmelina*, PKE and *Nauclea* respectively. Also, increasing the residence time to 60 minutes causes further increase in the lignin content of the fuels and the ADL content for *Lophira, Terminalia, Gmelina*, PKE and *Nauclea* presented a value of 43.09%, 41.49%, 33.28%, 29.05% and 46.44% respectively. In addition to this, the ADL content for PKE which was torrefied at 290^{o}C for 30 minutes is lower than the ADL content in PKE which was torrefied at 270^{o}C for 60 minutes.

The results from Klason lignin are significantly different from those obtained from ADL. The estimated concentrations of Klason lignin in the fuels are much higher than ADL estimation- possible reasons for this were discussed in Section 4.3.2. After torrefaction, the concentration of Klason lignin in the fuels increased from 34.68 to 48.08%, 30.40 to 44.28%, 33.13 to 44.87%, 43.23 to 55.44% and 38.75 to 60.58% for *Lophira, Terminalia, Gmelina*, PKE and *Nauclea* respectively which were torrefied at 270^{o}C for 30 minutes. Similarly, the Klason lignin concentration became higher for samples torrefied at 270^{o}C for 60 minutes i.e L270-60, T270-60, G270-60, P270-60, and N270-60 presenting lignin content of 52.71%, 53.99%, 52.33%, 87.8% and 62.65% respectively.

The findings here agree with the studies reported by Stelte *et al.*[195], Kaushlendra and Litha [196], Biswas *et al.*[197], Kumar [198] and Khazraie *et al.*[199] that hemicellulose and cellulose content of the feedstock decreased while lignin content becomes concentrated upon torrefaction. Chen *et al.*[112] and Khazraie *et al.*[199] further stated that when cellulose undergoes thermal treatment during torrefaction, it experiences some depolymerization, particularly at temperatures of 270°C and above, and the breaking of the accessible bonds begins, which then proceeds to the more

internally placed glucosidic bonds [199]. However, as suggested by Nowakowaski and Jones [72], some minerals like potassium present in biomass could potentially catalyze partial cellulose decomposition at a lower temperature.

Additionally, the increasing content of lignin which was observed during torrefaction supports the conclusion of Khazraie *et al.*[199] which states that the effect is likely due to two main reasons which are; cellulose degradation products which potential result in acid-insoluble condensed and benzenoid aromatic groups, which can increase the acid-insoluble material. Also, some released compounds from hemicelluloses depolymersation, such as furfural, might react with lignin phenolic compounds, producing more acid-insoluble compounds[199].

Table 5-4: Lignocellulose component of the fuels and the corresponding loss (estimated) upon torrefaction.

Chemical constituents of the fuels before and after torrefaction					Estimated amount for chemical constituents loss upon torrefaction		
Sample	Cellulose %	Hemicellulose %	Lignin %	Klason Lignin %	Cellulose %	Hemicellulose %	Lignin %
Lophira	52.8	7.72	29.5	34.7	0	0	0
L270-30	48.9	0	41.0	48.1	33.8	100	0.8
L270-60	46.5	0	43.1	52.7	40.7	100	1.6
Terminalia	46.9	10.5	28.6	30.4	0	0	0
T270-30	46.0	0.1	41.4	44.3	33.1	99.7	1.4
T270-60	45.2	0	41.5	54.0	35.4	100	2.7
Gmelina	56.1	9.9	22.9	33.1	0	0	0
G270-30	52.0	2.0	32.0	44.9	34.8	85.6	1.9
G270-60	50.4	0	33.3	52.3	40.3	100	3.4
PKE	39.1	11.0	21.6	43.2	0	0	0
P270-30	33.6	6.0	24.8	55.4	33.8	58.2	11.9
P270-60	28.7	0	29.1	87.8	52.0	100	12.1
P290-30	32.8	2.2	28.1	64.3	43.1	86.8	12.1
Nauclea	50.0	7.0	33.0	38.7	0	0	0
N270-30	42.0	4.0	44.1	60.6	38.9	58.4	2.9
N270-60	41.4	2.2	46.4	62.6	43.7	78.3	4.3

5.3.7 Grindability and Particle Size Distribution

Grindability and particle size distribution tests were done using the method discussed in Section 3.11.

5.3.7.1 Grindability

This Section looks into grindability behaviour of the torrefied biomass fuels and how they compare to their raw counterparts and also to four reference coals of known Hardgrove Grindability Index values (26, 49, 69 and 94). Grindability tests were carried out in order to establish how easily each fuel can be milled with coal at increased co-milling rates during cofiring application.

The HGI_{equiv} values of the raw and torrefied samples were assessed using the calibration curve shown in Figure 3-17 and are listed in Table 5-4. The untreated biomass samples resulted in an HGI_{equiv} value that is less than 1, which reveals their poor grindability behaviour.

Table 5-5: HGI_{equiv} of untreated and treated samples and their corresponding interpretation according to Tichánek [46].

Sample	m%	HGI_{equiv}	HGI Interpretation
Raw *Gmelina*	0.4	0	Very hard
G270-30	1.7	14	Very hard
G270-60	3.2	23	Very hard
Raw *Terminalia*	0.5	0	Very hard
T270-30	2.0	16	Very hard
T270-60	7.0	45	Hard
Raw *Lophira*	0.7	0	Very hard
L270-30	1.7	15	Very hard
L270-60	2.0	16	Very hard
Raw *Nauclea*	1.0	10	Very hard
N270-30	8.0	51	Hard
N270-60	9.0	56	Hard
PKE	0	0	Very hard
P270-30	0.6	8	Very hard
P270-60	1.2	12	Very hard
P290-30	0.9	10	Very hard
wheat straw	1.2	11	Very hard
W270-30	32.4	190	Extremely soft
W270-60	37.7	220	Extremely soft

m% = amount of sample passing through 75 micron sieve.

Table 5-5 presents the amount of sample that passed through the 75 micron sieve (m%), their HGI_{equiv} and interpretations. The interpretation was obtained using the classification order for coal by Tichánek [130]. According to Tichánek [130], coal with HGI value less than 40 are considered to be very hard, coals with HGI value between 40 and 60 are said to be hard, 60 to 80 are classified as medium hard, 80 to 100 HGI are soft, 100 to 120 as very soft and finally, coals above 120 are considered to be extremely soft. The m% and HGI_{equiv} for the raw fuels is zero except for *Nauclea* and wheat straw which recorded m% as 1% and1.2% respectively and their corresponding HGI_{equiv} value

as 10 and 11 respectively. Also for torrefied fuels, their m% and HGI_{equiv} is between 0.6 – 37.7% and 10 – 220 respectively. Table 5-3 also reveals an upward trend for the amount of sample that passed through the 75 micron sieve and HGI_{equiv} as the untreated fuels become torrefied and as well as the torrefaction condition becomes more severe. The increasing trend of m% and HGI values of these samples was also observed in the grindability test that were performed by Bridgeman *et al.*[93] as described in Chapter 2. In comparison, the Nigerian fuels and wheat straw considered in this study appeared to have better grindability than willow and miscanthus which were investigated in Bridgeman *et al.*[93], except for PKE which revealed little improvement after torrefaction. Also, the HGI_{equiv} value for N270-30 (51) is the same for willow torrefied at a more severe condition (i.e. 290^0C for 60 minutes) while the HGI_{equiv} values for willow and miscanthus (24 and 26 respectively) torrefied at the same temperature (290^0C) and a shorter residence time (10 minutes) is comparable to the HGI value of G270-60 (23). Similarly, the HGI_{equiv} obtained for willow & miscanthus that were torrefied at a lower temperature of 240^0C for 10 minutes (i.e. W240-10 and M240-10) are 10 and 11 respecitively [93] and this comparison also revealed the poor grinding behaviour of PKE, as the HGI value of P290-30 is the same for willow torrefied at 240^0C for 10 minutes. Furthermore, the HGI value for P270-60 (12) is almost similar to that of M240-10 (11) [93], despite been torrefied at a more severe condition.

The result from this analysis in Table 5-3, shows that torrefied fuels are easier to grind than untreated fuels. This is probably due to the decomposition of hemicellulose during the torrefaction process, as hemicellulose is known to be the binding agent of the polymeric fibres, thus making the fibres less tenacious and easier to separate. Therefore, T270-60 (45), N270-30 (51) and N270-60 (56) were easily ground; hence these fuels will have relatively higher throughputs of fuel in the mill and lower mill power consumption than the other fuels.

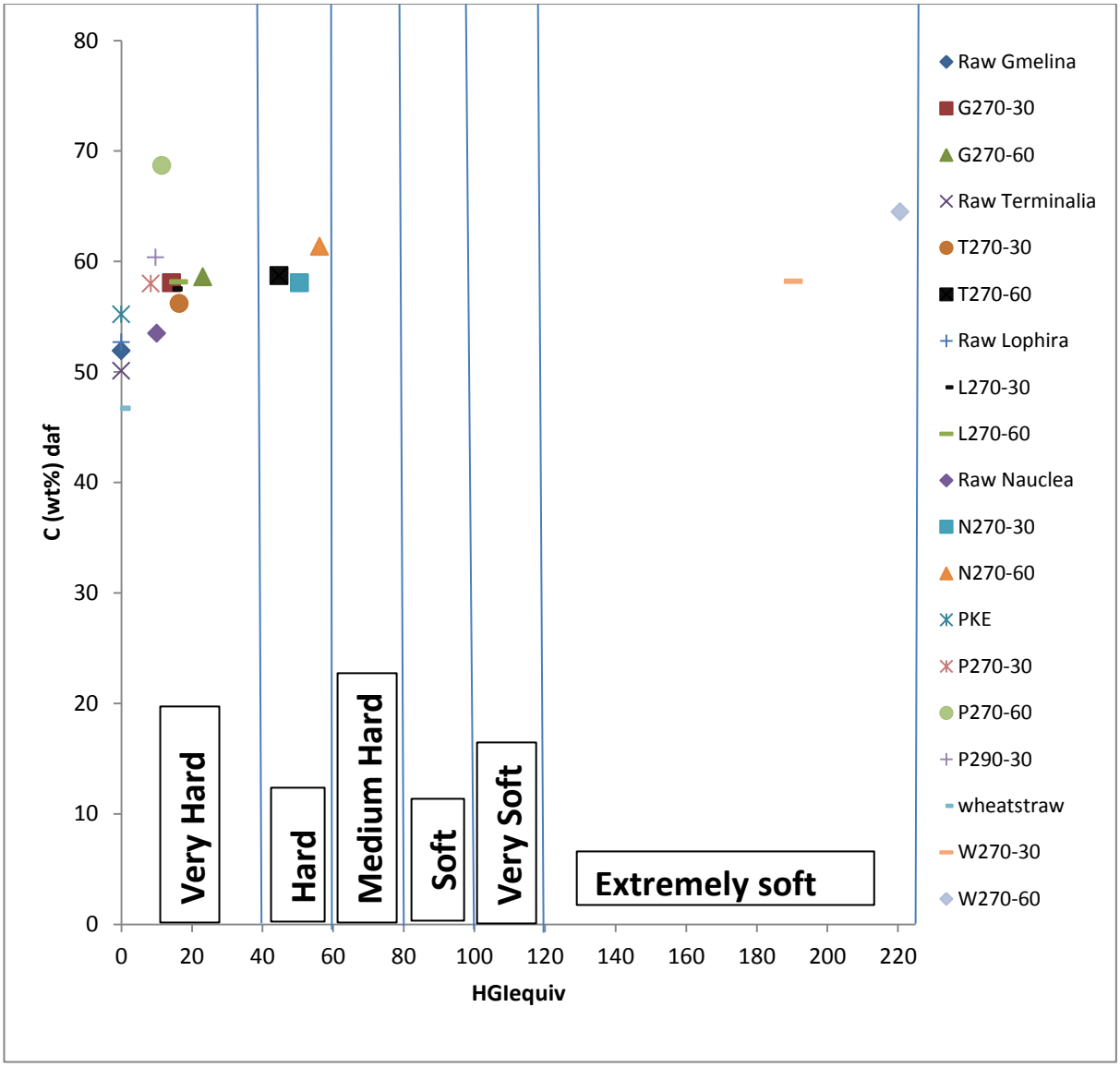

Figure 5-5: C (wt%) daf against HGI_{equiv} of raw and torrefied samples.

Figure 5-5 shows a plot of C(wt%) daf against HGI_{equiv} for all samples. From this plot, the influence of thermal pre-treatment on the grindability of a sample is seen as the torrefied fuels have a better grindability than the raw fuels which lie along zero HGI_{equiv} mark. The graph also establish the conclusion that increasing the severity of the torrefaction condition leads to higher the C(wt%) daf and better grindability. Here, although high C(wt%) daf value between 56-68% were recorded for the torrefied fuels, only T270-60, N270-30 and N270-60 fall within the hard grindability region, as well as W270-30 and W270-60 are found within the extremely soft grindability bound. Similarly, the effect of torrefaction on the heating value of the fuels is shown in Figure

5-6 (a&b). Since the carbon in the fuels becomes concentrated due to the loss of moisture and hydroxide compounds which is due to the degradation of hemicellulose during torrefaction [38], the resultant effect is observed as the heating value of the torrefied fuels become higher as presented in Figure 5-6 (a&b). There seems to be an immediate change in the slopes for the plots, where the HGI_{equiv} value appeared to increase considerably when the residence time for thermal pre-treatment is increased from 30 to 60 minutes and a significant increase in the heating value which is between 10 to 21%. Furthermore, the plot of PKE assessed from Figure 5-6a reveals the poor grindability of the fuel and it also shows slight increase in the HHV of the fuel when the torrefaction temperature changes from 270°C to 290°C but at the same residence time of 30 minutes.

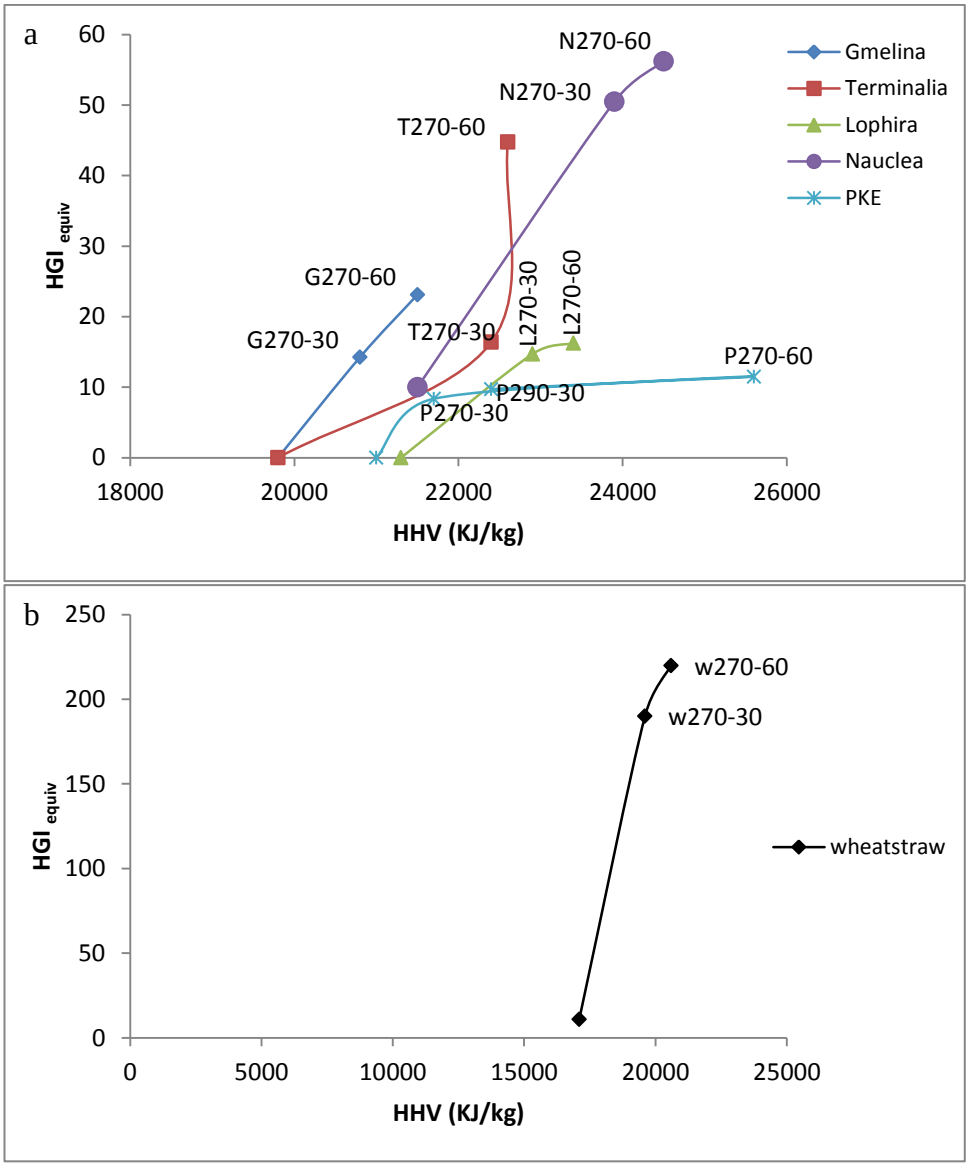

Figure 5-6: Plot of HGIequiv against HHV (KJ/kg) of the (a) raw and torrefied samples, alongside (b) raw and torrefied wheat straw.

5.3.7.2 Particle Size Distribution

Particle size distribution curve of the raw and torrefied biomass samples alongside the four standard reference coals were plotted in order to gain further information on the milling behaviour of the fuels and also to allow an in depth analysis into the changes in particle size distribution of the samples before and after torrefaction. The four standard reference coals were analysed initially in order to compare the information with the raw and torrefied samples. The distribution curves for the coals are shown in Figure 5-7 and

the result indicated that softer coals milled better and have finer particle sizes after grinding. Similar results were observed in Bridgeman *et al*.[93], who carried out similar investigations on raw and torrefied willow and miscanthus using standard reference coals of HGI 32, 49, 66 and 92.

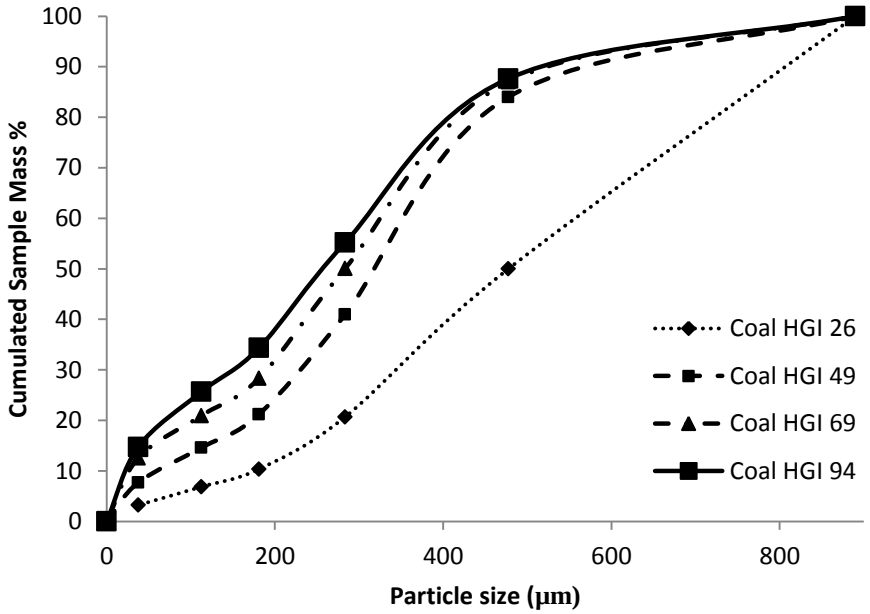

Figure 5-7: Particle size distribution curves for four standard reference coals of HGI 26, 49, 69 and 94.

The fibrous nature of the raw biomass samples are more clearly illustrated in Figure 5-8. Raw *Nauclea* seemed to have the best grindability behaviour amongst the raw fuels, but its grindability cannot be compared to the least rank coal of HGI 26.

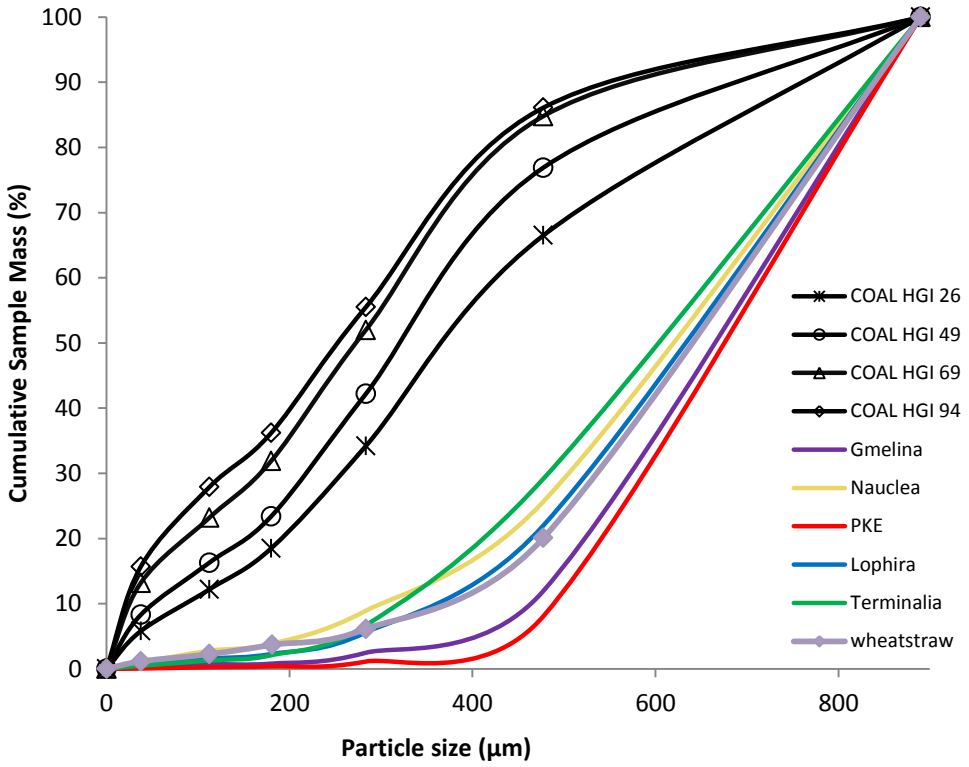

Figure 5-8: Particle size distribution curves for raw samples alongside with from the four standard reference coals of HGI 26, 49, 69 and 94.

Figure 5-9 shows the particle size distribution curves for raw and torrefied *Gmelina* with the four standard reference coals. From the curve, it is noted that increasing the severity of the torrefaction condition by increasing the residence time from 30 to 60 minutes improves the grindability behaviour of the fuel. However, both fuels (G270-30 & G270-60), still presented very different particle size distribution profiles to those of coals. Although, in the case of G270-60, a similar proportion of it had passed through the 75µm sieve just like coal of HGI 26, but the rest of the sample had a higher proportion of larger particle sizes. This observation was also reported in Bridgeman *et al.*[93], for willow torrefied at 290^{o}C for 10 minutes.

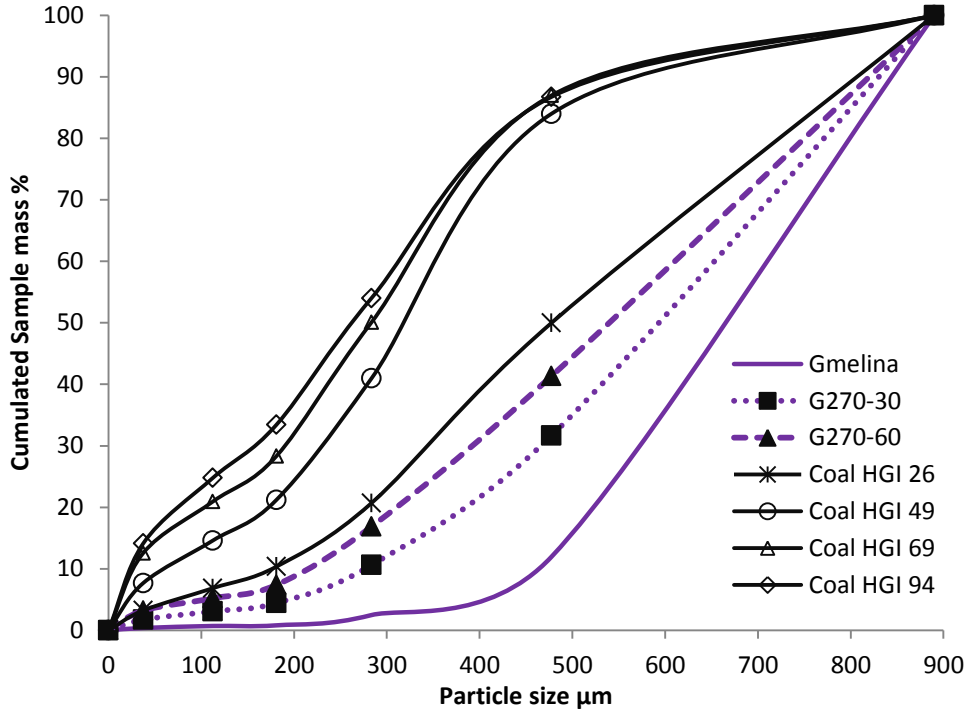

Figure 5-9: Particle size distribution curves for raw and torrefied *Gmelina* alongside four standard reference coals of HGI 26, 49, 69 and 94.

The particle size distribution curve of raw and torrefied *Lophira* with the four standard reference coals is shown in Figure 5-10. There is an overlapping profile between L270-30 and L270-60 which means that approximately the same proportion of L270-30 and L270-60 passed through the sieves. In this case, the effect of longer residence time during torrefaction did not have much impact on the particle size distribution of the sample when the torrefaction temperature remains the same. However, L270-60 still lies closer to the standard reference coals than L270-30. This is an indication that L270-60 will be slightly easier to pulverize than L270-30.

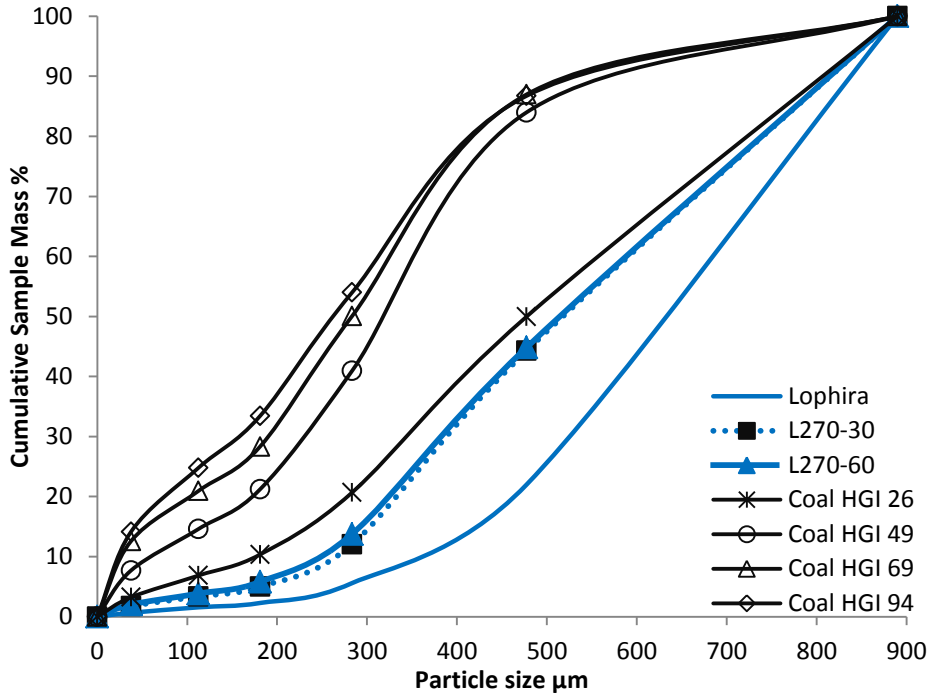

Figure 5-10: Particle size distribution curves for raw and torrefied *Lophira* alongside four standard reference coals of HGI 26, 49, 69 and 94.

Figure 5-11 shows the particle size distribution curve of raw and torrefied *Terminalia* with the four standard reference coals. From the graph, it can be seen that the samples become increasingly easier to grind with increasing torrefaction condition. The upper part of the profile for T270-30 appeared to lie very close to the upper profile of Coal HGI 26 signifying that about the same amount of sample passed through the 600µm sieve for both fuels. It is noted that there is an impressive improvement on the grindability behaviour of the *Terminalia* samples when torrefied at a more severe condition, with T270-60 showing better grindability behaviour than coal of HGI 26.

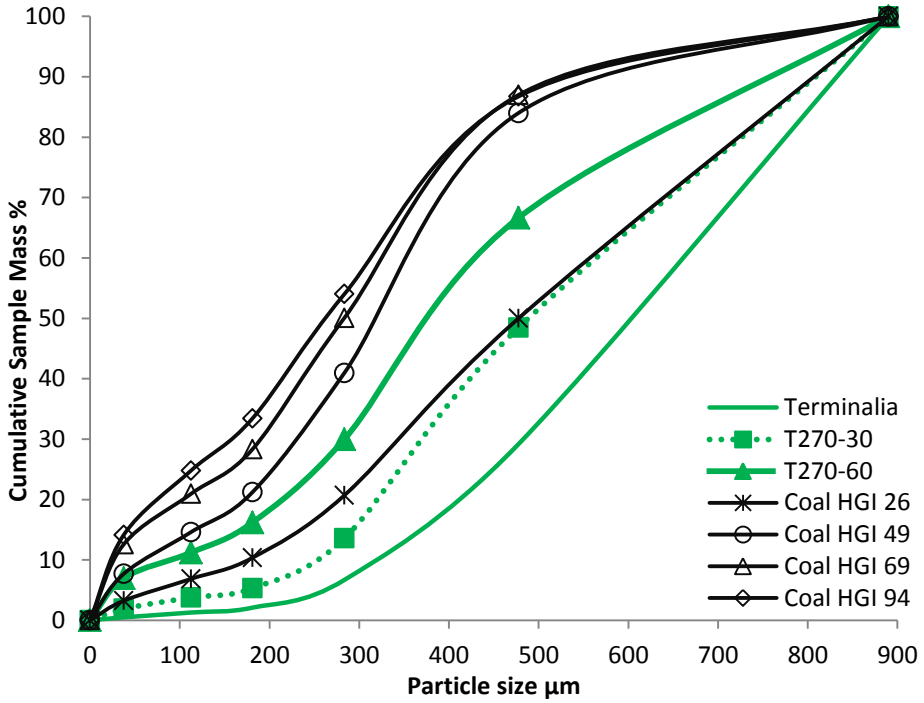

Figure 5-11: Particle size distribution curves for raw and torrefied *Terminalia* alongside four standard reference coals of HGI 26, 49, 69 and 94.

The particle size distribution curve of raw and torrefied *Nauclea* with the four standard reference coals is shown in Figure 5-12. The profile of the raw samples (see Figure 5-8) showed that untreated *Nauclea* have better grindability behaviour compared to the rest of the raw samples, but a very small proportion of this sample is reduced in particle size. However in Figure 5-12, N270-30 and N270-60 both showed great modification in their particle size distribution profiles and were similar to those of the four standard reference coals. The particle size distribution profile of N270-30 with an HGI_{equiv} of 51 has a comparable profile to the coal with HGI of 49, and N270-60 with an HGI_{equiv} of 56 presented a profile that can be compared to the profiles of coals with HGI values of 49 and 69. The profiles shown by N270-30 and N270-60 are similar to those shown by miscanthus torrefied at 290^{o}C at 10 minutes and 290^{o} C at 60 minutes respectively in Bridgeman *et al*.[93]. A possible explanation for the high grindability of *Nauclea* is due to the natural medium hardness physical characteristic it possesses [200].

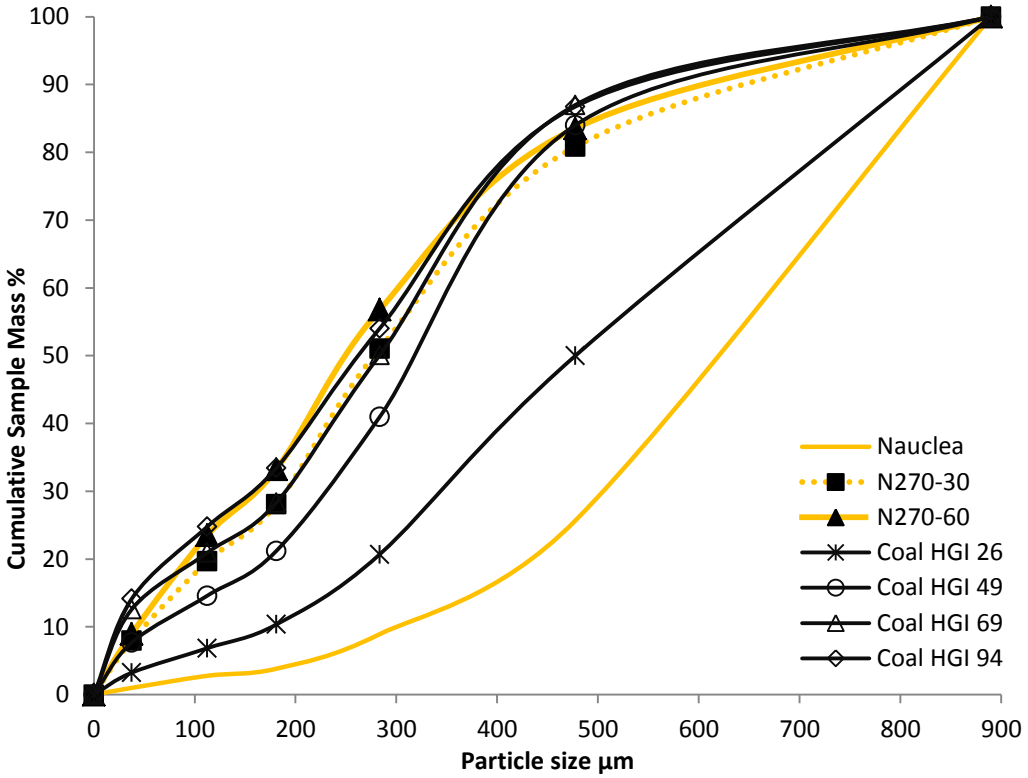

Figure 5-12: Particle size distribution curves for raw and torrefied *Nauclea* alongside four standard reference coals of HGI 26, 49, 69 and 94.

The particle size distribution curve of raw and torrefied PKE with the four standard reference coals is shown in Figure 5-13. From the curve, it is noted that increasing the severity of the torrefaction condition by increasing the residence time from 30 to 60 minutes showed little effect on the grindability behaviour of the fuel. However, both fuels (P270-30 & P270-60), still gave different particle size distribution profiles to those of coals. The Figure also reveal the poor grindability of PKE as it became obvious that the fuel was less affected by increasing the severity of the torrefaction conditions to become more critical. For example, the distribution profile of PKE torrefied at 290^{o}C for 30 minutes showed little change and is comparable to that of PKE torrefied at 270^{o}C for 60 minutes, since a similar proportion of the samples passed through the 75µm sieve for both P270-60 and P290-30 but the difference was in their upper profiles.

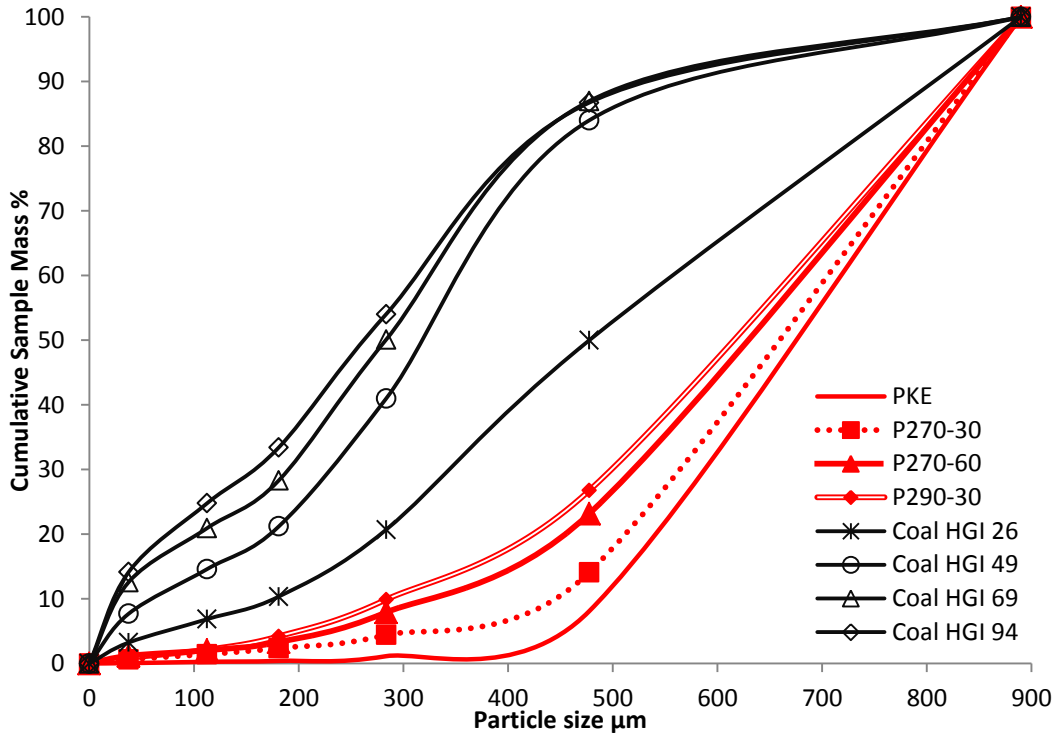

Figure 5-13: Particle size distribution curves for raw and torrefied PKE alongside four standard reference coals of HGI 26, 49, 69 and 94.

Figure 5-14 illustrates the plot of the particle size distribution of the raw wheat straw and its torrefied counterparts after milling with the four standard reference coals. Torrefaction has a large effect on the milling properties of wheat straw as shown in Figure 5-14 with the gindability of the fuel improved greatly. The lower and upper parts of the profiles of W270-30 and W270-60 are seen to be overlapping and are widely above the profiles of the coals. This evidence revealed the significant effect of torrefaction on the strength of the cell wall in wheat straw. Raw wheat straw contains a high proportion of hemicellulose which is the most reactive lignocellulose component during torrefaction. The fuel upon torrefaction, as discussed in Section 5.3.3, produced the lowest mass yield (65.39 and 58.38%), owing to the loss of its major constituent which is hemicellulose, and partly lignin (the binding agent) and cellulose. The partial decomposition and depolymerization of the aforementioned constituent during torrefaction reduces the fibre length and mechanical stability of the fuel and as a result improves its grinding characteristics. Also since wheat straw contains a high content of potassium, a catalyst that lowers the pyrolysis temperature thereby causing the fibres

between the biomass cell wall to breakdown quickly [165], making it very easy to pulverise with less power consumption for the milling process.

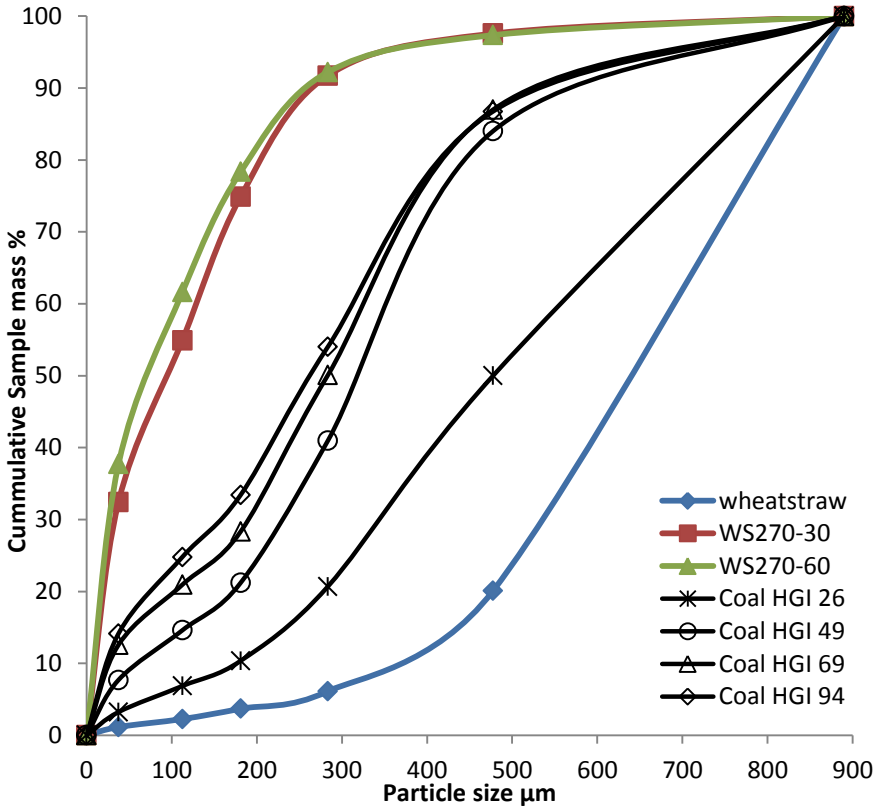

Figure 5-14: Particle size distribution curves for raw and torrefied wheat straw alongside four standard reference coals of HGI 26, 49, 69 and 94.

Generally, for all untreated samples, PKE will be the toughest to pulverise while *Nauclea* will be the easiest. For samples torrefied at the same conditions of 270^{o} C at 30 minutes, P270-30 will be the most difficult to pulverise while N270-30 and W270-60 will be the easiest to pulverise. For severe torrefaction conditions, N270-60 and W270-60 will be the easiest to grind. Therefore, N270-60 and W270-60 will have lower mill power consumption during co-milling than the other woody biomass and residue respectively and relatively higher throughputs.

5.3.8 Analysis of Liquid Products from Torrefaction.

The organic fractions were analysed using the methods described in Section 3.6 and 3.15.2.1 for elemental compositions and compound identification respectively. Table 5-5 (see **Appendix 5-1**) shows the CHNS and calorific values for the tars. This is

significant because the elemental composition is used to estimate the amount of nitrogen that is retained in the tar fraction. The nitrogen in the treated fuel and the tar can then be compared to the nitrogen in the raw fuel in order to have a mass balance analysis. Figure 5-15 shows the mass balance for the nitrogen distribution in tars and the torrefied fuels, alongside with their raw fuel counterparts. Some of the nitrogen in the original fuels were retained in the torrefied biomass after torrefaction and were also found in the tar counterparts as shown in Figure 5-15a. Figure 5-15b shows the percentage of nitrogen (%N) in original fuel that ends up in tar. For example, approximately 5, 8, 11, 13, 15 and 25% of nitrogen (of the original fuel) is found in the tar of *Terminalia, Nauclea*, PKE, wheat straw, *Lophira* and *Gmelina* respectively. It is worth noting that the nitrogen in the torrefied fuel and the tar does not add up to the nitrogen in the original fuel (raw counterpart). This is probably due to the occurrence of some nitrogen in the gas phase.

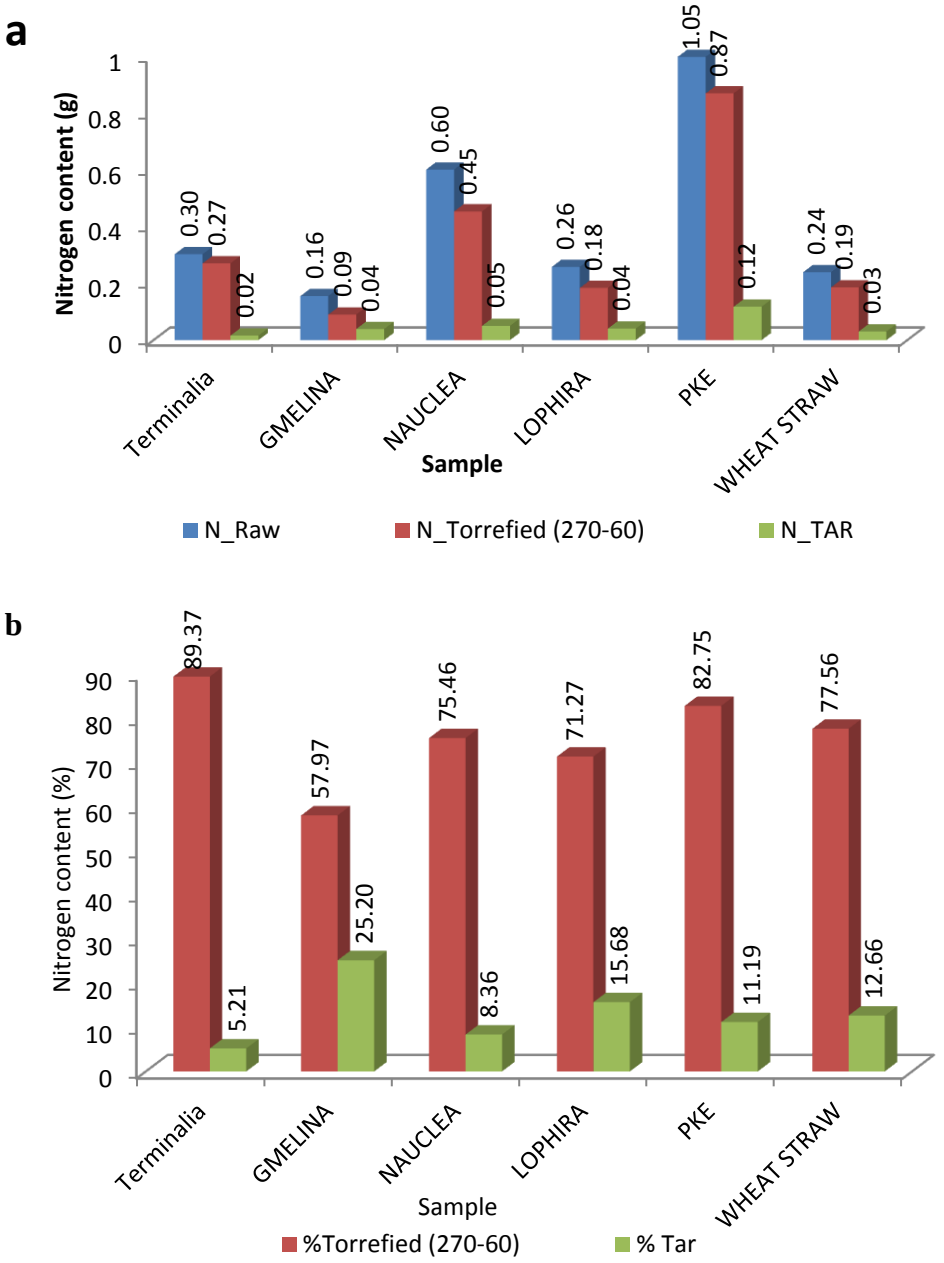

Figure 5-15: Mass balance for nitrogen distribution in tars, raw and the torrefied fuels in (a) gram and (b) percentage composition of nitrogen in tars and torrefied fuels.

Also, further knowledge about the content of the tar was also needed, and GC-MS was used to identify the major constituents. The chromatograms obtained from the liquid-GC-MS of the tar which were assigned to the main peaks are shown in Figures 5-16 to 21 and their corresponding components which were found in the tar; mainly monoaromatics are listed in Tables 5-6 to 11. The component in the organic fractions as presented in Tables 5-6 to 11 show a wide range of degradation products mainly from hemicellulose

degradation are obtainable for different fuels and torrefaction severities. The major reoccurring compounds which are identified at higher quantities as shown in the tables were furfural and phenol derivates with chains including methoxy, hydroxyl, aldehydes and alkanes groups. Generally the condensable fraction consists primarily of water, acetic acid, methanol, furfural, hydroxyacetone and phenols derivates as observed by Bergman *et al.*[35], and Prins *et al.*[89]. According to Bridgeman *et al.*[37], the formation of water and acetic acid found in the condensable fraction are caused by the dehydration reaction and thermolysis of acetyl groups particularly from hemicellulose respectively while the formation of methanol and furfural has resulted from demetoxylation of lignin as reported in Akinrinola *et al.*[200].

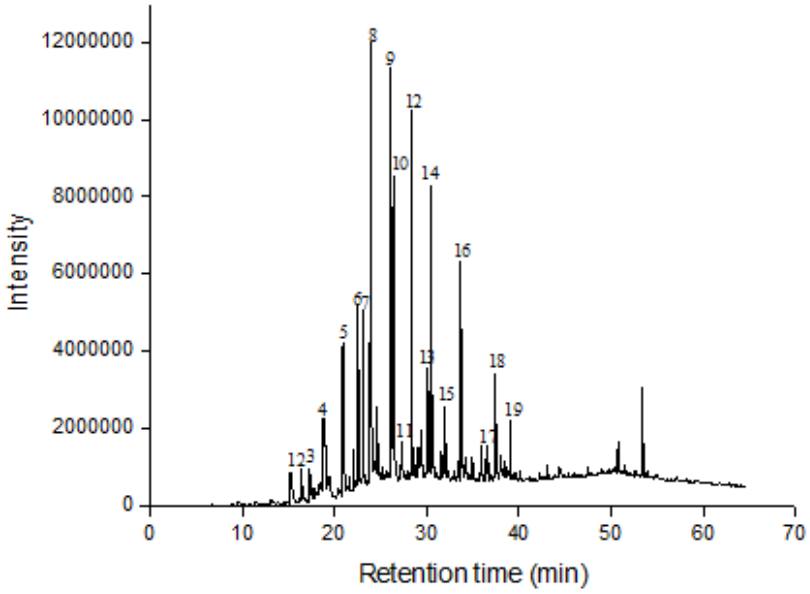

Figure 5-16: GC-MS of liquid extracts from torrefaction for L270-60 tar.

Table 5-6: Peak assignment to products of Liquid-GC-MS for L270-60 tar.

Peak No.	RT (min)	Compound
1	15.2	1,2-Cyclopentanedione, 3-methyl-
2	16.3467	Phenol, 2-methoxy-
3	17.2599	2-Cyclopenten-1-one, 3-ethyl-2-hydroxy-
4	18.7646	Phenol, 2-methoxy-4-methyl-
5	20.8764	Phenol, 4-ethyl-2-methoxy-
6	23.8806	Phenol, 2,6-dimethoxy-
7	24.5966	Phenol, 2-methoxy-4-(1-propenyl)-, (E)-
8	26.0961	Phenol, 2-methoxy-4-(1-propenyl)-, (Z)-
9	26.3504	4-Methoxy-2-methyl-1-(methylthio)benzene
10	27.2221	Vanillin
11	29.3183	Ethanone, 1-(4-hydroxy-3-methoxyphenyl)-
12	30.4598	Homovanillyl alcohol
13	31.9852	Phenol, 2,6-dimethoxy-4-(2-propenyl)-
14	33.656	Phenol, 2,6-dimethoxy-4-(2-propenyl)-
15	34.9428	Benzaldehyde, 4-hydroxy-3,5-dimethoxy-
16	36.3281	Benzoic acid, 4-hydroxy-3,5-dimethoxy-, hydrazide
17	36.5305	Ethanone, 1-(4-hydroxy-3,5-dimethoxyphenyl)-
18	37.4281	Desaspidinol
19	37.9833	4-Hydroxy-2-methoxycinnamaldehyde

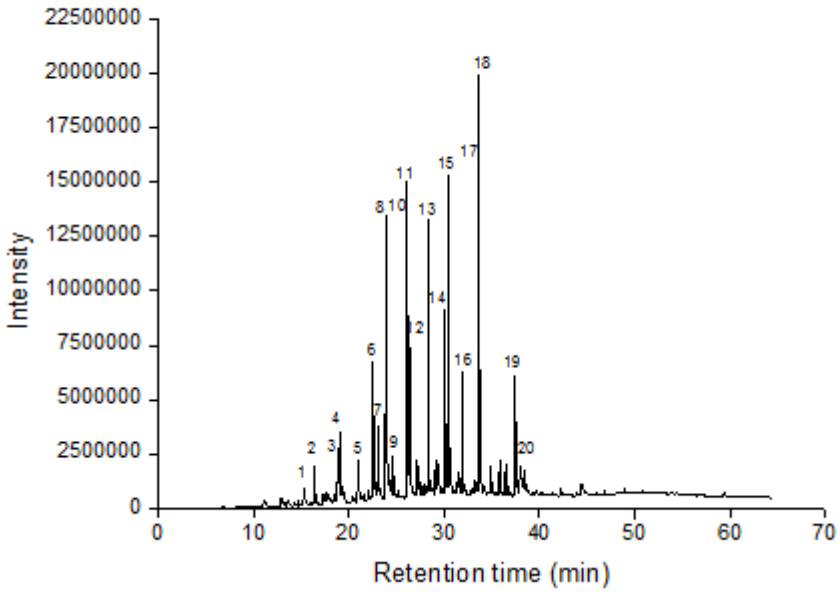

Figure 5-17: GC-MS of liquid extracts from torrefaction for T270-60 tar.

Table 5-7: Peak assignment to products of Liquid-GC-MS for T270-60 tar.

Peak No.	RT (min)	Compound
1	15.2311	1,2-Cyclopentanedione, 3-methyl-
2	16.2948	Phenol, 2-methoxy-
3	18.7853	Phenol, 2-methoxy-4-methyl-
4	20.9075	Phenol, 4-ethyl-2-methoxy-
5	22.5159	2-Methoxy-4-vinylphenol
6	23.04	Phenol, 2-methoxy-4-(1-propenyl)-, (Z)-
7	23.8857	Phenol, 2,6-dimethoxy-
8	24.5758	Phenol, 2-methoxy-4-(1-propenyl)-, (E)-
9	26.0961	Phenol, 2-methoxy-4-(1-propenyl)-, (Z)-
10	26.3555	Benzoic acid, 4-hydroxy-3-methoxy-
11	28.3376	5-tert-Butylpyrogallol
12	29.0536	Benzoic acid, 4-hydroxy-3-methoxy-, methyl ester
13	29.2716	Ethanone, 1-(4-hydroxy-3-methoxyphenyl)-
14	29.3442	Ethanone, 1-(4-hydroxy-3-methoxyphenyl)-
15	31.9437	Phenol, 2,6-dimethoxy-4-(2-propenyl)-
16	33.6559	Phenol, 2,6-dimethoxy-4-(2-propenyl)-
17	34.8649	Benzaldehyde, 4-hydroxy-3,5-dimethoxy-
18	37.4333	Desaspidinol
19	37.9729	4-Hydroxy-2-methoxycinnamaldehyde
20	38.4399	Aspidinol

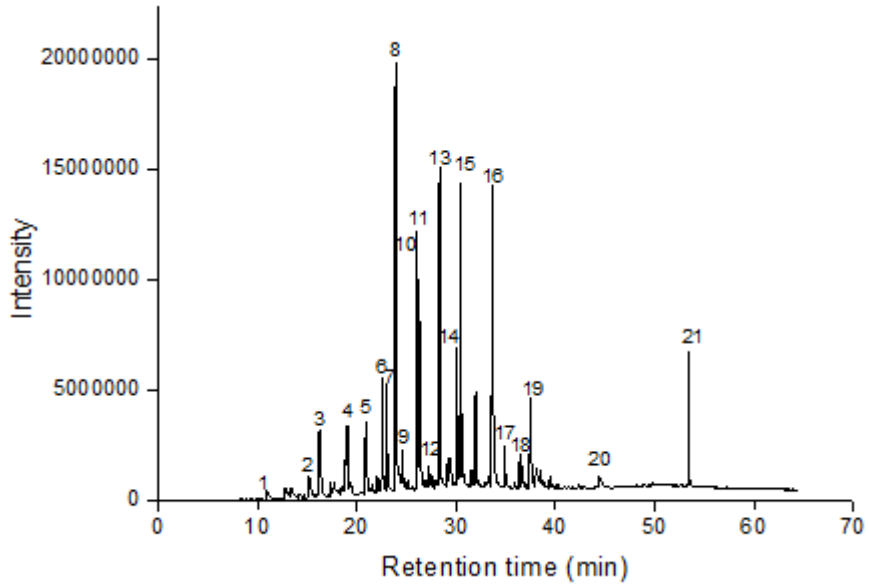

Figure 5-18: GC-MS of liquid extracts from torrefaction for N270-60 tar.

Table 5-8: Peak assignment to products of Liquid-GC-MS for N270-60 tar.

Peak No.	RT (min)	Compound
1	10.8727	2-Furanmethanol
2	15.1896	1,2-Cyclopentanedione, 3-methyl-
3	16.2377	Phenol, 2-methoxy-
4	18.7749	Phenol, 2-methoxy-4-methyl-
5	20.9126	Phenol, 4-ethyl-2-methoxy-
6	22.5263	2-Methoxy-4-vinylphenol
7	23.0452	Phenol, 2-methoxy-4-propyl-
8	23.8961	Phenol, 2,6-dimethoxy-
9	24.5654	Phenol, 2-methoxy-4-(1-propenyl)-, (Z)-
10	26.0961	Phenol, 2-methoxy-4-(1-propenyl)-, (Z)-
11	26.3607	1,2,3-Trimethoxybenzene
12	27.2169	Vanillin
13	28.3376	5-tert-Butylpyrogallol
14	29.3182	Ethanone, 1-(4-hydroxy-3-methoxyphenyl)-
15	31.9644	Phenol, 2,6-dimethoxy-4-(2-propenyl)-
16	33.6404	Phenol, 2,6-dimethoxy-4-(2-propenyl)-
17	34.9324	Hexadecanoic acid, methyl ester
18	36.5356	Ethanone, 1-(4-hydroxy-3,5-dimethoxyphenyl)-
19	38.0611	4-Hydroxy-2-methoxycinnamaldehyde
20	39.5139	8,11-Octadecadienoic acid, methyl ester
21	44.4224	3,5-Dimethoxy-4-hydroxycinnamaldehyde
22	53.4766	2,6,10,14,18,22-Tetracosahexaene, 2,6,10,15,19,23-hexamethyl-, (all-E)-

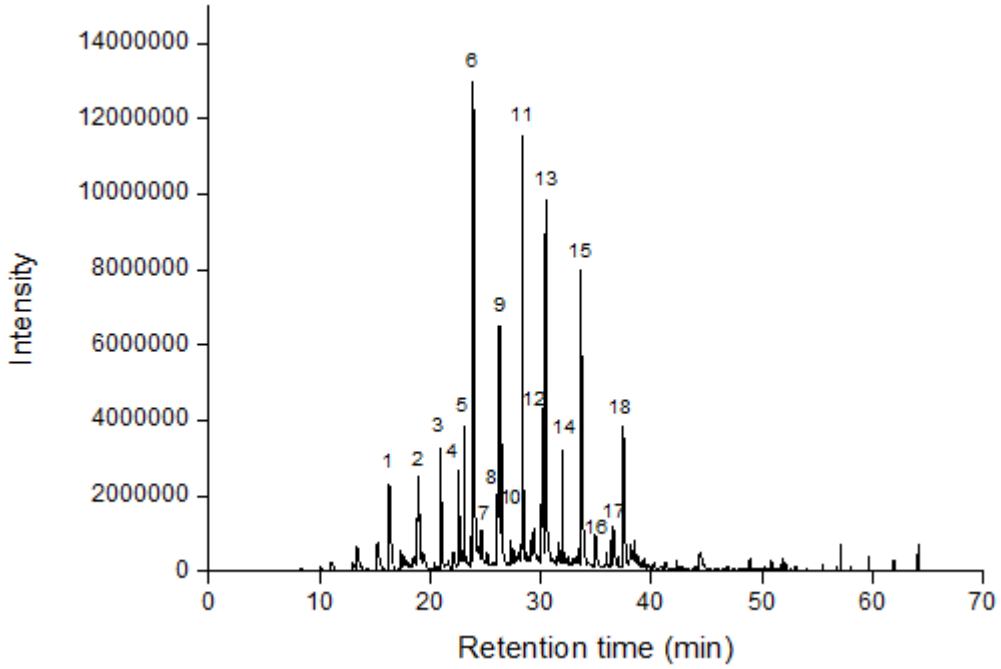

Figure 5-19: GC-MS of liquid extracts from torrefaction for G270-60 tar.

Table 5-9: Peak assignment to products of Liquid-GC-MS for G270-60 tar.

Peak No.	RT (min)	Compound
1	16.2998	Phenol, 2-methoxy-
2	18.8267	Phenol, 2-methoxy-4-methyl-
3	20.9437	Phenol, 4-ethyl-2-methoxy-
4	22.5729	2-Methoxy-4-vinylphenol
5	23.6625	2-Propenoic acid, 3-phenyl-, methyl ester
6	23.896	Phenol, 2,6-dimethoxy-
7	24.638	Phenol, 2-methoxy-4-(1-propenyl)-, (Z)-
8	26.1168	Phenol, 2-methoxy-4-(1-propenyl)-, (Z)-
9	26.3658	2H-Pyran-2-one, 3-acetyl-4-hydroxy-6-methyl-
10	27.2842	Vanillin
11	28.3479	5-tert-Butylpyrogallol
12	29.3908	Ethanone, 1-(4-hydroxy-3-methoxyphenyl)-
13	30.4804	Homovanillyl alcohol
14	31.9747	Phenol, 2,6-dimethoxy-4-(2-propenyl)-
15	33.6351	Phenol, 2,6-dimethoxy-4-(2-propenyl)-
16	34.9426	Benzaldehyde, 4-hydroxy-3,5-dimethoxy-
17	36.5615	Ethanone, 1-(4-hydroxy-3,5-dimethoxyphenyl)-
18	37.4695	2-Pentanone, 1-(2,4,6-trihydroxyphenyl)

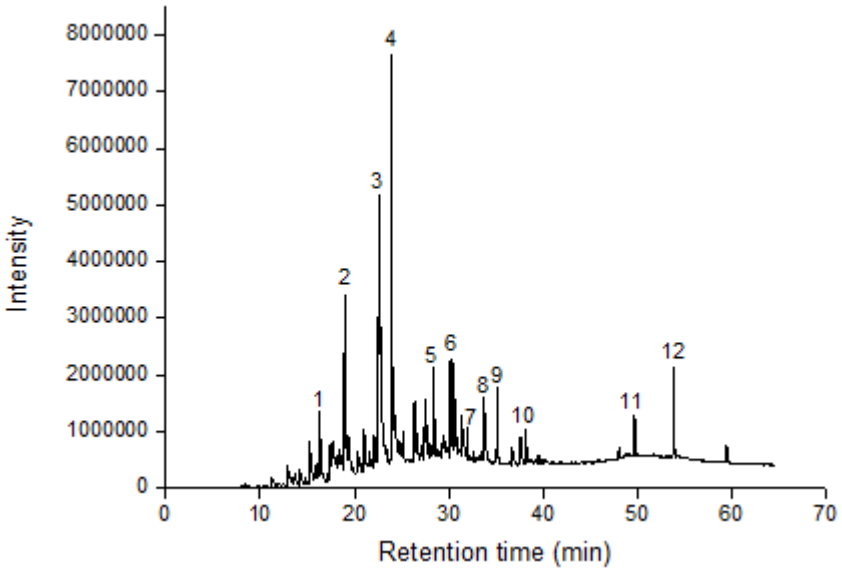

Figure 5-20: GC-MS of liquid extracts from torrefaction for W270-60 tar.

Table 5-10: Peak assignment to products of Liquid-GC-MS for W270-60's tar.

Peak No.	**RT**	**Compound**
1	15.2624	1,2-Cyclopentanedione, 3-methyl-
2	16.3364	Phenol, 2-methoxy-
3	22.5835	2-Methoxy-4-vinylphenol
4	23.9429	Phenol, 2,6-dimethoxy-
5	26.283	Phenol, 2-methoxy-4-(1-propenyl)-, (Z)-
6	27.3934	Vanillin
7	32.032	Phenol, 2,6-dimethoxy-4-(2-propenyl)-
8	33.682	2-Pentadecanone, 6,10,14-trimethyl-
9	33.7598	Phenol, 2,6-dimethoxy-4-(2-propenyl)-
10	35.249	2-Heptadecanone
11	49.7408	Heptacosane
12	53.954	Nonacosane

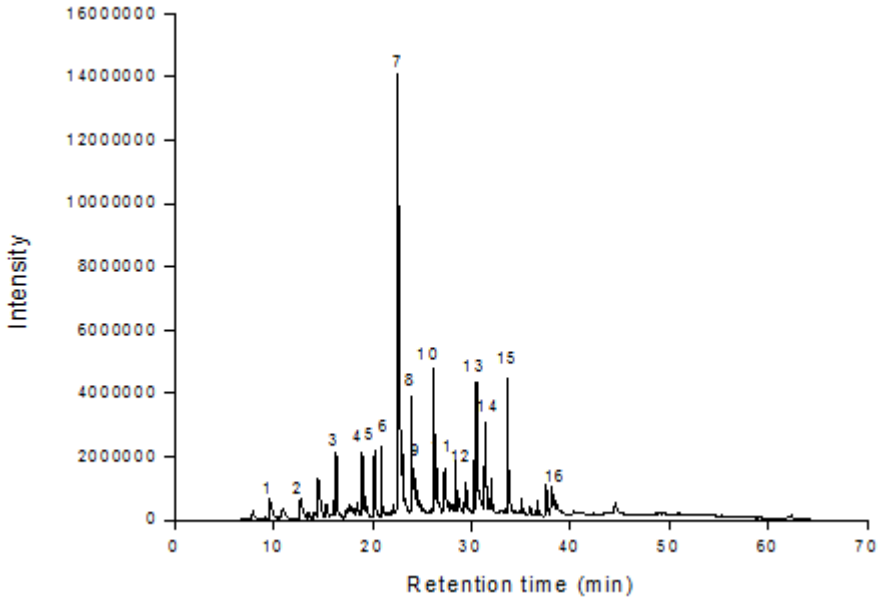

Figure 5-21: GC-MS of liquid extracts from torrefaction for P270-60‘s tar.

Table 5-11: Peak assignment to products of Liquid-GC-MS for P270-60’s tar.

Peak No.	RT (min)	Compound
1	9.5599	Furfural
2	12.725	1,2-Cyclopentanedione
3	16.025	Phenol
4	16.3259	Phenol, 2-methoxy-
5	20.207	Phenol, 4-ethyl-
6	20.9179	Phenol, 4-ethyl-2-methoxy-
7	22.5367	Pyridine, 3-ethyl-2,6-dimethyl-
8	23.9221	Phenol, 2,6-dimethoxy-
9	24.223	Phenol, 2,6-dimethoxy-
10	26.2103	Phenol, 2-methoxy-4-(1-propenyl)-, (Z)-
11	28.7008	Phenol, 2-methoxy-4-propyl-
12	29.4532	Ethanone, 1-(4-hydroxy-3-methoxyphenyl)-
13	30.5324	Homovanillyl alcohol
14	31.98	Phenol, 2,6-dimethoxy-4-(2-propenyl)-
15	33.6611	Phenol, 2,6-dimethoxy-4-(2-propenyl)-
16	36.6809	Ethanone, 1-(4-hydroxy-3,5-dimethoxyphenyl)-

5.4 Conclusions

Torrefaction and its effect on the fuel properties of some selected Nigerian biomass have been investigated. For this purpose, the fuels were torrefied at two different temperatures (270 and 290^{o}C) and residence times (30 and 60 mins). The mass yields of all torrefied samples ranged from 65.6% to 92.7% except for wheat straw while energy yield for all the fuels ranged from 70.6% to 93.3%. After the torrefaction, it was observed that the samples had reduced moisture contents, which should lead to a reduction in the susceptibility of the samples to bio-degradation, therefore extending its storage window. An increase in carbon content and a decrease in volatiles, oxygen and hydrogen contents was recorded after torrefaction and this led to an improved energy yield. Generally, the carbon content in some of the Nigerian raw fuels and their torrefied counterparts is relatively high. The high carbon content found in the fuels that were studied was validated by their corresponding relatively higher experimental HHVs obtained. Studies on the four the Nigeria torrefied samples showed that T270-30 had the lowest HHV value (21,200KJ/kg), while P270-60 had the highest HHV value (25,600KJ/kg). As expected, it is quite evident that torrefaction improves the heating value of biomass as most of the torrefied samples like G270-30 (23,100KJ/kg), G270-60 (23,100KJ/kg), N270-30 (23,200KJ/kg), N270-60 (24,600KJ/kg) and P270-60 (25,600KJ/kg) have heating values which are comparable to that of coal which is usually between 23,000KJ/kg to 28,000KJ/kg. Measured and calculated HHV were in very good agreement (<4% difference).

Studies show that during torrefaction process at a temperature of 270^{o}C, almost all the hemicellulose content of the fuels is gone especially at a longer residence time (60 minutes). Similarly the cellulose content decreases and it decreases further when the fuels are torrefied at the same temperature for longer residence time of 60 minutes. Furthermore, Lignin becomes concentrated upon torrefaction at a mild condition and increases more and more when the torrefaction condition becomes more critical.

The process also results in loss of nitrogen from the fuel, mainly in the tar (condensibles) – while wt% N generally increases in the torrefied fuel compared to the

starting material, the N contents on an energy basis, generally decrease. The main compounds detected in the tar/condensibles are monoaromatics.

From the grindability and particle size distribution results, apart from T270-60 (45), N270-30 (51) and N270-60 (56) which fell between 40 and 60, all other samples showed very hard grindability because their HGI_{equiv} fell below 40 according to the HGI ranking for coal carried out by Tichanek. For torrefied samples, N270-60 (56) was the easiest to grind, while torrefied PKE showed little improvement, even when a more critical torrefaction condition was applied; P270-30 (8), P270-60 (12), and P290-30 (10). However, the grindability of all samples increased as the torrefaction condition increased.

CHAPTER 6. PYROLYSIS STUDIES ON TORREFIED BIOMASS

6.1 Introduction

The significance of torrefaction on the properties of woods was discussed in Chapter 5. The process produces premium fuels that have less nitrogen content, high energy content, improved grindability and are less susceptible to moisture absorbtion. Thermal decomposition of biomass is the fundamental stage in biomass combustion and is receiving considerable attention. The process is also used to produce chemicals and bio-oil [83]. Consequently, it is important to understand pyrolysis behaviour of the treated fuels that are investigated in Chapter 5. During fuel pyrolysis, the fuels undergo thermal decomposition to form volatile, gases and a solid residue called char. Thermal decomposition of biomass is highly complex due to the heterogeneous nature of biomass composition. The biomass constituents i.e. hemicelluloses, cellulose, and lignin as mentioned in Chapter 2 decomposed at a range of temperatures and rates. The decomposition of hemicelluloses and cellulose in biomass occurs relatively fast and at a low temperatures between 200 to 350 °C, while lignin decomposes slowly over a wide range of temperatures between 280 to 600 °C with complete breakdown occurring at high temperature up to 900°C [124]. This explains the complexity in the thermal decomposition of biomass and consequently makes the reaction kinetics complicated. According to literature [46, 116, 133], thermal decomposition of treated fuels (torrefied) in an inert environment reveals different decomposition behaviours owing partly to the loss of some of the lignocellulose fraction during torrefaction. For example, the remains of lignin in torrefied fuels (after torrefaction) undergoes a degree of breakdown during the pyrolysis process and so at high temperatures, completion of breakdown occurs, and the initial cross-linked and elongated structure become less visible.

Generally, the volatile matter in torrefied fuels is lower and the char and ash contents becomes concentrated due to the partial devolatisation (mass loss) that occurred in the pretreatment process (as discussed in Chapter 5). During torrefaction, some volatile matter are lost which mostly results from the decomposition of hemicellulose and the partial decomposition of lignin. The char that is left i.e. torrefied fuel shows different decomposition characteristics due to the removal of hemicelluloses and modification of

cellulose and lignin in torrefaction [112, 116]. Different kinetics are expected for different biomass, since the composition of lignin is not the same for hardwood and softwood [79-82], and the contents of catalytic metals, particularly potassium differ[37]. The solid fraction (torrefied fuels) is composed mainly of unreacted cellulose, unreacted lignin as well as the non-volatile by-products of hemicellulose degradation. Discrete amounts of degradation may occur in the cellulose or lignin during torrefaction [114], and this has limited the conclusive characterisation of torrefied biomass. Thus the solid product, called "torrefied biomass" or "char", is always the target material.

Understanding of the kinetics of thermal decomposition of torrefied fuel is vital in the modelling of both its combustion processes and reactor kinetics. The rate of release, quantity, and composition of the volatiles influence flame ignition, stability, and the temperature profile in the radiant part of the furnace [83]. Therefore, these elements are significant in reactor design in pulverized fuel power stations. Similarly, in fast pyrolysis the relative rates of decomposition, cracking, repolymerization, and condensation reactions affect the quantity and quality of bio-oil produced as well as the thermal stability [83]. Thus, it is essential to understand the pyrolytic characteristics for torrefied fuels and to derive the kinetic parameters from the data of the thermogravimetric analysis.

6.2 Materials and Experimental Methods

6.2.1 Sample Preparation

The samples studied are detailed in Sections 3.2.1 to 3.2.7. All the samples were prepared and milled to particle sizes < 53μm according to the procedures stated in Section 3.3.

6.2.2 Experimental Methods

The details for all the experiments conducted in this Chapter are found in Section 3.12 and 3.13.

6.3 Results and Discussion

6.3.1 Thermogravimetric Analysis (TGA), and Differential Thermogravimetric Analysis (DTA).

The plots of the first derivative of mass loss curve with temperature (DTG) for the pyrolysis of the raw and torrefied samples are shown in Figures 6-1 to 6-7. The DTG pyrolysis curves show at least two peaks per samples for pyrolysis characteristic of the fuels i.e. the moisture peak and the volatiles release stages. The first stage of the curve is the moisture loss stage, which occurs between 25^{o}C and 110^{o}C (this is less evident in torrefied fuels as they are much drier); this stage is immediately followed by the devolatilization stage (peaks are between 200 and 500^{o}C), which shows the greatest mass loss due to volatile release. Avila *et al.*[66], studied the morphology and reactivity characteristics of ten different biomass particles and suggested that these DTG peaks are formed primarily by the influence of three main reactions linked to the thermal decomposition of lignocellulose at different temperatures [201].

The temperature which initiates the commencement of pyrolysis is denoted with T_o and the maximum temperature needed to begin the pyrolysis reaction is called peak maximum temperature of pyrolysis and it is denoted with $T_{p1.}$ This is obtained from the DTG, which presents the decomposition rate of a sample with temperature. The devolatilization process proceeds slowly after T_{p1} is reached and ends at a final programmed temperature of 700^{o}C which signifies the end of devolatilization.

In this instance, some of the curves revealed a shoulder on the pyrolysis peak, *Lophira*, *Terminalia*, wheat straw and miscanthus or two partially resolved peaks for PKE. (see Figure 6-5). Both the unresolved peak at a lower temperature and the shoulder on the main peak are due to hemicellulose decomposition, but the main peak is predominantly due to the degradation of cellulose. The DTG curves of raw and torrefied *Terminalia* show more peaks at higher temperatures. The last two peaks in the DTG pyrolysis curve for *Terminalia* result from the decomposition of calcium oxalate in the fuel ash which are converted into CO_2 [81] and possibly a further thermal cracking of some resultant organic compounds, whose formation may have been precipitated in the preceding reactions[45], as reported by Lasode *et.al.*[45] in the DTG analysis for untreated and

torrefied *Terminalia ivorensis*. This was confirmed by TGA pyrolysis of $CaC_2O_4.xH_2O$ and also of a small amount of CaC_2O_4 mixed with *Terminalia.* The DTG pyrolysis plots for *Terminalia*, $CaC_2O_4.xH_2O$, and a mixture of both *Terminalia a*nd $CaC_2O_4.xH_2O$ were plotted, as shown in Figure 6-8.

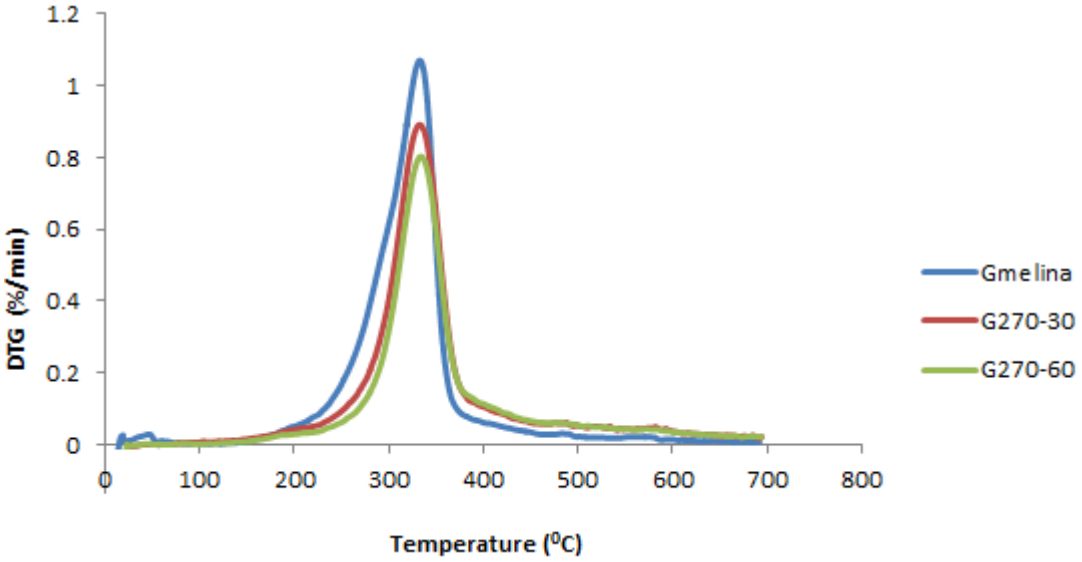

Figure 6-1: DTG pyrolysis profile of raw and torrefied *Gmelina* in nitrogen at 10^{o}C/min.

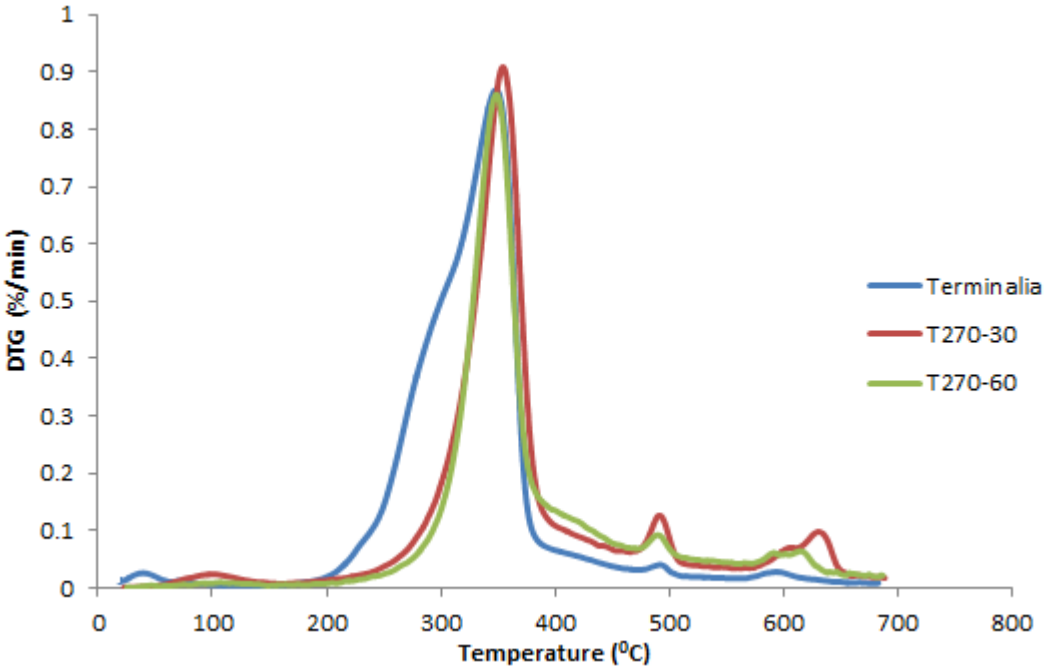

Figure 6-2: DTG pyrolysis profile of raw and torrefied *Terminalia* in nitrogen at 10°C/min.

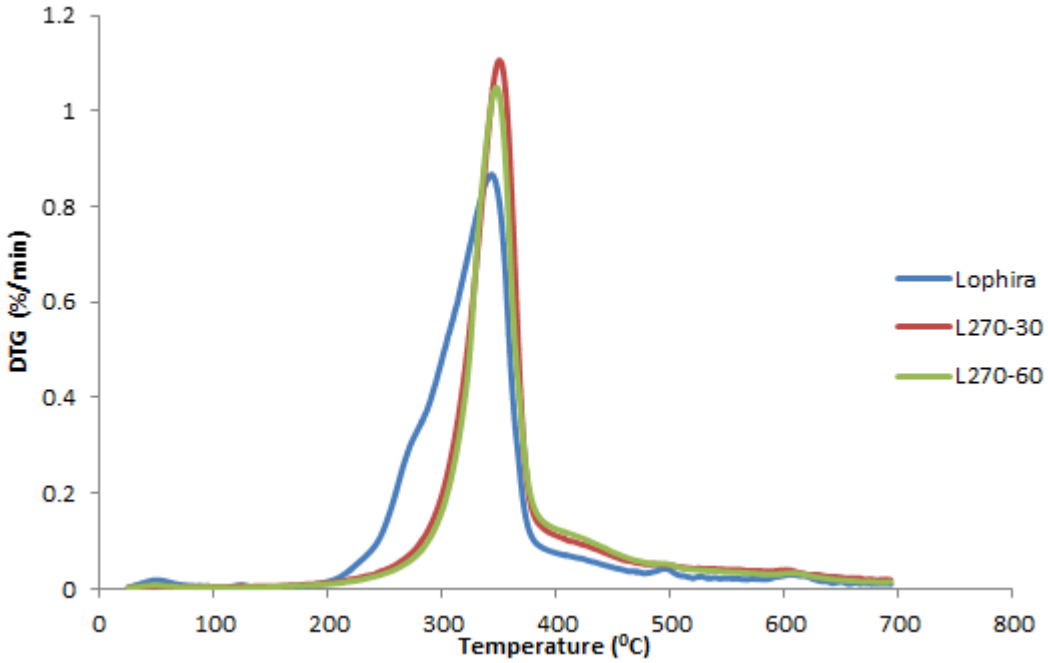

Figure 6-3: DTG pyrolysis profile of raw and torrefied *Lophira* in nitrogen at 10°C/min.

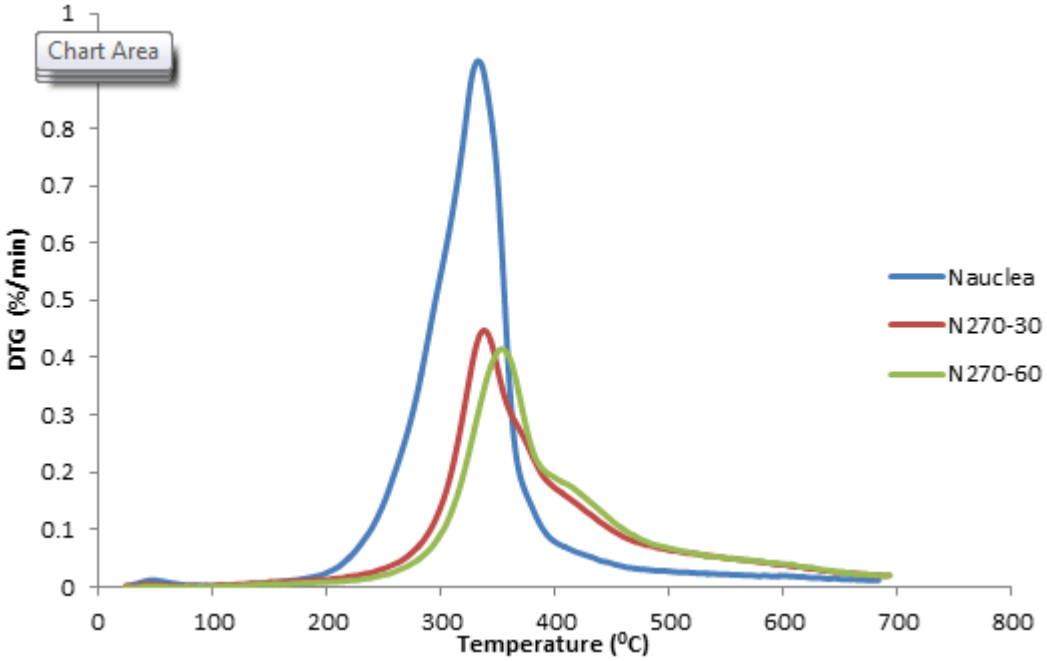

Figure 6-4: DTG pyrolysis profile of raw and torrefied *Nauclea* in nitrogen at 10°C/min.

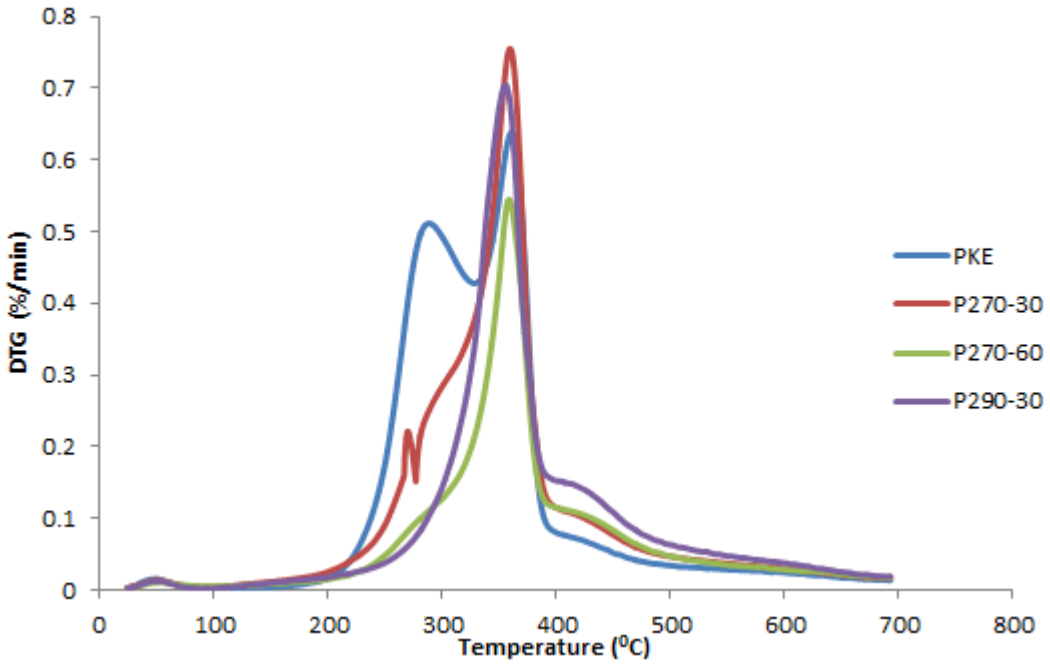

Figure 6-5: DTG pyrolysis profile of raw and torrefied PKE in nitrogen at 10°C/min.

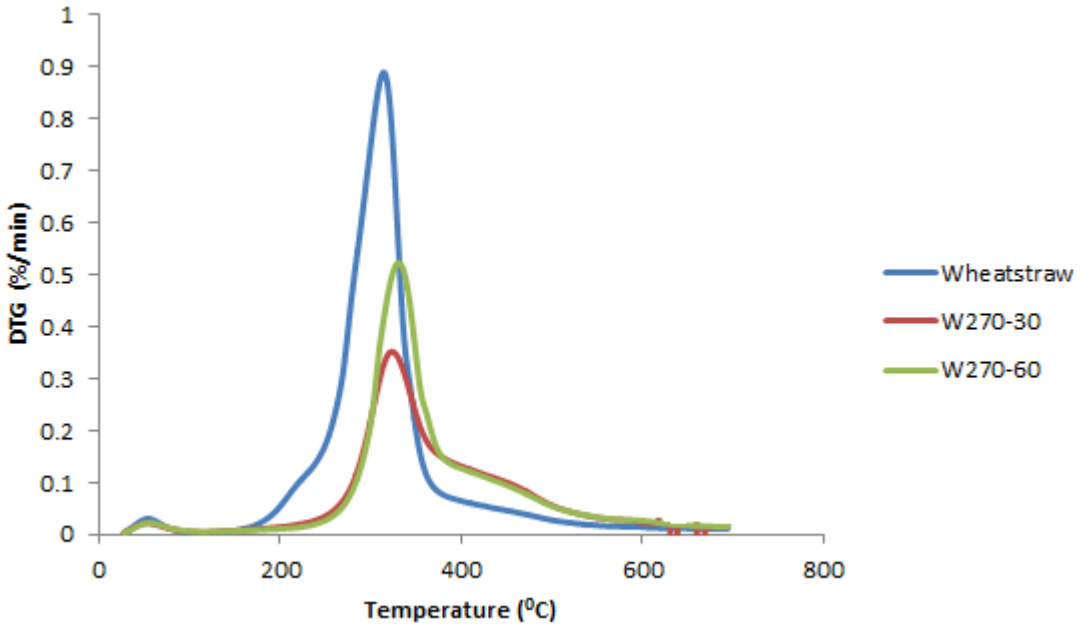

Figure 6-6: DTG pyrolysis profile of raw and torrefied wheat straw in nitrogen at 10°C/min.

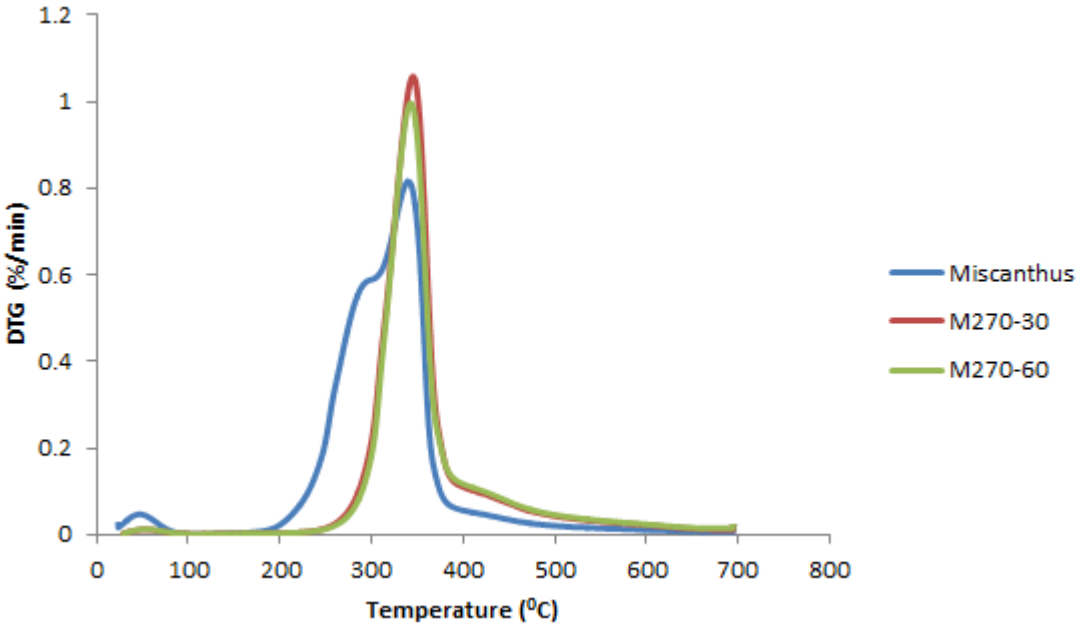

Figure 6-7: DTG pyrolysis profile of raw and torrefied miscanthus in nitrogen at 10°C/min.

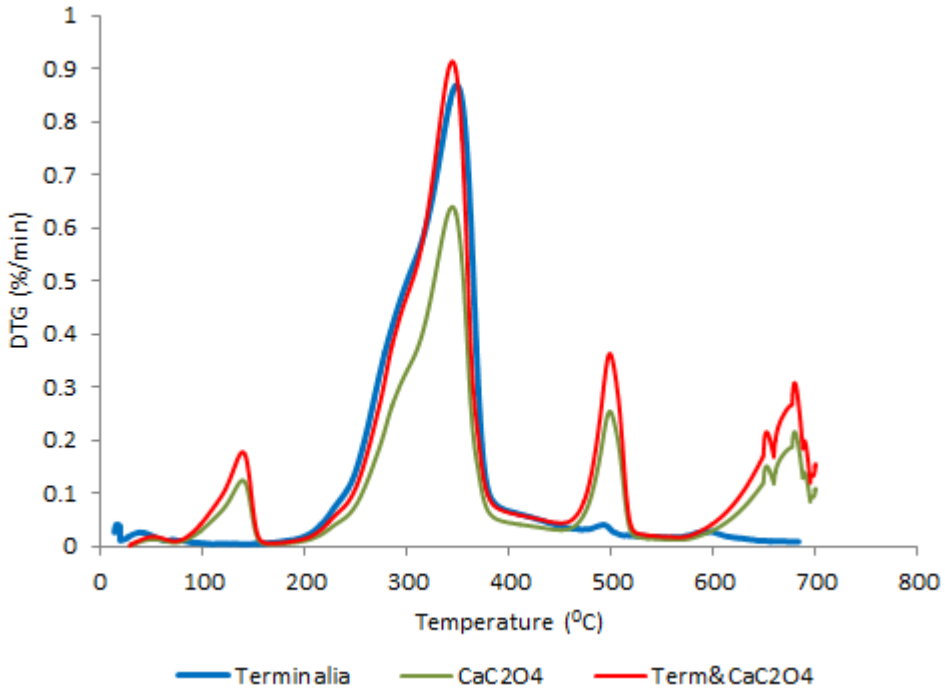

Figure 6-8: DTG pyrolysis profile of raw *Terminalia*, $CaC_2O_{4.x}H_2O$, & a mixture of $CaC_2O_{4.x}H_2O$ and *Terminalia*.

It is evident from these plots that the last two weight loss steps at T >450^{0}C on the DTG pyrolysis curve for *Terminalia* are due to the decomposition of $CaC_2O_{4.x}H_2O$ present in the fuel (since it has high CaO content ~41.7 wt% as reported in previous publication [202]) and some chemical species in the biomass structure; this is consistent with the findings from the literature [63, 203, 204]. Fisher *et al.*[43] reported similar peak at a temperature above 400^{O}C after primary DTG pyrolysis peak in their study on the effect of heating rate on the devolatilization of biomass residue. Biagini *et al.*[204] suggested that in this instance, the peaks within the aforementioned temperature region are due to the degradation of chemical species that may have been formed during the main thermal devolatilization.

Table 6-1 shows the onset temperature (T_o) and peak temperature of pyrolysis (T_{p1}) for the raw and torrefied fuels which were obtained from the DTG plots. It can be observed that the DTG peak pyrolysis temperatures for fuels torrefied at same temperature but different residence time have almost the same values. The pyrolysis peak temperature is often used as an indicator for fuel reactivity, where the fuel with the lowest T_{p1} value is considered the most reactive [74, 120, 133]. For this study, wheat straw is ranked as the most reactive fuel, while *Nauclea* and *Gmelina* (325^{0}C) are ranked as the most reactive

untreated woody biomass, and torrefied PKE (357^0C) is expected to be the least reactive of the fuels considered in this work. The effect of torrefaction is seen on the fuels reactivity as the process lowers the reactivity of the fuels. This is revealed in Table 6-1, as the torrefied fuels are seen to have lower Tp_1 values when compared to their raw conterparts and fuels that were subjected to a more critical torrefaction conditions (by increasing the residence time) appeared less reactive. This is seen in the case of *Gmelina, Nauclea,* wheat straw and miscanthus as they become less reactive upon torrefaction at a slightly lower condition (270^oC for 30min) and have lower reactivities when torrefied at a slightly higher condition (270^oC for 60min). The T_{p1} value for T270-30, L270-30 and P270-30 is slightly lower than that of their raw counterpart but this value remains unchanged for T270-60, L270-60, P270-60 and P290-30 (for same fuels torrefied at a more severe torrefaction conditions) as shown in Table 6-1. Meng *et al* .[205] mentioned that during torrefaction, the moisture content in the fuel evaporates, hemicellulose which is the most reactive compound decomposes, cellulose and lignin partially decompose. Some organic acids (e.g. acetic acid) are released from the biomass during decomposition of hemicellulose and oxygen is lost in form of water, carbon dioxide and carbon monoxide, consequently reducing the oxygen-carbon ratio of the biomass and increasing its thermal resistance [205]. Also increasing the severity of torrefaction condition causes rapid escape of volatiles from the biomass particles with associated development of the porous structure [133]. The removal of the thermally-reactive lignocellulose components through the loss of volatiles during torrefaction yields a higher concentration of biomass in thermally non-reactive carbon and hence lower reactivity [205]. This partly explains the reasons for lower reactivity of torrefied fuels at the same pyrolysis conditions compared to raw biomass than raw biomass. Another important consideration for fuel reactivity during biomass pyrolysis is the natural presence of potassium, a metal that is well-known to catalyse pyrolysis reactions [46, 72, 74, 75, 120]. The respective peak temperatures for the devolatilisation of raw and torrefied wheat straw, *Gmelina* and *Nauclea* are lower compared to the rest of the fuels, suggesting that these fuels would be the most reactive. Their tendency to pyrolyse faster than the other fuels is likely due to their relatively high potassium content (see Table 4-2).

Table 6-1: Characteristics temperature for the pyrolysis of the raw & torrefied samples

Sample	Pyrolysis onset temp (^{o}C) T_o	Pyrolysis peak max temp (^{o}C) T_{p1}
Gmelina	247	325
G270-30	273	328
G270-60	274	329
Terminalia	261	343
T270-30	290	348
T270-60	296	348
Lopira	264	345
L270-30	290	346
L270-60	292	346
Nauclea	252	325
N270-30	275	331
N270-60	292	345
PKE	251	352
P270-30	272	357
P270-60	292	357
P290-30	296	357
wheat straw	256	310
W270-30	266	316
W270-60	276	328
miscanthus	253	336
M270-30	290	341
M270-60	297	341

For samples torrefied at 270^{o}C for 30 minutes, W270-30 is the most reactive, while P270-30 is the least reactive. However, for all torrefied samples, W270-30 is the most reactive, while P270-30, P270-60 and P290-30 are the least reactive.

Determination of moisture, volatile, ash and fixed carbon are obtained using the data from TGA analysis and are reported in Table 6-2. The results for proximate analysis of the fuels are obtained from the TGA data and are comparable to the one which was

determined using British standards (presented in Table 4-1 in Chapter 4). The results of both analyses show the same trend of decreasing moisture and volatile contents as well as increasing fixed carbon contents and ash contents, as the severity of the torrefaction condition increases. It is worth noting that the content of moisture, volatile and ash (proximate analysis) for the fuels which are assessed from the TGA data is slightly less than the ones presented in Table 4-1 (Chapter 4). This is because smaller amounts of fuel and particle size are used for TGA analysis, and the rate of heat transfer becomes faster, thus, leading to more mass loss.

Table 6-2: Proximate analysis of the torrefied samples from TGA

Samples	Moisture content (%)	Volatile content (%)	Ash Content (%)	Fixed Carbon[a] (%)
Gmelina	3.5	80.2	0.9	15.4
G270-30	2.2	70.7	2.6	24.5
G270-60	1.5	63.5	4.1	30.9
Terminalia	4.8	78.8	2.4	14.5
T270-30	2.5	69.2	5.9	22.4
T270-60	1.5	64.5	6.0	28.0
Lophira	2.5	77.9	1.6	18.0
L270-30	1.6	71.9	1.7	24.8
L270-60	1.1	67.6	1.9	29.4
Nauclea	3.8	78.6	1.9	16.7
N270-30	1.8	53.3	3.4	41.5
N270-60	1.4	51.2	4.9	42.5
PKE	2.6	75.2	3.4	18.8
P270-30	2.4	66.9	4.9	25.8
P270-60	1.9	47.2	10.3	40.6
P290-30	2.2	62.0	5.6	30.2
wheat straw	3.1	73.6	5.0	18.3
W270-30	2.1	52.1	14.7	31.1
W270-60	1.7	42.9	19.9	35.5
miscanthus	6.6	77.4	1.5	14.5
M270-30	2.7	68.8	2.0	26.5
M270-60	1.8	65.1	2.6	30.5

a: assessed by difference.

6.3.2 Pyrolysis Kinetics

The kinetic parameters for the pyrolysis of the fuels were derived from the data of the TGA using equation (3-15) in Section 3.4.9.2. The pre-exponential factors, A (s^{-1}), activation energies, Ea (kJ/mol) and correlation co-efficient, R^2 obtained are presented in Table 6-3. It has been observed that torrefaction of biomass results in an increase in activation energy, Ea and therefore a slower apparent reactivity in pyrolysis [76]. This

effect can also be observed from the data in Table 6-3, which show that increasing the torrefaction temperature and/or residence time resulted in higher pre-exponential factors and activation energies required for the pyrolysis reaction. The reason for the high activation energies and slower kinetics of torrefied samples is that the global kinetics derived from the TGA data is no longer dominated by the kinetics of hemicellulose decomposition (which was decomposed during torrefaction) rather it represents the kinetics for the decomposition of the solid residue which is high in cellulose [46]. Table 6-3 also show that samples torrefied at a more severe condition have higher activation energies and slower kinetics than samples torrefied at a lower condition. This is probably due to the complete removal of hemicellulose or thermally-reactive lignocellulose components through the loss of volatiles during torrefaction; a process that produces char residue (mostly cellulose) which is thermally less reactive carbon [205].

Table 6-3: First-order kinetic parameters for the pyrolysis of the torrefied fuels.

Sample	ln (A) (s^{-1})	Ea (kJ/mol)	Correlation co-efficient, R^2	Reactivity at 573K, k_{573} (s^{-1})
Gmelina	10	78.8	0.9947	0.00150
G270-30	17.3	114	0.9956	0.00144
G270-60	20	128	0.9951	0.00108
Terminalia	15.6	110	0.9982	0.00052
T270-30	19.5	131	0.999	0.00035
T270-60	24.5	155	0.9961	0.00033
Lophira	15.9	112	0.9801	0.00051
L270-30	23.3	148	0.9985	0.00045
L270-60	24.9	156	0.9927	0.00042
Nauclea	9.87	77.8	0.9953	0.00157
N270-30	18.2	120	0.9959	0.00092
N270-60	16.7	116	0.9953	0.00050
PKE	14.5	108	0.9985	0.00033
P270-30	19.8	133	0.9797	0.00033
P270-60	23.2	149	0.9948	0.00031
P290-30	19.7	133	0.9848	0.00028
wheat straw	14	94.5	0.9904	0.00276
W270-30	17.9	115	0.9993	0.00175
W270-60	22.2	137	0.9956	0.00144
miscanthus	13.9	99.5	0.9761	0.00090
M270-30	20.6	132	0.9952	0.00079
M270-60	27.2	164	0.9937	0.00069

For all torrefied samples, W270-30 had the lowest activation energy and the fastest kinetics, while P290-30 had the highest activation energy and the slowest kinetics. Therefore, the former would require the least amount of energy to initiate a chemical reaction, while latter would require the most amount of energy to initiate a chemical reaction.

As mentioned earlier, one possible explanation for the low activation energy of W270-30 is the relatively high amount of potassium in the feedstock, a metal which is known to catalyse a chemical reaction [46]. Similar activation energies and pre-exponential factors have been published by Saddawi *et al.* [46] for wheat straw, willow, eucalyptus, and miscanthus torrefied at 290^{o}C for 60 minutes with values of 90.4 kJ/mol, 130kJ/mol, 141kJ/mol, and 151kJ/mol with pre-exponential factors, 11.8s^{-1},19.4s^{-1}, 21.9s^{-1}, 23.6s^{-1} respectively.

In order to establish a ranking of the reactivity of the samples, the kinetic parameters obtained were used to estimate the reactivity of the fuels at 573K (300^{o}C) and are listed in Table 6-3, for comparison purposes. The temperature, 573K is used as reference because at that temperature, all samples would have commenced pyrolysis. Equation 6-1 was used to assess the reaction rate constant at 573K:

$$k_{573} = A \exp\left(-Ea/RT\right) \qquad \text{Equation 6-1.}$$

Where k_{573} = reaction rate constant at 573K

A = pre-exponential factor (s^{-1})

Ea = activation energy (kJ/mol)

R = gas constant = 8.314J/mol K

T = temperature (K)

As expected, the raw samples were found to be more reactive than their torrefied counterparts, and the reactivity follows the order wheat straw > W270-30 > *Nauclea* > *Gmelina* > W270-60 > G270-30 > G270-60 > N270-30 > miscanthus > M270-30 > M270-60 > *Terminalia* > *Lophira* > N270-60 > L270-30 > L270-60 > T270-30 > T270-60> PKE > P270-30> P270-60 > P290-30. The order of reactivity calculated at 573K follows the same order of ranking obtained when comparing the peak pyrolysis temperature order. From the Nigerian fuels, it can be noted that both *Nauclea* and *Gmelina* resulted in very similar Ea values (77.8 & 78.8 KJ/mol repectively), which

were the lowest activation energies observed and resulted in the fastest reactivities calculated. A possible reason for the low activation energy of *Gmelina* and *Nauclea* could be the abundance of potassium in the fuels [202]; a metal that catalyses the pyrolysis reaction [46]. Also listed in Table 6-3 are the R^2 values which were used for calculating the kinetic parameters. The R^2 values reported here are high and are an indication that the results of activation energies are considered accurate. Figure 6-8 show the reaction rate and peak maximum temperature profiles of pyrolysis for raw and torrefied samples while Figure 6-9 is the plot of reaction rate against peak maximum temperature of pyrolysis. A relationship can be established between reaction rate and peak maximum temperature as shown in Figures 6-8 & 6-9. For instance, the reaction rate is observed to be slower (the value of K reduces) as the peak maximum temperature increases.

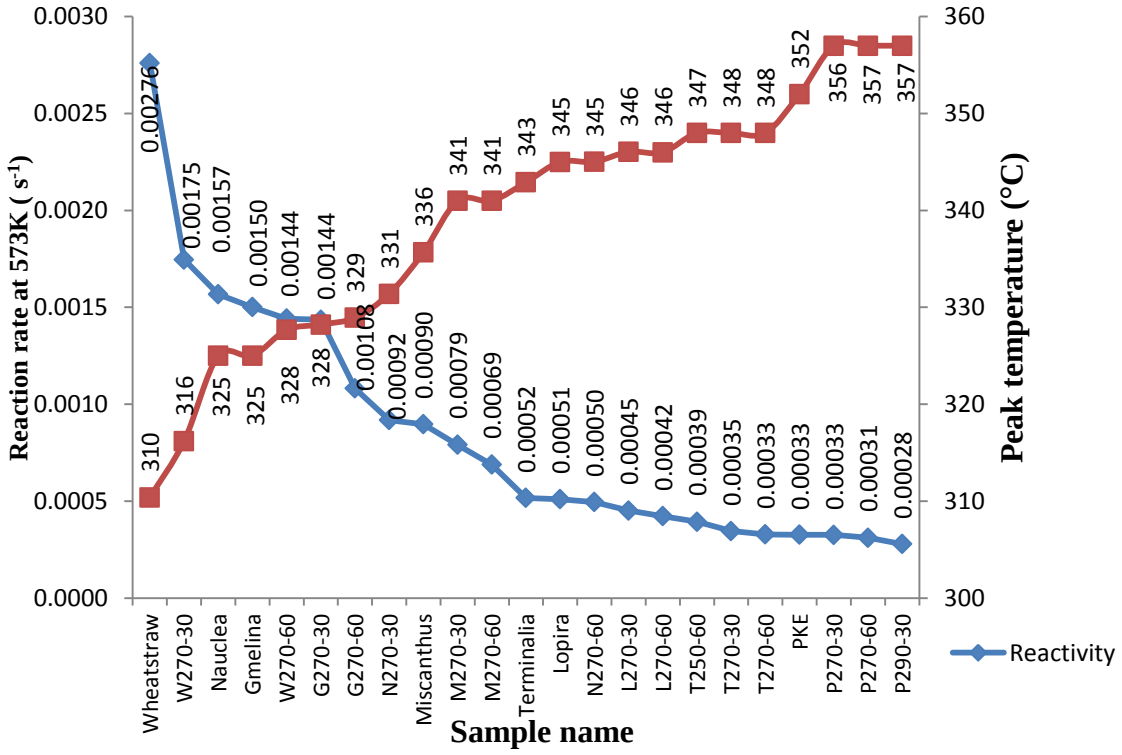

Figure 6-9: Reaction rate at 573K and peak maximum temperature profiles of pyrolysis for raw and torrefied samples.

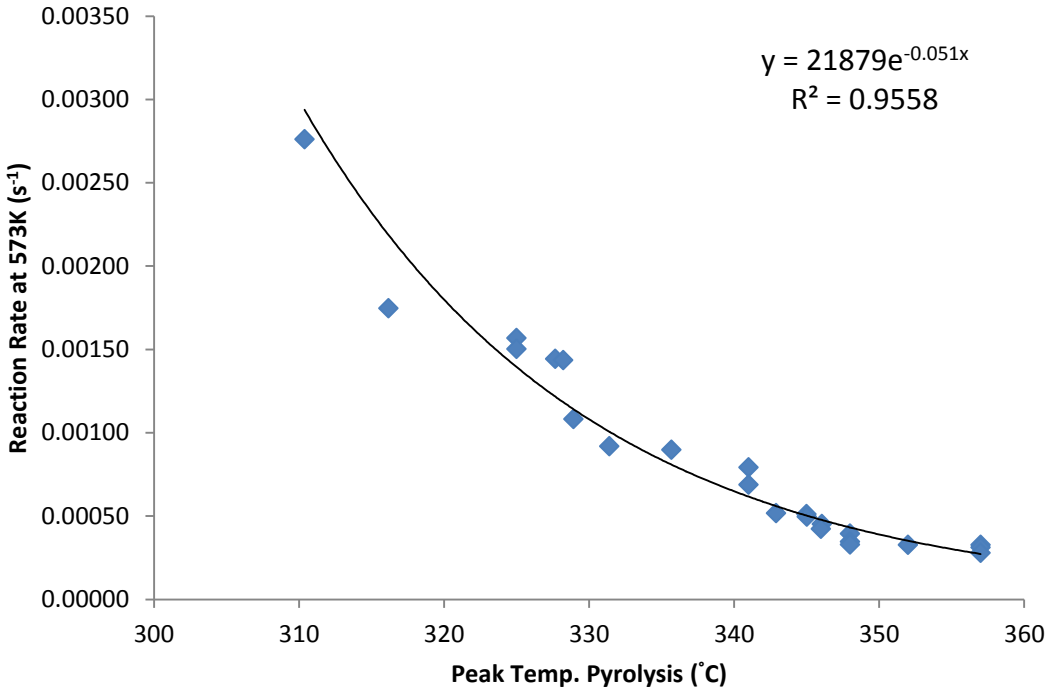

Figure 6-10: A plot of reaction rate at 573K against peak maximum temperature of pyrolysis for raw and torrefied samples.

6.3.3 Pyrolysis-Gas Chromatography-Mass Spectrometry (Py-GC-MS)

The rapid heating of the torrefied samples (Nigerian fuels) were carried out using the Py-GC-MS technique in order to recognise and semi-quantify the medium volatiles from the pyrolysis of the fuels. The fingerprint of the released volatiles for the torrefied samples are compared to that of the raw samples. The peak area percentages were estimated from the chromatograms and were normalised per mg of volatile products. The main peaks were identified, and assigned from the mass spectral detection NIST05A MS library and also from the literature [45, 120, 157, 186, 206]. Most of the products detected are from lignocelluloses and extractives and are classified into lignocellulose groupings in Table 6-4. For direct comparison, the peak area percentages for the decomposition compounds in the torrefied fuels are plotted together with that of the raw counterpart in Figures 6-10 to 6-16. As expected, Figures 6-10 to 6-16 show that some of the compounds (mostly hemicellulose products) that were identified during Py-GC-

MS analysis of the raw fuels cannot be found during the same analysis for their torrefied fuels. This is partly due to the released of low organic volatiles during decomposition of hemicellulose in torrefaction process [205] and also the presence of potassium in the fuel, a metal that is well-known to catalyse pyrolysis reactions [46, 72, 74, 75, 120].

Figures 6-10 to 6-16 also indicate that the proportion of phenolic organic compounds identified is more than one-third of the peak areas; especially methoxy-phenol and methyl-phenol. The peak area for methoxy-phenol and methyl-phenol increases for torrefied fuels and further increases are observed with fuels that were torrefied at a more severe condition. The increase in the peak area for the above-mentioned products is from the deconstruction of lignin fraction [185, 206, 207] and is consistent with findings from literature [45, 208]. Greenhalf *et al.* [208], reported that phenols constituted about one-third of the released volatile products among the group of compounds identified during fast pyrolysis of straw, perennial grasses and hardwoods. Lasode *et al.*[45] also observed that phenolic compounds made up more than one-third of the group of compounds identified during torrefaction of *Albizia pedicellaris, Tectona grandis* , *Terminalia ivorensis, Sorghum bicolour glume* and *Sorghum bicolour* stalk.

Table 6-4(a): Classification of identified compounds into lignocellulose component.

S/N	Compound Name	Lignocellulosic component
1	1,3-Pentadiene,	Hemicellulose
2	3-Furaldehyde	Cellulose
3	methyl-Furan	Cellulose
4	Furfural	Cellulose
5	Furanmethanol	Cellulose
6	2(5H)-Furanone	Cellulose
7	tetrahydro-2-Furanmethanol	Cellulose
8	5-methyl-2-Furancarboxaldehyde	Cellulose
9	Acetic acid	Hemicellulose
10	2-Cyclopenten-1-one	Hemicellulose
11	methyl-Cyclopenten-1-one	Hemicellulose
12	2-hydroxy-3-methyl-2-Cyclopenten-1-one	Hemicellulose
13	3-ethyl-2-hydroxy-2-Cyclopenten-1-one	Hemicellulose
14	1,2-Cyclopentanedione	Hemicellulose
15	3-methyl-1,2-Cyclopentanedione	Cellulose
16	4,4-dimethyl-2-Cyclohexen-1-one	Hemicellulose
17	Cyclohexanol, 1-methyl-4-(1-methylethenyl)-, acetate	Hemicellulose
18	Toluene	Lignin
19	o-Xylene	Lignin
20	Phenol	Lignin
21	methyl-Phenol,	Lignin
22	methoxy-Phenol	Lignin
23	ethyl-Phenol	Lignin
24	Vanillin	Lignin
25	vinylfuran	Cellulose
26	3',5'-Dimethoxyacetophenone	Lignin
27	2-methoxy-4-(1-propenyl)- Phenol	Lignin

Table 6-4b: Classification of identified compounds into lignocellulose component (cont'd).

S/N	Compound Name	Lignocellulosic component
28	3,4-dimethyl-, methylcarbamate- Phenol,	Lignin
29	Eugenol	Lignin
30	5-tert-Butylpyrogallol	Lignin
31	Hexadecanoic acid	Extractive
32	Octadecanoic acid	Extractive
33	Hexadecanamide	Extractive

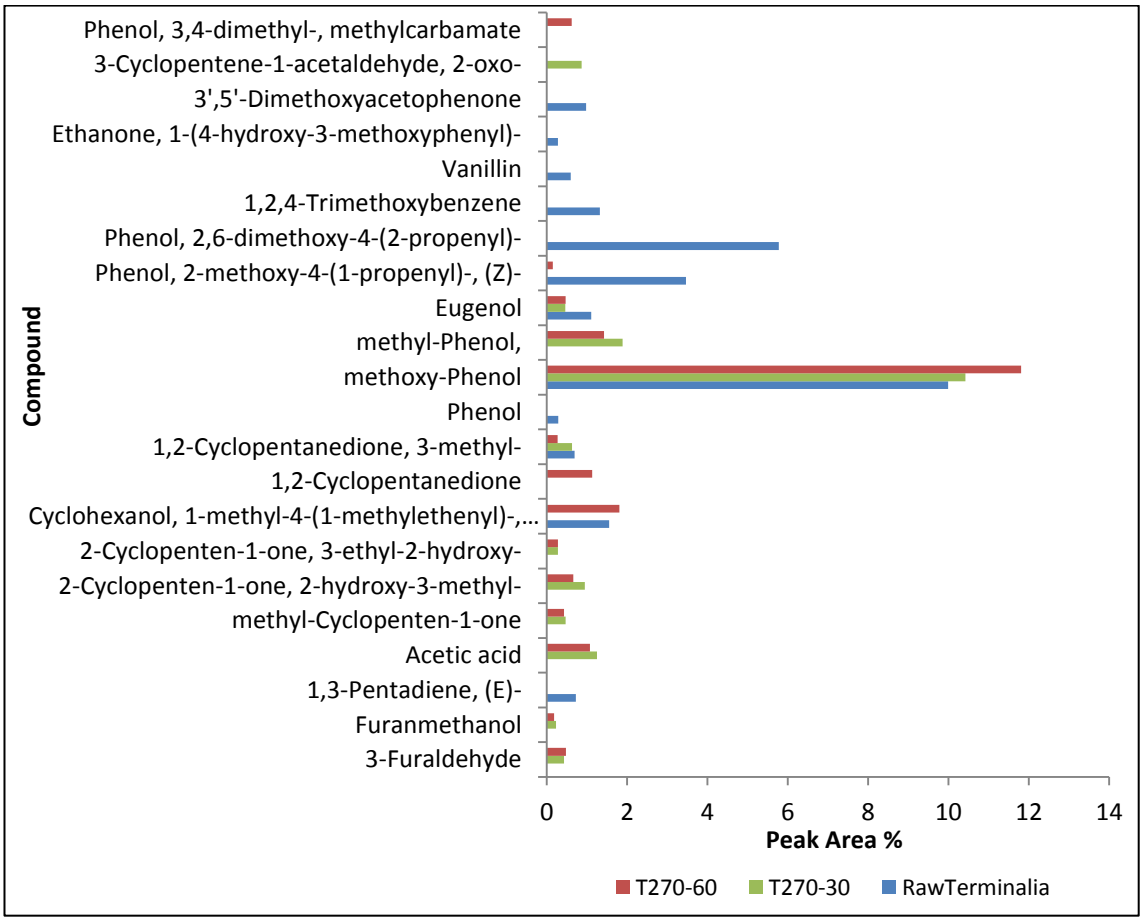

Figure 6-11: Decomposition products from Py-GC-MS analysis of raw and torrefied *Terminalia*.

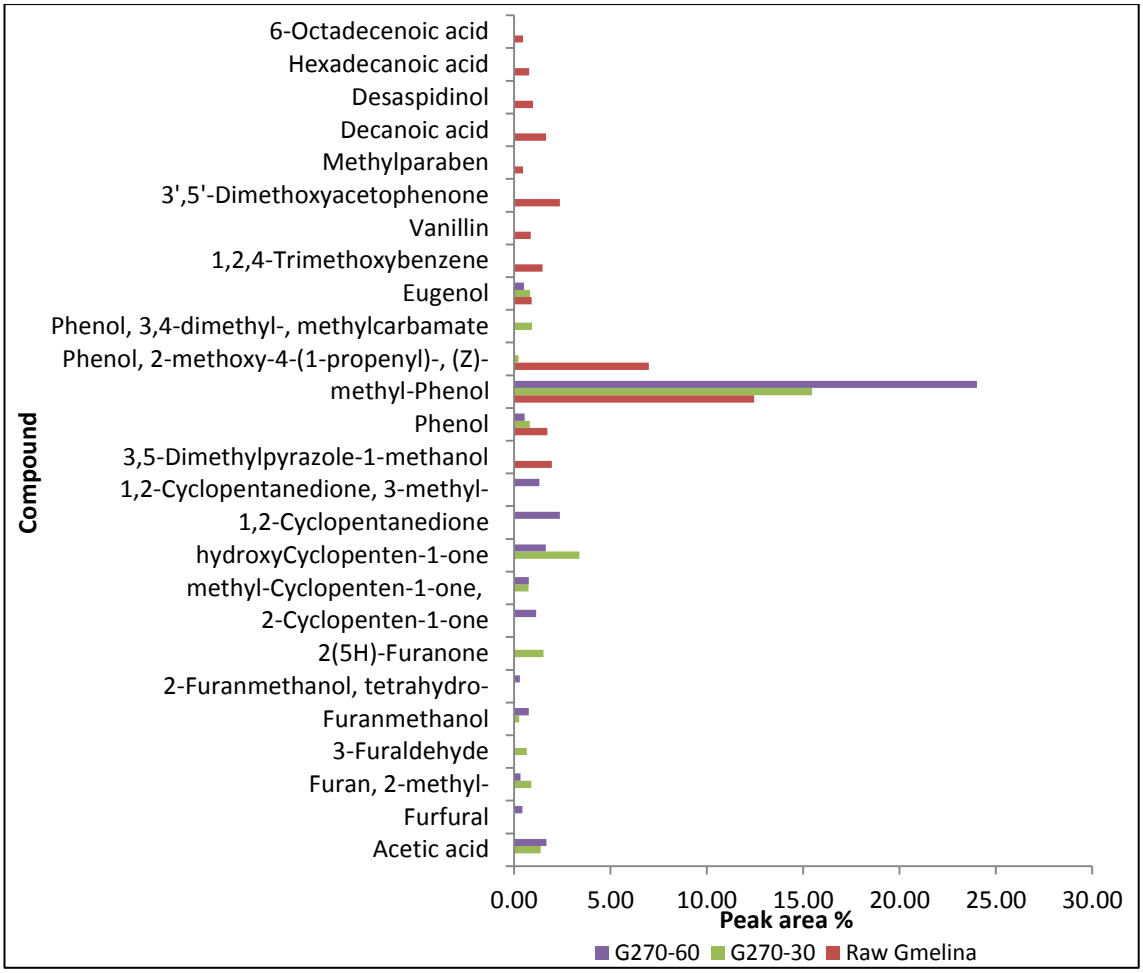

Figure 6-12: Decomposition products from Py-GC-MS analysis of raw and torrefied *Gmelina*.

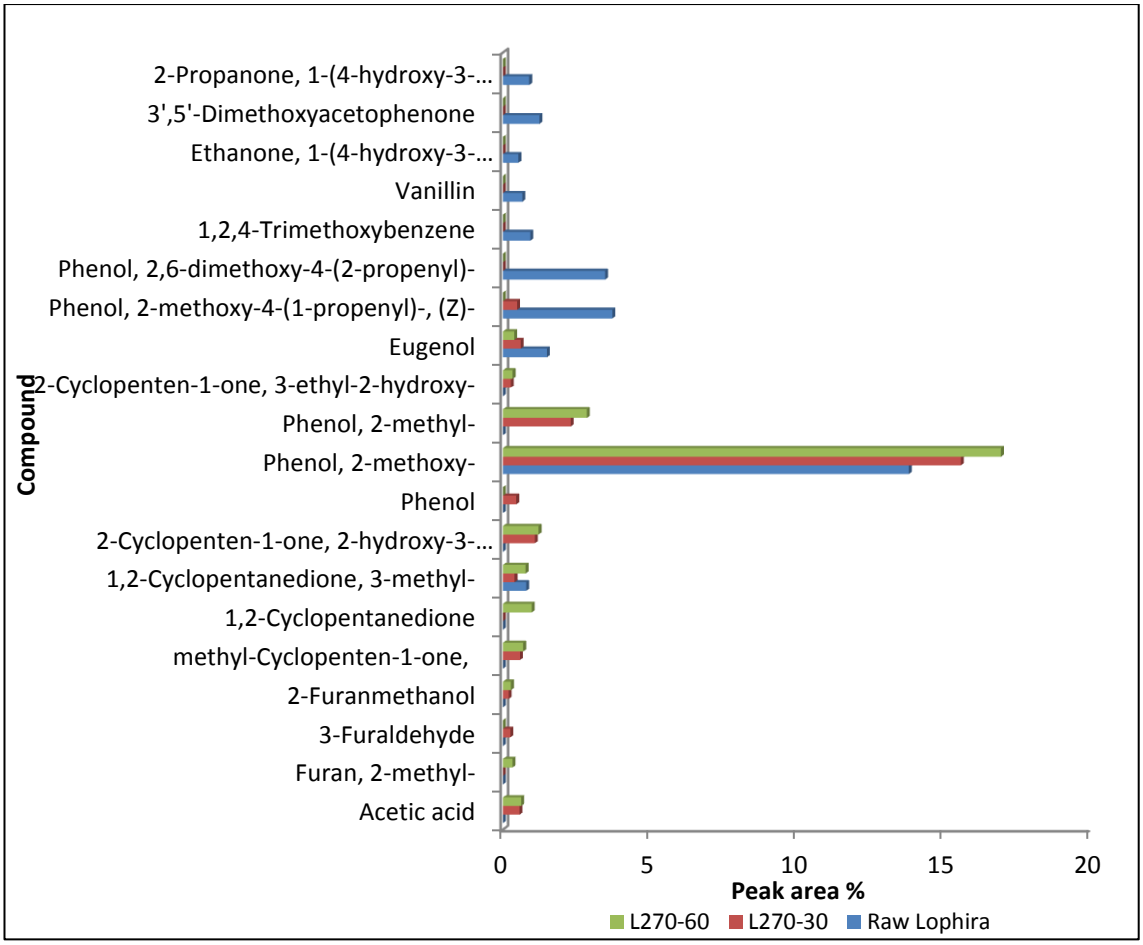

Figure 6-13: Decomposition products from Py-GC-MS analysis of raw and torrefied *Lophira.*

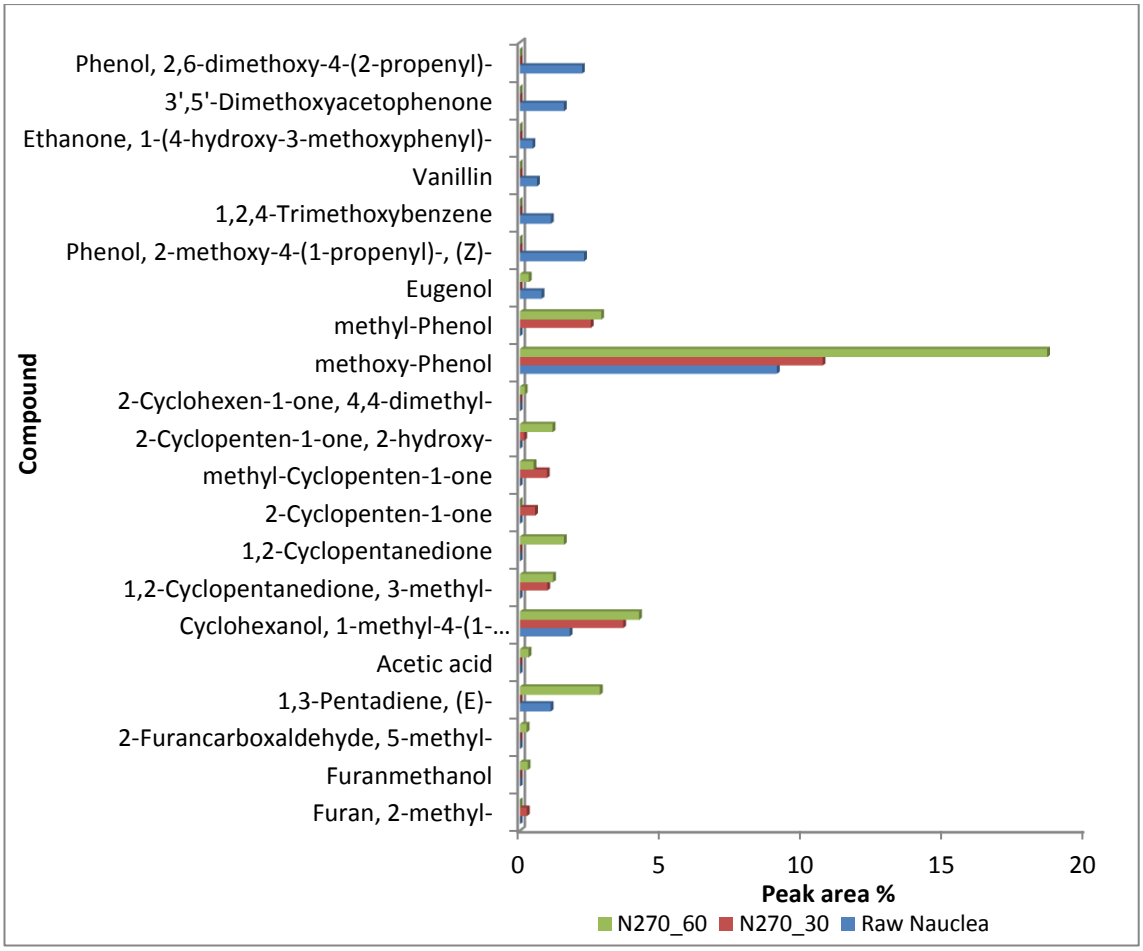

Figure 6-14: Decomposition products from Py-GC-MS analysis of raw and torrefied *Nauclea.*

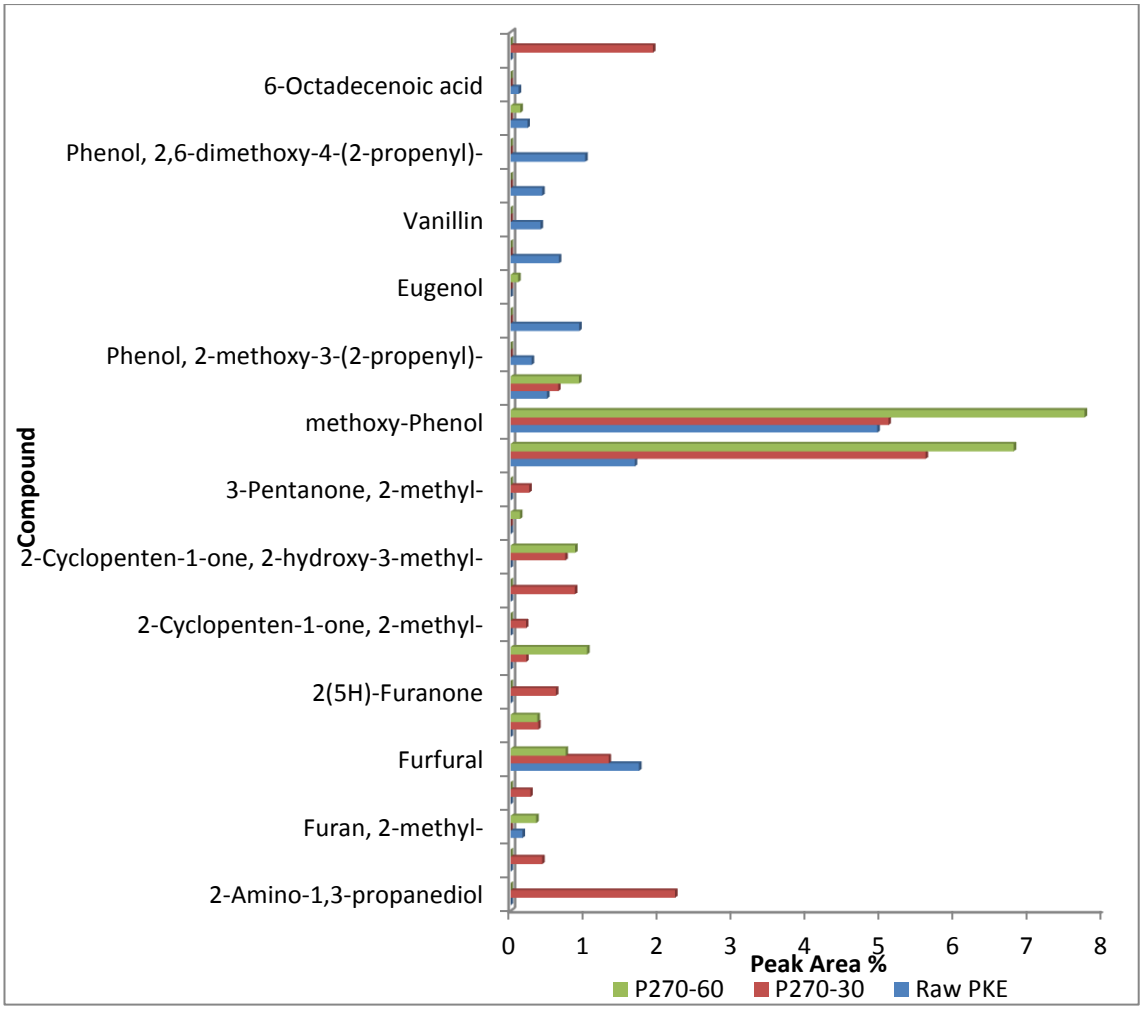

Figure 6-15: Decomposition products from Py-GC-MS analysis of raw and torrefied PKE.

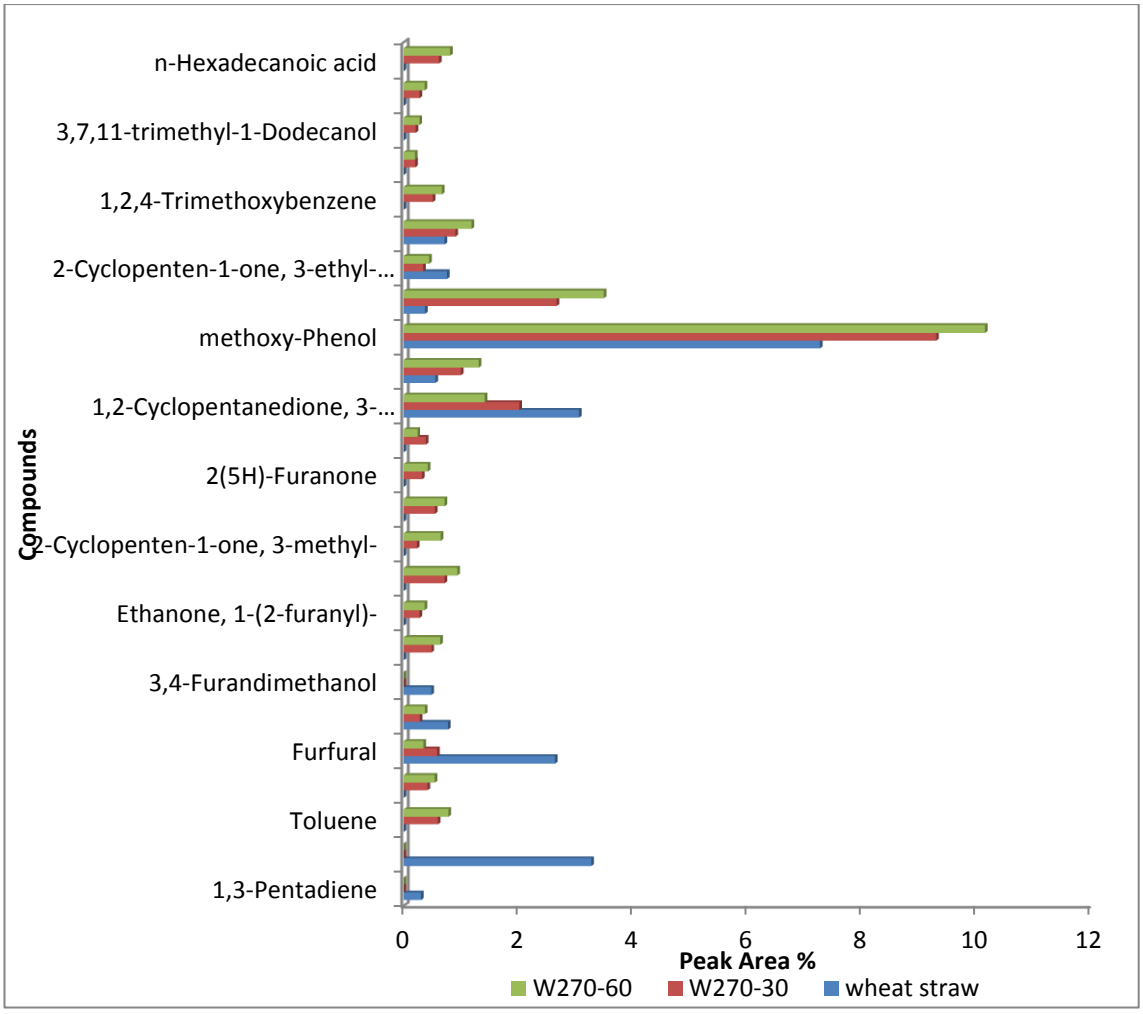

Figure 6-16: Decomposition products from Py-GC-MS analysis of raw and torrefied wheat straw.

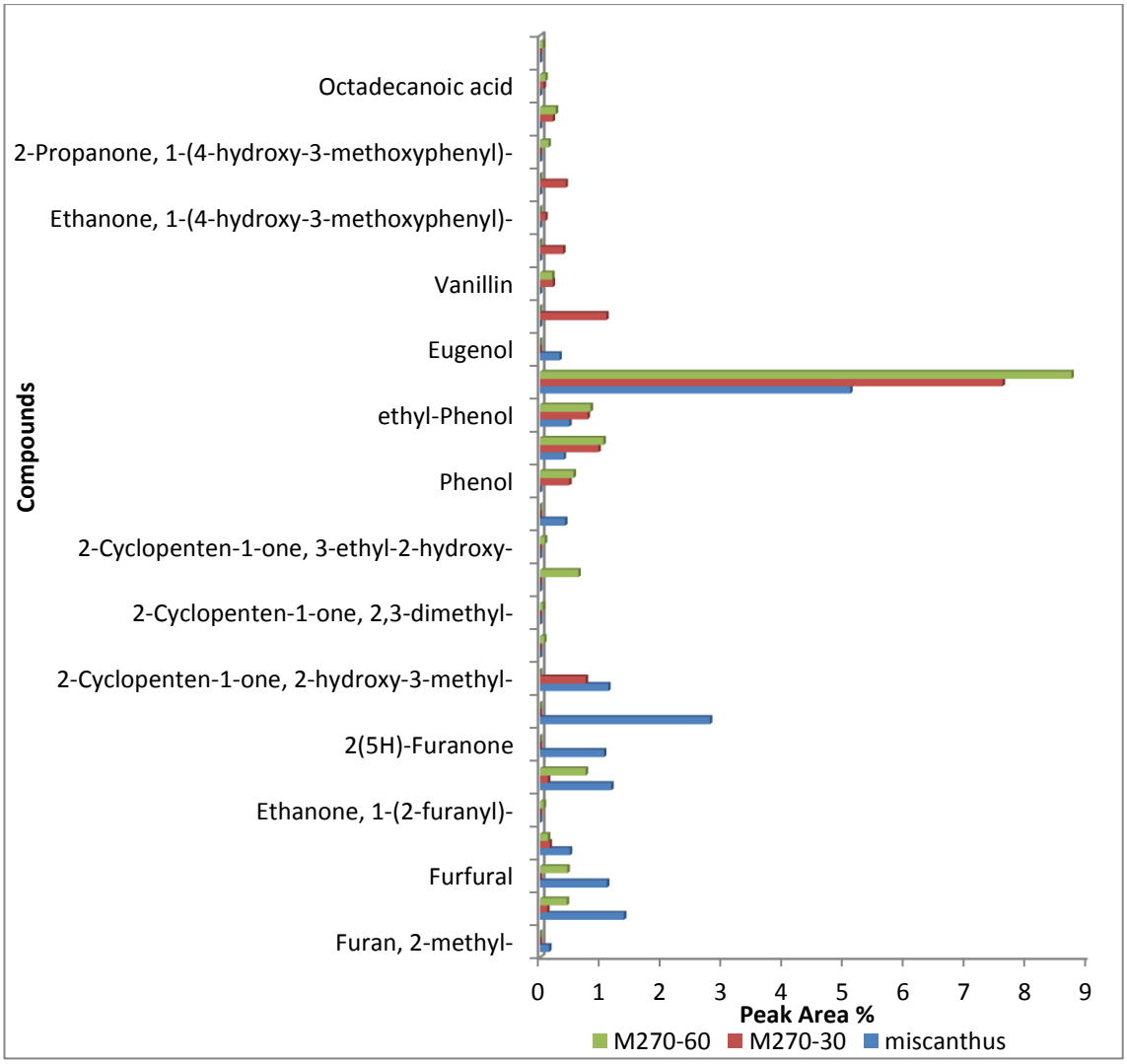

Figure 6-17: Decomposition products from Py-GC-MS analysis of raw and torrefied miscanthus.

6.4 Conclusion

The effects of torrefaction on the thermal properties of some Nigerian and UK fuels have been investigated. For this purpose, TGA and Py-GC-MS analysis was carried out using the treated fuels obtained from torrefaction experiment reported in Chapter 5.

TGA analysis showed that torrefied fuels are less reactive in pyrolysis than their raw counterparts, and, the more severe the torrefaction conditions, the less reactive the fuels become. Based on the temperature of maximum volatile combustion rate, T_{p1}, wheat straw, *Gmelina* and *Nauclea* are the most reactive fuels, while torrefied PKE fuels are

the least reactive. The reactivity of the torrefied fuels was also assessed from the reaction rate constant at 573K and followed the order wheat straw > W270-30 > *Nauclea* > *Gmelina* > W270-60 > G270-30 > G270-60 > N270-30 > miscanthus > M270-30 > M270-60 > *Terminalia* > *Lophira* > N270-60 > L270-30 > L270-60 > T270-30 > T270-60> PKE > P270-30> P270-60 > P290-30 i.e. it follows the same order of ranking as the DTG peak pyrolysis temperature order. The results obtained for determination of moisture, volatile and ash content from TGA analysis is similar to the results obtained from proximate analysis using British standards procedures.

The Py-GC-MS analytical technique revealed that the presence of extractives (oil compounds) in the fuels, while phenolic compounds made up more than one-third of the group of compounds identified; mainly methoxy-phenol and methyl-phenol. The presence of methoxy-phenol and methyl-phenol is more evident in torrefied fuels. Analysis also showed that some of the products which were not seen in the group of compounds identified during pyrolysis of torrefied fuels may have been released during decomposition of hemicellulose in the torrefaction process.

CHAPTER 7. COMBUSTION STUDIES ON TORREFIED BIOMASS

7.1 Introduction

The use of biomass for large scale power generation is increasing rapidly all around the globe, especially in the Europe where many coal-fired pulverized fuel plants are fully converted or retrofitted to burn biomass in boilers designed for pulverised coal. According to Jones *et al.* [133], the amounts of biomass used in co-firing range from a few percentages up to 100%, but are typically < 20% of the feedstock. In such applications, a good knowledge of the combustion behaviour of the solid biomass fuels is vital and therefore needs careful consideration to ensure effective operation and prevention of performance and environmental issues when considering biomass as a potential source for electricity generation.

Recently, computer models used for predicting the combustion behaviour of pulverised coal has been extended to the combustion of untreated biomass [209]. This level of knowledge has not yet been well developed on an industrial scale for the combustion of torrefied fuels other than some laboratory and CFD modelling studies [133]. The properties of the torrefied biomass are significantly influenced by the process conditions, such as reaction time and more importantly the reaction temperature [93, 133]. Some studies of combustion behaviour of torrefied biomass in comparison to the raw biomass can be found in the literature [37, 40, 133, 178], although most authors focus on the physical and chemical characteristics of the thermally treated biomass [93, 106, 118, 126, 128, 192]. During combustion, raw biomass produces smoke, and can have a low thermal efficiency due to its high moisture content [111]. When substituting coal with biomass, the impact on NOx during combustion is generally good (i.e. lower), because of the lower nitrogen content in the fuel. However, changes in flame shape, flame temperature, and the gaseous environment in the near and far burner regions, also impact on NOx production. Therefore understanding the combustion behaviour and properties of biomass is very important in order to enhance its performance in the combustion chamber. This will also help in identifying the environmental issues surrounding the burning of biomass as a potential substitute for fossil fuels.

Single particle combustion is an experimental method used in investigating the combustion behaviour of biomass but there are only a few studies documented in the

literature [177, 178, 210-213] using this approach. The method is used to model the combustion behaviour of pulverised biomass in large scale boilers since smaller biomass particle sizes (between 0.5 -3mm) can be used for this study. However the volume of data that can be easily generated using this method is limited since the process is time consuming and is labour intensive for preparing, burning and analysing individual particles.

A popular, more rapid approach for the prediction of combustion rate and kinetics parameters is using data from thermogravimetric analysis (TGA). Also, by analysing data from TGA, it is possible to determine different stages of combustion such as ignition temperature, and peak char combustion using the derivative thermogravimetric analysis (DTG).

In this study, single particles of untreated and torrefied biomass (particle size of about 2mm cube) were suspended in a methane-air flame, modelling biomass combustion in a furnace. Measurements of ignition delay, duration of volatile combustion and duration of char combustion were assessed using a high speed camera for both untreated and torrefied fuels. The temperature of the flame at the location of the particle and the oxygen concentration were measured using thermocouples and a gas-analyser probe respectively.

Also, low heating rate combustion studies were investigated under TGA for torrefied fuels in order to determine ignition temperature, peak char combustion, kinetics parameters and consequently reaction rate for char burn out. The results obtained are then compared to their raw counterparts in order to investigate the effect of torrefaction on the combustion process.

7.2 Materials and Experimental Methods

7.2.1 Sample Preparation

The samples studied were detailed in Sections 3.2.1 to 3.2.6. For single particle combustion studies, samples were prepared using a hand blade to 2x2x2 mm size fraction, and further milled to smaller particle size < 53μm for TGA analysis.

7.2.2 Experimental Methods

The details for all the experiments conducted in this Chapter are found in Section 3.12 and 3.14.

7.3 Results and Discussion

7.3.1 Single Particle Combustion Studies

There are a series of chemical reactions in the mechanism of biomass combustion. In complete combustion, the carbon in the biomass is oxidised to carbon dioxide, and hydrogen to water. According to Yang *et al.*[178], the process involved in burning a fixed single particle of biomass is described most often with about five combustion stages; the first stage is the evaporation of moisture (often called the drying stage), whose progress is assumed to be limited by the pattern of heat transfer inside the sample; the second stage is the removal of volatiles from the biomass, leaving just char behind (devolatilisation stage); the third stage is char combustion, (the second and third stages are usually catalysed by potassium in the fuel); the fourth is evaporation of metals; and finally the fifth stage which is the decomposition of ash (shrinking stage).

Lu *et al.*[214] in their studies on the combustion behaviour of poplar wood and hardwood in a single particle reactor with pre-heated air, suspended single particles of poplar wood and hardwood sawdust particles in the size range 0.3 – 9.5mm, in an enclosed chamber reactor. They described the processes involved as the biomass enters the reactor as; (1) heating and drying, (2) devolatilisation, and (3) char combustion. They further mentioned that these three processes depend on the properties of the particle such as the particle size and the chemical composition of the fuel.

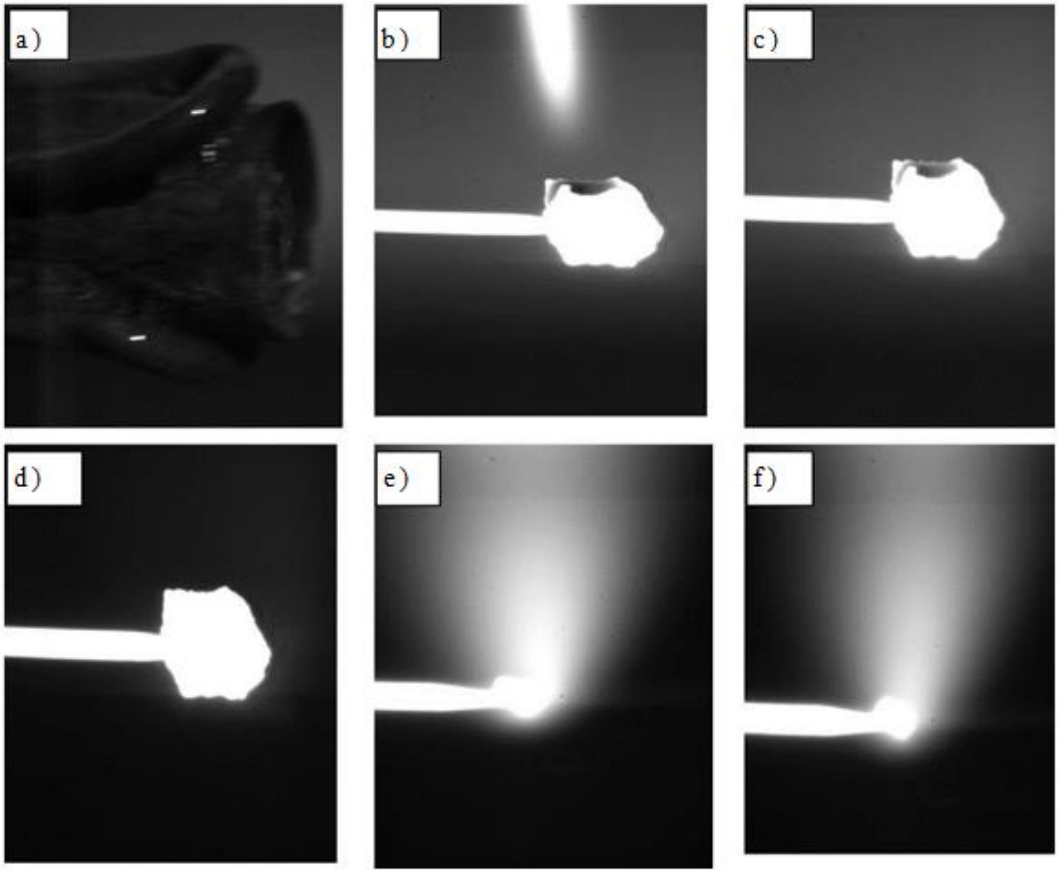

Figure 7-1(a – f): Images taken during the combustion of sample G270-60

The visual study of the images allowed the estimation of the ignition delay, and of the duration of the volatile and char combustion stages. Here, when analysing the images of the recorded video from the single particle combustion experiments to understand the behaviour of the fuels, the following combustion stages were clearly identified from these images: ignition, volatile combustion, and char combustion as shown in Figure 7-1(a-f).

For this study, only the raw fuels and the fuels torrefied at a process condition of 270°C for 60 min were investigated in order to establish a clear distinction between their combustion properties. Figure 7-1 (a) marks the exposure of the particle to the flame. The fuel particle was assumed to be ignited once flaming combustion was visible after exposure to the methane-air flame and can be observed in Figure 7-1 (b). The Biot Number (Bi) fundamentally describes how fast heat flows through a material, and in this case, it is vital to the heating-up and ignition process of the fuel particle, which can be considerably influenced by the moisture content. The Bi is a dimensionless ratio of surface convective heat transfer to internal heat conductivity and it decides whether the

conduction of heat inside a particle is faster than the transport of heat to the exterior of the particle from the gases [215]. According to Scott *et al.*[215], a Bi value <0.1 will result in a more or less uniform temperature throughout the particle. In this instance, the Biot number for the untreated and treated fuels is different, consequently, the effect is observed in the heating-up process and the ignition delay of the fuels (untreated and torrefied), due to the differences in the thermal conductivity of the woods [216]. The thermal conductivity of the torrefied fuels is higher, since the thermal resistance of the wood was lowered by the torrefaction process, and this caused transfer of heat to be faster in the ignition process of torrefied fuel than untreated fuels.

7.3.1.1 Delay on Ignition

In this study, as the biomass particle is exposed to the methane-air flame, it exchanges heat energy by both radiation and convection, and by chemical reactions. It then undergoes the following processes- drying, ignition, devolatilization and char combustion, sequentially or simultaneously, depending on particle properties and reactor conditions [177, 178]. The water content in the fuel particle is crucial because the energy required to dehydrate the particles in the flame results in a delay in the ignition process and can lead to lifted or unstable pulverized fuel flames [179]. Here ignition delay is obtained by the difference between the time at which the particle was exposed to the flame and the time at which the particle was ignited. A plot of the ignition delay against biomass particle dry mass is presented in Figure 7-2. From this figure, it can be observed that there are differences in the ignition delay of the raw and torrefied fuels. For the raw fuels, the effect of particle mass on the ignition delay of *Nauclea* and *Gmelina* is not as significant as in the case of miscanthus, *Terminalia* and *Lophira*. This is likely due to the chemical composition of *Nauclea* and *Gmelina* and also to both fuels having relatively low moisture contents when compared with miscanthus and *Lophira.* From Figure 7-2, it can be seen that the raw samples presented longer ignition delay times than the torrefied samples, as the latter were drier than their raw counterparts. The ignition delay of *Nauclea*, miscanthus, *Lophira, Terminalia*, and *Gmelina* ranged from 0.03 – 0.05s, 0.03 – 0.09s, 0.03 – 0.11s, 0.04 – 0.10s, and 0.04 – 0.06s respectively, with a standard error $\leq \pm$ 0.008s due to video frame speed. There is a significant improvement in the ignition of the torrefied fuels, as the delay in ignition was reduced to about 0.01 - 0.03s (standard error $\leq \pm$ 0.008s). It is

important to mention that any differences in the ignition delay may have also occurred in part from the difficulty in reducing particles to exactly the same size and shape, and also, in part to the differences in moisture contents of individual particles. Moisture contents were measured to be 4.2, 4.9, 5.2, 7.1 and 12% for *Nauclea*, *Gmelina*, *Terminalia*, miscanthus and *Lophira* respectively, and less than 3% for the torrefied fuels. The differences in the moisture contents of the fuels is possibly responsible for the variation in the ignition delay, as suggested by Borman and Ragland [217].

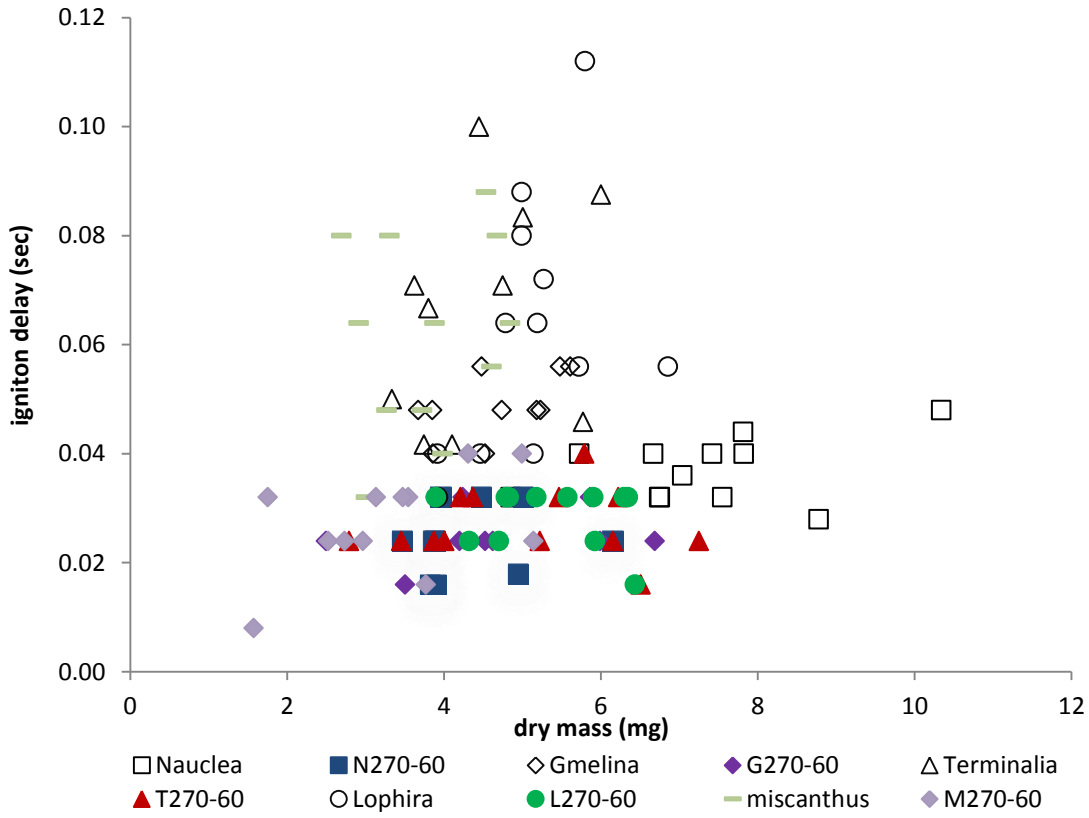

Figure 7-2: Plot of the ignition delay against particle mass (dry) for raw and torrefied fuels.

7.3.1.2 Volatile combustion

Volatile combustion proceeds after ignition, where the particle devolatilises and volatile organic materials are released and combusted rapidly. The release of volatiles through the biomass pores prevents the ingress of external oxygen into the particle, i.e. the flow of oxygen into the particle is obstructed by the large gaseous outflow of volatiles from the surface of the particles. Thus, char combustion proceeds after devolatilisation with the disappearance of the flame as shown in Figure 7-1(c), although in most cases here,

an overlapping occurrence of volatile (flaming) combustion and char (glowing particle) combustion was observed whereby char combustion proceeded at the bottom of the particle while flame combustion occurred from the top of the particle. Scott *et al.*[215] had described the thermal decomposition of biomass in an inert (pyrolysis) or oxidising environment (combustion) as a similar or parallel process because, during devolatilisation, volatile materials are released from the fuel, and this causes a reducing environment around the fuel; also the volatile matter burns in a diffusion flame at some distance from the fuel particle [215]. In this case, because of the orientation of the particle, the volatile release was non-uniform and enabled overlapping of char combustion during devolatilisation.

Figure 7-3 shows the duration of volatile combustion plotted against original particle dry mass. The time taken for volatile combustion was measured as the difference between the time (or frame) at which the particle was ignited and the time at which the flame ends. From Figure 7-3, it can be seen that the raw fuels showed longer duration for flaming combustion when compared to torrefied fuels. This is because the torrefied fuels have lost volatile matter during torrefaction as the process removes reaction water, lightweight hydrocarbon and gases from fuels; most of which are from hemicellulose and lignin components. Also noticeable is that all the torrefied fuels appear to have similar durations for volatile combustion. The flame duration for *Gmelina*, miscanthus, *Terminalia*, *Lophira* and *Nauclea* ranged from 2.02-3.74s, 2.32-3.79s, 2.38-3.53s, 3.22-4.21s, and 3.37-5.26s respectively (error $\leq \pm$ 0.008s). Whilst torrefied fuels are G270-60, M270-60, T270-60, N270-60 and L270-60 resulted in flame combustion durations of 1.48-3.31s, 1.57-3.31s, 1.62-3.38s, 2.21-2.80s and 2.25-3.12s respectively (error $\leq \pm$ 0.008s). The difference in the duration of flame combustion could also possibly be due to the presence of catalytic metals in the fuels, the variations in the density of the woods, and slow release of volatile materials (reactivity and pore development upon torrefaction) during combustion [75, 76, 83, 133, 202].

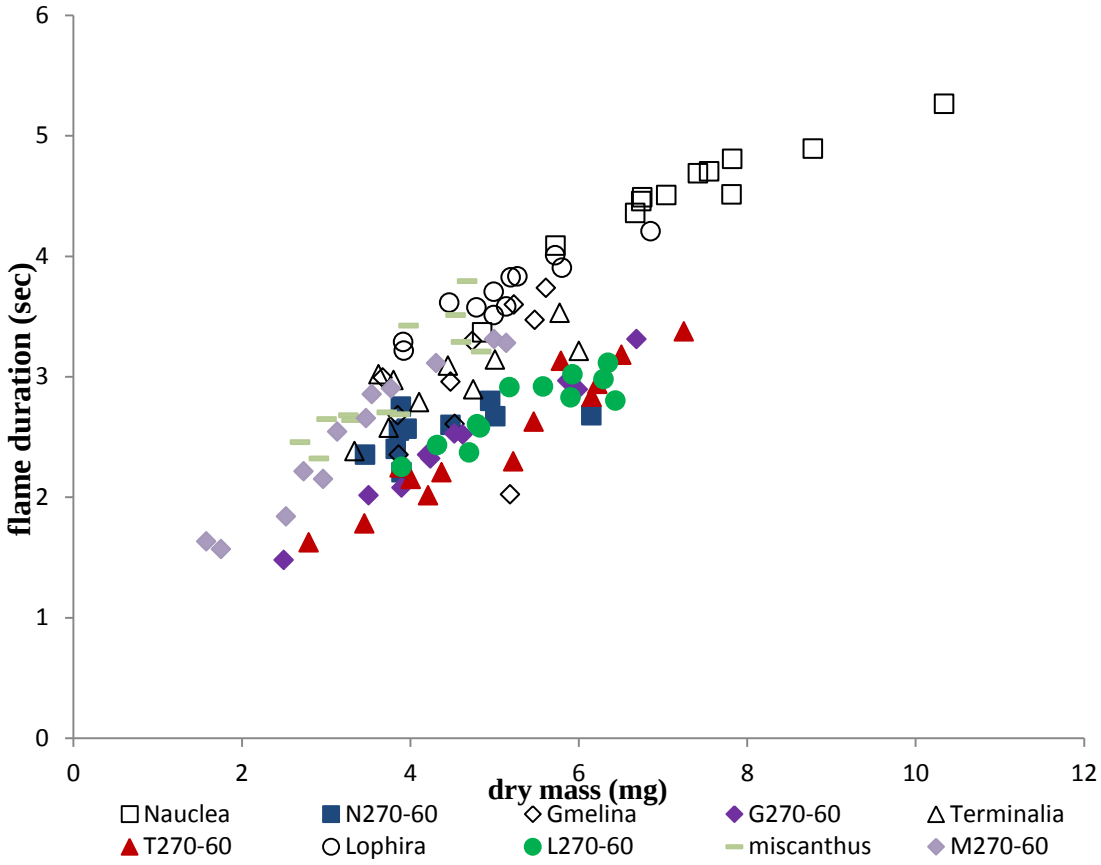

Figure 7-3: Plot of flame combustion duration against particle mass (dry) for raw and torrefied fuels.

7.3.1.3 Char Combustion

At the end of devolatilisation, when the volatile flame quenches, and oxygen is able to reach the residual char particle, then heterogeneous char combustion begins for the entire particle. This process continues until the char starts to shrink as shown in Figure 7-1 (d) which happens more rapidly towards the end of the combustion reaction, and finally reduces to a small mass of ash attached to the supporting needle as observed in Figure 7-1 (e) and (f). In some cases, video analysis revealed a "shrinking sphere" model for char combustion (Zone II or III) where diffusion processes influence the combustion rate, and diffusion limitations became more crucial towards the end of char combustion. The duration of char combustion was assessed as the time it takes for the char to completely burn out, and this was estimated from the end of flame combustion (even though overlapping of these two processes could be observed) until nothing but ash remaining on the supporting needle (end of particle shrinkage). It is important to note that this approach may over-estimate the char burn-out duration. Figure 7-4 shows the plot of duration of char burnout versus original particle dry mass for the raw and

torrefied fuels. From this figure, the char combustion step for raw *Lophira* and *Nauclea* particles showed different characteristics with longer char burnout stages, 9.74-19.15s and 21.64-39.52s respectively while the duration for char burnout of *Terminalia* and *Gmelina* ranged from 7.7-11.89s and 7.83-11.41s respectively (error ≤ ± 0.008s) and were comparable. As expected, miscanthus which contains the lowest amount of fixed carbon (~14%) recorded the least char burnout duration i.e. 2.47-4.75s. It can also be seen that torrefied samples take longer to complete char burnout than the raw samples. The duration for char burn out for M270-60, T270-60, G270-60, L270-60 and N270-60 is 3.31-12.26s, 17.74-45.02s, 10.66-23.88s, 39.94-47.27s and 34.43-54.60s respectively. The longer duration of the char combustion stage could result from the high char content (fixed carbon) of thermally pre-treated fuels caused by the increase in C-C bonds during decomposition of lignocellulose component of the biomass [37]. Moreover, diffusion rates, char porosity, the amount of catalytic metals present in the char, density of the wood, and elemental carbon content of the resultant char can also make up for the differences in char combustion rates [133].

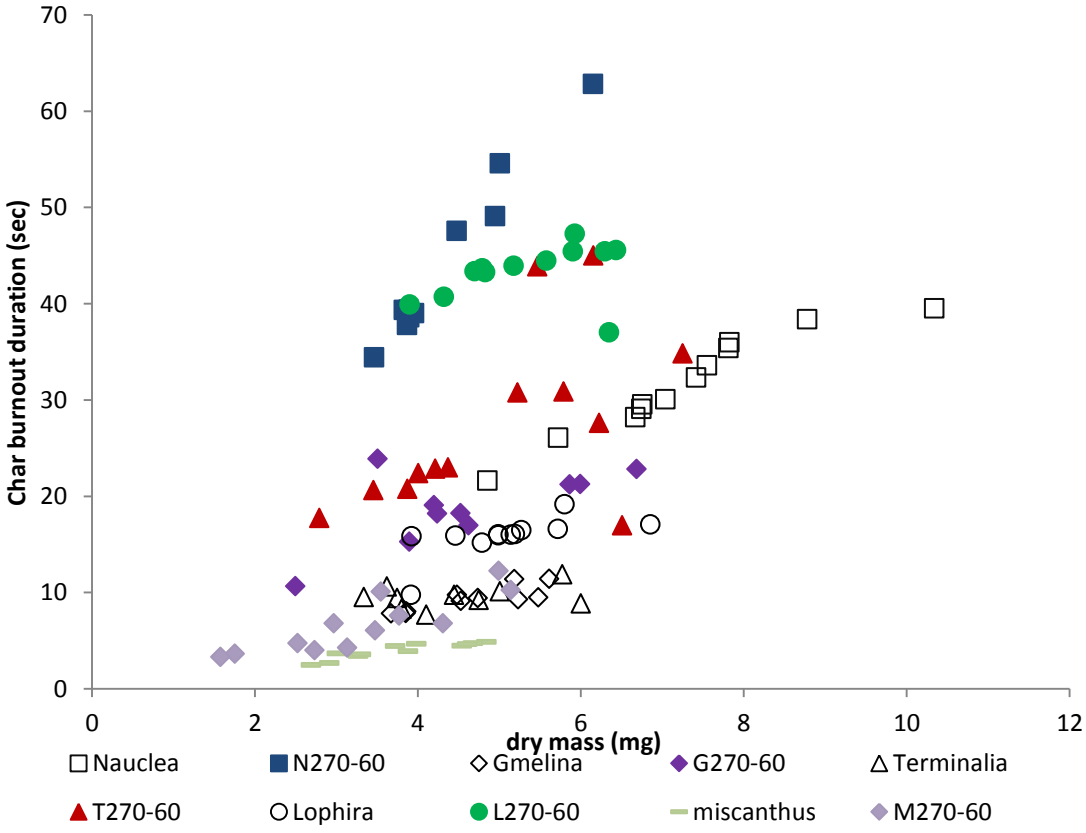

Figure 7-4: Plot of the char burnout duration against original dry particle mass for raw and torrefied fuels.

7.3.2 Thermogravimetric Analysis (TGA), and Differential Thermogravimetric Analysis (DTA) for char combustion.

The residue left at the end of the pyrolysis tests described in Section 3.12.1 is the char and ash content of the sample. This residue was cooled, and then underwent temperature programmed combustion.

The plots of the first derivative of mass loss curve with temperature (DTG) for the combustion of the raw and torrefied char samples are shown in Figures 7-5 to 7-11. The DTG combustion curves in most cases show a single decomposition stage of combustion characteristic of the fuels except for wheat straw and PKE which show a shoulder on the combustion peak, and a double peak in the case of *Terminalia*. The two stages char combustion peak found in *Terminalia* and the overlapping peak found in PKE could possibly be due to the presence of two different types of chars which could have resulted from the nature of different parts of the original fuels as reported in literature [9, 172, 218]. Also listed in Table 7-1 are char ignition temperatures (T_i) and the maximum peak temperature for combustion (T_{p2}), as obtained from the char burning profiles of the fuels studied. The ignition temperatures for miscanthus and PKE (raw and torrefied chars) are similar, with their combustion starting at higher temperatures compared to the other chars, while the start of char combustion of wheat straw (raw and torrefied) is at the lowest temperature as shown in Table 7-1. In contrast to the peak temperatures for pyrolysis; which appear almost unaffected by the longer reaction times in torrefaction, the peak temperatures for char combustion seems to be shifted to higher temperatures when the reaction time in torrefaction is increased from 30 to 60 min, with the exception of *Gmelina* and PKE, which show no change in peak temperature upon torrefaction. The order of reactivity using the maximum peak temperature of char combustion is as follows; wheat straw > *Gmelina* G270-30 > G270-60 > W270-30 > *Terminalia* > W270-60 > T270-30 > *Lopira* > *Nauclea* T270-60 > L270-30 > L270-60 > N270-30 > miscanthus > M270-60 > M270-30 > N270-60 PKE > P270-30 > P270-60 > P290-30.

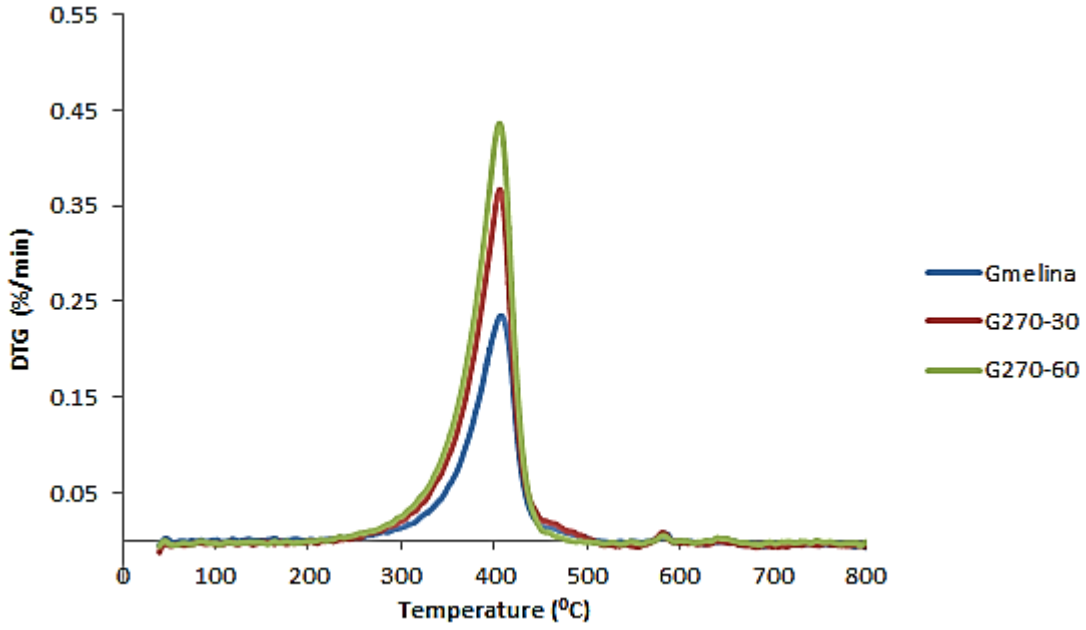

Figure 7-5: DTG char combustion profile of raw and torrefied *Gmelina*..

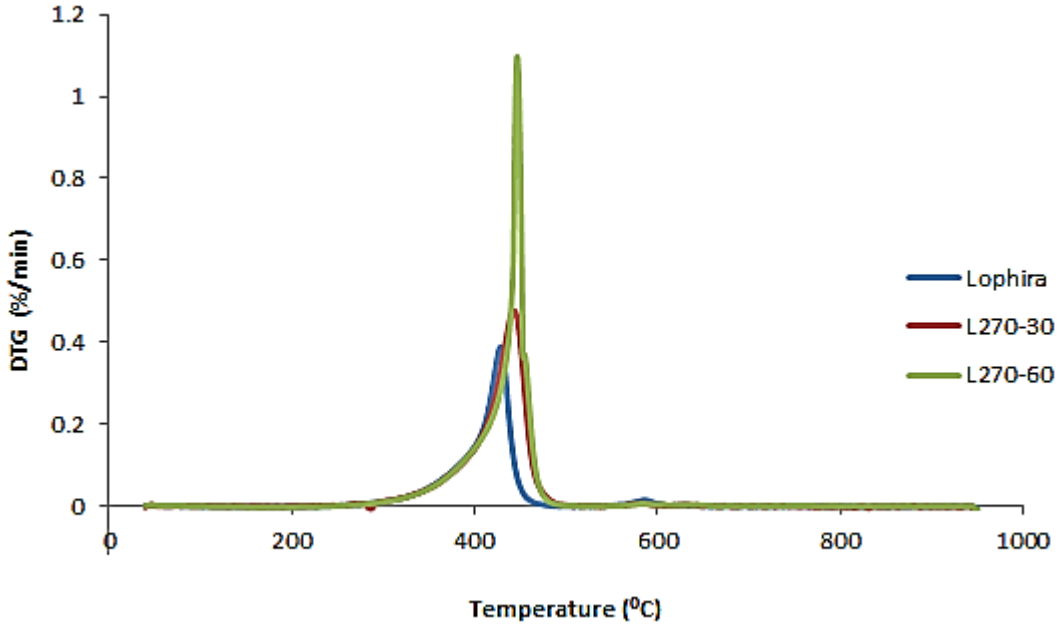

Figure 7-6: DTG char combustion profile of raw and torrefied *Lophira.*

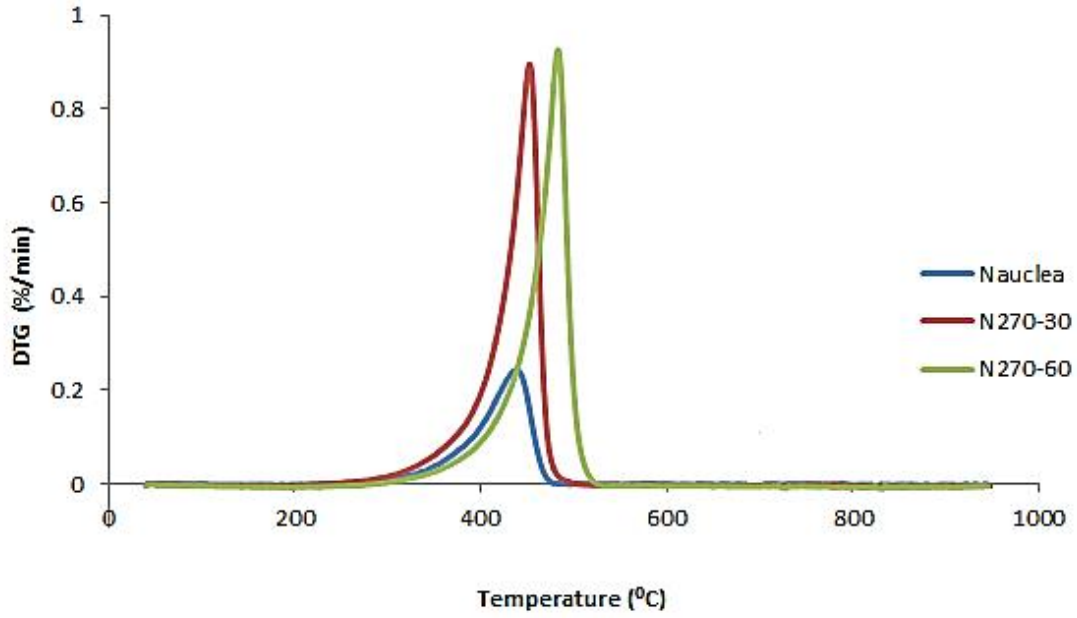

Figure 7-7: DTG char combustion profile of raw and torrefied *Nauclea*.

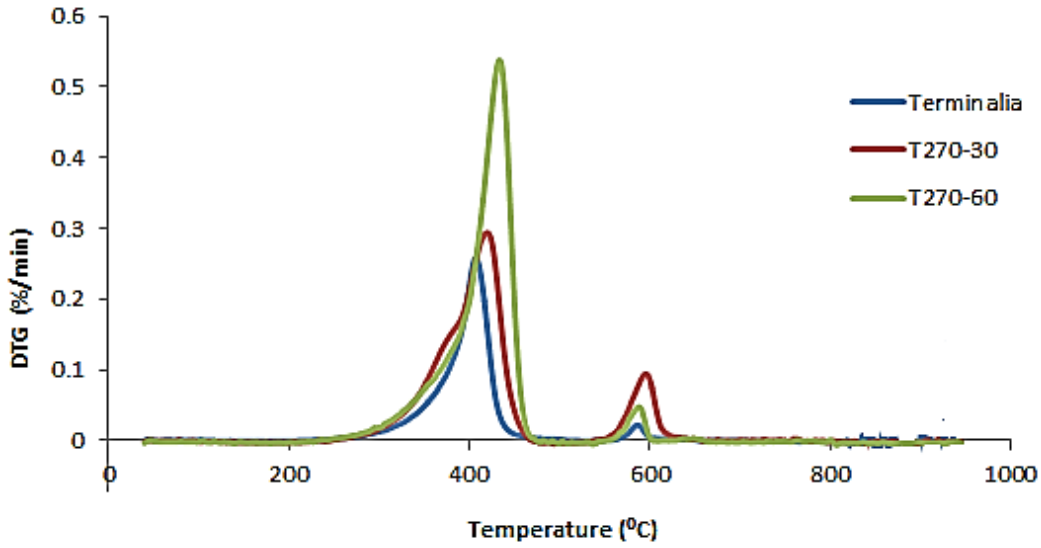

Figure 7-8: DTG char combustion profile of raw and torrefied *Terminalia.*

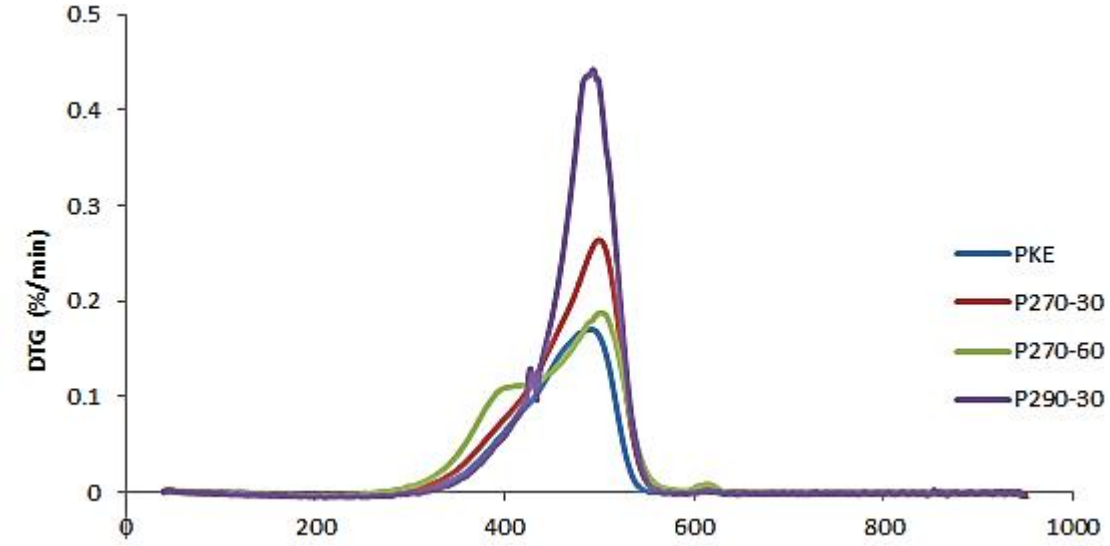

Figure 7-9: DTG char combustion profile of raw and torrefied PKE.

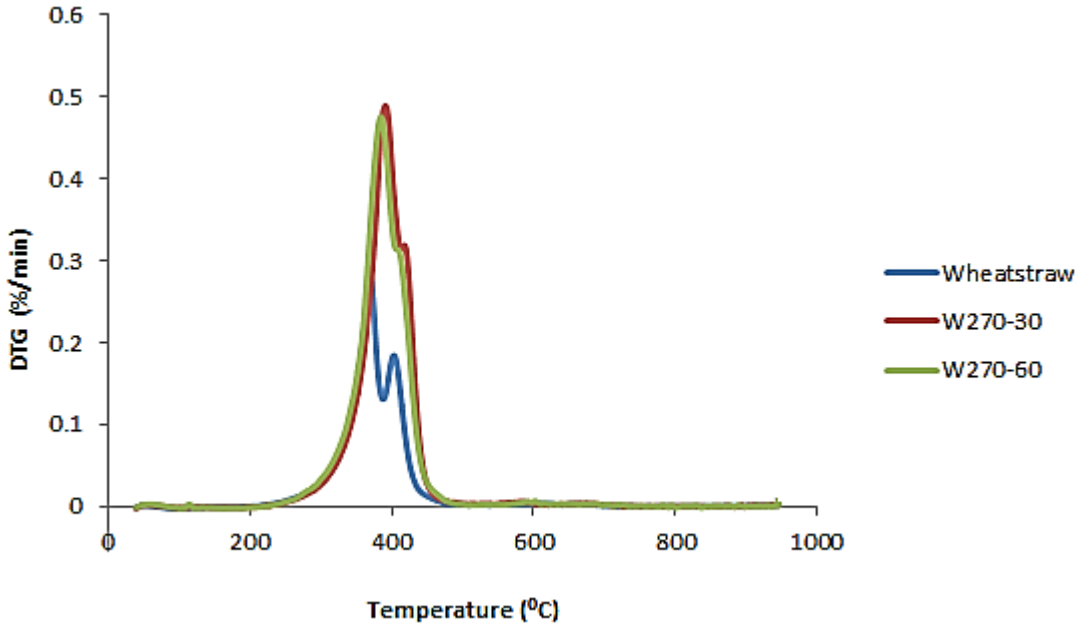

Figure 7-10: DTG char combustion profile of raw and torrefied wheat straw.

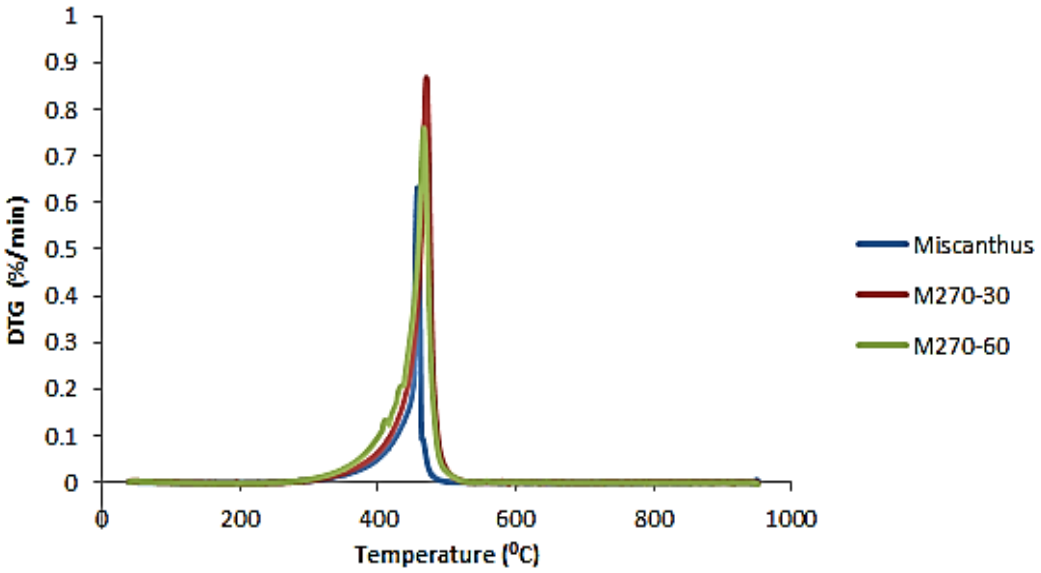

Figure 7-11: DTG char combustion profile of raw and torrefied miscanthus.

Table 7-1: Characteristic temperatures of char combustion for raw and torrefied samples.

Sample	Combustion ignition Temp (^{o}C) T_i	Combustion Max peak (^{o}C) T_{p2}
Gmelina	341	398
G270-30	345	401
G270-60	348	401
Terminalia	345	403
T270-30	352	411
T270-60	362	430
Lopira	391	425
L270-30	391	431
L270-60	393	446
Nauclea	360	428
N270-30	390	451
N270-60	409	485
PKE	390	485
P270-30	390	486
P270-60	390	486
P290-30	416	486
wheat straw	314	397
W270-30	330	402
W270-60	334	406
miscanthus	391	457
M270-30	420	469
M270-60	424	465

7.3.3 Char Combustion Kinetics

Apparent first order kinetic parameters for char combustion of the samples studied are derived from the data from the TGA using equation (3-15) in Section 3.4.9.2. The pre-exponential factors, A (s^{-1}), activation energies, Ea (kJ mol^{-1}) and correlation co-efficient, R^2 obtained are presented in Table 7-2. The kinetic parameters for char combustion of the fuels were derived from the data of the TGA using equation (3-15) in Section 3.4.9.2. The pre-exponential factors, A (s^{-1}), activation energies, Ea (kJ mol^{-1}) and correlation co-efficient, R^2 obtained are presented in Table 7-2. It has been

observed that torrefaction of biomass results in an increase in activation energy, Ea, which translates into a slower apparent reactivity in combustion [133]. This effect can also be observed in Table 7-2, as analysis showed that increasing the torrefaction temperature and/or residence time resulted in higher pre-exponential factors and activation energies required for the combustion reaction. According to Jones *et al.*[133], the possible reason for the high activation energies and lower reactivity of chars from torrefied biomass compared to chars from raw biomass is that the lower volatile content of the former, together with the different composition of volatiles (larger fraction of higher molecular weight material), results in a char with less developed porosity, and hence lower reactivity. Table 7-2 shows that the char of wheat straw had the lowest activation energy while the char of P270-60 had the highest activation energy. The activation energies listed in Table 7-2 for char of raw and torrefied woody biomass (~81 – 115 $kJmol^{-1}$) is similar to those reported by Jones *et al.*[133], for char of raw and torrefied willow (~82 – 88 $kJmol^{-1}$) with particle sizes less than 10mm and 20mm and conditions of 290^{o}C at 10 minutes and 60 minutes for both particle sizes.

From the rate constant calculated at 400°C, the values of k ranged from 0.00012 – 0.345s^{-1} and it can be seen that reactivity shows a slightly different order at this temperature, i.e. it follows the the order- wheat straw > *Gmelina* > G270-30 > G270-60 > W270-30 > W270-60 > *Terminalia* > T270-30 > *Lophira* > *Nauclea* > T270-60 > L270-30 > N270-30 > L270-60 > N270-60 > PKE > miscanthus > M270-30 > M270-60 > P270-30> P270-60 > P290-30.

A similar approach was used by Jones *et al.*[133], when comparing the reactivity of the chars of raw and torrefied willow with particle sizes less than 10mm and 20mm and conditions of 290^{o}C at 10minutes and 60minutes for both particle sizes. The rate constant was set at the same temperature 400^{o}C and consequently obtained values for k in the range of 0.000324 to 0.000825 s^{-1}. Ignoring wheat straw, the values are similar to those listed in Table 7-2 that ranged from 0.00012 – 0.0027 s^{-1}. The wheat straw chars are particularly reactive, probably due to high potassium, a catalyst in the reaction [46, 72, 74, 75, 120]. It is important to mention that the rate constant calculated at 400°C for char of raw *Nauclea* (0.000872 s^{-1}) & N270-30 (0.000613 s^{-1}) are similar to those obtained for char of raw willow (0.000874 s^{-1}) with particle sizes less than 10mm and

char of torrefied willow (0.000608 s^{-1}) with particle sizes less than 20mm in Jones *et al.*[133].

Table 7-2: Kinetics parameters of char combustion studies for raw and torrefied samples.

Sample	Ea ($kJmol^{-1}$)	ln A (s^{-1})	K_{400} (s^{-1})	R^2
wheat straw	70.51	11.54	0.345	0.9904
W270-30	113.12	13.38	0.0011	0.9793
W270-60	118.29	14.33	0.0011	0.9456
Gmelina	80.65	8.51	0.0027	0.9947
G270-30	85.72	8.81	0.0015	0.9956
G270-60	87.57	8.87	0.0011	0.9751
Terminalia	86.23	8.45	0.0009	0.9982
T270-30	90.85	9.23	0.0009	0.9991
T270-60	92.14	9.38	0.0008	0.9961
Lopira	93.16	9.63	0.0009	0.9801
L270-30	100.36	10.54	0.0006	0.9985
L270-60	115.36	13.2	0.0006	0.9927
Nauclea	89.63	8.97	0.0009	0.9953
N270-30	98.32	10.18	0.0006	0.9959
N270-60	110.75	12.36	0.0006	0.9953
PKE	132.89	15.93	0.0004	0.9985
P270-30	150.32	17.93	0.0001	0.9797
P270-60	161.05	19.84	0.0001	0.9948
P290-30	158.02	19.22	0.0001	0.9848
miscanthus	109.63	11.47	0.0003	0.9761
M270-30	125.42	13.9	0.0002	0.9952
M270-60	138.89	16.27	0.0002	0.9937

K_{400} reaction rate constant at 400^0C for comparison between fuels.

A relationship can be established between the maximum peak temperature, reaction rate for char combustion (Table 7-1:2) and the duration of char burnout from the single particle combustion experiments (Figure 7-4). For example, N270-60 which was the least reactive woody biomass in this studies with highest value of T_{p2} (485°C) and the lowest value of k (0.000592 s^{-1}) from TGA also had the longest char burnout time

(54.60s). The apparent slow reactivity of torrefied biomass char is evident in the single particle experiment as torrefied char particles burn more slowly, thus resulting into longer char burnout time.

7.4 Conclusions

Combustion behaviours of raw and torrefied fuels were studied in a methane air flame using a high speed camera. The images were recorded at a frame speed of 125fps. Video analysis revealed that torrefaction altered the combustion properties of biomass. The effect of torrefaction on the fuel properties is clearly seen, as torrefied fuels which contain lower moisture content than their raw counterparts have improved ignition characteristics, shorter duration of volatile combustion, and a longer duration of char burn out. The longer duration of the char burn out could result from the increasing fixed carbon content of thermally pre-treated fuels (The C-C bonds become concentrated during decomposition of lignocellulose component of the biomass in the torrefaction process). Also, diffusion rates, char porosity, the amount of catalytic metals present in the char, density of the wood, and elemental carbon content of the resultant char can also make up for the differences in char combustion rates [133].

TGA analysis of chars showed that torrefied chars are less reactive during combustion than their raw counterparts and the more severe the torrefaction conditions, the less reactive the fuels become. Also, the peak temperatures for char combustion were observed to be shifted to higher temperatures (in most cases) when the reaction time of the torrefaction process is increased from 30 to 60 min, with the exception of *Gmelina* and PKE, that show no change in peak temperature upon torrefaction. The order of reactivity using the maximum peak temperature of char combustion is as follows; wheat straw > *Gmelina* G270-30 > G270-60 > W270-30 > *Terminalia* > W270-60 > T270-30 > *Lopira* > *Nauclea* T270-60 > L270-30 > L270-60 > N270-30 > miscanthus > M270-60 > M270-30 > N270-60 PKE > P270-30 > P270-60 > P290-30.

Based on the temperature of maximum char combustion rate (T_{p2}), *Gmelina* and *Nauclea* are the most reactive fuels, while torrefied PKE fuels are the least reactive. The reactivity of the torrefied fuels was also assessed from the reaction rate constant at 400°C and followed the order *Nauclea* > *Gmelina* > G270-30 > G270-60 > N270-30 >

Terminalia > *Lophira* > N270-60 > L270-30 > L270-60 > T270-30 > T270-60> PKE > P270-30> P270-60 > P290-30.

Apparent first order kinetic parameters for char combustion of the samples studied showed that observed that torrefaction of biomass results in an increase in activation energy, Ea and therefore a slower apparent reactivity in combustion. Char from wheat straw had the lowest activation energy while the char of P270-60 had the highest activation energy. The activation energies for char of raw and torrefied woody biomass (~81 – 115 $kJmol^{-1}$) in this study is similar to those reported by Jones *et al.*[133], for char of raw and torrefied willow (~82 – 88 $kJmol^{-1}$) with particle sizes less than 10mm and 20mm and conditions of 290^{o}C at 10minutes and 60minutes for both particle sizes.

From the rate constant calculated at 400°C, the values of k ranged from 0.00012 s^{-1} – 0.345 s^{-1}. The wheat straw chars are much more reactive than the others (about 100-1000x faster reaction than the other biomass); presumably due to potassium catalysed char combustion. The rate of char combustion of *Nauclea* (0.000872 s^{-1}) & N270-30 (0.000613 s^{-1}) are similar to those obtained for willow (0.000874 s^{-1}) with particle sizes less than 10mm and torrefied willow (0.000608 s^{-1}) with particle sizes less than 20mm in Jones *et al.*[133]. A relationship was also established between the maximum peak temperature for combustion and the duration of char burnout from the single particle combustion experiments. For example, N270-60 (T_{p2} 485°C) which was the least reactive from TGA also had the longest char burnout time (54.60 s).

CHAPTER 8. CONCLUSIONS AND RECOMMEDATIONS FOR FURTHER WORK

8.1 Summary of Conclusions

Each chapter has included a number of conclusions and only the main conclusions are presented here along with recommendations for further work. This research includes a number of objectives that were aimed at investigating torrefaction and combustion properties of some Nigerian biomass. Some potential energy crops and woods from Nigeria, namely *Terminalia superba*, *Gmelina arborea*, *Lophira alata*, *Nauclea diderrichii*, and also one abundant agricultural residue, palm kernel expellers (PKE), were characterized for their combustion properties. Standard characterisation procedures such as ultimate proximate analyses, ash fusion test and metals analysis were used for this purpose and the results were compared with some European biomass. In addition, their thermal conversion was assessed by thermogravimetric analysis and pyrolysis−gas chromatography−mass spectrometry (Py- GC−MS). Combustion studies were conducted by suspending single biomass particles in a methane flame to obtain information on reactivities and combustion characteristics of the untreated fuels. Results show that the Nigerian fuels have low N, S, Cl and high carbon contents. The high carbon content in the Nigerian fuels resulted in the relatively higher calorific value than the European biomass. Also, the ash fractions in the Nigerian woods were low in K, Si, and Ca, resulting in low calculated alkali indices, hence these fuels are not predicted to cause severe fouling problems. These two together make the woods very attractive for energy production. Furthermore, the analysis of the evolved products during devolatilisation of these raw biomass from Py−GC−MS suggests that the content of extractives is high in *Gmelina*.

The fuels were torrefied at 270 and 290^{o}C for either 30 or 60 mins, and assessed for pyrolysis and combustion characteristics in comparison to their untreated (raw) counterparts. Optimisation of the torrefaction process for the investigated fuels was achieved and solid characterisation of torrefied fuels was carried out in detail. The fuels were analysed for proximate, ultimate and higher heating value, and mass and energy yields were calculated. For these fuels mass yields were in the range 70-93% and energy yields in the range 79-93%. Energy densities of the woods improved from 19.2-

21.2 MJ/kg for the raw fuels to 21.2-25.6 MJ/kg for the torrefied fuels. The torrefaction process also results in loss of nitrogen from the fuel, mainly in the tar (condensibles).

Generally, while the wt% N increases in the torrefied fuel compared to the original material, the N content on an energy basis, generally decrease. This is very significant since amount of NOx that is formed in combustion is related, in part, to fuel nitrogen (fuel dependent N/GJ).

A modified Hardgove Index test was used to study the milling behaviour of the torrefied fuels, which demonstrated improved grindability of the woods upon torrefaction, especially for *Nauclea*. This is important for pulverized fuel combustion applications where energy in milling and mill throughput are expected to decrease. However, torrefaction had very little effect on the grindability of PKE.

The apparent first order kinetics for pyrolysis were determined by thermogravimetric analysis (TGA). After torrefaction, the fuels become less reactive as evidenced by both the slightly higher temperature of maximum pyrolysis rate and by the lower reactivity rate (as calculated at 400^{o}C). The A and Ea values for the fuels ranged from 10 – 24.9 s^{-1} and 78.8 -156 kJ/mol respectively. Overall, *Nauclea* and *Gmelina* were the most reactive fuels, whilst PKE was the least reactive. The Py-GC-MS analytical technique indicated that phenolic compounds i.e. methoxy-phenol and methyl-phenol are more evident in the group of compounds identified during pyrolysis of torrefied fuels.

The combustion behaviour of the selected raw and some of the torrefied fuels was examined in a methane air flame using a high-speed camera. The observations showed that torrefaction changes the combustion properties of biomass resulting in shorter ignition delay, shorter duration of volatile combustion and longer duration of char burn out. TGA combustion analysis of chars showed that torrefied chars are less reactive than their raw counterparts and the more severe the torrefaction conditions, the less reactive the fuels become. Apparent first order kinetic parameters for char combustion revealed that torrefaction of biomass results in an increase in activation energy, Ea, resulting in a slower apparent reactivity in combustion. The fuels are becoming more coal-like in their combustion behaviour. The activation energies for char combustion of raw and torrefied biomass fuels in this studies range from ~71 – 161 $kJmol^{-1}$. The rate of char combustion of these fuels was also obtained. *Nauclea* (0.000872 s^{-1}) & N270-30 (0.000613 s^{-1}) in

particular have rates that are similar to those obtained for willow (0.000874) and torrefied willow (0.000608 s^{-1}) in the studies conducted by Jones *et al.*[133].

In summary, the Nigerian biomass and torrefied biomass show high potential for large scale electricity production. Their high calorific value, low nitrogen, low sulphur and high melting ash, together with their combustion properties make them an attractive resource. Future studies should examine the sustainability of supply chains for these fuels to ensure good carbon reduction. Torrefaction shows promise for improving many characteristics of the fuels for use in both large scale power stations and more widely for domestic purposes.

8.2 Future Work

8.2.1 Torrefaction and its Effect on Fuel Properties.

During torrefaction of biomass, hemicellulose degrades; leading to a loss of hydroxyl groups and making the biomass material hydrophobic in nature. The hydrophobicity test should be carried out to see how the torrefied biomass fuels resist moisture reabsorption. There is need to investigate the chemical structures of the torrefied biomass e.g. through the use of attenuated total reflectance Fourier transform infrared (ATR FT-IR) spectroscopy. This will help to understand how the hydroxyl groups decompose and result in a more hydrophobic solid.

There were some losses of liquids and vapours in the torrefaction testing and this reduced the number of analysis that could be carried out. Tars were only analysed for CHNS and liquid-GC-MS. For example, Karl Fischer titration, TOC, viscosity tests on the tar could have been carried out if the volume was enough. Therefore, it is important to have a good implementation and design that will ensure minimal loss during collection of liquids since the liquids are important for further analysis.

It had been planned that the gases were to be detected using the GC chromatography, but the gases could not be quantified using the output data that were obtained from the gas chromatography. The equilibration time (retention time) that was set for gas collection for a complete torrefaction run is shorter, and the peaks could not be resolved. Therefore would be a need to recalibrate the GC in order to obtain more meaningful data. Also for future work, the rig design should be revisited to allow a flow meter to be

placed between the traps and the GC. This will assist in quantifying the gases that are detected.

8.2.2 Pyrolysis studies on torrefied biomass.

Studies conducted during this research determined the properties of biomass and their behaviour during pyrolysis and combustion reactions. Parameters such as particle size and shape of biomass also influence both the convective and the conductive heat transfer rate from the reactor to the biomass and within the biomass, respectively. In order to overcome heat transfer limitations, the Biot number has to be small, where the heat conduction within the particle is faster than the heat going into the particle, and also, the pyrolysis number has to be large, where the heat convection rate is faster than the chemical reaction [90]. The Biot Number which fundamentally describes how fast heat flows through a material is a dimensionless ratio between the heat convection and conduction rates while pyrolysis number is the ratio of heat convection rate and reaction rate. If large particle size are used during torrefaction, the process will be controlled by conduction and may lead to a higher temperature in the interior of the biomass by decreasing the convective heat transfer rate [28]. It can also experience non- uniform heat distribution within the biomass due to the anisotropic and heterogeneous properties of the biomass [104]. Therefore, an investigation in to these parameters should be considered for future work.

8.2.3 Combustion studies on torrefied biomass

The work carried out in Chapter 7 deals with combustion studies of torrefied biomass fuels and can be further developed. For example, studies on porosity development during char formation can be examined to see how this impacts on char combustion rates. Char formation at high heating rate occurs with simultaneous development of the porous structure during the rapid release of volatiles from the biomass particles. The pore evolution and development could be studied by BET and SEM characterisation in further work.

Finally self-heating is another emerging area of research in biomass utilisation and this could also be investigated in further work. There have been several fire incidents from spontaneous combustion in the storage of wood pellets. Self-heating happens due to chemical reactions (i.e. oxidation) or when microorganism activity generates heat in the

stockpile at a sufficient rate to raise the temperature of surrounding material. The increase in temperature leads to ignition and loss of valuable feedstock if left unchecked. There is speculation that torrefied fuel would have a lower propensity for self-heating because of the hydrophobicity.

8.3 Reference

1. Renewable Energy Policy Network, *Renewable 2011 Global Status Report.* 2011, Renewable Energy Policy Network for the 21st Century: Paris, France.

2. World Energy Council, W.E.C., *Energy Policy Scenario Study to 2050 – Draft report for Africa"*, in *All Africa Data,*. 2010, World Energy Council, WEC

3. EIA, *International Energy Outlook 2013*. 2013, ENERGY INFORMATION ADMINISTRATION, [online]. [Accessed 12/01/14]. Available from: http://www.eia.gov/forecasts/ieo/pdf/0484(2013).pdf.

4. United-Nations. *Status of Ratification of the Kyoto Protocol*. United Nations Framework Convention on Climate Change 2011 [cited 2011 24/10/2011]; Available from: http://unfccc.int/kyoto_protocol/status_of_ratification/items/2613.php.

5. European Commission, *Renewable energy progress report.* 2013, The Commission to the European Parliament, The Council, The European Economic and Social Committee and The Committee Of The Regions

6. Parliament of the United Kingdom, *Climate Change Act 2008*. 2008: United Kingdom.

7. European Comission, *DIRECTIVE 2009/28/EC OF THE EUROPEAN PARLIAMENT AND OF THE COUNCIL of 23 April 2009 on the promotion of the use of energy from renewable sources and amending and subsequently repealing Directives 2001/77/EC and 2003/30/EC*. 2009.

8. Organisation for Economic Co-operation and Development, O.E.C.D., *Linking Renewable Energy to Rural Development*. OECD Green Growth Studies. 2012: OECD Publishing.

9. Gudka, B.A., *Combustion Characteristics of some Imported Feedstocks and Short Rotation Coppice (SRC) Willow for UK Power Stations*. 2012, University of Leeds: Unpublished PhD thesis.

10. International Energy Agency, I.E.A., *Energy Balances for Non-OECD Countries 2006 Edition.* 2006, International Energy Agency, I.E.A.: Paris.

11. Onoduku, U.S., *Chemistry of Maiganga Coal Deposit, Upper Benue Trough, North Eastern Nigeria.* Journal of Geosciences and Geomatics, 2014. **2**(3): p. 80-84.

12. Sambo, A.S., *The challenges of sustainable energy development in nigeria*, in *Nigerian Society of Engineers Forum*. 2009, Energy Commission of Nigeria: Shehu Yar'Adua Centre, Abuja. p. 1-39.

13. US Energy Information and Administration, E.I.A. *Nigeria Energy Profile*. 2011 [cited 2011 05/05/2011]; Available from: http://www.eia.gov/countries/cab.cfm?fips=NI.

14. US Energy Information Administration, E.I.A., *World Energy Projection System Plus Model Documentation 2010: Coal Model*. 2011, U.S. Department of Energy: Washington, DC 20585.

15. Sambo, A.S., *Strategic Developments In Renewable Energy In Nigeria*. 2009, Energy Commision of Nigeria, Goverment of Nigeria. p. 15-19.

16. Ohunakin, O.S., *Energy Utilization and Renewable Energy Sources in Nigeria.* Journal of Engineering and Applied Sciences, 2010. **5**(2): p. 171-177.

17. Oyedepo, S.O., *On energy for sustainable development in Nigeria.* Renewable and Sustainable Energy Reviews, 2012. **16**(5): p. 2583-2598.

18. Onyekwelu, J.C., R. Mosandl, and B. Stimm, *Productivity, site evaluation and state of nutrition of Gmelina arborea plantations in Oluwa and Omo forest reserves, Nigeria.* Forest Ecology and Management, 2006. **229**(1–3): p. 214-227.

19. Fall, L., *WEC Regional Forum on Energy Efficiency, "Recommendations & Follow-up"*. 2007: Abuja, Nigeria.

20. Food and Agriculture Organization of the United Nations, F.A.O., *Sustainable Forest Management Programme in African ACP Countries: Experience of Implementing National Forest Programmes in Nigeria.* . 2003, Forest Resources and Forestry Development in Nigeria.

21. Olaoye, J.O., *An Analysis of the Environmental Impacts of Energy Crops in Nigeria towards Environmental Sustainability*, in *3rd International Soil Tillage Research Organisation (ISTRO), Nigeria Symposium*. 2011: Ilorin, Nigeria. p. 204-212.

22. Abila, N., *Biofuels development and adoption in Nigeria: Synthesis of drivers, incentives and enablers.* Energy Policy, 2012. **43**(0): p. 387-395.

23. Brown, R.C., *Thermochemical Processing of Biomass*. 2011, West Sussex: Wiley.

24. Klass, D.L., *Biomass for Renewable Energy, Fuels, and Chemicals.* 1998, San Diego: Academic Press

25. Williams, A., J.M. Jones, L. Ma, and M. Pourkashanian, *Pollutants from the combustion of solid biomass fuels.* Progress in Energy and Combustion Science, 2012. **38**(2): p. 113-137.

26. Brown, R.C., *Biorenewable Resources* 2003, Lowa: Blackwell Publishing Company.

27. The Japan institute of energy, *The Asian biomass handbook: A guide for biomass productionand utilization.* 2008, Ministry of Agriculture, Forestry and Fisheries, Japan.: Japan.

28. Basu, P., S. Rao, and A. Dhungana, *An investigation into the effect of biomass particle size on its torrefaction.* The Canadian Journal of Chemical Engineering, 2013. **91**(3): p. 466-474.

29. Hall, D.O., *Biomass energy in industrialised countries—a view of the future.* Forest Ecology and Management, 1997. **91**(1): p. 17-45.

30. Hoogwijk, M., A. Faaij, B. Eickhout, B. de Vries, and W. Turkenburg, *Potential of biomass energy out to 2100, for four IPCC SRES land-use scenarios.* Biomass and Bioenergy, 2005. **29**(4): p. 225-257.

31. Thrän, D., T. Seidenberger, J. Zeddies, and R. Offermann, *Global biomass potentials — Resources, drivers and scenario results.* Energy for Sustainable Development, 2010. **14**(3): p. 200-205.

32. Sami, M., K. Annamalai, and M. Wooldridge, *Co-firing of coal and biomass fuel blends.* Progress in Energy and Combustion Science, 2001. **27**(2): p. 171-214.

33. Williams, A., M. Pourkashanian, and J.M. Jones, *Combustion of pulverised coal and biomass.* Progress in Energy and Combustion Science, 2001. **27**(6): p. 587-610.

34. Babbitt, C.W. and A.S. Lindner, *A life cycle inventory of coal used for electricity production in Florida.* Journal of Cleaner Production, 2005. **13**(9): p. 903-912.

35. Bergman, P.C.A., A.R. Boersma, R.W.R. Zwart, and J.H.A. Kiel, *Torrefaction for biomass co-firing in existing coal-fired power stations "BIOCOAL"*. 2005, ECN.

36. Bergman, P.C.A., J.H.A. Kiel, and H.J. Veringa, *Combined torrefaction and pelletisation: The TOP process*. 2005, Energy research Centre of the Netherlands (ECN).

37. Bridgeman, T.G., J.M. Jones, I. Shield, and P.T. Williams, *Torrefaction of reed canary grass, wheat straw and willow to enhance solid fuel qualities and combustion properties.* Fuel, 2008. **87**(6): p. 844-856.

38. Chen, W.-H., H.-C. Hsu, K.-M. Lu, W.-J. Lee, and T.-C. Lin, *Thermal pretreatment of wood (Lauan) block by torrefaction and its influence on the properties of the biomass.* Energy, 2011. **36**(5): p. 3012-3021.

39. Lipinsky, E.S., J.R. Arcate, and T.B. Reed, *Enhanced wood fuels via torrefaction*. 2002, Innovative Thinking, Inc. p. 408-410.

40. Pentananunt, R., A.N.M.M. Rahman, and S.C. Bhattacharya, *Upgrading of biomass by means of torrefaction.* Energy, 1990. **15**(12): p. 1175-1179.

41. Van der Stelt, M.J.C., H. Gerhauser, J.H.A. Kiel, and K.J. Ptasinski, *Biomass upgrading by torrefaction for the production of biofuels: A review.* Biomass and Bioenergy, 2011. **35**(9): p. 3748-3762.

42. Vattenfall, *Annual Report*. 2011, Vattenfall AB Stockholm, Sweden.

43. BBI International, *Vega Biofuels lands large bio-coal order from European company*, in *Biomass Magazine*. 2014, BBI International: Grand Forks, ND.

44. Svanberg, M., *A framework for supply chain configuration of a biomass-to-energy pre-treatment process*, in *Department of Technology Management and Economics, Division of Logistics & Transportation*. 2013, Chalmers University of Technology, Sweden: Unpublished PhD Thesis.

45. Lasode, O.A., A.O. Balogun, and A.G. McDonald, *Torrefaction of some Nigerian lignocellulosic resources and decomposition kinetics.* Journal of Analytical and Applied Pyrolysis, (0).

46. Saddawi, A., J.M. Jones, A. Williams, and C. Le Coeur, *Commodity Fuels from Biomass through Pretreatment and Torrefaction: Effects of Mineral Content on Torrefied Fuel Characteristics and Quality.* Energy & Fuels, 2011.

47. Aina, O.M. *Wood Waste Utilization for Energy Generation*. in *Renewable Energy for Developing Countries-2006*. 2006. Nigeria.

48. Jenkins, B.M., L.L. Baxter, T.R. Miles Jr, and T.R. Miles, *Combustion properties of biomass.* Fuel Processing Technology, 1998. **54**(1–3): p. 17-46.

49. Yang, H., R. Yan, H. Chen, D.H. Lee, and C. Zheng, *Characteristics of hemicellulose, cellulose and lignin pyrolysis.* Fuel, 2007. **86**(12–13): p. 1781-1788.

50. David, K. and A.J. Ragauskas, *Switchgrass as an energy crop for biofuel production: A review of its ligno-cellulosic chemical properties.* Energy & Environmental Science, 2010. **3**(9): p. 1182-1190.

51. Morris, J.R., *CourseSmart International E-Book for Biology: How Life Works*. 2013: Palgrave Macmillan.

52. Haygreen, J.G., J.L. Bowyer, and K. Lilley, *Forest products and wood science : an introduction*. 1987, Ames, Iowa: Iowa state university press.

53. Brown, R.M., J.I.M. Saxena, and Kudlicka, *Cellulose biosynthesis in higher plants.* Elsevier trends in plant sciences, 1996. **1**(5): p. 149-156.

54. Scheller, H.V. and P. Ulvskov, *Hemicelluloses.* Annual Review of Plant Biology, 2010. **61**(1): p. 263-289.

55. Zanzi, R., K. Sjöström, and E. Björnbom, *Rapid pyrolysis of agricultural residues at high temperature.* Biomass and Bioenergy, 2002. **23**(5): p. 357-366.

56. Ramos, L.P., *The chemistry involved in the steam treatment of lignocellulosic materials.* Química Nova, 2003. **26**: p. 863-871.

57. Hon, D.N.S. and N. Shiraishi, *Wood and cellulosic chemistry*. 2001, New York: Marcel Dekker.

58. Freudenberg, K. and A.A. Neish, *The Constitution and Biosynthesis of Lignin*. 1968, New York: Springer-Verlag.

59. Lewin, M. and S.I. Goldstein, *Wood structure and composition*. 1991, New York: Marcel Dekker.

60. Adler, E., *Structural Elements of Lignin.* Industrial & Engineering Chemistry, 1957. **49**(9): p. 1377-1383.

61. Bridgeman, T.G., L.I. Darvell, J.M. Jones, P.T. Williams, R. Fahmi, A.V. Bridgwater, T. Barraclough, I. Shield, N. Yates, S.C. Thain, and I.S. Donnison, *Influence of particle size on the analytical and chemical properties of two energy crops.* Fuel, 2007. **86**(1–2): p. 60-72.

62. Shen, D., R. Xiao, S. Gu, and K. Luo, *The pyrolytic behavior of cellulose in lignocellulosic biomass: a review.* RSC Advances, 2011. **1**(9): p. 1641-1660.

63. Fisher, T., M. Hajaligol, B. Waymack, and D. Kellogg, *Pyrolysis behavior and kinetics of biomass derived materials.* Journal of Analytical and Applied Pyrolysis, 2002. **62**(2): p. 331-349.

64. Shafizadeh, F., *Industrial pyrolysis of cellulosic materials.* Appl Polym Symp, 1975(28): p. 153-174.

65. Stefanidis, S.D., K.G. Kalogiannis, E.F. Iliopoulou, C.M. Michailof, P.A. Pilavachi, and A.A. Lappas, *A study of lignocellulosic biomass pyrolysis via the pyrolysis of cellulose, hemicellulose and lignin.* Journal of Analytical and Applied Pyrolysis, 2014. **105**(0): p. 143-150.

66. Avila, C., C.H. Pang, T. Wu, and E. Lester, *Morphology and reactivity characteristics of char biomass particles.* Bioresource Technology, 2011. **102**(8): p. 5237-5243.

67. Shen, D.K., S. Gu, and A.V. Bridgwater, *Study on the pyrolytic behaviour of xylan-based hemicellulose using TG–FTIR and Py–GC–FTIR.* Journal of Analytical and Applied Pyrolysis, 2010. **87**(2): p. 199-206.

68. Gu, P., R.K. Hessley, and W.-P. Pan, *Thermal characterization analysis of milkweed flos.* Journal of Analytical and Applied Pyrolysis, 1992. **24**(2): p. 147-161.

69. Fahmi, R., A.V. Bridgwater, I. Donnison, N. Yates, and J.M. Jones, *The effect of lignin and inorganic species in biomass on pyrolysis oil yields, quality and stability.* Fuel, 2008. **87**(7): p. 1230-1240.

70. Patwardhan, P.R., R.C. Brown, and B.H. Shanks, *Product Distribution from the Fast Pyrolysis of Hemicellulose.* ChemSusChem, 2011. **4**(5): p. 636-643.

71. Yang, H., R. Yan, H. Chen, C. Zheng, D.H. Lee, and D.T. Liang, *In-Depth Investigation of Biomass Pyrolysis Based on Three Major Components: Hemicellulose, Cellulose and Lignin.* Energy & Fuels, 2005. **20**(1): p. 388-393.

72. Nowakowski, D.J. and J.M. Jones, *Uncatalysed and potassium-catalysed pyrolysis of the cell-wall constituents of biomass and their model compounds.* Journal of Analytical and Applied Pyrolysis, 2008. **83**(1): p. 12-25.

73. Fahmi, R., A.V. Bridgwater, L.I. Darvell, J.M. Jones, N. Yates, S. Thain, and I.S. Donnison, *The effect of alkali metals on combustion and pyrolysis of Lolium and Festuca grasses, switchgrass and willow.* Fuel, 2007. **86**(10–11): p. 1560-1569.

74. Jones, J.M., L.I. Darvell, T.G. Bridgeman, M. Pourkashanian, and A. Williams, *An investigation of the thermal and catalytic behaviour of potassium in biomass combustion.* Proceedings of the Combustion Institute, 2007. **31**(2): p. 1955-1963.

75. Nowakowski, D.J., J.M. Jones, R.M.D. Brydson, and A.B. Ross, *Potassium catalysis in the pyrolysis behaviour of short rotation willow coppice.* Fuel, 2007. **86**(15): p. 2389-2402.

76. Saddawi, A., J.M. Jones, and A. Williams, *Influence of alkali metals on the kinetics of the thermal decomposition of biomass.* Fuel Processing Technology, 2012. **104**(0): p. 189-197.

77. Wang, S., X. Guo, K. Wang, and Z. Luo, *Influence of the interaction of components on the pyrolysis behavior of biomass.* Journal of Analytical and Applied Pyrolysis, 2011. **91**(1): p. 183-189.

78. Hosoya, T., H. Kawamoto, and S. Saka, *Cellulose–hemicellulose and cellulose–lignin interactions in wood pyrolysis at gasification temperature.* Journal of Analytical and Applied Pyrolysis, 2007. **80**(1): p. 118-125.

79. Gil, M.V., D. Casal, C. Pevida, J.J. Pis, and F. Rubiera, *Thermal behaviour and kinetics of coal/biomass blends during co-combustion.* Bioresource Technology, 2010. **101**(14): p. 5601-5608.

80. Zhang, X., M. Xu, R. Sun, and L. Sun, *Study on Biomass Pyrolysis Kinetics.* Journal of Engineering for Gas Turbines and Power, 2006. **128**(3): p. 493-496.

81. Tumuluru, J.S., B. Richard, W. Christopher, and J. Heintzelman, *Changes in moisture, carbon, nitrogen, sulphur, volatiles, and calorific value of miscanthus during torrefaction*. 2001. Medium: ED.

82. White, J.E., W.J. Catallo, and B.L. Legendre, *Biomass pyrolysis kinetics: A comparative critical review with relevant agricultural residue case studies.* Journal of Analytical and Applied Pyrolysis, 2011. **91**(1): p. 1-33.

83. Saddawi, A., J.M. Jones, A. Williams, and M.A. Wójtowicz, *Kinetics of the Thermal Decomposition of Biomass.* Energy & Fuels, 2009. **24**(2): p. 1274-1282.

84. Varhegyi, G., E. Jakab, and M.J. Antal, *Is the Broido-Shafizadeh Model for Cellulose Pyrolysis True?* Energy & Fuels, 1994. **8**(6): p. 1345-1352.

85. Bradbury, A.G.W., Y. Sakai, and F. Shafizadeh, *A kinetic model for pyrolysis of cellulose.* Journal of Applied Polymer Science, 1979. **23**(11): p. 3271-3280.

86. Koufopanos, C.A., A. Lucchesi, and G. Maschio, *Kinetic modelling of the pyrolysis of biomass and biomass components.* The Canadian Journal of Chemical Engineering, 1989. **67**(1): p. 75-84.

87. Prins, M.J., K.J. Ptasinski, and F.J.J.G. Janssen, *Torrefaction of wood: Part 1. Weight loss kinetics.* Journal of Analytical and Applied Pyrolysis, 2006. **77**(1): p. 28-34.

88. Di Blasi, C. and M. Lanzetta, *Intrinsic kinetics of isothermal xylan degradation in inert atmosphere.* Journal of Analytical and Applied Pyrolysis, 1997. **40–41**(0): p. 287-303.

89. Prins, M.J., K.J. Ptasinski, and F.J.J.G. Janssen, *Torrefaction of wood: Part 2. Analysis of products.* Journal of Analytical and Applied Pyrolysis, 2006. **77**(1): p. 35-40.

90. Ibrahim, R.H.H., *Fundamentals of torrefaction of biomass and its environmental impacts*. 2013, University of Leeds: Unpublished PhD thesis.

91. Borchardt, H.J. and F. Daniels, *The Application of Differential Thermal Analysis to the Study of Reaction Kinetics1.* Journal of the American Chemical Society, 1957. **79**(1): p. 41-46.

92. Weber, R., *Extracting mathematically exact kinetic parameters from experimental data on combustion and pyrolysis of solid fuels.* Journal of the Energy Institute, 2008. **81**(4): p. 226-233.

93. Bridgeman, T.G., J.M. Jones, A. Williams, and D.J. Waldron, *An investigation of the grindability of two torrefied energy crops.* Fuel, 2010. **89**(12): p. 3911-3918.

94. Chen, W.-H. and P.-C. Kuo, *Isothermal torrefaction kinetics of hemicellulose, cellulose, lignin and xylan using thermogravimetric analysis.* Energy, (0).

95. Gaur, S. and Reed, *Thermal Data for Natural and Synthetic Fuels*. 1998, New York: Marcel Dekker.

96. Chen, W.-H. and P.-C. Kuo, *Torrefaction and co-torrefaction characterization of hemicellulose, cellulose and lignin as well as torrefaction of some basic constituents in biomass.* Energy, 2011. **36**(2): p. 803-811.

97. Ferro, D.T., V. Vigouroux, A. Grimm, and R. Zanzi, *Torrefaction of agricultural and forest residues*, in *Cubasolar 2004*. 2004: Guantánamo, Cuba.

98. Dhungana, A., *Torrefaction of biomass*. 2011, Dalhousie University, Nova Scotia: Unpublished work.

99. Chew, J.J. and V. Doshi, *Recent advances in biomass pretreatment – Torrefaction fundamentals and technology.* Renewable and Sustainable Energy Reviews, 2011. **15**(8): p. 4212-4222.

100. Bergman, P.C.A., M.J. Prins, A.R. Boersma, K.J. Ptasinski, J.H.A. Kiel, and F.J.J.G. Janssen, *Torrefaction for entrained-flow gasification of biomass*. 2004.

101. Phanphanich, M. and S. Mani, *Impact of torrefaction on the grindability and fuel characteristics of forest biomass.* Bioresource Technology, 2011. **102**(2): p. 1246-1253.

102. Sandoval-Torres, S., W. Jomaa, F. Marc, and J.R. Puiggali, *Causes of color changes in wood during drying.* Forestry Studies in China, 2010. **12**(4): p. 167-175.

103. Aydemir, D., G. Gunduz, and S. Ozden, *The influence of thermal treatment on color response of wood materials.* Color Research & Application, 2012. **37**(2): p. 148-153.

104. Nhuchhen, D.R., P. Basu, and B. Acharya, *A comprehensive review on biomass torrefaction* International Journal of Renewable Energy & Biofuels 2014. **2014**(2014).

105. Sundqvist, B., *Color changes and acid formation in wood during heating*. 2004, Lulea University of Technology: Unpublished work.

106. Arias, B., C. Pevida, J. Fermoso, M.G. Plaza, F. Rubiera, and J.J. Pis, *Influence of torrefaction on the grindability and reactivity of woody biomass.* Fuel Processing Technology, 2008. **89**(2): p. 169-175.

107. Repellin, V., A. Govin, M. Rolland, and R. Guyonnet, *Energy requirement for fine grinding of torrefied wood.* Biomass and Bioenergy, 2010. **34**(7): p. 923-930.

108. Almeida, G., J.O. Brito, and P. Perré, *Alterations in energy properties of eucalyptus wood and bark subjected to torrefaction: The potential of mass loss as a synthetic indicator.* Bioresource Technology, 2010. **101**(24): p. 9778-9784.

109. Medic, D., M. Darr, A. Shah, B. Potter, and J. Zimmerman, *Effects of torrefaction process parameters on biomass feedstock upgrading.* Fuel, 2012. **91**(1): p. 147-154.

110. Bates, R.B. and A.F. Ghoniem, *Biomass torrefaction: Modeling of reaction thermochemistry.* Bioresource Technology, 2013. **134**(0): p. 331-340.

111. Pimchuai, A., A. Dutta, and P. Basu, *Torrefaction of Agriculture Residue To Enhance Combustible Properties†.* Energy & Fuels, 2010. **24**(9): p. 4638-4645.

112. Chen, W.-H. and P.-C. Kuo, *A study on torrefaction of various biomass materials and its impact on lignocellulosic structure simulated by a thermogravimetry.* Energy, 2010. **35**(6): p. 2580-2586.

113. Ciolkosz, D. and R. Wallace, *A review of torrefaction for bioenergy feedstock production.* Biofuels, Bioproducts and Biorefining, 2011. **5**(3): p. 317-329.

114. Nimlos, M.N., E.B.M.J. Looker, and R.J. Evans, *Biomass torrefaction studies with a molecular beam mass spectrometer*. 2003, National Bioenergy Center: Colorado.

115. Ohliger, A., M. Förster, and R. Kneer, *Torrefaction of beechwood: A parametric study including heat of reaction and grindability.* Fuel, 2013. **104**(0): p. 607-613.

116. Wannapeera, J., B. Fungtammasan, and N. Worasuwannarak, *Effects of temperature and holding time during torrefaction on the pyrolysis behaviors of woody biomass.* Journal of Analytical and Applied Pyrolysis, 2011. **92**(1): p. 99-105.

117. Tapasvi, D., R. Khalil, G. Várhegyi, Ø. Skreiberg, K.-Q. Tran, and M. Grønli, *Kinetic Behavior of Torrefied Biomass in an Oxidative Environment.* Energy & Fuels, 2013. **27**(2): p. 1050-1060.

118. Jaya, S.T., S. Shahab, H.J. Richard, W.C. T, and B.R. D., *A review on biomass torrefaction process and product properties for energy applications.* Industrial Biotechnology, 2011. **7**(5): p. 384-401.

119. Vassilev, S.V., D. Baxter, and C.G. Vassileva, *An overview of the behaviour of biomass during combustion: Part II. Ash fusion and ash formation mechanisms of biomass types.* Fuel, 2014. **117, Part A**(0): p. 152-183.

120. Darvell, L.I., J.M. Jones, B. Gudka, X.C. Baxter, A. Saddawi, A. Williams, and A. Malmgren, *Combustion properties of some power station biomass fuels.* Fuel, 2010. **89**(10): p. 2881-2890.

121. Darvell, L.I., L. Ma, J.M. Jones, M. Pourkashanian, and A. Williams, *Some Aspects of Modeling NOx Formation Arising from the Combustion of 100% Wood in a Pulverized Fuel Furnace.* Combustion Science and Technology, 2014. **186**(4-5): p. 672-683.

122. Li, J., A. Brzdekiewicz, W. Yang, and W. Blasiak, *Co-firing based on biomass torrefaction in a pulverized coal boiler with aim of 100% fuel switching.* Applied Energy, 2012. **99**(0): p. 344-354.

123. Li, J., E. Biagini, W. Yang, L. Tognotti, and W. Blasiak, *Flame characteristics of pulverized torrefied-biomass combusted with high-temperature air.* Combustion and Flame, 2013. **160**(11): p. 2585-2594.

124. Ren, S., H. Lei, L. Wang, Q. Bu, S. Chen, and J. Wu, *Thermal behaviour and kinetic study for woody biomass torrefaction and torrefied biomass pyrolysis by TGA.* Biosystems Engineering, 2013. **116**(4): p. 420-426.

125. Chen, W.-H., S.-W. Du, C.-H. Tsai, and Z.-Y. Wang, *Torrefied biomasses in a drop tube furnace to evaluate their utility in blast furnaces.* Bioresource Technology, 2012. **111**(0): p. 433-438.

126. Li, H., X. Liu, R. Legros, X.T. Bi, C.J. Lim, and S. Sokhansanj, *Torrefaction of sawdust in a fluidized bed reactor.* Bioresource Technology, 2012. **103**(1): p. 453-458.

127. Felfli, F.F., C.A. Luengo, J.A. Suárez, and P.A. Beatón, *Wood briquette torrefaction.* Energy for Sustainable Development, 2005. **9**(3): p. 19-22.

128. Ibrahim, R.H.H., L.I. Darvell, J.M. Jones, and A. Williams, *Physicochemical characterisation of torrefied biomass.* Journal of Analytical and Applied Pyrolysis, 2013. **103**(0): p. 21-30.

129. Sadaka, S. and S. Negi, *Improvements of biomass physical and thermochemical characteristics via torrefaction process.* Environmental Progress & Sustainable Energy, 2009. **28**(3): p. 427-434.

130. Tichánek, F., *Contribution to Determination of Coal Grindability Using Hardgrove Method.* GeoScience Engineering GSE, 2008. **54**(1): p. 27-32.

131. Wu, K.-T., C.-J. Tsai, C.-S. Chen, and H.-W. Chen, *The characteristics of torrefied microalgae.* Applied Energy, 2012. **100**(0): p. 52-57.

132. Tumuluru, J.S., S. Sokhansanj, C.T. Wright, and R.D. Boardman, *Biomass torrefaction process review and moving bed torrefaction system model development.* 2010, U.S. Department of Energy: Unpublished work.

133. Jones, J.M., T.G. Bridgeman, L.I. Darvell, B. Gudka, A. Saddawi, and A. Williams, *Combustion properties of torrefied willow compared with bituminous coals.* Fuel Processing Technology, 2012. **101**(0): p. 1-9.

134. Chan, M.L., J.M. Jones, M. Pourkashanian, and A. Williams, *The oxidative reactivity of coal chars in relation to their structure.* Fuel, 1999. **78**(13): p. 1539-1552.

135. Fisher, E.M., C. Dupont, L.I. Darvell, J.M. Commandré, A. Saddawi, J.M. Jones, M. Grateau, T. Nocquet, and S. Salvador, *Combustion and gasification characteristics of chars from raw and torrefied biomass.* Bioresource Technology, 2012. **119**(0): p. 157-165.

136. Ogbonna, P.C. and V.I. Okeke, *Metal Content of Soil and Macronutrient of Gmelina leaves in Umuahia, Nigeria.* Journal of Applied Science in Environmental Sanitation, 2011. **6**(1): p. 15-22.

137. Onyekwelu, J.C., *Above-ground biomass production and biomass equations for even-aged Gmelina arborea (ROXB) plantations in south-western Nigeria.* Biomass and Bioenergy, 2004. **26**(1): p. 39-46.

138. Fuwape, J.A. and S.O. Akindele, *Biomass yield and energy value of some fast-growing multipurpose trees in Nigeria.* Biomass and Bioenergy, 1997. **12**(2): p. 101-106.

139. Adekunle, V.A.J., A.A. Alo, and F.O. Adekayode, *Yields and nutrient pools in soils cultivated with Tectona grandis and Gmelina arborea in Nigerian rainforest ecosystem.* Journal of the Saudi Society of Agricultural Sciences, 2011. **10**(2): p. 127-135.

140. Fuwape, J.A., J.C. Onyekwelu, and V.A.J. Adekunle, *Biomass equations and estimation for Gmelina arborea and Nauclea diderrichii stands in Akure forest reserve.* Biomass and Bioenergy, 2001. **21**(6): p. 401-405.

141. Orwa, C., A. Mutua, R. Kindt, R. Jamnadass, and A. Simons, *Agroforestree Database:a tree reference and selection guide* 2009.

142. Ola-Adams, B.A., *Effects of spacing on biomass distribution and nutrient content of Tectona grandis Linn. f. (teak) and Terminalia superba Engl. & Diels. (afara) in south-western Nigeria.* Forest Ecology and Management, 1993. **58**(3–4): p. 299-319.

143. Oriola, E.O., *Forestry for Sustainable Development in NigeriaForestry for Sustainable Development in Nigeria.* International Journal of African Studies, 2009: p. 11-16.

144. Alamu, L.O. and B.O. Agbeja, *Deforestation and endangered indigenous tree species in South-West Nigeria.* International Journal of Biodiversity and Conservation, 2011. **3**(7): p. 291-297.

145. White, L.J.T. and J.F. Oates, *New data on the history of the plateau forest of Okomu, southern Nigeria: an insight into how human disturbance has shaped the African rain forest: RESEARCH LETTER.* Global Ecology & Biogeography, 1999. **8**(5): p. 355-361.

146. Kelly, C.K. and A. Purvis, *Seed size and establishment conditions in tropical trees.* Oecologia, 1993. **94**(3): p. 356-360.

147. Onyekwelu, J.C., *Growth, biomass yield and biomass functions for plantation-grown Nauclea diderrichii (de wild) in the humid tropical rainforest zone of south-western Nigeria.* Bioresource Technology, 2007. **98**(14): p. 2679-2687.

148. Sichaem, J., W. Worawalai, and S. Tip-pyang, *Chemical constituents from the roots of Nauclea orientalis.* Chemistry of Natural Compounds, 2012. **48**(5): p. 827-830.

149. Uemura, Y., W.N. Omar, T. Tsutsui, and S.B. Yusup, *Torrefaction of oil palm wastes.* Fuel, 2011. **90**(8): p. 2585-2591.

150. Balogun, A.O., O.A. Lasode, and A.G. McDonald, *Thermo-Analytical and Physico-Chemical Characterization of Woody and Non-Woody Biomass from an Agro-ecological Zone in Nigeria.* BioResources, 2014. **9**(3).

151. Akinwole, A.O. and A.B. Dauda, *Performance of Palm Kernel Shell as Nitrification Media for Aquaculture Wastewater at Varying Drying Time* Global Journal of Science Frontier Research, 2014. **14**(5): p. 30-40.

152. Poku, K. *Small-Scale Palm Oil Processing in Africa.* . FAO Agricultural Services Bulletin, 2002.

153. Matlaga, D.P. and A.S. Davis, *Minimizing invasive potential of Miscanthus × giganteus grown for bioenergy: identifying demographic thresholds for population growth and spread.* Journal of Applied Ecology, 2013. **50**(2): p. 479-487.

154. Reed, T.B., *Biomass gasification: Principles and Technology* 1981, Park Ridge, New Jersey: Noyes Data Corporation.

155. Friedl, A., E. Padouvas, H. Rotter, and K. Varmuza, *Prediction of heating values of biomass fuel from elemental composition.* Analytica Chimica Acta, 2005. **544**(1-2): p. 191-198.

156. Van Soest, P.J., *The use of detergents in the analysis of fibrous feeds: II. a rapid method for the determination of fibre and lignin.* Journal of the Association of official Agricultural Chemists, 1963. **46**: p. 829-835.

157. Nowakowski, D.J., C.R. Woodbridge, and J.M. Jones, *Phosphorus catalysis in the pyrolysis behaviour of biomass.* Journal of Analytical and Applied Pyrolysis, 2008. **83**(2): p. 197-204.

158. Lai, Y.Z. and K.V. Sarkanen, *Isolation and structural studies in Lignins: Occurrence, Formation, Structure and Reactions*, ed. K.V. Sarkanen and C.H. Ludwig. 1971, New York: Wiley-Interscience.

159. Hatfield, R.D., H.G. Jung, J. Ralph, D.R. Buxton, and P.J. Weimer, *A comparison of the insoluble residues produced by the Klason lignin and acid detergent lignin procedures.* J. Sci. Food Agric., 1994. **65**: p. 51-58.

160. Kondo, T., K. Mizuno, and T. Kato, *Variation in solubilities of lignin in acid detergent and in alkali.* J. Jpn. Grassl. Sci., 1987. **33**: p. 296-299.

161. Lowry, J.B., L.L. Conlan, A.C. Schlink, and C.S. McSweeney, *Acid detergent dispersible lignin in tropical grasses.* J. Sci. Food Agric., 1994. **65**: p. 41-49.

162. Bryers, R.W., *Fireside slagging, fouling, and high-temperature corrosion of heat-transfer surface due to impurities in steam-raising fuels.* Progress in Energy and Combustion Science, 1996. **22**(1): p. 29-120.

163. Baxter, X.C., L.I. Darvell, J.M. Jones, T. Barraclough, N.E. Yates, and I. Shield, *Study of Miscanthus x giganteus ash composition – Variation with agronomy and assessment method.* Fuel, 2012. **95**(0): p. 50-62.

164. Miles, T.R., T.R. Miles Jr, L.L. Baxter, R.W. Bryers, B.M. Jenkins, and L.L. Oden, *Boiler deposits from firing biomass fuels.* Biomass and Bioenergy, 1996. **10**(2–3): p. 125-138.

165. Darvell, L.I., J.M. Jones, B. Gudka, X.C. Baxter, A. Saddawi, R.H. Ibrahim, and W. A., *Combustion properties of imported biomass feedstocks for co-firing in the UK*. 2010, 18th European biomass congress and exhibition: Lyon, France.

166. Vassilev, S.V., D. Baxter, L.K. Andersen, C.G. Vassileva, and T.J. Morgan, *An overview of the organic and inorganic phase composition of biomass.* Fuel, 2012. **94**(0): p. 1-33.

167. Werkelin, J., B.-J. Skrifvars, and M. Hupa, *Ash-forming elements in four Scandinavian wood species. Part 1: Summer harvest.* Biomass and Bioenergy, 2005. **29**(6): p. 451-466.

168. Kaltschmitt, M. and M. Weber, *Markets for solid biofuels within the EU-15.* Biomass and Bioenergy, 2006. **30**(11): p. 897-907.

169. Lewandowski, I. and A. Kicherer, *Combustion quality of biomass: practical relevance and experiments to modify the biomass quality of Miscanthus x giganteus.* European Journal of Agronomy, 1997. **6**(3–4): p. 163-177.

170. Kauter, D., I. Lewandowski, and W. Claupein, *Quantity and quality of harvestable biomass from Populus short rotation coppice for solid fuel use—a review of the physiological basis and management influences.* Biomass and Bioenergy, 2003. **24**(6): p. 411-427.

171. Gudka, B.A., *Combustion Characteristics of some Imported Feedstocks and Short Rotation Coppice (SRC Willow for UK Power Stations*, in *School of Process, Environmental and Materials Engineering*. 2012, The University of Leeds, Leeds: White Rose Etheses Online.

172. Kastanaki, E. and D. Vamvuka, *A comparative reactivity and kinetic study on the combustion of coal–biomass char blends.* Fuel, 2006. **85**(9): p. 1186-1193.

173. Antal M, J., G. Varhegyi, and E. Jakab, *Cellulose pyrolysis kinetics : Revisited.* Industrial & engineering chemistry research, 1998. **37**(4): p. 1267-1275.

174. Chen, W.-H. and P.-C. Kuo, *Isothermal torrefaction kinetics of hemicellulose, cellulose, lignin and xylan using thermogravimetric analysis.* Energy, 2011. **36**(11): p. 6451-6460.

175. Conesa, J.A., A. Marcilla, J.A. Caballero, and R. Font, *Comments on the validity and utility of the different methods for kinetic analysis of thermogravimetric data.* Journal of Analytical and Applied Pyrolysis, 2001. **58–59**(0): p. 617-633.

176. Miranda, T., A. Esteban, S. Rojas, I. Montero, and A. Ruiz, *Combustion Analysis of Different Olive Residues.* International Journal of Molecular Sciences, 2008. **9**(4): p. 512-525.

177. Gubba, S.R., L. Ma, M. Pourkashanian, and A. Williams, *Influence of particle shape and internal thermal gradients of biomass particles on pulverised coal/biomass co-fired flames.* Fuel Processing Technology, 2011. **92**(11): p. 2185-2195.

178. Yang, Y.B., V.N. Sharifi, J. Swithenbank, L. Ma, L.I. Darvell, J.M. Jones, M. Pourkashanian, and A. Williams, *Combustion of a Single Particle of Biomass.* Energy & Fuels, 2007. **22**(1): p. 306-316.

179. Kanury, A.M., *Combustion Characteristics of Biomass Fuels.* Combustion Science and Technology, 1994. **97**(4-6): p. 469-491.

180. Babrauskas, V., *Ignition Handbook.* 2003, Issaquah, WA 98027 USA: Fire Science

181. Bridgwater A.V, *Review of fast pyrolysis of biomass and product upgrading.* Biomass and Bioenergy, 2012. **38**(0): p. 68-94.

182. Alén, R., E. Kuoppala, and P. Oesch, *Formation of the main degradation compound groups from wood and its components during pyrolysis.* Journal of Analytical and Applied Pyrolysis, 1996. **36**(2): p. 137-148.

183. Vamvuka, D., *Bio-oil, solid and gaseous biofuels from biomass pyrolysis processes—An overview.* International Journal of Energy Research, 2011. **35**(10): p. 835-862.

184. Dong, C.-q., Z.-f. Zhang, Q. Lu, and Y.-p. Yang, *Characteristics and mechanism study of analytical fast pyrolysis of poplar wood.* Energy Conversion and Management, 2012. **57**(0): p. 49-59.

185. Azeez, A.M., D. Meier, J.r. Odermatt, and T. Willner, *Fast Pyrolysis of African and European Lignocellulosic Biomasses Using Py-GC/MS and Fluidized Bed Reactor.* Energy & Fuels, 2010. **24**(3): p. 2078-2085.

186. Fahmi, R., A.V. Bridgwater, S.C. Thain, I.S. Donnison, P.M. Morris, and N. Yates, *Prediction of Klason lignin and lignin thermal degradation products by Py–GC/MS in a collection of Lolium and Festuca grasses.* Journal of Analytical and Applied Pyrolysis, 2007. **80**(1): p. 16-23.

187. Lu, Q., Z.-F. Zhang, C.-Q. Dong, and X.-F. Zhu, *Catalytic Upgrading of Biomass Fast Pyrolysis Vapors with Nano Metal Oxides: An Analytical Py-GC/MS Study.* Energies, 2010. **3**(11): p. 1805-1820.

188. Lu, Q., W.-M. Xiong, W.-Z. Li, Q.-X. Guo, and X.-F. Zhu, *Catalytic pyrolysis of cellulose with sulfated metal oxides: A promising method for obtaining high yield of light furan compounds.* Bioresource Technology, 2009. **100**(20): p. 4871-4876.

189. Chen, W.-H., W.-Y. Cheng, K.-M. Lu, and Y.-P. Huang, *An evaluation on improvement of pulverized biomass property for solid fuel through torrefaction.* Applied Energy, 2011. **88**(11): p. 3636-3644.

190. Melkior, T., S. Jacob, G. Gerbaud, S. Hediger, L. Le Pape, L. Bonnefois, and M. Bardet, *NMR analysis of the transformation of wood constituents by torrefaction.* Fuel, 2012. **92**(1): p. 271-280.

191. Felfli, F.F., C.A. Luengo, G. Bezzon, and P. Beaton Soler. *Bench unit for biomass residues torrefaction*. in *10th European biomass conference for energy & industry*. 1998. Würzburg, Germany.

192. Yan, W., T.C. Acharjee, C.J. Coronella, and V.R. Vásquez, *Thermal pretreatment of lignocellulosic biomass.* Environmental Progress & Sustainable Energy, 2009. **28**(3): p. 435-440.

193. Rousset, P., C. Aguiar, N. Labbé, and J.-M. Commandré, *Enhancing the combustible properties of bamboo by torrefaction.* Bioresource Technology, 2011. **102**(17): p. 8225-8231.

194. Peng, J.H., H.T. Bi, S. Sokhansanj, and J.C. Lim, *A Study of Particle Size Effect on Biomass Torrefaction and Densification.* Energy & Fuels, 2012. **26**(6): p. 3826-3839.

195. Stelte, W., C. Clemons, J.K. Holm, A.R. Sanadi, J. Ahrenfeldt, L. Shang, and U.B. Henriksen, *Pelletizing properties of torrefied spruce.* Biomass and Bioenergy, 2011. **35**(11): p. 4690-4698.

196. Singh, K. and L. Sivanandan, *Changes in wood during mild thermal decay and its detection using ATR-IR: a review*. Journal of Agricultural Science and Applications, 2014. **3**(1): p. 1-7.

197. Biswas, A.K., W. Yang, and W. Blasiak, *Steam pretreatment of Salix to upgrade biomass fuel for wood pellet production.* Fuel Processing Technology, 2011. **92**(9): p. 1711-1717.

198. Kumar, S., *Co-liquefaction of coal and biomass for liquid fuel synthesis*. 2012, West Virginia University, Morgantown, WV.

199. Khazraie, S.T., N.A. DeMartini, S.M. Willför, A. Pranovich, A.I. Smeds, T. Virtanen, S.L. Maunu, F. Verhoeff, J.H.A. Kiel, and M. Hupa, *Impact of Torrefaction on the Chemical Structure of Birch Wood.* Energy & Fuels, 2014.

200. Akinrinola, F.S., L.I. Darvell, J.M. Jones, A. Williams, and J.A. Fuwape, *Characterization of Selected Nigerian Biomass for Combustion and Pyrolysis Applications.* Energy & Fuels, 2014.

201. Lester, E., M. Gong, and A. Thompson, *A method for source apportionment in biomass/coal blends using thermogravimetric analysis.* Journal of Analytical and Applied Pyrolysis, 2007. **80**(1): p. 111-117.

202. Akinrinola, F.S., L.I. Darvell, J.M. Jones, A. Williams, and J.A. Fuwape, *Characterization of Selected Nigerian Biomass for Combustion and Pyrolysis Applications.* Energy & Fuels, 2014. **28**(6): p. 3821-3832.

203. Naik, S., V.V. Goud, P.K. Rout, K. Jacobson, and A.K. Dalai, *Characterization of Canadian biomass for alternative renewable biofuel.* Renewable Energy, 2010. **35**(8): p. 1624-1631.

204. Biagini, E., A. Fantei, and L. Tognotti, *Effect of the heating rate on the devolatilization of biomass residues.* Thermochimica Acta, 2008. **472**(1–2): p. 55-63.

205. Meng, J., J. Park, D. Tilotta, and S. Park, *The effect of torrefaction on the chemistry of fast-pyrolysis bio-oil.* Bioresource Technology, 2012. **111**(0): p. 439-446.

206. Jablonský, M., J. Kočiš, A. Ház, A. Sládková, and I. Šurina, *The approach the isolation of lignins and its characterization* in *5th International Scientific Conference, Renewable Energy Sources 2014*. 2014: High Tatras - Tatranske Matliare, Slovak Republic

207. Gao, N., A. Li, C. Quan, L. Du, and Y. Duan, *TG–FTIR and Py–GC/MS analysis on pyrolysis and combustion of pine sawdust.* Journal of Analytical and Applied Pyrolysis, 2013. **100**(0): p. 26-32.

208. Greenhalf, C.E., D.J. Nowakowski, A.B. Harms, J.O. Titiloye, and A.V. Bridgwater, *A comparative study of straw, perennial grasses and hardwoods in terms of fast pyrolysis products.* Fuel, 2013. **108**(0): p. 216-230.

209. Ma, L., M. Gharebaghi, R. Porter, M. Pourkashanian, J.M. Jones, and A. Williams, *Modelling methods for co-fired pulverised fuel furnaces.* Fuel, 2009. **88**(12): p. 2448-2454.

210. Flower, M. and J. Gibbins, *A radiant heating wire mesh single-particle biomass combustion apparatus.* Fuel, 2009. **88**(12): p. 2418-2427.

211. Lu, H. and L.L. Baxter, *Biomass Combustion Characteristics and Implications for Renewable Energy*, in *Solid Biofuels for Energy*, P. Grammelis, Editor. 2011, Springer London. p. 95-121.

212. Lu, H., E. Ip, J. Scott, P. Foster, M. Vickers, and L.L. Baxter, *Effects of particle shape and size on devolatilization of biomass particle.* Fuel, 2010. **89**(5): p. 1156-1168.

213. Momeni, M., C. Yin, S.K. Kær, T.B. Hansen, P.A. Jensen, and P. Glarborg, *Experimental Study on Effects of Particle Shape and Operating Conditions on Combustion Characteristics of Single Biomass Particles.* Energy & Fuels, 2012. **27**(1): p. 507-514.

214. Lu, H., W. Robert, G. Peirce, B. Ripa, and L.L. Baxter, *Comprehensive Study of Biomass Particle Combustion.* Energy & Fuels, 2008. **22**(4): p. 2826-2839.

215. Scott, S.A., J.F. Davidson, J.S. Dennis, and A.N. Hayhurst, *The devolatilisation of particles of a complex fuel (dried sewage sludge) in a fluidised bed.* Chemical Engineering Science, 2007. **62**(1–2): p. 584-598.

216. Oluyamo, S.S., O.R. Bello, and Y.O. Johnson, *Thermal Conductivity of Three Different Wood Products of Combretaceae Family; Terminalia superb, Terminalia ivorensis and Quisqualis indica.* Journal of Natural Sciences Research, 2012. **2**: p. 36-44.

217. Borman, G.L. and K.W. Ragland, *Combustion engineering*. 1998, New York: McGraw-Hill.

218. Munir, S., S.S. Daood, W. Nimmo, A.M. Cunliffe, and B.M. Gibbs, *Thermal analysis and devolatilization kinetics of cotton stalk, sugar cane bagasse and shea meal under nitrogen and air atmospheres.* Bioresource Technology, 2009. **100**(3): p. 1413-1418.

219. Corbitt, R.A., *Standard Handbook of Environmental Engineering*. Second Edition ed. 1998, New York: McGraw-Hill Inc.

8.4 APPENDICES

8.4.1 Appendix 5-1: CHNS and HHVvalues for the tars.

Sample	C (wt %)	H (wt %)	N (wt %)	O (wt %) *	HHV (MJ/kg)
T270-60_tar	58.37	6.30	0.14	35.19	22.49
G270-60_tar	54.70	6.35	0.41	38.54	20.72
L270-60 _tar	57.18	6.40	0.34	36.08	22.07
M270-60_tar	52.15	5.66	0.74	41.46	18.33
W270-60_tar	54.94	6.25	0.43	38.37	20.69
P270-60_tar	62.87	6.15	0.21	30.77	24.59
N270-60_tar	57.57	6.46	0.61	35.36	22.42

HHV calculated using DuLong formula [219]. Elemental composition C, H, N, O and S are the mass fractions of carbon, hydrogen, oxygen and sulphur respectively in wt.% on a dry basis. ***** Calculated by difference. The tars are sulphur free.

8.4.2 Appendix 5-2: Nitrogen in Fuel (wt% and gram)

Sample	***Terminalia***	***GMELINA***	***NAUCLEA***	***LOPHIRA***	**PKE**	**WHEAT STRAW**
N_Raw (%)	0.30	0.16	0.60	0.24	0.42	0.50
N_Torrefied (270-60) %	0.35	0.14	0.70	0.27	0.53	0.67
N_TAR (%)	0.14	0.41	0.61	0.34	0.21	0.43
N_Raw (g)	0.30	0.16	0.60	0.26	1.05	0.24
N_Torrefied (270-60) g	0.23	0.09	0.45	0.18	0.87	0.19
N_TAR (g)	0.02	0.04	0.05	0.04	0.12	0.03
%Torrefied (270-60)	77.08	57.97	75.46	71.27	82.75	77.56
% Tar	5.21	25.20	8.36	15.68	11.19	12.66

8.4.3 Appendix 5-3: Nitrogen in fuel (per kg of Fuels).

Fuels	N(db)	HHV(db)	HHV(GJ/kg)	(0.01*Wt%N)	N in kg/GJ:
Gmelina	0.16	20,400	0.0204	0.0016	0.08
G270-30	0.14	22,900	0.0229	0.0014	0.06
G270-60	0.14	23,000	0.023	0.0014	0.06
Terminalia	0.32	19,200	0.0192	0.0032	0.17
T270-30	0.34	21,200	0.0212	0.0034	0.16
T270-60	0.35	21,500	0.0215	0.0035	0.16
Lophira	0.26	20,200	0.0202	0.0026	0.13
L270-30	0.27	22,200	0.0222	0.0027	0.12
L270-60	0.27	22,600	0.0226	0.0027	0.12
Nauclea	0.62	21,200	0.0212	0.0062	0.29
N270-30	0.67	23,200	0.0232	0.0067	0.29
N270-60	0.68	24,600	0.0246	0.0068	0.28
PKE	0.45	21,000	0.021	0.0045	0.21
P270-30	0.47	21,700	0.0217	0.0047	0.22
P270-60	0.54	25,600	0.0256	0.0054	0.21
P290-30	0.53	22,400	0.0224	0.0053	0.24
wheat straw	0.50	17,100	0.0171	0.0050	0.29
W270-30	0.72	19,600	0.0196	0.0072	0.37
W270-60	0.68	20,600	0.0206	0.0068	0.33